Computer Assisted Orthopaedic Surgery for Hip and Knee

Current State of the Art in Clinical Application and Basic Research

Nobuhiko Sugano
Editor

Springer

Computer Assisted Orthopaedic Surgery for Hip and Knee

Nobuhiko Sugano
Editor

Computer Assisted Orthopaedic Surgery for Hip and Knee

Current State of the Art in Clinical Application and Basic Research

Springer

Editor
Nobuhiko Sugano
Department of Orthopaedic Medical Engineering
Osaka University Graduate School of Medicine
Suita, Osaka, Japan

ISBN 978-981-10-5244-6 ISBN 978-981-10-5245-3 (eBook)
https://doi.org/10.1007/978-981-10-5245-3

Library of Congress Control Number: 2018936913

Printed on acid-free paper

This Springer imprint is published by the registered company Springer Nature Singapore Pte Ltd.
part of Springer Nature
The registered company address is: 152 Beach Road, #21-01/04 Gateway East, Singapore 189721, Singapore

Preface

It has been more than two decades since the clinical application of computer-assisted orthopedic surgery (CAOS) was introduced. During this time, the uses for CAOS have expanded from spine surgery to total knee/hip arthroplasty, trauma surgery, ligament reconstruction, osteotomies, and tumor surgery. The main goal of CAOS is to help surgeons improve the accuracy and precision of their surgical endeavors with the use of preoperative planning, navigation, custom-made instruments/implants, and robotic devices. With the advances in computer hardware and software, it is not difficult for even novice surgeons to use CAOS technology nowadays. The accumulation of three-dimensional data sets and the availability of statistical shape modeling methods have led to simpler means by which to measure the three-dimensional morphology of the joints and improve implant alignment. These advances have made the development of custom implant designs and automated preoperative planning easier without CT images and complex manual works.

A year ago, in 2016, I hosted the CAOS international annual meeting, where I realized that it was a good time to review the clinical status of CAOS and its applications emerging from basic research and the continuous development of computer technology. I asked clinicians and basic researchers familiar with the use of CAOS—all experts in their fields—to write chapters for what would eventually become this book. They graciously agreed to share their specific knowledge about using CAOS to address pelvic, hip, and knee revisions and repairs—the major areas of advancement in the use of CAOS.

I hope this compendium—the end result of our efforts—will be a useful resource for specialists interested in this technology. It was our belief that orthopedic surgeons, clinical technologists, and computer scientists could benefit from this update on CAOS and that it might steer these same innovators to think about the future directions of CAOS technology and research.

Suita, Osaka, Japan — Nobuhiko Sugano

Contents

Part I
Computet-Assisted TKA

Chapter 1
Navigation of Alignment and Balancing During Knee Replacement

Norberto Confalonieri, Alessio Biazzo, and Alfonso Manzotti

Abstract Neutral mechanical alignment is currently considered the "gold standard" and primary aim of every total knee replacement (TKR). It can be achieved via various surgical techniques, such as with extramedullary and intramedullary guides, patient-specific instrumentation, and navigation, each with advantages and disadvantages. Between 1998 and 2003, we compared three alignment systems in 115 TKRs: the Orthopilot navigation system in 38 patients (group A), totally intramedullary alignment system in 40 patients (group B), and totally extramedullary alignment system in 37 patients (group C). At the 12-month postoperative follow-up, the mean hip–knee–ankle angle (HKA) was 179.1° (range 176°–184°) for group A, 178.6° (173°–186°) for group B, and 177.8° (172°–186°) for group C. Differences among the three groups were not statistically significant. The number of prostheses aligned within 2° of an ideal HKA (180°) in the three groups was 33 (86.8%) in group A, 33 (82.5%) in group B, and 23 (62.1%) in group C. There was a statistically significant difference between groups A and C (A > C) ($p = 0.02$). Thus, the accuracy of the implant's alignment was significantly improved by using a navigation system compared with alignment using an extramedullary guide. In the navigation group (A), there were no cases of malalignment of >3° away from an ideal implant alignment in either the frontal or sagittal plane. Navigation has proved to be a useful tool for achieving a more accurate postoperative mechanical axis via precise, reproducible bone resection and ligament balancing. Navigation for TKR has been reported to provide more precise component placement in coronal, sagittal, and rotational alignments, more accurate bone cuts, and better restoration of coronal limb alignment.

Keywords Computer-assisted navigation · Total knee replacement · Knee balancing · Mechanical alignment

N. Confalonieri (✉) • A. Biazzo
1st Orthop Department, CTO Hospital, Milan, Italy
e-mail: norberto.confalonieri@gmail.com

A. Manzotti
Orthop Department, "Luigi Sacco" Hospital, Milan, Italy

N. Sugano (ed.), *Computer Assisted Orthopaedic Surgery for Hip and Knee*,
https://doi.org/10.1007/978-981-10-5245-3_1

1.1 Introduction

Total knee replacement (TKR) is one of the most frequent orthopedic procedures performed every year. The number of TKRs carried out in the United States is estimated to increase by 673% before 2030 [1]. At the same time 20% of patients who underwent TKR are not satisfied with the outcome [2, 3]. The reasons are unknown, but we think that a mechanical alignment beyond 3° of varus–valgus can represent the most important cause of mechanical failure of a TKR and consequently patient dissatisfaction.

Restoring the mechanical axis in TKR is a key factor to optimize the load sharing and prevent the eccentric loading through the prosthesis, which could avoid implant loosening, instability, or early failure [4, 5]. The concept of mechanical axis was introduced by Insall et al. [6] in 1985: it requires that both femoral and tibial cuts must be perpendicular to the mechanical axis of the femur and tibia. The purpose is to create equal load distribution on the new joint line.

Although Parratte et al. [7] found that a postoperative mechanical axis of 0° did not improve the rate of survival 15 years postoperatively, several authors suggested that restoration of a neutral mechanical axis improves durability following TKR [8–10]. Nowadays, neutral mechanical alignment is considered the "gold standard" and the primary aim in every TKR. This can be achieved through different surgical techniques, such as extramedullary and intramedullary guides, patient-specific instrumentation (PSI), and navigation, and each one has advantages and disadvantages. Regarding the intramedullary guide, there is an increased risk of fat embolism [11]; there are great limitations on its use, or even impossibility, in cases of bone deformity, sequelae of trauma, or presence of osteosynthesis devices that obliterates the medullary canal. Regarding the extramedullary guide, it becomes more difficult to use in cases of great obesity or increased soft tissue volume around the tibia. PSI for TKR has been introduced to improve alignment and reduce outliers, operation time, and the risk of fat embolism by avoidance of intramedullary canal violation. Recent randomized controlled trails and meta-analysis proved no advantage of PSI in improving mechanical axis and implant survivorship [12, 13].

Navigation has provided a useful tool in assisting the surgeon to achieve more accurate postoperative mechanical axis through precise and reproducible bone resection and ligament balancing [14]. Navigation for TKR has been reported to provide more precise component placement in coronal, sagittal, and rotational alignment, more accurate bone cuts, and better restoration of coronal limb alignment [15–17]. In a meta-analysis of 29 studies comparing navigation with conventional technique, Mason et al. [18] demonstrated 90.4% of patients with a femoral varus/valgus alignment within 2° of the femoral mechanical axis (versus 65.9% in the conventional group) and 95.2% of patients with a tibial varus/valgus alignment within 2° of the tibial mechanical axis (versus 79.7% of the conventional group). While it has been proved that navigation improves mechanical alignment and consequently implant survivorship, improved patient outcomes have been harder to demonstrate.

1.2 Clinical Experience

Between 1998 and 2003, we performed 115 TKRs, using the Orthopilot navigation system in 38 patients (group A), a totally intramedullary alignment system in 40 patients (group B), and a totally extramedullary alignment system in 37 patients (group C). Patients were enrolled in this retrospective, comparative study with the aim of evaluating the radiological results of these alignment systems. The inclusion criteria were a diagnosis of primary osteoarthritis, a body mass index ≤35 kg/m^2, a preoperative hip–knee–ankle angle (HKA) in the frontal plane of 165°–195°, and a preoperative knee flexion deformity not exceeding 10° (the latter two parameters were calculated on preoperative radiographs). At 12 months postoperatively, each patient underwent standing, long leg, anteroposterior and lateral radiography of the operated knee. For the standing long leg radiographs, the patient had to maintain the knee in maximum extension, with the patella pointing forward and with both hips and ankles visible on the film. The groups are summarized as follows.

- Group A: 38 knees operated using computer navigator-assisted alignment (Orthopilot, version 3.0; Aesculap, Tuttlingen, Germany), using the search total knee prosthesis (Aesculap), and retaining the posterior cruciate ligament (PCL)
- Group B: 40 knees operated using a totally intramedullary alignment system for both the tibia and femur, using the prosthesis Genius Triccc (Astro Medical, Vimercate, Milan, Italy), and sacrificing the PCL
- Group C: 37 knees operated using a totally extramedullary alignment system for both the tibia and femur, using the scan prosthesis (Mitab, Shenjoborg, Sweden), and retaining the PCL

An anterior mid-patellar approach and medial arthrotomy were used in all cases. Each of the three alignment instruments was set to achieve an ideal HKA of 180° in the frontal plane and a tibial slope according to the implant design in the sagittal plane (0° for search, 5° for scan and Tricc).

1.3 Computer-Assisted TKR (Surgical Technique)

Since 1998, our department has utilized various computer-assisted navigation systems, without the use of computed tomography (CT), in >2000 joint replacements (knees and hips). With these navigation systems, all data were acquired in the operating theater during the procedures. The procedure was performed in steps.

Step 1. The surgical field is prepared according to the surgeon's preferences. Overall, however, the patient should be in supine position with just the feet outside, allowing the knee to be easily flexed at 90°. A support is placed by the side of the thigh to maintain the lower limb position even with the knee flexed. The surgeon is in front of the patient and able to check the mechanical axis constantly.

Step 2. A metal locator is positioned at the center of the hip as a further limb alignment reference during the surgery, thereby maintaining a constant check on the axial adjustments and the correct positioning of the prosthetic femoral component (plain radiography of the hip indicates the position of the metal locator).

Step 3. With the patient under anesthesia, the surgeon clinically evaluates the limb deformity and determines how much can be reduced manually by exercising the knee.

Step 4. The skin incision with the limb flexed at 90° should not exceed 12–14 cm in a median or paramedian medial direction. The surgeon then performs knee arthrotomy, evaluates all compartments, and confirms (or not) the surgical indication.

Step 5. Screws for the infrared reflecting diodes (LED) of the localizer are inserted through a tiny (<1 cm) skin incision. One diode should be located on the femur and one on the tibia, both 10 cm away from the joint line. Lower limb data can now be acquired using the computer. Just moving the limb and using mathematical models, the navigator determines the axis, which goes through the rotation center of the femoral head and the center of the knee and ankle. Using a mobile pointer, the deepest point in the more damaged tibial plateau, the center of the tibial plateau, both posterior femoral condyles, the superior femoral cortex, and the medial and lateral epicondyles are identified step-by-step, always according to the indications on the screen.

Step 6. With the data reported on the screen, the surgeon can recalculate the deformity with numbers and then determine how much can be corrected. Data processing empowers the system to produce on-screen the information related to the mechanical axes in frontal and lateral projections within the entire range of movement (Fig. 1.1). It suggests an implant size, the amount of bone that needs to be cut according to the deformity, and tridimensional implant alignment.

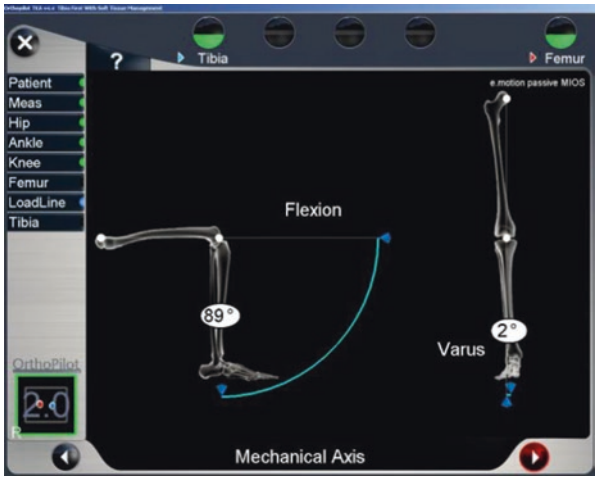

Fig. 1.1 Flexion and extension mechanical axis

Step 7. The deformity should always be reducible manually. If it is not, the surgeon should proceed with slight release of the ligaments under direct control of the system.

Step 8. The tibial cut guide is positioned and connected to the computer using a mobile diode. The height of the resection is based on the concept of the "minimum bone cut"—a simple rule with which we have been experimenting since 2001. The amount of bone to be resected is determined by the difference between the prosthesis thickness and the arthritic knee deformity. For example, if a patient has a valgus deformity of 8°—and assuming a total prosthesis thickness of 19 mm—the minimum bone planned to be resected is 11 mm (19 − 8 = 11) (Fig. 1.2). The tibial cut orientation (varus/valgus) is then planned and checked on the display (Fig. 1.3). The slope is then determined according to the implant slope. After fixing the guide, a blade is used for the horizontal cut.

Step 9. The femoral cuts have been already planned according to the joint space in flexion and extension, both in the medial and lateral compartments, using spreaders (Fig. 1.4). If the gap balancing is not correct, the femoral cuts, rotation of the femoral component, size of the prosthesis, and polyethylene thickness are then reconsidered to equalize the gaps (Table 1.1). In difficult cases with deformities >10°, ligament release must be performed to equalize the gaps. For impossible cases, a hinge prosthesis could be used.

Step 10. A distal femoral cut is then performed and checked on the screen. The chamfers of the corresponding size are then positioned, with adequate femoral rotation, and checked on the screen. The remaining cuts are then made (Fig. 1.5).

Step 11. The tibial and femoral trial components are positioned using polyethylene thicknesses, the mechanical axis is checked, and the ligament balance in full

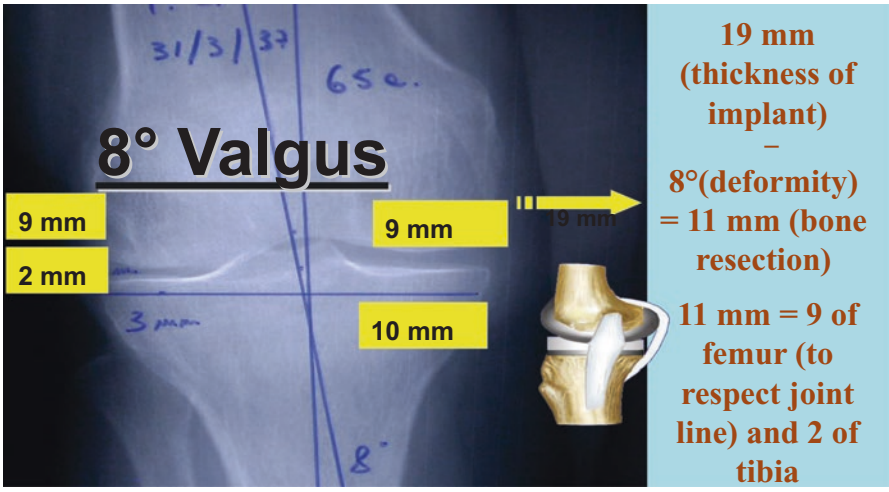

Fig. 1.2 Valgus knee 8°. The minimum bone to be resected is defined as the difference between the prosthesis thickness and the axial deviation angle. Here, we must resect 9 mm of the femur because it drives the joint line

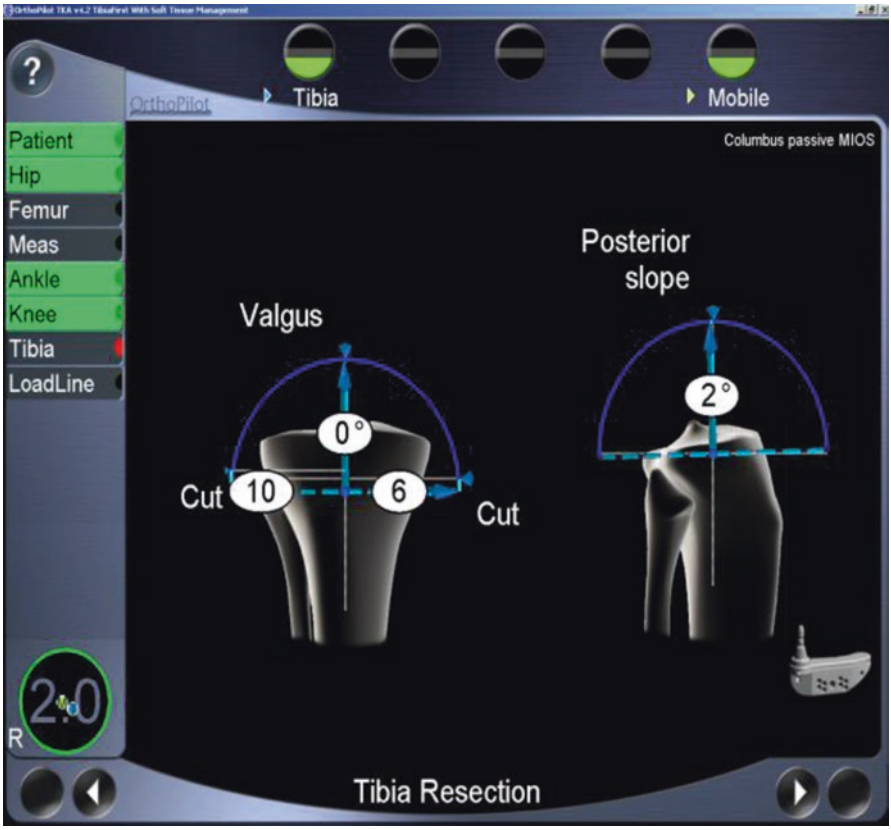

Fig. 1.3 Navigated tibial cut

Fig. 1.4 Gap balancing in extension (0°) and flexion (90°)

Table 1.1 Gap balancing algorithm for total knee replacement

TKR	Extension space balanced	Extension space is tight	Laxity in extension space
Flexion space balanced	Perfect	Release posterior capsule Increase distal femoral cut with the same polyethylene thickness Removal of osteophytes and posterior condyles	Distal femoral wedges Increase tibial slope with higher polyethylene thickness Decrease femoral size component with higher polyethylene thickness
Flexion space is tight	Undersize femoral component with the same poly Release PCL in CR implant Increase tibial slope with the same poly thickness	Increase tibial cut with the same polyethylene thickness	Decrease femoral size with higher polyethylene thickness Distal femoral wedges and increase distal cut and/or tibial slope
Laxity in flexion space	Increase tibial cut and decrease tibial slope with higher polyethylene Increase femoral size with the same polyethylene thickness Increase distal femoral cut with bigger polyethylene	Increase distal femoral cut with bigger polyethylene thickness Increase femoral size component and/or augmentation with posterior femoral wedges with the same polyethylene thickness	Bigger polyethylene thickness

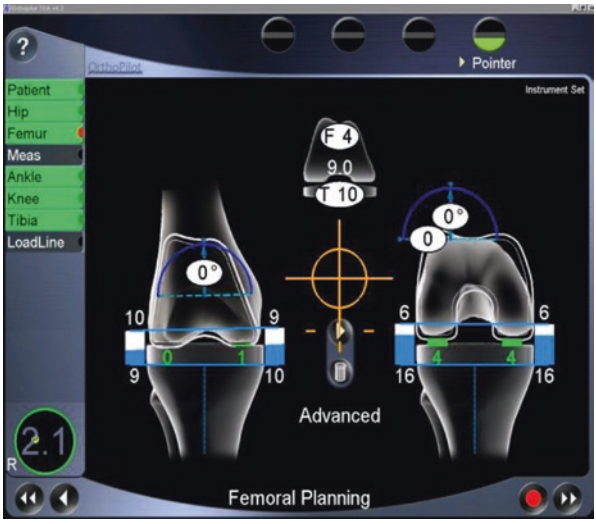

Fig. 1.5 Navigated femoral planning

range of motion is confirmed, always reading the values and the morphology of the inferior limb in motion on the computer screen.

Step 12. The tibial component is then implanted, followed by the femoral component, with the limb then extended and compressed securely against the chest of the operator to complete the operation. The final data are recorded for the computerized patient file charts.

Step 13. The wound is sutured, and a postoperative plain radiograph is obtained. This is the only check for those who do not use computer-assisted surgery.

1.4 Results

According to the surgical charts, the mean operative time was 109.2 min (range 89–133 min) in the navigator group (group A), 91.2 min (74–112 min) for group using the intramedullary alignment guide (group B), and 82.2 min (65–106 min) for the group using the extramedullary alignment guide (group C). The operative time was statistically longer in group A than either group B or group C ($p < 0.05$). Even in group B, the operative time was statistically significantly longer than in group C ($p < 0.05$).

At the 12-month postoperative follow-up, the mean HKA was 179.1° (range 176°–184°) for group A, 178.6° (173°–186°) for group B, and 177.8° (172°–186°) for group C, with no statistically significant differences among the three groups.

The mean frontal femoral component angle was 90.5° (range 87°–94°) for group A, 91.05° (85°–95°) for group B, and 91.19° (85°–96°) for group C. There were no statistically significant differences among the three groups.

The mean frontal tibial component angle was 89.9° (range 83°–97°) for group A, 90.6° (87°–95°) for group B, and 90.8° (86°–95°) for group C. There were no statistically significant differences among the three groups. The mean tibial component inclination in the sagittal plane was 1° (range 0°–3°) for group A, 3.6° (0°–7°) for group B, and 3.1° (0°–6°) for group C.

Regarding the number of patients with femoral components aligned within 2° of 90° in the three groups, there were 33 (86.8%) in group A, 32 (80%) in group B, and 23 (62.1%) in group C. There was a statistically significant difference ($p = 0.03$) between groups A and C (A > C).

Regarding the number of patients with tibial components aligned within 2° of 90°, there were 34 (89.4%) in group A, 34 (85%) in group B, and 26 (70.2%) in group C. There were no statistically significant differences among the three groups.

Regarding the number of prostheses aligned within 2° of an ideal HKA (180°), there were 33 (86.8%) in group A, 33 (82.5%) in group B, and 23 (62.1%) in group C. There was a statistically significant difference ($p = 0.02$) between groups A and C (A > C).

In terms of the number of prostheses aligned within 4° of an ideal HKA (180°), all the implants in group A were aligned, 35 (89.5%) prostheses in group B were aligned, and 28 (75.7%) prostheses in group C were aligned. Again, there was a statistically significant difference ($p = 0.002$) between groups A and C (A > C).

1.5 Discussion and Conclusions

Several studies have reported significant differences in implant survivorship when a traditionally safe zone of 0°–3° was used to define aligned versus malaligned knees with respect to a neutral mechanical axis. For example, Berend et al. [8] reported a statistically significantly increased rate of failure of tibial components positioned in >3.9° of varus. Ritter et al. [9] found an increased rate of failure in knees with a femoral component in >8° of anatomical valgus and in those with a varus tibial component relative to the tibial axis. Collier et al. [10] reported a significantly greater loss of thickness of polyethylene in the medial compartment when the limb was aligned in >5° of varus.

In contrast, some authors have found no statistically significant differences in survivorship between aligned versus malaligned knees with respect to a neutral mechanical axis. One of the most influential studies is that reported by Parratte et al. [7], who retrospectively reviewed the clinical and radiological data of 398 TKRs. They found that a postoperative mechanical axis of 0° did not improve the 15-year postoperative survival rate and stated that the description of alignment as a dichotomous variable (aligned vs. malaligned) provided little value in regard to durability. Nevertheless, they concluded that "until additional data can be generated to more accurately determine the ideal postoperative limb alignment in individual patients, a neutral mechanical axis remains a reasonable target and should be considered as the standard for comparison if other alignment targets are introduced." Similar to the findings of Parratte et al. [7], other authors found that the relation between coronal alignment and survivorship was weak [19–21].

Several studies reported that, with the conventional technique, the percentage of malaligned knees was 20–30% [22–26]. It has been shown that only 70–80% of cases would obtain ideal positioning of the prosthesis when using the intramedullary system [27]. Our results for the intramedullary and extramedullary groups are consistent with those reported in other studies. Oswald et al., using an extramedullary alignment system, reported a malalignment of >4° in the sagittal plane in only 8% of their series [28]. More recently, Reed et al. conducted a randomized, prospective comparison of extramedullary and intramedullary tibial alignment guides in the frontal plane. They reported that 15% of tibial components were not aligned within 2° of 90° in the intramedullary group and 35% were not aligned within 2° of 90° in the extramedullary group, similar to our findings [29].

Navigation for TKR was introduced to improve limb axis correction and component alignment. In 2003, Sparmann et al., in a randomized study, found statistically better alignment in both the frontal and sagittal planes for computer-assisted alignment implants than without navigation support, emphasizing the immediate benefits of applying computer-assisted techniques to TKR [30].

Navigation guidance also provides more accurate bone cuts; more precise component placement in the coronal, sagittal, and rotational planes; and better restoration of coronal limb alignment and lower gap asymmetry [31–35]. Our results demonstrate the significant improvement in the accuracy of the implant's alignment

using a navigation system versus extramedullary guidance. Although the postoperative HKA angles were similar among our three groups (without statistical differences), in the navigation group, there was no implant with an alignment of >4° away from 180°.

Three recent meta-analyses definitively proved that navigation improves mechanical axis and implant survivorship, but currently there is no clinical evidence of improved functional outcomes [36–38]. Hence, the question is: Does navigation improve clinical TKR outcomes? Up to now, we do not know. We are strongly convinced, however, that the improved implant position and coronal and sagittal alignment are decisive for the final outcome and could justify its application to TKR.

References

1. Kurtz S, Ong K, Lau E, Mowat F, Halpern M. Projections of primary and revision hip and knee arthroplasty in the United States from 2005 to 2030. J Bone Joint Surg Am. 2007;89-A:780–5.
2. Bourne RB, Chesworth BM, Davis AM, Mahomed NN, Charron KD. Patient satisfaction after total knee arthroplasty: who is satisfied and who is not? Clin Orthop Relat Res. 2010;468:57–63.
3. Dossett HG, Swartz GJ, Estrada NA, LeFevre GW, Kwasman BG. Kinematically versus mechanically aligned total knee arthroplasty. Orthopedics. 2012;35:e160–9.
4. Blakeney WG, Khan RJ, Wall SJ. Computer-assisted techniques versus conventional guides for component alignment in total knee arthroplasty: a randomized controlled trial. J Bone Joint Surg Am. 2011;93:1377–84.
5. Tingart M, Lüring C, Bäthis H, et al. Computer-assisted total knee arthroplasty versus the conventional technique: how precise is navigation in clinical routine? Knee Surg Sports Traumatol Arthrosc. 2008;16:44–50.
6. Insall JN, Binazzi R, Soudry M, Mestriner LA. Total knee arthroplasty. Clin Orthop Relat Res. 1985;192:13–22.
7. Parratte S, Pagnano MW, Trousdale RT, Berry DJ. Effect of postoperative mechanical axis alignment on the fifteen-year survival of modern, cemented total knee replacements. J Bone Joint Surg Am. 2010;92:2143–9.
8. Berend ME, Ritter MA, Meding JB, et al. Tibial component failure mechanisms in total knee arthroplasty. Clin Orthop Relat Res. 2004;428:26–34.
9. Ritter MA, Davis KE, Meding JB, et al. The effect of alignment and BMI on failure of total knee replacement. J Bone Joint Surg Am. 2011;7(93):1588–96.
10. Collier MB, Engh CA Jr, McAuley JP, Engh GA. Factors associated with the loss of thickness of polyethylene tibial bearings after knee arthroplasty. J Bone Joint Surg Am. 2007;89:1306–14.
11. Fahmy NR, Chandler HP, Danylchuk K, et al. Blood-gas and circulatory changes during total knee replacement. Role of the intramedullary alignment rod. J Bone Joint Surg Am. 1990;72:19–26.
12. Huijbregts HJ, Khan RJ, Sorensen E, et al. Patient-specific instrumentation does not improve radiographic alignment or clinical outcomes after total knee arthroplasty. Acta Orthop. 2016;1:1–9.
13. Nunley RM, Ellison BS, Zhu J, et al. Do patient-specific guides improve coronal alignment in total knee arthroplasty? Clin Orthop Relat Res. 2012;470:895–902.
14. Pitto RP, Graydon AJ, Bradley L, et al. Accuracy of a computer-assisted navigation system for total knee replacement. J Bone Joint Surg Br. 2004;88:601–5.

15. Rosenberger RE, Hoser C, Quirbach S, et al. Improved accuracy of component alignment with the implementation of image-free navigation in total knee arthroplasty. Knee Surg Sports Traumatol Arthrosc. 2007;16:249–57.
16. Scuderi GR, Fallaha M, Masse V, et al. Total knee arthroplasty with a novel navigation system within the surgical field. Orthop Clin North Am. 2014;45:167–73.
17. Stöckl B, Nogler M, Rosiek R, et al. Navigation improves accuracy of rotational alignment in total knee arthroplasty. Clin Orthop Relat Res. 2004;426:180–6.
18. Mason JB, Fehring TK, Estok R, et al. Meta-analysis of alignment outcomes in computer-assisted total knee arthroplasty surgery. J Arthroplast. 2007;22:1097–106.
19. Bonner TJ, Eardley WG, Patterson P, Gregg PJ. The effect of post-operative mechanical axis alignment on the survival of primary total knee replacements after a follow-up of 15 years. J Bone Joint Surg Br. 2011;93:1217–22.
20. Choong PF, Dowsey MM, Stoney JD. Does accurate anatomical alignment result in better function and quality of life? Comparing conventional and computer-assisted total knee arthroplasty. J Arthroplast. 2009;24:560–9.
21. Magnussen RA, Weppe F, Demey G, et al. Residual varus alignment does not compromise results of TKAs in patients with preoperative varus. Clin Orthop Relat Res. 2011;469: 3443–50.
22. Bäthis H, Perlick L, Tingart M, et al. Alignment in total knee arthroplasty. A comparison of computer-assisted surgery with the conventional technique. J Bone Joint Surg Br. 2004;86:682–7.
23. Manjunath KS, Gopalakrishna KG, Vineeth G. Evaluation of alignment in total knee arthroplasty: a prospective study. Eur J Orthop Surg Traumatol. 2015;25:895–903.
24. Matziolis G, Krocker D, Weiss U, et al. A prospective, randomized study of computer-assisted and conventional total knee arthroplasty. Three-dimensional evaluation of implant alignment and rotation. J Bone Joint Surg Am. 2007;89:236–43.
25. Mielke RK, Clemens U, Jens JH, Kershally S. Navigation in knee endoprosthesis implantation—preliminary experiences and prospective comparative study with conventional implantation technique. Z Orthop Ihre Grenzgeb. 2011;139:109–16.
26. Petersen TL, Engh GA. Radiographic assessment of knee alignment after total knee arthroplasty. J Arthroplast. 1988;3:67–72.
27. Mahaluxmivala J, Bankes MJ, Nicolai P, et al. The effect of surgeon experience on component positioning in 673 Press Fit Condylar posterior cruciate-sacrificing total knee arthroplasties. J Arthroplast. 2001;16:635–40.
28. Oswald MH, Jakob RP, Schneider E, Hoogewoud HM. Radiological analysis of normal axial alignment of femur and tibia in view of total knee arthroplasty. J Arthroplast. 1993;8: 419–26.
29. Reed MR, Bliss W, Sher JL, et al. Extramedullary or intramedullary tibial alignment guides: a randomised, prospective trial of radiological alignment. J Bone Joint Surg Br. 2002;84: 858–60.
30. Sparmann M, Wolke B, Czupalla H, et al. Positioning of total knee arthroplasty with and without navigation support. A prospective, randomised study. J Bone Joint Surg Br. 2003;85: 830–5.
31. Decking R, Markmann Y, Fuchs J, et al. Leg axis after computer-navigated total knee arthroplasty: a prospective randomized trial comparing computer-navigated and manual implantation. J Arthroplast. 2005;20:282–8.
32. Fehring TK, Mason JB, Moskal J, et al. When computer-assisted knee replacement is the best alternative. Clin Orthop Relat Res. 2006;452:132–6.
33. Jenny JY, Clemens U, Kohler S, et al. Consistency of implantation of a total knee arthroplasty with a non-image-based navigation system: a case-control study of 235 cases compared with 235 conventionally implanted prostheses. J Arthroplast. 2005;20:832–9.
34. Kim YH, Park JW, Kim JS. Computer-navigated versus conventional total knee arthroplasty: a prospective randomized trial. J Bone Joint Surg Am. 2012;94:2017–24.

35. Weng YJ, Hsu RW, Hsu WH. Comparison of computer-assisted navigation and conventional instrumentation for bilateral total knee arthroplasty. J Arthroplast. 2009;24:668–73.
36. Fu Y, Wang M, Liu Y, Fu Q. Alignment outcomes in navigated total knee arthroplasty: a meta-analysis. Knee Surg Sports Traumatol Arthrosc. 2012;20:1075–82.
37. Hetaimish BM, Khan MM, Simunovic N, et al. Meta-analysis of navigation vs conventional total knee arthroplasty. J Arthroplast. 2012;27:1177–82.
38. Rebal BA, Babatunde OM, Lee JH, et al. Imageless computer navigation in total knee arthroplasty provides superior short term functional outcomes: a meta-analysis. J Arthroplast. 2014;29:938–44.

Chapter 2
CT-Based Navigation for Total Knee Arthroplasty

Tetsuya Tomita, Toshitaka Fujito, Dai Kiyotomo, Kazuma Futai, and Kazuomi Sugamoto

Abstract Image-free computer-assisted surgery systems have been used worldwide for total knee arthroplasty (TKA). We present a computed tomography (CT)-based system that provides preoperative images. Although there is additional cost for preoperative CT-based navigation, it provides useful kinematic data to surgeons for preoperative planning and in the operating room without imageless navigation. In addition to rotation, varus/valgus instability, and anteroposterior translation data, a recent CT-based navigation system provides information about changes in the lengths of the cruciate ligaments during all ranges of movement. Our preliminary results suggest that intraoperative knee kinematics can predict postoperative in vivo kinematics. Reconstructed knee kinematics is one of the key issues for improving patients' satisfaction after TKA. The CT-based navigation system also supports the surgical procedure by optimizing soft tissue balance, with good clinical results.

Keywords Navigation · Total knee arthroplasty · Computer-assisted surgery
CT-based · 3D template

2.1 Introduction

The main goals of total knee arthroplasty (TKA) are long-term durability and good clinical function that allow the patient to maintain activities of daily life and sometimes participate in sports activities. Achieving these goals, however, requires accurate implant positioning, reconstruction of an optimal mechanical axis of the lower extremity, and proper soft tissue balance during all ranges of movement [1]. During the past decade, patients' satisfaction has been reported to be significantly lower after TKA

T. Tomita (✉) • T. Fujito • D. Kiyotomo • K. Futai • K. Sugamoto
Department of Orthopedic Biomaterial Science, Osaka University Graduate School of Medicine, Osaka, Japan
e-mail: tomita@ort.med.osaka-u.ac.jp

N. Sugano (ed.), *Computer Assisted Orthopaedic Surgery for Hip and Knee*,
https://doi.org/10.1007/978-981-10-5245-3_2

than after total hip arthroplasty (THA) [2]. A possible action that might improve patients' satisfaction after TKA is to optimize the knee's postoperative kinematics [3].

Systems for computer-assisted surgery (CAS) for TKA were introduced during the 1990s. Many reports showed substantially better implant positioning and mechanical axes using the CAS systems than with the use of the standard techniques (intramedullary or extramedullary guidance systems). It has been reported that CAS systems play a role in achieving well-aligned knee joints (<3°–4° varus/valgus) and in reducing the number of outliers [4].

There are two main CAS systems for TKA: image-free and image-based. The image-free CAS system has been widely accepted and used for TKA. Its advantages are that there is no need for preoperative computed tomography (CT) or for the extra time required for preoperative planning. Regarding the latter, although with CT image-based CAS for TKA it is necessary to measure numerous landmarks to accomplish registration of the targeted bone, errors in data collection of landmark points intraoperatively with image-free CAS may lead to registration error [5, 6].

To achieve proper implant positioning and to reconstruct an appropriate mechanical lower extremity axis, the image-free CAS system is an excellent tool for TKA. To

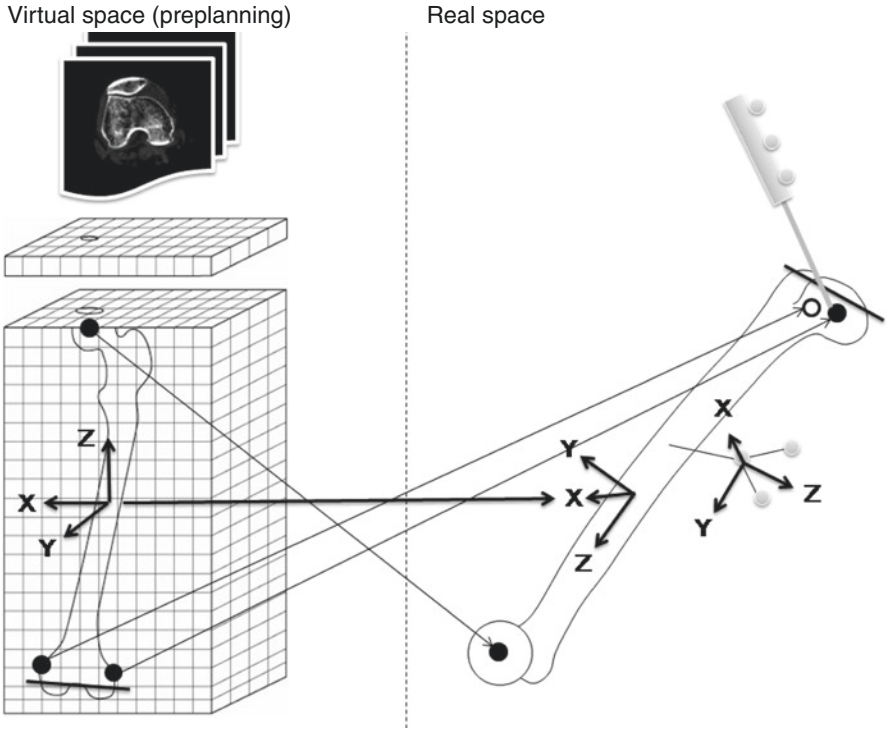

Fig. 2.1 Basic principles of registration with the computed tomography-based (with images) navigation system

Fig. 2.2 CT-based navigation system for total knee arthroplasty (TKA) developed by Teijin Nakashima Ltd. in collaboration with Osaka University

improve patients' satisfaction and provide a higher-functioning reconstructed knee, however, the CT-based navigation system is potentially more useful for TKA.

The main role of the CT-based navigation system for TKA is to guide the level and inclinations of osteotomy planes for both the femur and tibia to the preoperatively three-dimensionally (3D) planned osteotomy planes based on the CT images. The position of the cutting block relative to the femur or tibia is computed in the operating room, and its position relative to preoperative planning in the virtual space is measured and visualized. The surgeons can then achieve an accurate osteotomy in accordance with preoperative planning (Fig. 2.1).

The aim of this chapter is to introduce the CT-based navigation system for TKA (Teijin Nakashima Medical Co., Ltd., Okayama, Japan, developed in collaboration with Osaka University) (Fig. 2.2) to help readers understand the advantages of this guidance system.

2.2 Preoperative Planning

Preoperatively, we obtained CT images from the hip to the distal end of the ankle. To ensure navigational accuracy within 1 mm and 1° [7], the minimum slice thickness and pitch of the hip, knee, and ankle joint CT images should be ≤1.25 mm. To minimize radiation exposure at the femoral and tibial diaphyses, automatic exposure control should be applied during CT scanning. CT images are stored in Digital Imaging and Communication in Medicine format and transferred to a computer for preoperative planning. One of the recent prominent improvements in CT-based navigation for TKA is the accuracy of the automatic reconstruction of surface bone models for surface registration, which was the result of a new segmentation system that had been developed (Fig. 2.3a). With this technical advancement, it has been easy to minimize the registration error between 3D reconstructed bone models and actual bones during the procedure (Fig. 2.3b).

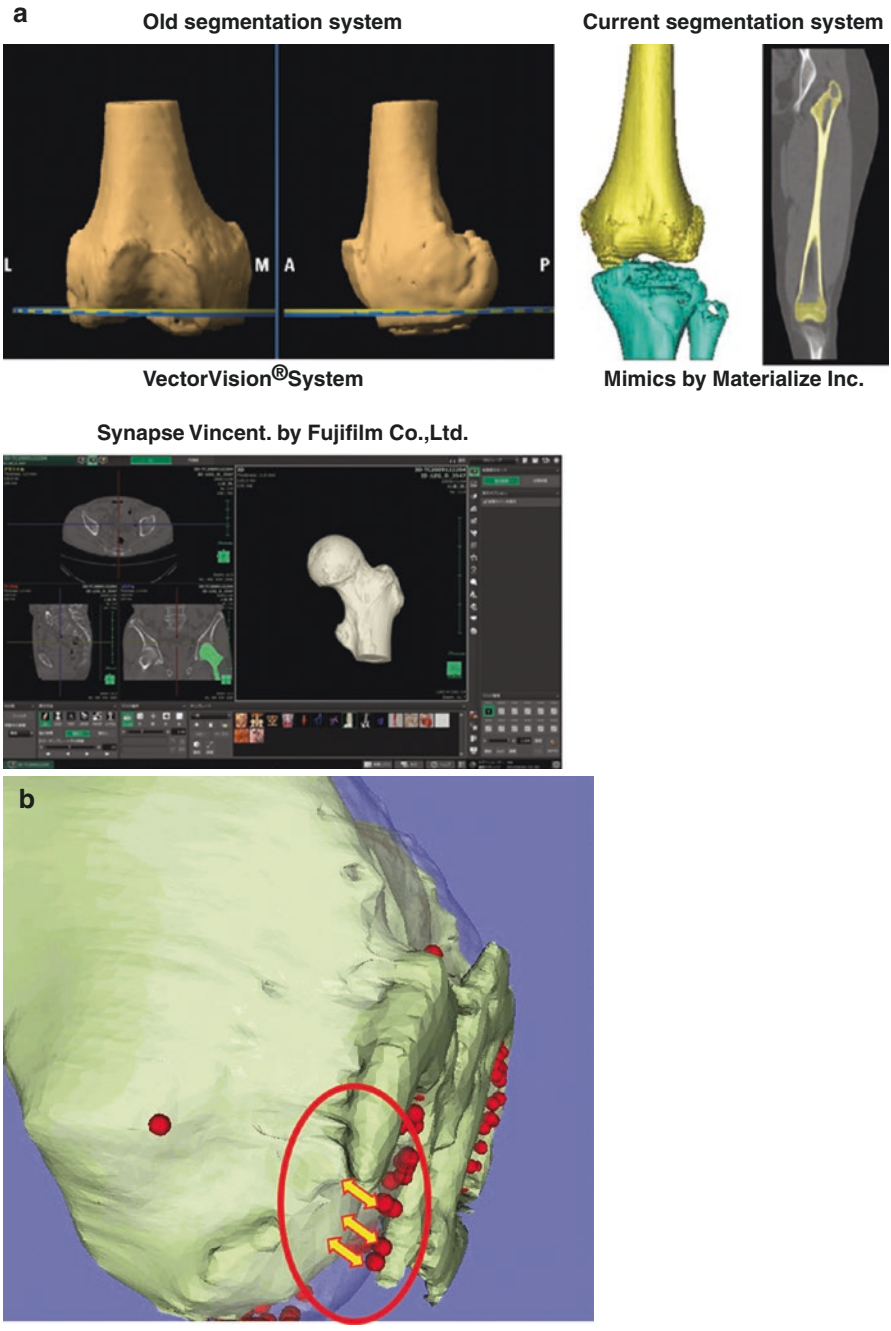

Fig. 2.3 Reconstruction of target bone according to CT data. (**a**) The bearing surface of the bone joint can be reconstructed precisely with the segmentation process developed during the last decade. (**b**) Inaccurate three-dimensional (3D) bone model reconstructed using the old segmentation system, which resulted in a wide registration error during the surgery

The femoral axis is defined as the line through the center of the femoral head and the midpoint of the medial and lateral epicondyles. The tibial axis is defined as the line through the midpoint of the tibial tuberosity, the posterior cruciate ligament (PCL) insertion, and the midpoint of the medial and lateral malleoli. The level and inclinations of the osteotomy planes for both femur and tibia are planned based on these established axes. These landmarks are just defaults, however, and the surgeon can change the landmarks according to bone morphology, surgical technique, and implant design. The implant size is predicted by superimposing the computer-aided design models of the implants on the CT-based 3D digital model of the knee joint. Preoperative planning using the FINE TKA system (Teijin Nakashima Medical Co., Ltd., Okayama, Japan) is outlined in Fig. 2.4.

2.3 Registration and Confirmation of Accuracy

Before registration, the data should be checked to determine if the installed patient data are correct. At the beginning of the operation, a dynamic reference base with three non-collinearly distributed, light-reflecting markers is rigidly fixed to the distal femur

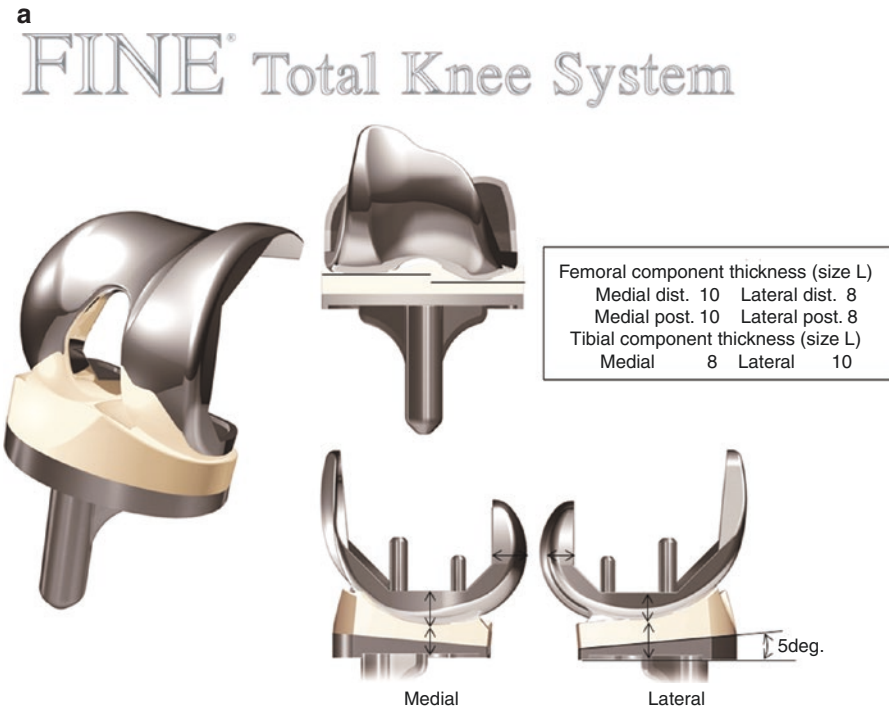

Fig. 2.4 Preoperative planning using the FINE TKA system. (**a**) Features of the FINE TKA system. (**b**) Default reference axis and landmarks for the femoral bone cut. (**c**) 3D template for the femur. (**d**) Default reference axis and landmarks for the tibial bone cut. (**e**) 3D template for the tibia

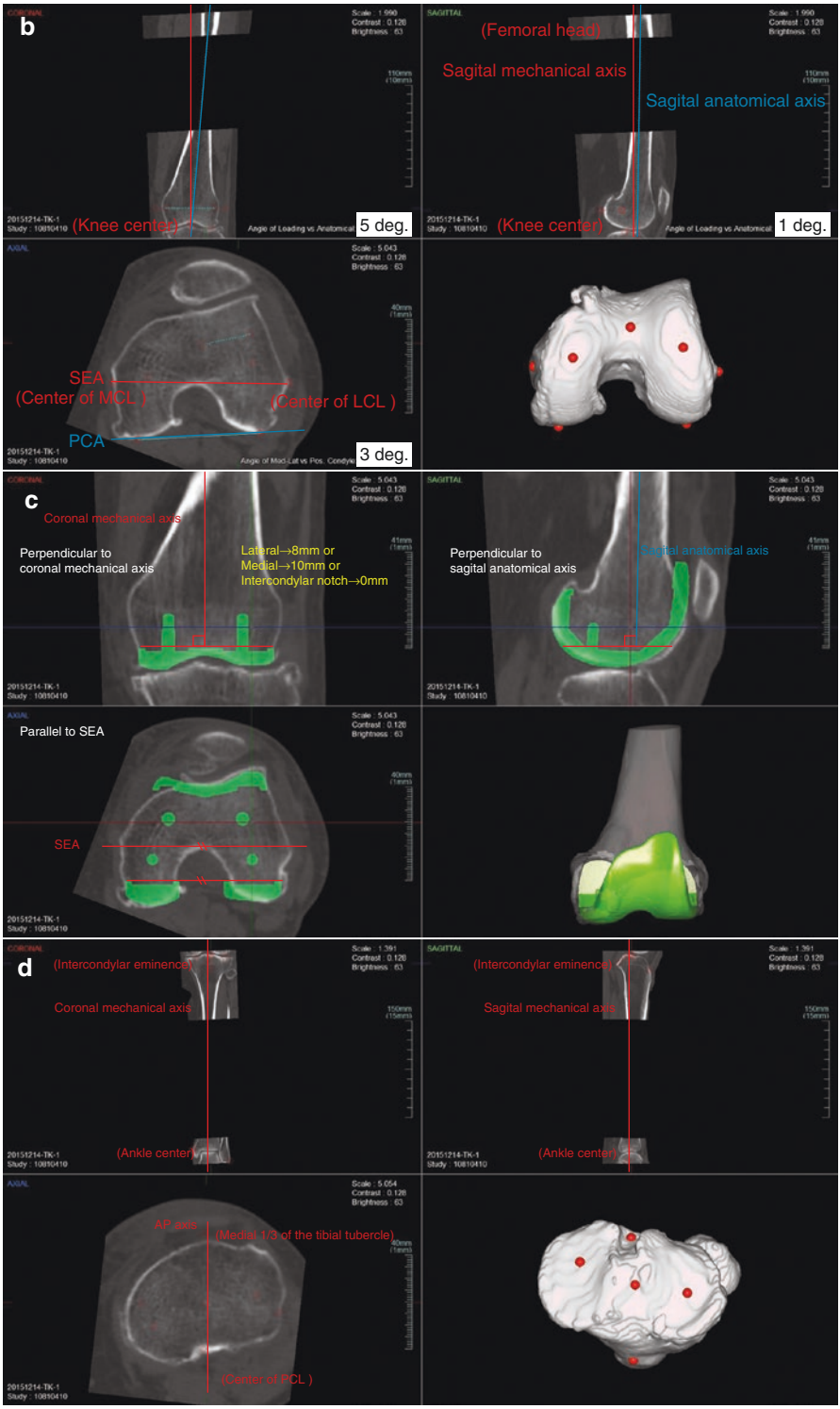

Fig. 2.4 (continued)

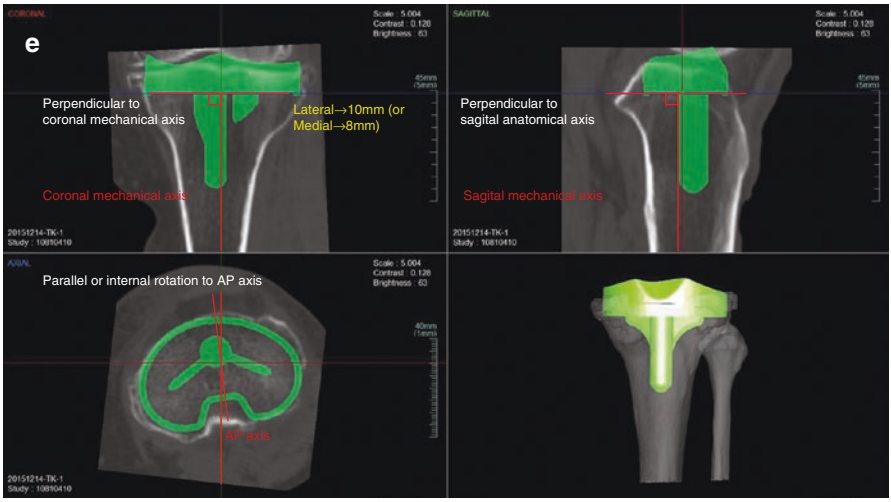

Fig. 2.4 (continued)

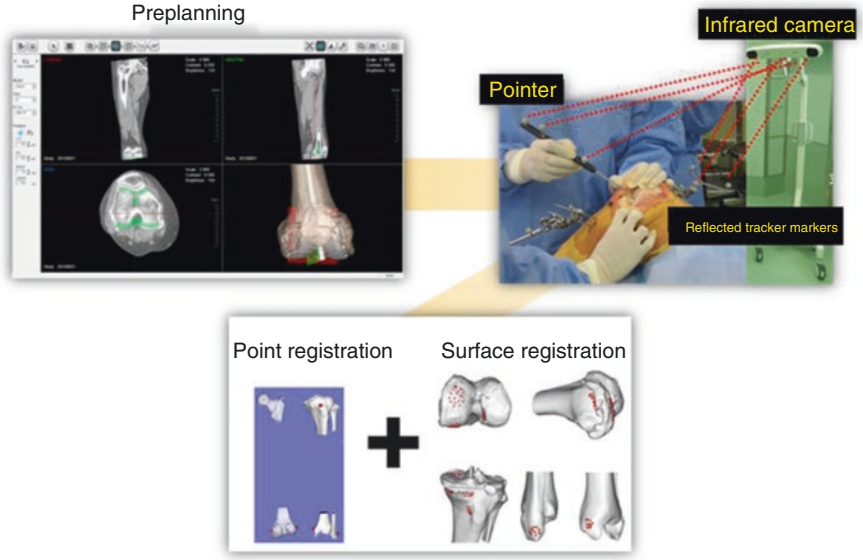

Fig. 2.5 Registration process. Surface registration is performed after paired-point registration

and proximal tibia to track the position of the bones. The bones with these dynamic reference bases are recognized using a charged coupled device camera system at any position of the knee joint. Registration is performed to match the patient's anatomy (real space) to the computer model (virtual space). Paired-point registration is initially performed with the center of the femoral head (rotational center of the femoral movement), medial and lateral epicondyles of the femur and the tibial tubercle, and medial and lateral malleoli of the tibia (Fig. 2.5). This surface registration is then followed by digitizing the medial aspects of the exposed femur and tibia to accommodate minimally invasive TKA and unicompartmental knee arthroplasty (Fig. 2.6).

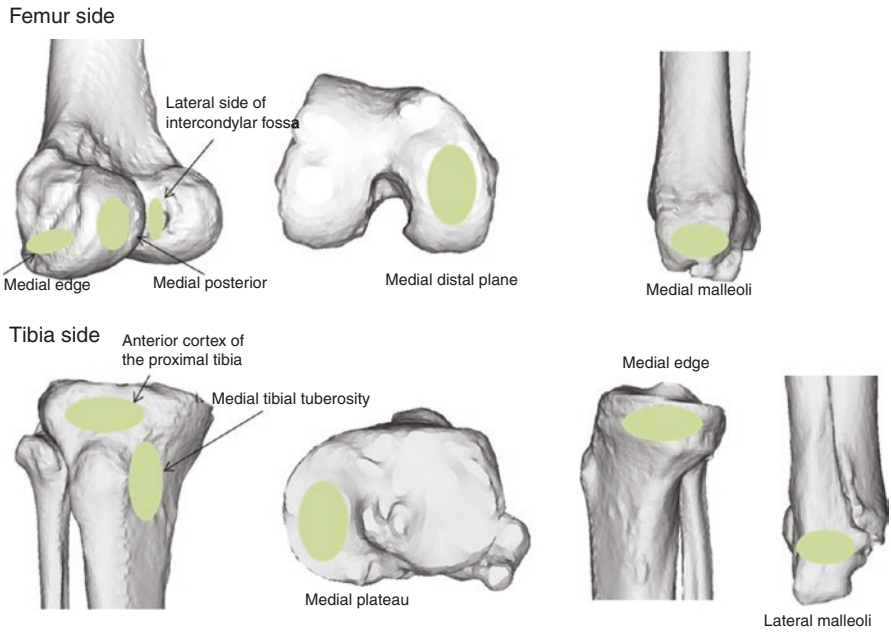

Fig. 2.6 Registration areas. With our system, the registration is performed by measuring only the medial side for easier application during minimally invasive TKA and unicompartmental knee arthroplasty

After registration, the root mean square of registration residue is calculated, which is a reliable parameter for judging the accuracy of the registration. It should be $\leq$1 mm. Nonetheless, it is important to verify the accuracy by touching several bone surfaces in both the medial and lateral compartments with a pointer tool. If the pointer tip is just on a bone surface without articular cartilage, or separated from a bone surface with articular cartilage by 1–2 mm, the registration accuracy is considered acceptable.

2.4 Intraoperative Measurements: Bone Preparation

The varus/valgus alignment, soft tissue balance, and kinematics during all ranges of movement are evaluated and recorded before releasing the soft tissue and cutting the bone. In cases of PCL-preserving and bi-cruciate-preserving TKAs, the origins and insertions of the ligaments are identified to measure any changes in the length of the anterior cruciate ligament or the PCL during all ranges of movement before and after implantation.

Soft tissue balance can be adjusted by removing osteophytes or releasing soft tissue. The position of the cutting blocks for the distal femur and proximal tibia is then guided by real-time visualization using the navigation system. After the distal cut of the femur, the rotation of the anteroposterior femoral cut block is guided according to the posterior condylar line or the epicondylar axis.

After preparing the bone and adjusting the soft tissue balance, the knee alignment (Fig. 2.7), kinematics (Fig. 2.8), and changes in the lengths of the cruciate ligaments, changes in length (preserved ligaments case) (Fig. 2.9) are corrected during all ranges of movement with trial implants. At this point, the surgeon can determine the thickness of the tibial implant needed.

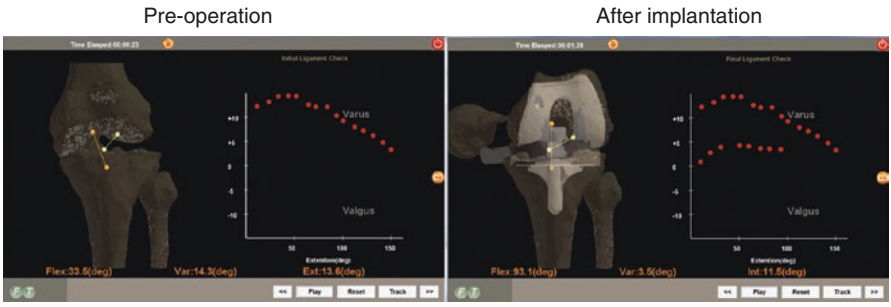

Fig. 2.7 Analysis of a varus/valgus deformity during all ranges of knee motion before and after implantation

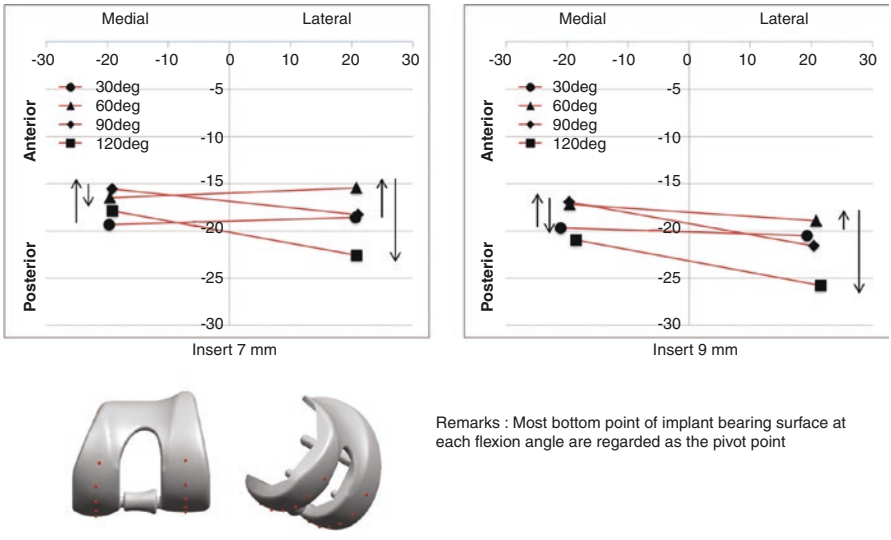

Fig. 2.8 Analysis of kinematics during all ranges of knee motion. Using this system, useful information can be provided in terms of the thickness of the implant for its effect on knee kinematics

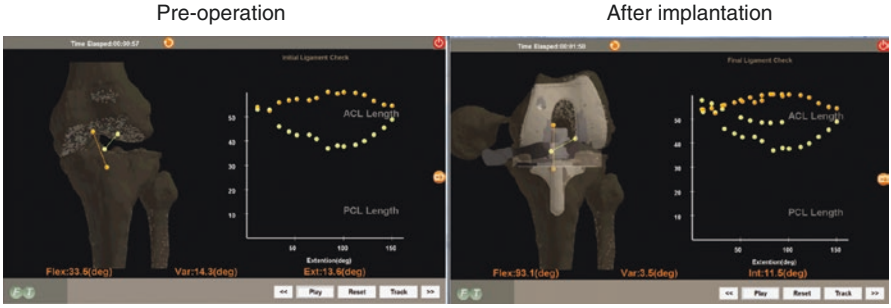

Fig. 2.9 Analysis of changes in the lengths of the anterior (ACL) and posterior (PCL) cruciate ligaments during all ranges of knee motion when performing ACL- and PCL-preserving TKA

2.5 Postoperative Evaluation of Navigated Knee Kinematics

It is well accepted that both CT-based and image-free navigation systems have improved leg axes and component alignments by decreasing the number of outliers requiring TKA even though there was no significant difference in postoperative functional scores between the navigated and traditional TKAs. The lower patients' satisfaction rate after TKA than that after THA, however, remains an issue, and we believe that achieving proper medial pivot pattern kinematics after TKA is the key to addressing this issue. One of the advantages of CT-based navigation is its greater ability than imageless systems to evaluate knee kinematics during TKA. With our CT-based system, we could measure the nearest medial and lateral points between the femoral and tibial components after implantation. Using the same coordinate system, the kinematics of the reconstructed knee could be evaluated in terms of rotation, varus/valgus instability, and anteroposterior translations between the femur and tibia. We have preliminarily compared the intraoperative and postoperative in vivo kinematics after TKA and investigated whether intraoperative knee kinematics could predict postoperative in vivo knee kinematics [8]. Rotation and anteroposterior translation of the posterior nearest points during all ranges of passive knee movement revealed no significant difference between the intraoperative and postoperative kinematics (Figs. 2.10 and 2.11). There was also less varus/valgus instability according to the postoperative kinematics compared with the intraoperative kinematics. These results suggest that the intraoperative knee kinematics evaluated by CT-based navigation can predict postoperative in vivo knee kinematics following TKA.

2.6 Summary

The CT-based navigation system allows kinematic measurements of the knee during every step of the TKA procedure, which is key to improving patients' satisfaction postoperatively. To evaluate and compare the preoperative, intraoperative, and postoperative knee kinematics, the coordinates on the femur and tibia must be matched. Only

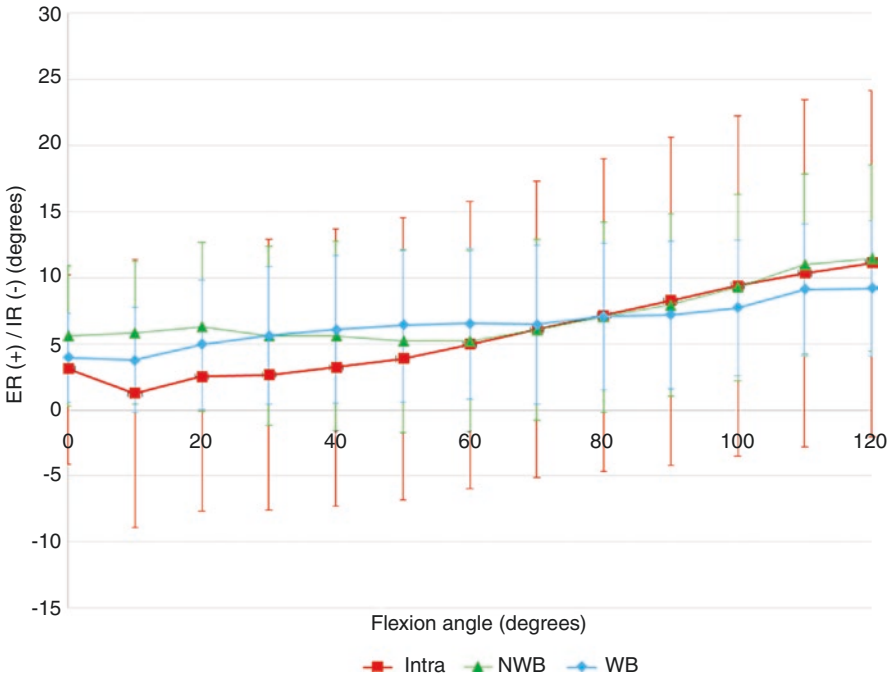

Fig. 2.10 Comparison of external rotation of the femoral component relative to the tibial component. There were no significant differences between intraoperative and postoperative non-weight-bearing deep knee bending and squatting

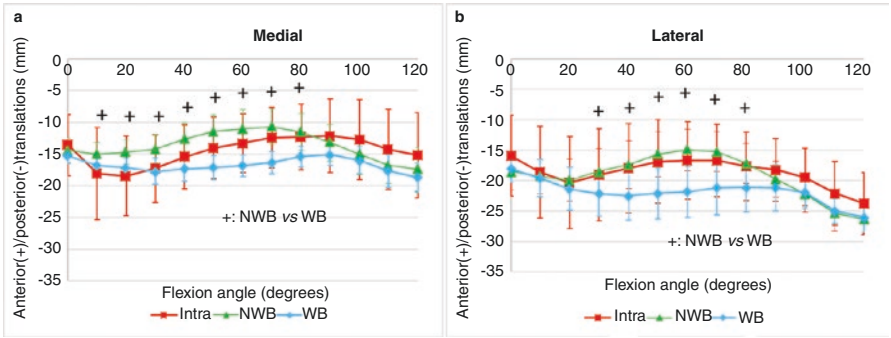

Fig. 2.11 Comparison of medial (**a**) and lateral (**b**) anteroposterior translation during deep knee bending. There was no significant difference between intraoperative and postoperative non-weight-bearing deep knee bending. The only significant difference seen was between postoperative non-weight-bearing and weight-bearing conditions

CT-based navigation can provide these coordinates. Although extra time for preoperative planning is a major disadvantage of CT-based navigation, the software that allows automatic accurate segmentation has been improved, with a reduction in the time required. TKA has become a standard procedure among orthopedic surgeons, although

it still requires that attention be paid to every aspect of the preoperative planning, including bone morphology, accurate bone cutting, and soft tissue balancing. Patients' expectations for postoperative function are currently quite high, including their return to sports activities, squatting, and kneeling after TKA. CT-based navigation for TKA can play a role in optimizing the procedure and satisfying even highly demanding patients.

References

1. Sharkey PF, Hozack WJ, Rothman RH, Shastri S, Jacoby SM. Insall Award paper. Why are total knee arthroplasties failing today? Clin Orthop Relat Res. 2002;(404):7–13.
2. Bourne RB, Chesworth B, Davis A, Mahomed N, Charron K. Comparing patient outcomes after THA and TKA: is there a difference? Clin Orthop Relat Res. 2010;468(2):542–6.
3. Scott CE, Howie CR, MacDonald D, Biant LC. Predicting dissatisfaction following total knee replacement: a prospective study of 1217 patients. J Bone Joint Surg Br. 2010;92(9):1253–8.
4. Bae DK, Song SJ. Computer assisted navigation in knee arthroplasty. Clin Orthop Surg. 2011;3(4):259–67.
5. Jenny JY, Boeri C. Low reproducibility of the intra-operative measurement of the transepicondylar axis during total knee replacement. Acta Orthop Scand. 2004;75(1):74–7.
6. Matziolis G, Krocker D, Weiss U, Tohtz S, Perka C. A prospective, randomized study of computer-assisted and conventional total knee arthroplasty. Three-dimensional evaluation of implant alignment and rotation. J Bone Joint Surg Am. 2007;89(2):236–43.
7. Yokoyama Y, Abe N, Fujiwara K, Suzuki M, Nakajima Y, Sugita N, Mitsuishi M, Nakashima Y, Ozaki T. A new navigation system for minimally invasive total knee arthroplasty. Acta Med Okayama. 2013;67(6):351–8.
8. Fujito T, Tomita T, Futai K, Yamazaki T, Kono K, Yoshikawa H, Sugamoto K. In vivo kinematic analysis of total knee arthroplasty: comparison between intra- and post-operative measurements. Orthop Proc. 2017;29:2393–6.

Chapter 3
Robotic Total Knee Arthroplasty

Eun-Kyoo Song and Jong-Keun Seon

Abstract Various robotic systems have been developed to improve the accuracy of implant selection, its positioning and alignment, and bone resection. These systems are currently used worldwide for total knee arthroplasty. Many studies have clearly demonstrated that robotic systems can accurately and reliably control variables such as lower leg alignment, joint-line maintenance, soft tissue balance, and component positioning. In addition, they are more accurate and reliable than those used for conventional total knee arthroplasty. To date, however, few studies have assessed the survivorship and functional outcomes of robot-assisted surgery, and we found no sufficiently powered studies that compared these two parameters between robot-assisted and conventional knee arthroplasty. Although larger survivorship studies are necessary for these comparisons, robotics will continue to progress toward becoming a valuable tool for decreasing the revision rate and improving functional outcomes.

Keywords Total knee arthroplasty · Robotic-assisted · Implant position · Mechanical axis · Outcomes

3.1 Introduction

Total knee arthroplasty (TKA) is a reliable treatment for alleviating pain and achieving functional recovery of the knee joint in end-stage arthritic knees, providing satisfactory outcomes in more than 90% of patients [1–3]. Mechanical alignment, implant position, and soft tissue balance play important roles in treatment success and implant longevity [4–6]. Despite carefully performed procedures and improved instruments, however, various studies have described significant axial or rotational malalignment and unsatisfactory implant positioning [7, 8]. None of the contemporary improvements in implant design, instrumentation, or surgical techniques have resolved these problems completely.

E.-K. Song (✉) • J.-K. Seon
Chonnam National University Hwasun Hospital, Hwasun, South Korea
e-mail: eksong@chonnam.ac.kr

N. Sugano (ed.), *Computer Assisted Orthopaedic Surgery for Hip and Knee*,
https://doi.org/10.1007/978-981-10-5245-3_3

Robotic surgery has been increasingly chosen as an option to address these problems. The use of robots has proved that human errors made when placing and moving surgical tools could be reduced. Robotic systems are referred to as "active" systems that aid with preoperative imaging, planning, registration, and cutting. Orthopedic surgeons first performed total hip arthroplasty (THA) using a robotic system (ROBODOC) in 1992 [9] (Fig. 3.1a), and the first robot-assisted TKA was performed with the computer-assisted surgical planning and robotics (CASPAR) system in 2000 [10] (Fig. 3.1b). Thus, robot-assisted orthopedic surgery has been available clinically in some form for more than two decades. It is claimed that it has improved the results of total joint arthroplasty by enhancing the surgeon's ability to reproduce the correct alignment and therefore restore normal kinematics [11].

Robotic systems serve as an offline, computerized tool for planning a surgical procedure prior to surgery [12]. Some robotic platforms have been introduced to increase the accuracy and precision of component positioning during total joint arthroplasty. Improved alignment might lead to longer implant survival and less need for revision surgery.

3.2 Contemporary Systems

Many robotic systems have been developed and prototyped, but only a handful have been used successfully in a clinical setting. More recent and commonly used systems include the following: ROBODOC/TSolution One Surgical System (Curexo Technology, Fremont, CA), Navio PFS (Blue Belt Technologies, Plymouth, MN), iBlock robotic cutting guide (OMNIlife Science, East Taunton, MA), and RIO Robotic Arm Interactive Orthopedic System (Mako Surgical Corporation, Fort Lauderdale, FL) (Table 3.1).

3.2.1 ROBODOC/TSolution One Surgical System

The ROBODOC/TSolution One Surgical System, initially called the ROBODOC system (Curexo Technology, Fremont, CA), was one of the first to be used for joint replacement (Fig. 3.1b). The ROBODOC is an image-based, active robotic milling system [11]. Once the system is placed and fixed to the patient, dynamic reference markers (e.g., for navigation) are not needed to track the patient. The robotic arm controls the milling device within a rigid frame according to the preoperative planning based on computed tomography (CT) images after registration. A bone motion sensor is placed on the target bone to detect unacceptable movement of the bone within the frame. Initial clinical trials for use during THA

Fig. 3.1 Robotics in arthroplasty. (**a**) ROBODOC. (**b**) CASPAR system. (**c**) MAKO

Table 3.1 Contemporary robotic platforms

Name	Company	FDA approval	Applications	Control	Resection type	Planning image
ROBODOC	Curexo Technology, Fremont, CA	2008	TKA, THA (femur)	Autonomous	Mill	CT scan
Mako	Stryker, Fort Lauderdale, FL	2006	UKA, THA, TKA	Semiautonomous haptic	Burr, reamer, saw	CT scan
Navio PFS	Blue Belt Technology, Plymouth, MN	2012	UKA	Semiautonomous	Burr	None
iBlock	OMNIlife Science, East Taunton, MA	2010	TKA (femur)	Autonomous	Manual saw	None

TKA total knee arthroplasty, *THA* total hip arthroplasty, *UKA* unicondylar knee arthroplasty, *CT* computed tomography

began in 1994 and were approved by the US Food and Drug Administration (FDA) in 2008 [13, 14].

Preoperatively, the surgeon starts planning the surgery on the ORTHODOC workstation (part of the ROBODOC system) based on CT images. Planning includes outlining the segmentation of the femur and tibia, defining the femoral and tibia coordinates to evaluate implant alignment, and determining the implant size and positioning before engaging and operating the robot intraoperatively. Its clinical success and usefulness have been reported in a series of clinical trials. The advantages of using the ROBODOC system include improved alignment and positioning accuracy as well as its ability to track where the robot is milling. It also achieves a consistent radiological outcome. Its disadvantage is that the planning, registration, and milling take a longer time than when performed with the other contemporary robotic systems [11].

3.2.2 Navio PFS

Navio PFS—a handheld, image-free, open-platform instrument that provides freehand sculpting for unicondylar and patellofemoral knee arthroplasty—was approved for clinical use by the FDA in 2012 [15]. This lightweight robotic tool combines image-free intraoperative registration, planning, and navigation for bone preparation. The Navio system has certain benefits. It is imageless, thereby reducing the risk of radiation exposure and the cost of preoperative imaging. The safety of the burr retraction, however, is limited because of its sensitivity and retraction speed. Thus, bone outside the planned volume could be removed inadvertently before burr retraction if the burr is moved too quickly.

3.2.3 iBlock

The iBlock robotic cutting guide was previously known as Praxiteles and gained FDA approval in 2010 [16]. It is a motorized, bone-mounted cutting guide that positions the saw guide for all femoral resections according to the surgeon's plan, allowing the surgeon to complete the resection with a standard oscillating saw. Intraoperatively, all anatomical data are acquired with digitization. The system allows planning the implant's size and positioning. It allows visualization of the planned bone cuts. The iBlock system does have some limitations. It provides no tactile feedback, is available only for TKA applications, has a closed platform, and allows only limited kinematic assessment after implantation for evaluating the implant's behavior.

3.2.4 Mako

The RIO Robotic Arm Interactive Orthopedic System is a tactile system used in such clinical procedures as unicondylar knee arthroplasty (UKA), THA, and TKA (Fig. 3.1c). Preoperative CT images are used in this system to determine the component's size and positioning and the amount of bone resection required. This information is then confirmed—with accommodations made as necessary—intraoperatively based on the patient's specific kinematics prior to the surgical procedure. During the operation, the robotic system provides tactile feedback to prevent excessive bone resection [17]. Currently, the RIO system is ordinarily used for robot-assisted UKA and THA. Recently, the FDA approved it for TKA.

3.3 Surgical Technique

Robot-assisted TKA consists of four steps: CT scanning, preoperative planning, registration, and surgery. The surgical process described herein is based on the ROBODOC system.

3.3.1 Preoperative Planning

CT images of the femoral head, distal femur, proximal tibia, and ankle are obtained preoperatively and transferred to the ORTHODOC workstation. The ORTHODOC combines the CT data and displays three-dimensional cross sections of bone on a high-resolution screen. The first planning step is to identify the centers of the hip, knee, and ankle for determining the femoral and tibial mechanical axes. Virtual implantation is carried out by fitting computer-assisted design files of implants to

the bone. Then, the size, position, and alignment of the implant is fine-tuned for the corresponding bone (Fig. 3.2a). After verifying the correct position during virtual surgery, the data for the robotic milling path are created and uploaded to the control unit of the surgical robot.

3.3.2 Registration

A standard incision, with medial parapatellar arthrotomy and lateral eversion of the patella, is performed. The patient's leg (placed in a leg holder) is flexed and rigidly connected to the robot by two transverse Steinmann pins inserted percutaneously through the proximal tibia and distal femur (Fig. 3.2b). These two pins are connected to a frame, which is linked to the robot. Surface-based registration of the femur and tibia is then performed by digitizing a predetermined area of bone surface with a ball-tipped probe, and the accuracy of registration is verified by measuring the discrepancy between the probe tip touching several bone surface points and the bone surface models reconstructed from the CT data (Fig. 3.2c, d).

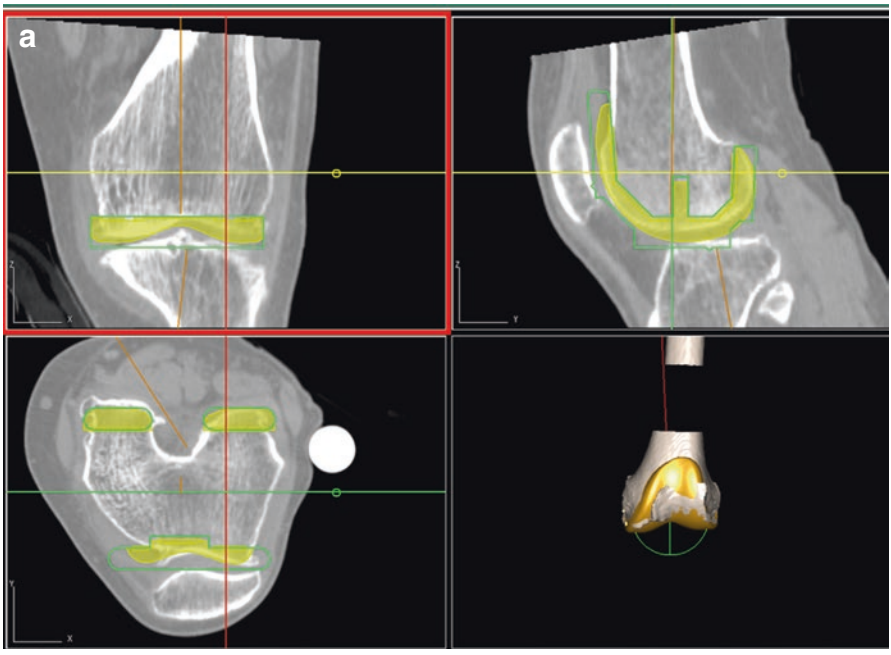

Fig. 3.2 Surgical process of ROBODOC system. (**a**) Planning, (**b**) arthrotomy and fixation, (**c**) registration, (**d**) verification, (**e**) milling, (**f**) cutting surface, (**g**) implantation

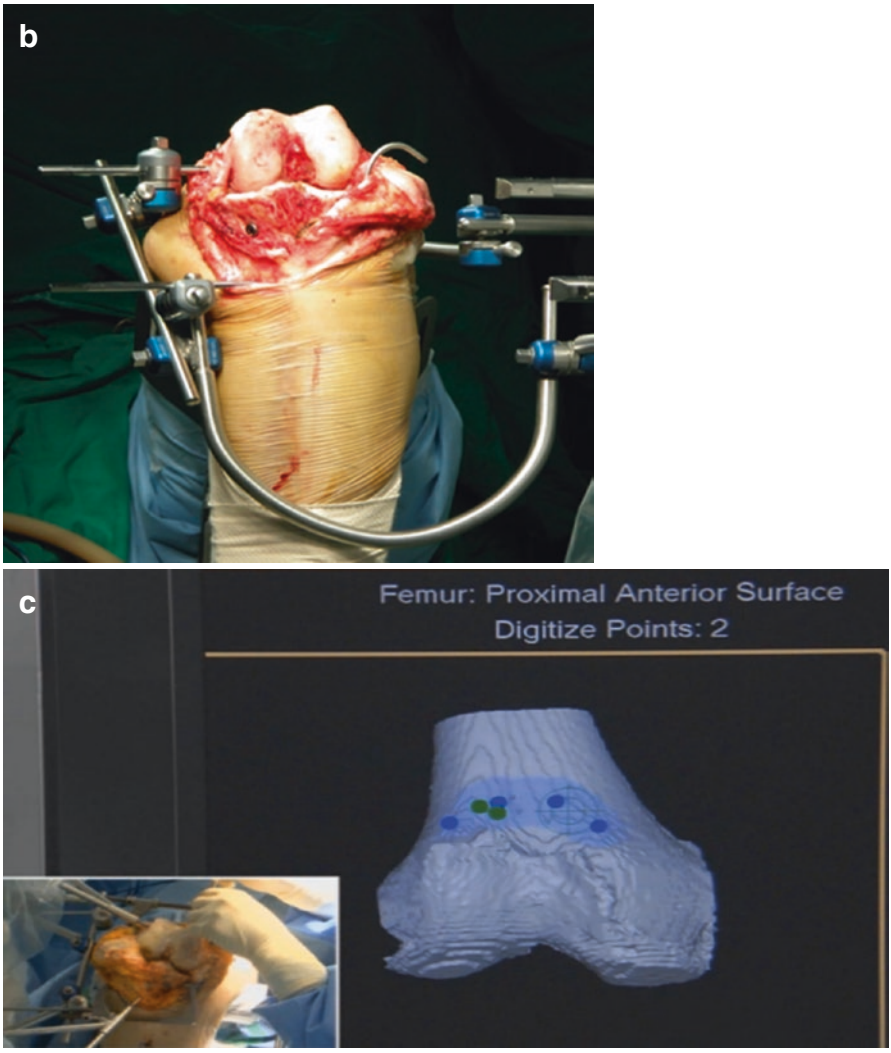

Fig. 3.2 (continued)

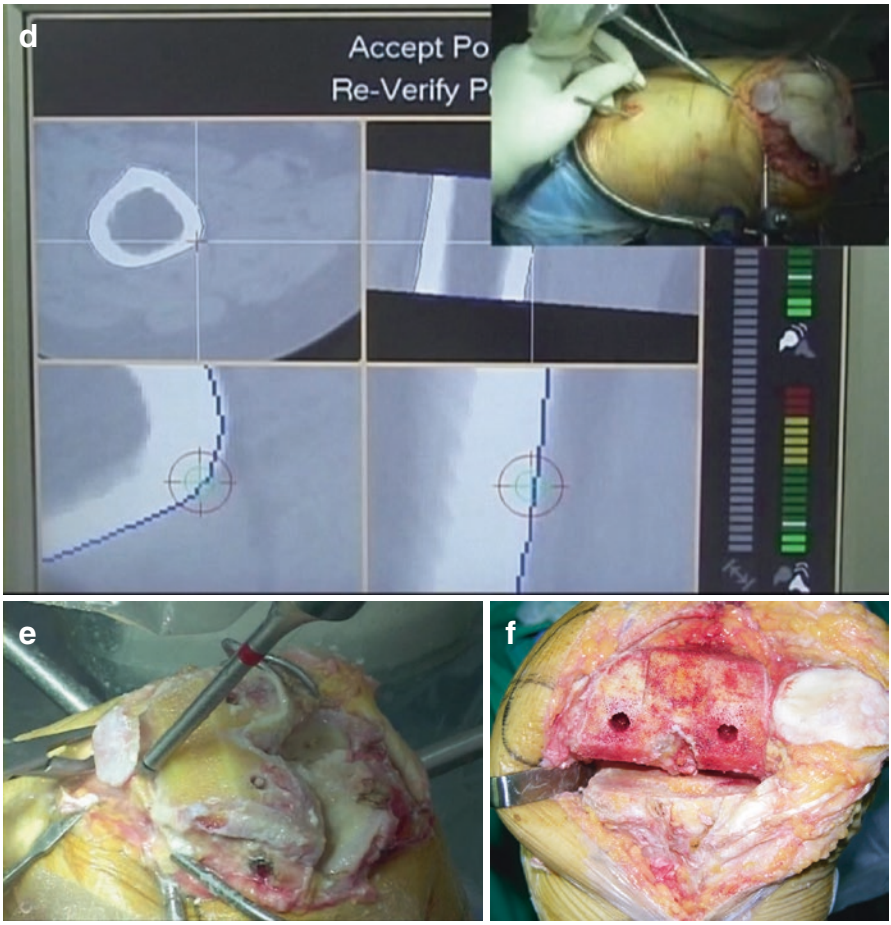

Fig. 3.2 (continued)

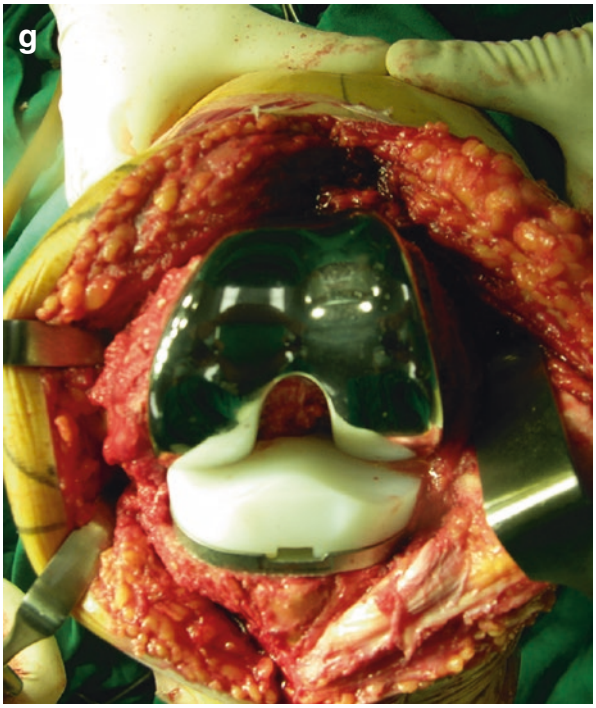

Fig. 3.2 (continued)

3.3.3 Cutting, Soft Tissue Balancing, and Implantation

After successful registration, the ROBODOC carries out intraoperative precise bone cutting for the implant according to the preoperative plan. This step is accomplished using a milling cutter, with constant normal saline irrigation for cooling and debris removal (Fig. 3.2e). After the bone cuts, the ROBODOC is disconnected and removed (Fig. 3.2f).

Soft tissue balancing is performed in a stepwise manner by releasing only what is required to achieve balance. The order of release for medial soft tissues is as follows: deep medial collateral ligament, posterior medial capsule, and superficial medial collateral ligament. Femoral and tibial implants are manually fixed with cement (Fig. 3.2g).

3.4 Current Outcomes

3.4.1 Radiologic Results

Although robot-assisted TKA is accurate, it is necessary to compare these systems with the gold standard, conventional TKA. Published studies in which robot-assisted systems were used for TKA are summarized in Table 3.2.

Siebert et al. [10] assessed mechanical axis accuracy and mechanical outliers following robot-assisted TKA surgery using the CASPAR system versus conventional TKA. They reported that the difference between preoperative and postoperative mechanical alignment was 0.8° for robot-assisted TKA and 2.6° for conventional TKA. Moreover, they showed that one patient (1.4%) in the robot-assisted group and 18 patients in the conventional group (35.0%) had mechanical alignment of >3° from the neutral mechanical axis.

Liow et al. [18] performed a prospective randomized study and reported that there were no outliers >3° from the neutral mechanical axis in the robot-assisted group, whereas 19.4% of the patients in the conventional group had mechanical axis outliers. They also assessed the joint-line outliers in both groups and found that 3.2% of patients had joint-line outliers of >5 mm in the robot-assisted group compared with 20.6% in the conventional group. Kim et al. [19] assessed the implant accuracy achieved with robot-assisted surgery using the ROBODOC system versus

Table 3.2 Overview of studies that compared clinical and radiologic outcomes between robotic-assisted and conventional TKA

Author	Journal (year)	Mean F/U (years)	Number of patients		Clinical result	Mechanical axis[a]		
			Robotic	Conventional		Robotic	Conventional	*P*
Liow et al. [18]	JOA (2014)	0.5	31	29	No significant difference	1.3 ± 0.9	1.8 ± 0.2	0.095
Song et al. [12]	KSSTA (2011)	2.0	30	30		0.2 ± 1.6	1.2 ± 2.1	0.035
Kim et al. [19]	Orthopedics (2012)	3.9	32	30		0.2 ± 1.1	−0.5 ± 2.8	0.611
Song et al. [20]	CORR (2013)	5.5	50	50		0.5 ± 1.4	1.2 ± 2.9	0.06
Siebert et al. [10]	Knee (2002)	1	70	52		0.8 ± 1.0	2.6 ± 2.2	0.01

N.S, nonspecific

[a]±, "+" means varus alignment, and "–" means valgus alignment

conventional surgery. They found that robot-assisted TKA had higher implant accuracy and fewer outliers than were seen following the conventional technique.

Finally, Song et al. [12, 20] performed two randomized clinical trials in which they compared mechanical axis alignment, component positioning, soft tissue balancing, and patient preference between conventional TKA surgery and robot-assisted surgery using the ROBODOC system. In the first study [12], they simultaneously performed robot-assisted surgery on one leg and conventional TKA surgery on the other leg. They found that the robot-assisted surgery resulted in fewer outliers regarding the mechanical axis and component positioning. They also found that flexion–extension balance was achieved in 92% of patients treated with robot-assisted TKA surgery but in only 77% of patients treated with conventional TKA surgery. In the other study [20], the authors found that more patients treated with robot-assisted surgery had a <2 mm flexion–extension gap and more satisfactory posterior cruciate ligament tension when compared with those who underwent conventional surgery (Fig. 3.3).

3.4.2 Clinical Results and Survivorship

Despite the better radiological outcomes, no significant differences were detected in functional outcomes between the robot-assisted and conventional techniques. The studies comparing functional outcomes following robot-assisted TKA and conventional TKA, however, were frequently underpowered because of their small sample sizes [12]. Furthermore, we found no studies that compared the survivorship of robot-assisted TKA with that of conventional TKA. A few studies, however, reported that robot-assisted TKA has lower rates of mechanical complications and revisions than conventional TKA. Hence, the superior mechanical alignment may result in better long-term outcomes and increased survival rate of implant.

3.5 Limitations of Robotics

Robotic surgery does have some limitations. First, the operative time might be longer, especially during the learning curve, than that for conventional surgery. Second, in addition to the cost associated with the robotic apparatus in the operating room, significant education is required for surgeons and staff to optimize the safety and effectiveness of the surgery. Third, a robotic system cuts according to the bone-cutting path established during the preoperative planning—regardless of what it may actually be cutting. Therefore, the surgeon must be alert to retracting the soft tissues (e.g., patellar tendon, capsule) in the planned path to avoid unnecessary damage.

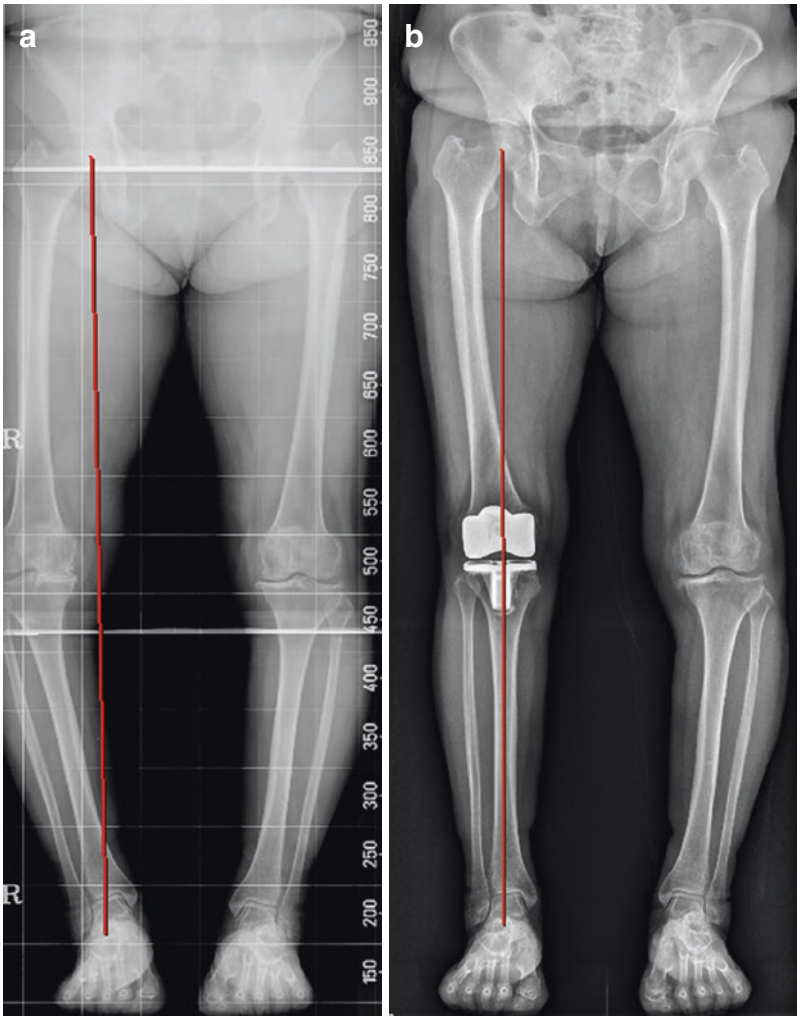

Fig. 3.3 Preoperative (**a**) and 3-year postoperative (**b**) plain radiographs of a 72-year-old woman who underwent total knee arthroplasty with ROBODOC system, showing postoperative neutral alignment

3.6 Future of Robotics

Robot-assisted TKA already safely and effectively enhances the accuracy of the implant's position and decreases the number of outliers of knee arthroplasty by avoiding major adverse events. Future innovations will continue to improve the planning, registration, and cutting methods during robot-assisted arthroplasty. Such developments will be implemented in a way that simplifies the process and minimizes the learning curve. Preoperative planning will be used to create the desired

anatomical and kinematic framework. Whereas earlier implant designs were limited by the preparation possible with traditional jigs/instruments and traditional visualization abilities, the future of implant development appears very different. The combination of robotic technology with navigation systems for real-time monitoring of soft tissue balance achieves the principles of knee arthroplasty, such as accurate bone cutting and precise gap balancing.

3.7 Conclusion

Robotic assistance can clearly improve the accuracy of implant positioning and mechanical alignment during TKA. These benefits may lead to a decrease in complications such as loosening and instability, thereby improving survivorship and functional outcomes. Although few studies have yet identified improved survivorship or better functional outcomes of robot-assisted knee arthroplasty over conventional knee arthroplasty, future well-designed long-term comparative studies will prove the improved survivorship and functional outcomes of robot-assisted knee arthroplasty. Innovation to simplify the process and minimize the learning curve will lead to robotic assistance becoming an invaluable adjunct to the surgeon. The development of this technology will certainly provide better outcomes than we can presently achieve.

References

1. Laskin RS. The Genesis total knee prosthesis: a 10-year followup study. Clin Orthop Relat Res. 2001;388:95–102.
2. Rodriguez JA, Bhende H, Ranawat CS. Total condylar knee replacement: a 20-year followup study. Clin Orthop Relat Res. 2001;388:10–7.
3. Scott WN, Rubinstein M, Scuderi G. Results after knee replacement with a posterior cruciate-substituting prosthesis. J Bone Joint Surg Am. 1988;70:1163–73.
4. Griffin FM, Insall JN, Scuderi GR. Accuracy of soft tissue balancing in total knee arthroplasty. J Arthroplast. 2000;15:970–3.
5. Ritter MA, Faris PM, Keating EM, et al. Postoperative alignment of total knee replacement. Its effect on survival. Clin Orthop Relat Res. 1994;299:153–6.
6. Takahashi T, Wada Y, Yamamoto H. Soft-tissue balancing with pressure distribution during total knee arthroplasty. J Bone Joint Surg Br. 1997;79B:235–9.
7. Aglietti P, Buzzi R, Gaudenzi A. Patellofemoral functional results and complications with the posterior stabilized total condylar knee prosthesis. J Arthroplast. 1988;3:17.
8. Jeffery RS, Morris RW, Denham RA. Coronal alignment after total knee replacement. J Bone Joint Surg Br. 1991;73:709.
9. Börner M, Bauer A, Lahmer A. Rechnerunterstützter Robotereinsatz in der Hüftendoprothetik. Orthopade. 1997;26:251.
10. Siebert W, Mai S, Kober R, et al. Technique and first clinical results of robot-assisted total knee replacement. Knee. 2002;9(3):173–80.
11. Jacofsky D, Allen M. Robotics in arthroplasty: a comprehensive review. J Arthroplast. 2016;31:2353–63.

12. Song EK, Seon JK, Park SJ, et al. Simultaneous bilateral total knee arthroplasty with robotic and conventional technique: a prospective, randomized study. Knee Surg Sports Traumatol Arthrosc. 2011;19:1069–76.
13. Bargar WL. Robots in orthopedic surgery. Clin Orthop Relat Res. 2007;463:31.
14. Chun YS, Kim KI, Cho YJ, et al. Causes and patterns of aborting a robot-assisted arthroplasty. J Arthroplast. 2011;26:621.
15. NavioPFS FDA. http://www.accessdata.fda.gov/cdrh_docs/pdf12/K121936.pdf. 2006. Accessed 05 Jan 2006.
16. Plaskos C, Cinquin P, Lavallee S, et al. Praxiteles: a miniature bone-mounted robot for minimal access total knee arthroplasty. Int J Med Robot. 2005;1(4):67.
17. Lang JE, Mannava S, Floyd AJ, et al. Robotic systems in orthopaedic surgery. J Bone Joint Surg Br. 2011;93:1296.
18. Liow MH, Xia Z, Wong MK, et al. Robot-assisted total knee arthroplasty accurately restores the joint line and mechanical axis. A prospective randomized study. J Arthroplast. 2014;29(12):2373–7.
19. Kim SM, Park YS, Ha CW, et al. Robot-assisted implantation improves the precision of component position in minimally invasive TKA. Orthopedics. 2012;35(9):e1334–9.
20. Song EK, Seon JK, Yim JH, et al. Robotic-assisted TKA reduces postoperative alignment outliers and improves gap balance compared to conventional TKA. Clin Orthop Relat Res. 2013;471(1):118–26.

Chapter 4
Patient-Specific Templates for Total Knee Arthroplasty

Mahmoud A. Hafez and Hosamuddin Hamza

Abstract Advances in computer-assisted techniques, such as patient-specific templates (PSTs), have revolutionized total knee arthroplasty (TKA). Available clinically for more than a decade, PSTs have a TKA success rate comparable to that of traditional knee replacement and that with navigation. With its accurate preoperative calculations, PST allows precise, atraumatic bone cutting and optimal mechanical axis and limb alignment. A surgical procedure may be planned, or the plan supervised, by the surgeon. In addition, the surgery itself can be simulated a priori to confirm the best fit of the template and determine the accurate amount and shape of the subsequent bone cutting. Manufacturing the templates has been made easier with the availability of three-dimensional printers and printing materials. This chapter outlines the history of the development, as well as the clinical and technical setups, of PSTs for use in TKA.

Keywords Total knee arthroplasty · Patient-specific templates · Hospital-based system · Bilateral simultaneous TKA

4.1 Introduction

The incidence of knee osteoarthritis continues to increase in our aging populations, mandating the continuing development of surgical techniques using cutting-edge technology to improve total knee arthroplasty (TKA) methods. The aim of patient-specific surgery for TKA is to restore knee function by replacing the deformed knee joint to its original, healthy condition [1]. Widespread application of TKA is still limited because of its technical difficulty, high cost, and the claim that it is useful only in straightforward cases—not for those with severe intra-articular or extra-articular deformities [2]. Another limitation of the current TKA technique is that the knee implants currently available are designed based on

M.A. Hafez (✉) • H. Hamza
The Orthopaedic Department, October 6 University, Cairo, Egypt
e-mail: mhafez@msn.com

N. Sugano (ed.), *Computer Assisted Orthopaedic Surgery for Hip and Knee*,
https://doi.org/10.1007/978-981-10-5245-3_4

Caucasian knees. Recent studies have identified anthropometric differences between Asian/Arab populations and those of Caucasians, which could cause component mismatch and subsequent failure [3].

Patient-specific instruments, also known as patient-specific templates (PSTs), have been introduced in orthopedics as a minimally invasive surgical tool that allows precise execution of preoperative planning, which results in better function and survival rate, shorter operative time, shorter hospitalization and recovery time, and lower complication rate and cost. The PST is therefore considered an alternative to conventional techniques, robotics, and navigation for TKA surgery [4]. It aims to overcome the technical limitations of robotics and navigation while eliminating the drawbacks of the conventional technique. PST for TKA is a custom-made, image-based surgical tool that allows preoperative planning and simulation using computer software, followed by production of the cutting templates according to the surface anatomy of the individual's bony structures.

Compared with imageless navigation and robotic systems, it has the advantage of preoperative planning, with the surgeon becoming familiar with the given bony structures prior to surgery [5]. The PST system is also considered a simpler, more user-friendly, more affordable tool than surgery that depends on navigation and robotics. It does not require an intraoperative setup or a large operating theater. It has a short operative time because some of the steps usually performed intraoperatively are now done preoperatively. It has a short learning curve and is easily accepted by surgeons, nurses, and patients as a simple modality of computer-assisted orthopedic surgery [6]. Its disadvantage is that it lacks a tool that navigational and conventional techniques have that would provide intraoperative verification of errors, allowing the surgeon to correct the error immediately [7].

4.2 Technical Setup

The PST requires a rapid prototyping machine—i.e., three-dimensional (3D) printer—for its production via additive manufacturing. 3D printers use liquid, powder, sheets, or filaments to form complex models with predesigned dimensions and structures. The printers are also used to create physical anatomical models reconstructed from computed tomographic (CT) images, such as fractured or deformed bony models for educational purposes or for provisional practice prior to its use in the clinical setting [8]. The use of 3D printing in orthopedics is not limited to TKA. It is also useful for spinal pedicle screw insertion, other joint arthroplasties, and osteotomy.

Currently, the femoral and tibial cutting guides are fabricated with selective laser sintering (SLS) 3D printers using nylon as the material for the cutting guides. This production cycle takes place outside the hospital (being outsourced to other facilities) to avoid the cost of purchasing an expensive machine. The cycle includes writing the patient's initials and code number, whether it is the right or left knee to be operated on, and the surgeon's name on the cutting guides [9]. The use of nylon as the material of choice for producing the cutting guides is based on its being

autoclavable, hard enough to withstand the cutting forces without flaking at the operating site, and reproducible when used for finely detailed objects. The surgical staff is given information preoperatively regarding the size and type of knee implant and the instruments to be used. Neither traditional instruments nor intramedullary rods are required for the procedure [10].

The concept of PST was first utilized by industrial companies to produce pin locators. The planning is based on either CT or magnetic resonance imaging (MRI) images. The disadvantage of using MRI is that it sometimes gives unpredictable results for obese, unfit, or claustrophobic patients or those with a pacemaker. The only known drawback for CT is its associated radiation exposure [8]. In addition to MRI or CT, long-leg topography, extending from the hip to the ankle in anteroposterior and lateral projections, is required. This long-leg film could be useful for measuring changes in leg length preoperatively and postoperatively [11].

The first author applies an "open-platform" technique, wherein a PST could be used for any type or size of knee implant, unlike commercially available implants. MRI systems have an average waiting time of 6 weeks from acquiring the MRI scan to production of the PST and its delivery to the hospital. This long interval carries the risk of anatomical changes in cartilage due to daily activities or as a result of abnormal loading during this waiting time, which may cause misaligned templates and subsequent failure. Failure can also result from inaccurate bone segmentation, which is more likely to occur when using MRI than CT images [4].

The most critical step of TKA is intraoperative positioning of the templates because malpositioning could lead to error in the cutting, with subsequent malalignment of the lower limb. A previous laboratory study tested the accuracy and reliability of PSTs on cadaveric and plastic knees. Its analysis of postoperative CT scans showed that the mean errors for alignment and bone cutting were within 1.7° and 0.8 mm, respectively [12], which is higher than those reported for conventional and navigational techniques (3.0°) in the clinical setting. Another study included five independent observers, who examined the postoperative results (bone cutting, alignment of the prosthesis) of patient-specific TKA performed on plastic knees [4]. The observers were given a navigational tool for measuring the position. Even "naive" users were able to produce acceptable sizing errors (0.32–1.0 mm) and alignment errors (0.67°–2.5°). That is, positioning the PST was reliable, and there were no significant intraobserver/interobserver variations regarding alignment or the levels of bone cutting of the femur and tibia. These studies were useful for evaluating the reliability of the TKA with PSTs. It is not the case clinically, however, as kinematics are more important than mechanical alignment [13].

4.3 Clinical Setup

During TKA, the knee joint is exposed via the medial parapatellar approach. The femoral template is positioned in a best-fit fashion—that is, by locating probes at the bottom surface of the template that are touching the distal femur at the center

and at median and lateral points, this position should be the unique, single point at which the template could be fixed by pins onto the distal femur with an angle or wing to verify the amount of bone to be removed from the distal and frontal sides [14]. Bone is then cut with saw blades of known thickness, inserted through a slit for the distal cut and then for the anterior, posterior, and chamfer cuts. The tibial template is positioned over the proximal tibia at the frontal and medial surfaces and the tibial plateau, as close as possible to the patellar tendon insertion, which requires good clearance of the surrounding soft tissues. This position could be verified with surface matching (i.e., a single, unique matching position) that is secure enough to avoid dislodgement during bone cutting [4]. The template is fixed by the fixation pins at the front and top surfaces with an angle or wing to verify the amount of bone to be removed. Bone cutting is done through the cutting slits, with the cut bone removed from the medial and lateral sides. The templates could be modified by adding lug holes [15]. Stem and keel preparation is done through the corresponding hole/slit at the top of the tibial cutting guide to determine the rotational angle of the tibial implant [16].

After removing the templates, trial implants could be inserted for primary verification of the accuracy of the bone cuts and to adjust the soft tissue balance for the mediolateral and flexion–extension planes. Such trial implants are plastic (polyamide) and are fabricated in a manner similar to that used for producing the PST [17]. This technique could be used for simple, routine, straightforward TKAs, complex cases that are difficult to manage with the conventional technique, and those for which surgery is contraindicated because of an extra-articular deformity or retained hardware (e.g., nails, screws, plates) [6]. The PST is also useful for patients with bleeding tendencies (e.g., hemophiliacs), medically unfit patients at high risk of anesthesia, those with severe osteoarthritis combined with severe bone/cartilage loss, patients with complex articular anatomy, and those at increased risk of infection. The common feature of these patients is that conventional TKA would be difficult as it carries a risk of bleeding, infection, and prolonged operative time because of the use of intramedullary guides [18].

The first author's experience with PST has focused on the CT-based technique, although the CT scans are performed using a tailored protocol. The drawback of this system is that it is limited to use in patients who previously underwent TKA on the contralateral knee that must now be bent during scanning to avoid interference. Nevertheless, CT-based software is easy to use because tissue segmentation is done automatically with the possibility for manual adjustment [3]. Also, it allows the surgeon to participate in the preoperative planning and to design the templates. (In contrast, MRI-based software requires an experienced technician to perform manual segmentation of the tissues.) The original clinical trials included patients with extra-articular deformities, a high bleeding tendency, bilateral deep vein thromboses, and/or a pulmonary embolism. They also included bilateral procedures for patients seeking speedy recovery of both limbs simultaneously and medically compromised individuals with cardiorespiratory problems. These patients had been denied conventional TKA by anesthetists or surgeons.

In each of these patients, PST was applied successfully according to the preoperative planning without resorting to conventional instrumentation, intramedullary guides, or alignment rods. Sizing was applied, as accurately predicted from preoperative planning, and a tourniquet (not drains) was used for all cases. Postoperatively, full extension and >100° flexion were achieved [13].

Preoperative anteroposterior and lateral view radiographs of the planned surgery were used for superimposing the implants. The surgeon was guided by screen shots or other visual aids while placing the templates and implants during surgery. The final plan was printed out and taken to the operating room for any verification required throughout the surgery. It gave full details about positioning and fixing the templates over bone for accurate implementation, double checking to avoid inaccurate positioning of the PST and subsequent inaccurate bone cutting, implant malpositioning, and limb malalignment. Placing each template over sound-receptive bone in a satisfactory matching manner took an average of 5 min [4]. It was longer for patients with a severe flexion deformity (>30°), where two femoral templates were designed to have a second option for excessive distal cutting and were used intraoperatively for optimal bone cutting [13].

Nearly all major implant companies currently use PSTs as standard technique. The PSTs were approved by the US Food and Drug Administration as Class 2 instruments. The major use of PSTs currently is as pin locators for conventional instruments. A set of conventional jigs is costly, however, as it contains more than 150–200 instruments, needs a special sterilization setup, and may cause staff confusion during surgery. This issue has long been a subject of debate as many authors believe that the main objective of PSTs is to replace conventional TKA instruments because the clinical applicability of PSTs has been confirmed [18]. Other studies criticized this technique and found that it provided suboptimal clinical results. For example, Klatt et al. used image-free navigation to evaluate PST bone cuts and postoperative alignment and found that there was >3° deviation from the mechanical axis [19]. The reason for this error was a faulty preoperative plan carried out on MRI software. Another report compared the results of custom-fit guides to traditional TKA and found a shorter operative time in 14% of the PST procedures and an average deviation from the mechanical axis by 1.2° varus [20]. Howell et al. documented 48 consecutive TKAs done with PSTs in which all subjects rapidly showed acceptable clinical outcomes (speedy recovery, well-restored motion, good stability, postoperative mechanical axis alignment, and high patient satisfaction). None of these patients required soft tissue release from the collateral or retinacular ligaments. Only three tibial and three femoral guides were improperly positioned owing to improper alignment on the preoperative planning using MRI software [15].

In the current setup, 3D printers had been modified to serve a variety of architects, surgeons, and dentists, among others, with specific features to produce complex structures. These modifications involved a variety of materials, each with differing physical and thermal properties and, consequently, different uses. It allowed the production of PSTs with a variety of materials (plastics), each with its specific biocompatibility, heat stability, sterilization method (autoclave or gamma rays), durability, and price. Other modifications in 3D printers included the addition

of extruders or increasing the surface area of the printing bed to allow printing of larger or longer objects [8]. The manufacturers of these 3D printers were able to produce small, compact printers of the same size as paper printers. Called "desktop 3D printers," they are easy to carry, can be placed in a room or office, and are less expensive than industrial 3D printers. These desktop 3D printers could be purchased by hospitals and stored in a laboratory room, imaging department, or even an outpatient clinic. Thus, imaging, preoperative planning, and PST production could be done in one workplace, thereby saving time and resources. In addition, 3D CT scanning tools with a cone beam have become a feasible tool to use in orthopedic surgery [21].

4.4 New Features of PST

The development of PST for clinical use allowed new users to benefit from this approach. The learning curve starts with performing surgery on 3D-printed plastic knees according to a patient's CT scan, thereby allowing the surgeon to predict the surgical results prior to operating on a living patient. Training involves positioning the PST over bony surfaces accurately and marking the level/inclination of bone cutting using conventional instruments or navigation guidance to compare and evaluate the cuts. The surgeon thus develops familiarity with the technique and gains confidence using it by seeing how simple instruments (e.g., angel wings) could be used to level bone cuts, visually inspect the surgical site, and confirm the appropriateness of the surgical procedure. After an average of five to ten cases, the surgeon should be ready to become involved in clinical, comparative trials [9, 10].

PSTs are useful in active young patients who need to preserve good bony stock. Its advantage lies in the fact that the amount of bone to be cut is quantified before the actual surgery. Accurate preoperative planning for PSTs is most advantageous when applied to revision TKA, unicompartmental TKA, bicondylar replacement of only the medial and lateral compartments while preserving the anterior and posterior cruciate ligaments, patellofemoral arthroplasty, and high tibial osteotomy (Fig. 4.1) [22]. PSTs are also useful for hip resurfacing and total hip arthroplasty, comprising a powerful and inexpensive training tool.

The currently used software provides a good opportunity for surgeons to participate and modify the preoperative planning of TKA and to learn how to interpret dynamic and kinematic data regarding the size, alignment, rotation, and virtual bone cutting. It also allows simulation of the surgery, which allows the surgeon to identify and analyze any error in the 3D planes in real time [9]. Moreover, this training improves cognitive and motor skills as it is based on repetitive practice while committing and correcting errors. Reusable 3D-printed plastic bones and PSTs are used in arthroplasty workshops. It has been noted that training for the PST technique for TKA is easier than that for the conventional technique as it involves fewer instruments and operative steps.

Fig. 4.1 Patient-specific orthopedics

Medical and legal staff have referred to PST usage as a complex process, and surgeons are held responsible in case of failure as PST manufacturers cannot proceed with developing the procedure without obtaining acceptance from the surgeon [23]. For current company-based PST systems, planning is considered a serious limitation as it is done by technicians, not the surgeon, and the whole process is controlled by the implant company, with the surgeon able only to review the treatment plan. For example, improper fitting of a PST could cause overhang of a knee prosthesis, in turn causing irritation of the surrounding soft tissues. Alternatively, under-coverage could cause subsidence and instability [3].

PSTs offer the advantage of trial (simulated) surgery so the results of the surgical outcome could be foreseen and the surgeon can validate the accuracy, leveling, and inclination of the bone resection. PST technology is still in its early stages, and more work is needed to investigate the accurate placement of jigs over the bony surfaces [8]. This accurate placement demands proper soft tissue management. (For example, it is unprofitable to detach all soft tissues from bone to find an optimal fit for the PST.) When MRI is used for preoperative planning, cartilage thickness could cause inaccurate planning and subsequent placement of the PST. This is especially true for the tibial jig, which is usually weak and requires good assessment prior to the final placement and bone cutting. Inaccurate segmentation or planning would result in malpositioning of the PST and erroneous cuts in three dimensions [24].

The amount of intraoperative information on navigation and robotics is enormous. An average of 1° of deviation with navigation is considered accurate with regard to implant positioning and bony cuts. Verification is then done with much ease so changes could be made prior to the definitive cuts. The PST system, however, lacks verification tools, and minor malalignment with the risk of notching cannot be detected by the human eye. This disadvantage of PST has been well documented [25]. Thus, surgeons in training must verify their cuts by navigation or extramedullary rods in at least their first ten cases. This safeguard could significantly help junior surgeons understand the concept of PSTs and shorten the learning curve. The verification step could help these learners clarify their preferences regarding the usefulness of the various arthroplasty techniques, implant designs, and surgical approaches. The primary results of training usually show higher accuracy with femoral bone cutting, during which utmost attention must be focused on the tibial cutting position. Neophyte surgeons should not rely on medical representatives when choosing appropriate PST systems as the company representatives usually promise that their system is the most accurate [24].

The currently available PSTs are mostly produced by implant companies and are specific for their own knee prostheses. In contrast, the use of an open-platform technique allows coordination of the PST with any surgical instruments. This integration, or coupling, could be done by various methods based on connecting the custom-made guides to any instrument system from any implant manufacturer. The same concept can be applied for other joint arthroplasty procedures such as for the hip, shoulder, elbow, ankle, and others (Fig. 4.1) [13]. This technique is suitable for any commercially available instrument or prosthesis, and it gives the surgeons the option of using any implant and any instrumentation system. The technique involves different designs and shapes of PST to fit available instruments and implants. For example, using computer software, deep indents could be designed on the back of the cutting block to offer secure fitting [26]. Another design could be "housing," created by interlocking the block from three sides and mounting it over a custom-made guide. To ensure accurate mounting, additional pins could be used to fix the cutting block over the custom-made guide. Several variations could be accomplished with the PST design using slots, grooves, or boxes with variable inclinations and angulations. These designs make PST more universal and applicable for patients with variable anatomy and deformities [4].

4.5 Modern Applications of PST

Current training strategies to familiarize junior surgeons and nurses with PST systems vary among surgeons and hospitals. The first author introduced the self-contained, or hospital-based, PST system (Fig. 4.2). With this setup, imaging, planning, sizing, designing, and fabrication of the PST are completed by a technical team directly supervised by the operating surgeon [24]. Thus, the staff could communicate rapidly and easily, and the planned design could be instantly adjusted. This system is based on CT images because the waiting time is shorter and the cost

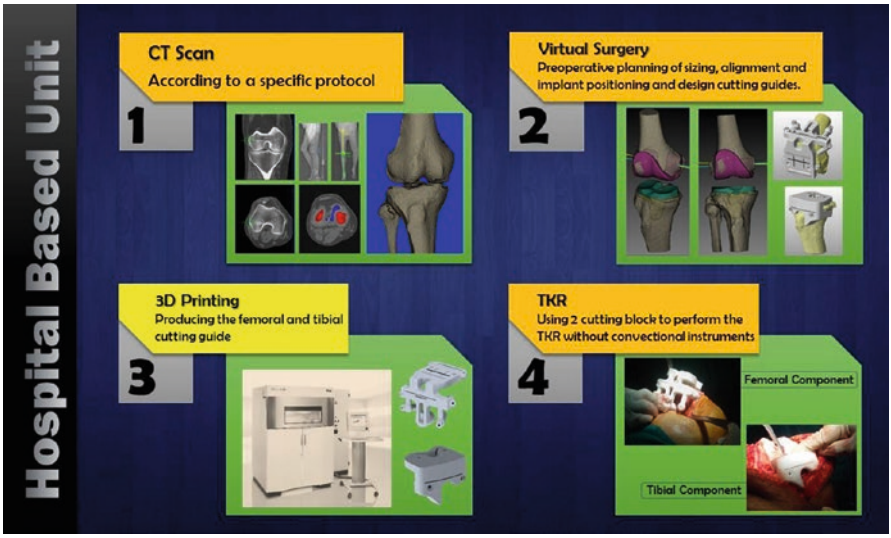

Fig. 4.2 Hospital-based patient-specific template system for total knee arthroplasty. *CT* computed tomography, *3D* three-dimensional, *TKR* total knee replacement

of CT is less than that of MRI by an average of USD 40–300 in developing countries, Europe, and the United States. The overall cost of a PST in a hospital-based setup is nearly USD 500 and ranges from USD 800 to USD 2000 in company-based systems for cutting blocks or pin locators [15]. In addition to the cost element, the number of instruments used in a hospital-based system are 2 PSTs and 15 instruments, whereas for a company-based system, it is 2 PSTs and an average of 30–43 instruments, which is significantly more. It is worth mentioning that the fewer instruments needed, the less complicated is their sterilization and packing setup and the less disturbance there is in the operating room [16]. All of the steps for TKA in the hospital-based system can be carried out within the same workplace (the hospital), including the examination, imagining, planning, fabrication, packing, sterilization, surgery, and rehabilitation. There is no need for any company representative or special method for transferring data, radiographs, or documents.

The one obstacle to applying hospital-based PST is the cost of the 3D printers (average USD 500,000) that are used to produce the templates. The currently available desktop 3D printers, however, have replaced industrial machines and are capable of producing the physical PST and trial implant models. These physical models are made of nylon, which is known to be heat stable, autoclavable, sufficiently durable to resist the force of saw blades, inexpensive, and easily manufactured within a short time and in easily available settings [24]. Another material used to produce PSTs is ABS plastics, which is also not expensive but requires sterilization with gamma rays, low-temperature steam, or other special chemicals. Another material that could be used is polycarbonate which could be sterilized by autoclave, gamma rays, or chemicals [8, 9].

Another advantage of the PST is its applicability for bilateral one-stage TKA procedures. Simultaneous bilateral TKA is considered a good option for patients with bilateral knee osteoarthritis because it offers a single anesthesia exposure and simultaneous rehabilitation of both limbs with better functional outcome, although there remain some concerns about its safety. The Swedish Knee Arthroplasty Register and the Swedish Cause of Death Register showed a difference in the early mortality rate among patients treated with simultaneous bilateral TKA versus others who underwent staged procedures [27]. Previous reports showed that blood loss is one of the major complications associated with bilateral TKA. Because the risk of bleeding was 2.2 units per single TKA (caused by extensive osteotomy and soft tissue cuts), it would be logical to assume that treating two knees would double the risk of bleeding and the need for blood transfusion. During TKA, however, the need for blood transfusion has several predisposing factors, such as the surgical technique, operating time, and clotting factors. As computer-assisted orthopedic surgery techniques have the general advantages of avoiding intramedullary perforation and preserving soft tissues—which shorten the recovery time and reduce the rate of blood loss—PST is useful for simultaneous bilateral TKA while eliminating the need for intramedullary rods and subsequent bleeding, fat embolism, and infection. It is also useful for treating bilateral cases of severe articular deformities (valgus, varus, and fixed flexion deformity) during a single hospitalization, with a shorter accumulative operating time and, accordingly, less cost [28].

References

1. Weeks WB, Schoellkopf WJ, Sorensen LS, Masica AL, Nesse RE, Weinstein JN. The High Value Healthcare Collaborative: observational analyses of care episodes for hip and knee arthroplasty surgery. J Arthroplast. 2017;32(3):702–8.
2. Koenig JH, Maheshwari AV, Ranawat AS, Ranawat CS. Extra-articular deformity is always correctable intra-articularly: in the affirmative. Orthopedics. 2009;32(9)
3. Hafez MA, Sheikhedrees SM, Saweeres ES. Anthropometry of Arabian arthritic knees: comparison to other ethnic groups and implant dimensions. J Arthroplast. 2016;31(5):1109–16.
4. Hafez MA, Chelule KL, Seedhom BB, Sherman KP. Computer-assisted total knee arthroplasty using patient-specific templating. Clin Orthop Relat Res. 2006;444:184–92.
5. Mattei L, Pellegrino P, Calò M, Bistolfi A, Castoldi F. Patient specific instrumentation in total knee arthroplasty: a state of the art. Ann Transl Med. 2016;4(7):126.
6. Chan WC, Pinder E, Loeffler M. Patient-specific instrumentation versus conventional instrumentation in total knee arthroplasty. J Orthop Surg (Hong Kong). 2016;24(2):175–8.
7. McCrory B, LaGrange CA, Hallbeck MS. Quality and safety of minimally invasive surgery: past, present, and future. Biomed Eng Comput Biol. 2014;6:1–11.
8. Qiu B, Liu F, Tang B, Deng B, Liu F, Zhu W, Zhen D, Xue M, Zhang M. Clinical study of 3D imaging and 3D printing technique for patient-specific instrumentation in total knee arthroplasty. J Knee Surg. 2017. https://doi.org/10.1055/s-0036-1597980.
9. Lee Ventola C. Medical applications for 3D printing: current and projected uses. P T. 2014;39(10):704–11.
10. Conteduca F, Iorio R, Mazza D, Ferretti A. Patient-specific instruments in total knee arthroplasty. Int Orthop. 2014;38(2):259–65.

11. Vaidya SV, Patel MR, Panghate AN, Rathod PA. Total knee arthroplasty: limb length discrepancy and functional outcome. Indian J Orthop. 2010;44(3):300–7.
12. Ritter MA, Berend ME, Meding JB, et al. Long-term followup of anatomic graduated components posterior cruciate retaining total knee replacement. Clin Orthop Relat Res. 2001;388:51–7.
13. Hafez MA. Patient specific instruments: past, present and future. In: Thienpont E, editor. Improving accuracy in knee arthroplasty. New Delhi: Jaypee Brothers Medical Publishers (P) Ltd.; 2012. p. 149–68.
14. Sanna M, Sanna C, Caputo F, Piu G, Salvi M. Surgical approaches in total knee arthroplasty. Joints. 2013;1(2):34–44.
15. Howell SM, Kuznik K, Hull ML, Siston RA. Results of an initial experience with custom-fit positioning total knee arthroplasty in a series of 48 patients. Orthopedics. 2008;31(9):857–63.
16. Tria AJ, Scuderi GR. Minimally invasive knee arthroplasty: an overview. World J Orthop. 2015;6(10):804–11.
17. Stulberg SD, Loan P, Sarin V. Computer-assisted navigation in total knee replacement: results of an initial experience of thirty-five patients. J Bone Joint Surg Am. 2002;84(Suppl 2):90–8.
18. Chauhan SK, Scott RG, Breidahl W, et al. Computer assisted knee arthroplasty versus a conventional jig-based technique. A randomised, prospective trial. J Bone Joint Surg Br. 2004;86(3):372–7.
19. Klatt BA, Goyal N, Austin MS, et al. Custom-fit total knee arthroplasty (OtisKnee) results in malalignment. J Arthroplast. 2008;23(4):637–8.
20. Spencer BA, Mont MA, McGrath MS, et al. Initial experience with custom-fit total knee replacement: intraoperative events and long-leg coronal alignment. Int Orthop. 2009;33(6):1571–5.
21. Mahmoud A. Hafez, Khaled Abdelghany, and Hosamuddin Hamza. Highlighting the medical applications of 3D printing in Egypt. Ann Transl Med. 2015;3(22):359.
22. Bäthis H, Shafizadeh S, Paffrath T, et al. Are computer assisted total knee replacements more accurately placed? A meta-analysis of comparative studies. Orthopade. 2006;35(10):1056–65.
23. Beswick AD, Wylde V, Gooberman-Hill R, Blom A, Dieppe P. What proportion of patients report long-term pain after total hip or knee replacement for osteoarthritis? A systematic review of prospective studies in unselected patients. BMJ Open. 2012;2(1):e000435.
24. Lal K, White GS, Morea DN, Wright RF. Use of stereolithographic templates for surgical and prosthodontic implant planning and placement. Part I. The concept. J Prosthodont. 2006;15(1):51–8.
25. Chan KY, Teo YH. Patient-specific instrumentation for total knee replacement verified by computer navigation: a case report. J Orthop Surg (Hong Kong). 2012;20(1):111–4.
26. A device and a technique of PSI for TKA with a universal and an open platform. PCT/EG2013/000014.
27. Stefánsdóttir A, Lidgren L, Robertsson O. Higher early mortality with simultaneous rather than staged bilateral TKAs: results from the Swedish Knee Arthroplasty Register. Clin Orthop Relat Res. 2008;466(12):3066–70.
28. Hafez MA, Ghazal I. Rate of blood transfusion in patients undergoing bilateral simultaneous total knee arthroplasty using patient-specific templates and conventional techniques: a comparative study. Remed Open Access. 2016;1:1028.

Chapter 5
UKA Computer Navigation

Pornpavit Sriphirom

Abstract Several factors are involved in the failure of unicompartmental knee arthroplasty (UKA), including the patient's age, anterior cruciate ligament deficiency, and alignment. To address these failures, a computer-aided navigation system that consistently provides accurate measurements was developed to reduce the errors committed with conventional UKA. The undercorrection with a minor varus alignment produced by this system provides appropriate outcomes and longevity for UKAs. The computer navigation system thus offered a procedure to attain optimal alignment. Although a learning period is required for computer-assisted surgery, the computer-assisted UKA produced comparable range of motion and WOMAC and Oxford scores with fixed-bearing UKA implantation.

Keywords Unicompartment knee arthroplasty · UKA · Longevity · Outcomes · Computer-assisted surgery · Navigation · Alignment

5.1 Introduction

Unicompartmental knee arthroplasty (UKA) provides a less invasive alternative to total knee arthroplasty (TKA) in selected patients [1]. Minimally invasive surgery (MIS) with a small incision and less damage has gained popularity for UKA. MIS has the advantage of a shorter recovery period and faster healing than TKA [2]. Joint registries indicate that MIS UKA was performed for at least half of the UKA procedures [3, 4]. As the number of UKAs has increased, however, it has led to an increased number of failures. Early reports of UKA with this technique showed higher failure rates than expected. For example, 43 (8.3%) of 517 medial MIS UKAs with fixed-bearing implants had reportedly failed at 6 years (Fig. 5.1) [2], which is in accord with recent orthopedic literature. The major reason for this failure was aseptic loosening (19/43, 44%), followed by progressive arthritis of the lateral compartment. Obesity has also been reported as a reason for UKA failure [5]. Although comparable revision rates were found in mobile and fixed UKA designs, progressive

P. Sriphirom
Department of Orthopaedic Surgery, Rajavithi Hospital, Rangsit University, Bangkok, Thailand
e-mail: pornpavit@yahoo.com

N. Sugano (ed.), *Computer Assisted Orthopaedic Surgery for Hip and Knee*,
https://doi.org/10.1007/978-981-10-5245-3_5

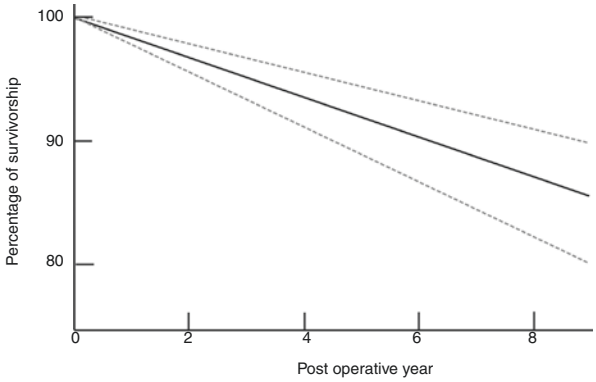

Fig. 5.1 Postoperative survival of fixed-bearing unicompartmental knee arthroplasties (UKAs) (Depuy, Johnson & Johnson Company, New Brunswick, NJ, USA). The dark linear plot represents the survival rate of unicondylar implants over an 8-year follow-up period. The dashed lines show the 95% confidence interval. Hamilton et al. reported that revision rate was only 8.3% (43/517) of cases with fixed-bearing UKAs at 6 years. This figure has been modified based on data from the Hamilton et al. study [2]

arthritis was seen somewhat less frequently with mobile implants (0.23%) than with fixed implants (0.29%) [6]. An oversized femoral component or patellofemoral impingement was reportedly related to promote progression of patellofemoral osteoarthritis [7], although there was no significant difference in revision rates between Oxford III UKAs with and without progressive patellofemoral osteoarthritis [8]. It is well established that the high failure rate of UKA is associated with anterior cruciate ligament (ACL) deficiency [9], although other causes remain but are controversial. Age may affect the survivorship of UKAs, which is based on two joint registries and prior studies having reported significantly higher revision rates for UKAs in young patients [3, 4, 10, 11]. In contrast, some independent cohorts showed that age did not relate to UKA survival [1]. An analysis of 23,400 medial cemented UKAs showed that the institutional and surgeons' case volumes had an effect on the revision rates following UKA (Fig. 5.2). These results suggested that there should be at least 13 [12] to 23 [13] UKAs performed per year before better outcomes could be expected.

Alignment was also associated with UKA failure. Overcorrected valgus (hip–knee–ankle angle >180°) was associated with a high risk of degenerative changes in the opposite compartment, and undercorrection in varus deformity (hip–knee–ankle angle <170°) increased polyethylene wear and tibial component loosening [14]. Excessive stress on the supporting cancellous bone can cause loosening and failure. Sawatari et al. reported that excessive varus alignment led to cancellous bone stress [15]. The short-term survival study by Vasso et al. showed better outcomes for minor varus alignment than for neutral or close-to-neutral alignment. They found that 70% of UKA deformities were not fully correctable to neutral alignment [16]. The full extension of correctability of varus deformity could be determined only after removing osteophytes [17].

Alterations in tibiofemoral kinematics have implications for the cumulative survival rate of UKA prostheses. The highest rate of implant survivorship was found

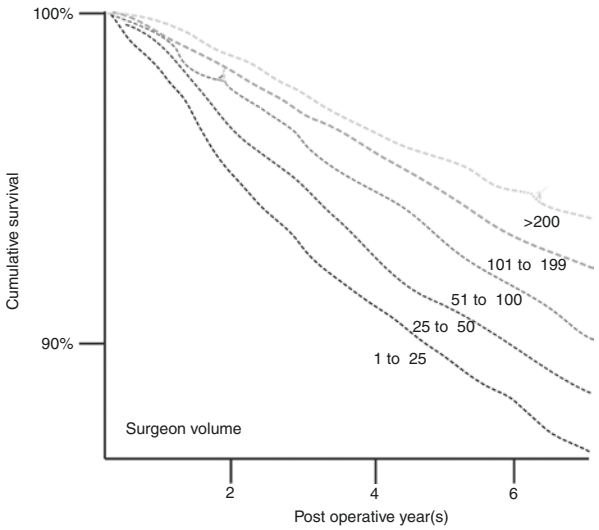

Fig. 5.2 Influence of the institutional and surgeon case volumes on the revision rate of unicompartmental knee replacement (UKR). The higher-volume of institutional and surgeon case rates produced higher cumulative survival rates. At least 13 such procedures per year have been suggested for better UKR outcomes. This figure has been modified based on data from the Baker et al. study [12]

with a tibiofemoral alignment of 4°–6° of valgus [17]. Overstuffing increased valgus at full extension and did not improve the tibiofemoral kinematics [18]. A posterior slope of the tibial implant must also be considered as a factor in UKA failure. Particularly, a compromise between physiological sagittal translation and excessive translation was detected in the posterior slope of tibial implants between 3° and 7° [19]. This notion was supported by the evidence that the posterior slope over this range would increase ACL stress, and frequent ACL ruptures occurred at slopes of >13° [19]. The wear rate of tibial prostheses was significantly decreased at slopes of 0°–4°, whereas a slope of 4°–8° shows no difference [20]. Thus, procedures that restored appropriated alignment were needed to prevent UKA failure.

The principle of restoring alignment consists of undercorrection, neutral correction, and overcorrection (Fig. 5.3). The traditional concept of TKA is to restoration neutral limb alignment for good outcomes. While the better UKA outcomes were obtained with under neutral alignment correction. It is essential that restoration of the alignment has undercorrection without ligament release, thereby leading to increased surgical efficiency when using the computer-assisted system. Jenny et al. showed that computer-assisted navigation achieved a higher rate of perfect alignment than conventional surgery (60% vs. 20%), including the coronal femorotibial mechanical angle and both coronal and sagittal orientations of the femoral and tibial components [21]. Several recent studies have suggested that navigation could significantly improve positioning of the posterior slope in the tibial component over that achieved with conventional UKA methods ($p = 0.04$) [22]. After a 10-year follow-up, UKA with navigation showed better outcomes regarding coronal alignment and clinical scores [23]. The Australian Joint Replacement Registry indicated that TKA with navigation had lower rates of revision than were achieved with conventional TKA [24], although this information was still lacking for UKAs. This evidence clearly suggested that the computer-assisted system could play an essential role in improving the restored alignment.

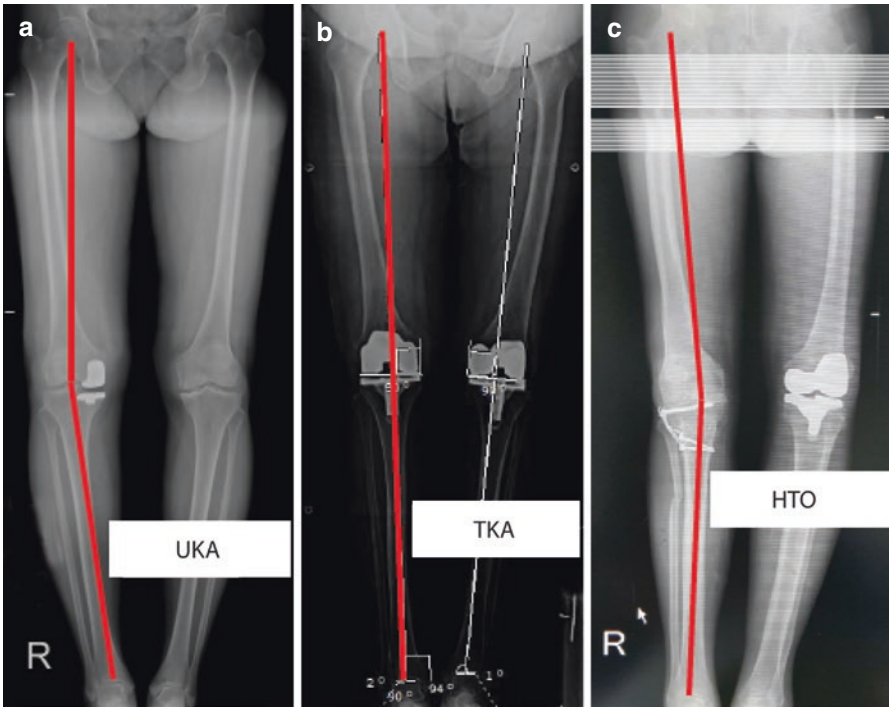

Fig. 5.3 Restoration of alignment. (**a**) Undercorrection in unicompartmental knee arthroplasty (UKA). (**b**) Neutral correction in total knee arthroplasty (TKA). (**c**) Overcorrection with high tibial osteotomy (HTO)

5.2 Surgical Technique

Our MIS technique included an imageless navigation system (OrthoPilot 3.0; B. Braun Aesculap, Tuttlingen, Germany). The UKA technique is similar to that of Jenny et al. [25]. For navigated UKA, it is mandatory to carry out adequate preoperative planning based on radiographic images, as is done when using the manual technique.

The skin incision is made via a medial parapatellar approach (Fig. 5.4a). Two infrared localizers are fixed on the distal femur and the proximal tibia (Fig. 5.4b). Registration of the femur and tibia was performed by touching the landmark points with a pointer at the knee center, the most distal point of the medial femoral condyle, the posterior point of the femoral condyle, the proximal tibial center and tibial plateau, the medial and lateral malleoli, and the center of the ankle joint (50% of the anterior ankle) (Fig. 5.4c–h). Kinetic registration of the hip center is performed by circumduction, flexion–extension, and rotation of the hip. These registration steps are used to define the mechanical axes of the femur and tibia in both anterior and sagittal views (Fig. 5.5a). The restoration of alignment or reducibility of the

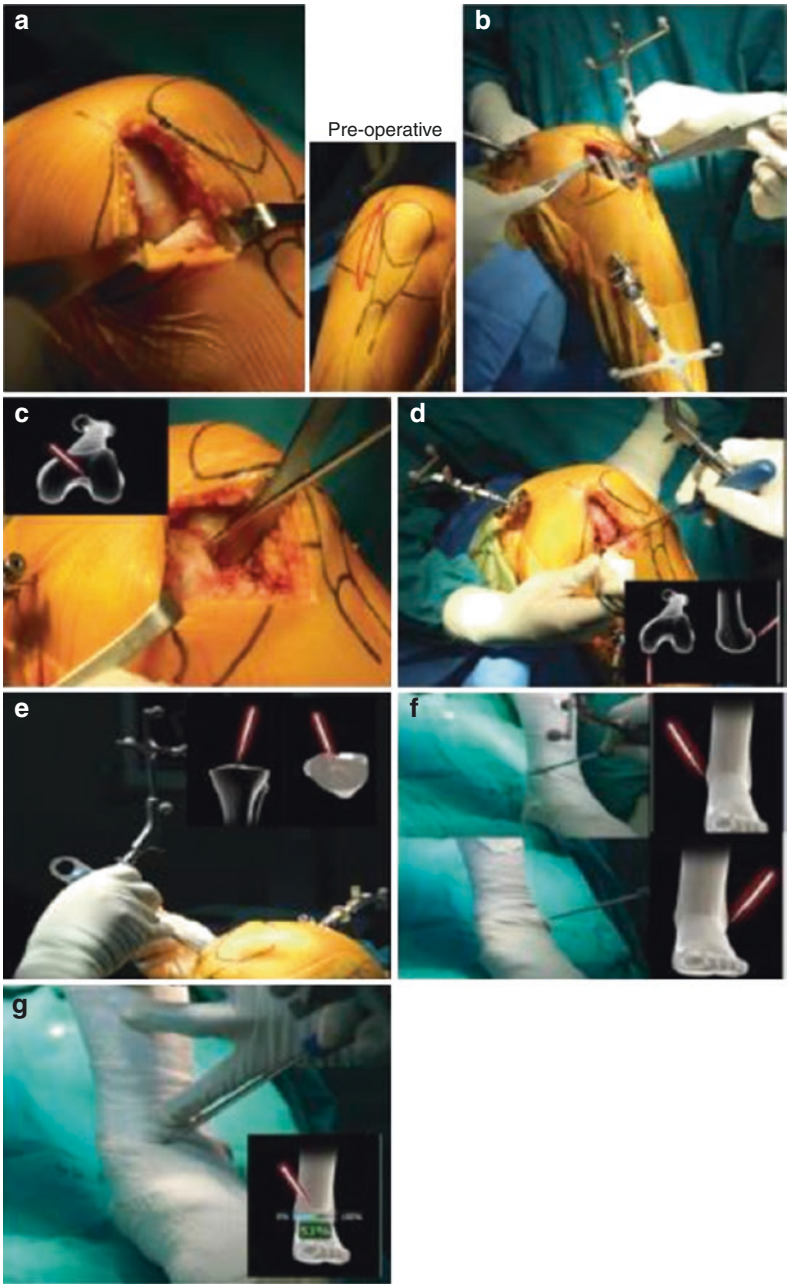

Fig. 5.4 Minimally invasive surgery navigated technique. The skin incision is made via a medial parapatellar approach (**a**) and restoration of the infrared localizer (**b**). Anatomical registry was then performed at the knee center (**c**), the most distal point of the medial femoral condyle and posterior point of the femoral condyle (**d**), proximal tibial center and tibial plateau (**e**), medial and lateral malleoli (**f**), and center of the ankle joint (50% pf the anterior ankle) (**g**)

deformation can be assessed by the mediolateral joint laxity test, wherein the joint is stressed on the opposite side from the opening. A localizer is then placed on the tibial cutting block (Fig. 5.5b), and the proximal tibial resection is guided using the navigated cutting block, with the position controlled using a freehand technique.

The medial meniscus and osteophytes are removed. The accuracy of each resection is verified by a navigated plate. The femorotibial gap is then measured by

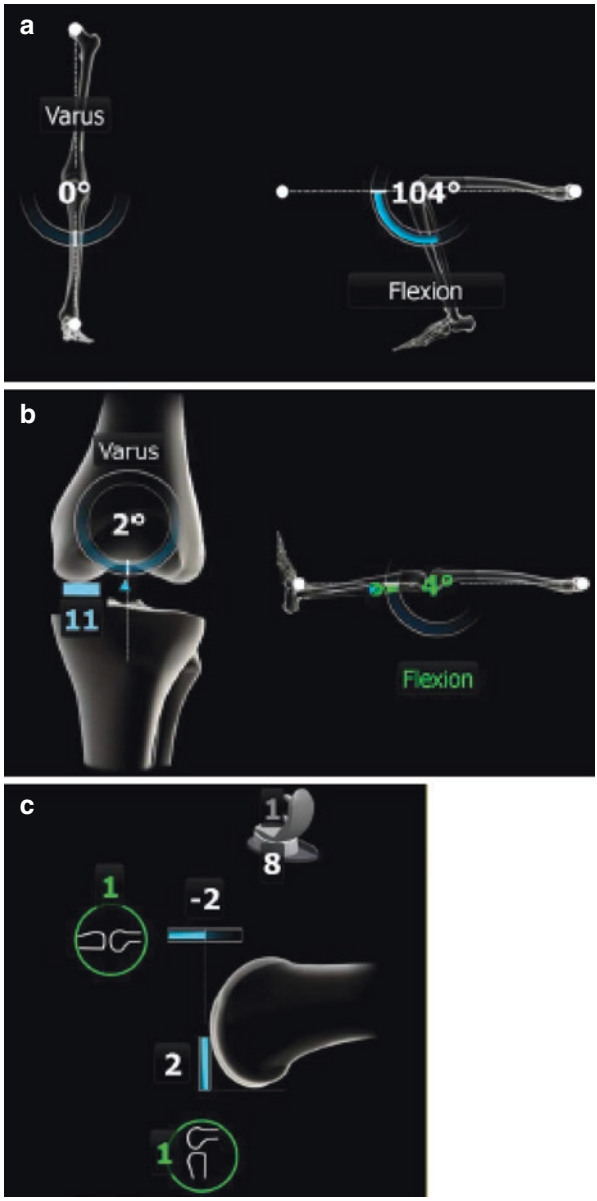

Fig. 5.5 Simulation display during computer-assisted surgery with OrthoPilot 3.0 software (B. Braun Aesculap, Tuttlingen, Germany). (**a**) Simulated mechanical axes of the femur and tibia in both coronal and sagittal views are shown after anatomical registration. (**b**) The planning screen also shows both tibial and femoral resections. (**c**) They consist of coronal and sagittal orientations, high distal and posterior resections, and thickness of the tibial component mediolateral laxity

applying a laminar spreader at 0° and 90° of knee flexion. The planning screen of the femoral resection consists of coronal and sagittal orientations, the thickness of the distal and posterior resections, thickness of the polyethylene liner, and mediolateral laxity (Fig. 5.5c). These data can be virtually adjusted to obtain appropriate conditions. When the values meet the surgeon's preference, the UKA components are cemented and implanted in the patient. The final axis correction is then checked again by the navigation system.

In all, 32 patients underwent UKA with implantation of a fixed bearing (Univation®, B. Braun Aesculap) at Rajavithi Hospital from June to December 2015. We used the classic technique of tibial cutting at a 0° slope in 17 patients and an anatomical technique at a 3° varus slope in the other 15 patients. The range of motion (ROM) and Oxford and WOMAC scores were collected before and after surgery.

A student's paired *t*-test was used to compare the two treatments. Differences were considered statistically significant at $p < 0.05$ and/or $p < 0.01$.

5.3 Results

The characteristics of both patient groups were comparable for age, weight, height, and body mass index (Table 5.1). The classic technique produced a significant difference between the preoperative and postoperative ROMs ($p = 0.019$), whereas there was no difference in the other group (Table 5.2). There was no significant difference in the postoperative ROMs between the two techniques ($p = 0.846$).

Both the classic and anatomical techniques significantly improved both the WOMAC and Oxford scores ($p < 0.01$), compared with the preoperative baseline

Table 5.1 Patients' demographics in the classic (tibial cutting at 0°) and anatomical (tibial cutting at 3°) groups

Characteristic	Classical technique ($n = 17$)	Anatomical technique ($n = 15$)	*p*-value
Age (year)	60.9 ± 5.1	58.9 ± 4.5	0.75
Weight (kg)	67.5 ± 12.5	73.1 ± 8.6	0.83
Height (cm)	156.7 ± 6.8	162.0 ± 5.4	0.82
BMI (kg/m^2)	25.1 ± 5.1	22.1 ± 7.2	0.69

Table 5.2 Influence of the two techniques (classic tibial cutting at 0°, anatomical cutting at 3°) on range of motion

Technique(s)	Pre-operative ROM degree (Mean)	Post-operative ROM degree (Mean)	*p*-value
Classical technique ($n = 17$)	115	123	0.019
Anatomical technique ($n = 15$)	121	122	0.667
p-value	0.032	0.846	

Table 5.3 Effects of the two techniques (classic tibial cutting at 0°, anatomical cutting at 3°) on WOMAC scores

Technique(s)	Pre-operative WOMAC score (Mean)	Post-operative WOMAC score (Mean)	*p*-value
Classical technique ($n = 17$)	73.60	25.67	<0.001
Anatomical technique ($n = 15$)	72.29	22.36	<0.001
p-value	0.512	0.467	

Table 5.4 Effects of the two techniques (classic tibial cutting at 0°, anatomical cutting at 3°) on Oxford scores

Technique(s)	Pre-operative Oxford score (Mean)	Post-operative Oxford score (Mean)	*p*-value
Classical technique ($n = 17$)	23.33	38.93	<0.001
Anatomical technique ($n = 15$)	20.71	42.21	<0.001
p-value	0.305	0.040	

scores (Tables 5.3 and 5.4, respectively). The mean postoperative WOMAC score showed no significant difference between the two groups (Table 5.3). More improvement in postoperative Oxford score was seen with the anatomical technique ($p = 0.04$) (Table 5.4).

5.4 Discussion

Undercorrection with minor varus was clearly shown to provide better outcomes and longevity than neutral alignment with UKA [26, 27]. Although such an exact degree of optimal correction has not been indicated, computer navigation assisted in reaching appropriate alignment [28]. In general, computer navigation significantly shortens the learning curve for surgeons performing TKA [29, 30]. The early failure phase of UKA was bearing dislocation which our experience found 3 cases in 23 cases with mobile bearing UKA. It was possible that these errors were influenced by the learning curve phenomenon.

Ligament balancing is an essential factor for knee joint stability. The femorotibial gap could be measured only at 0° and 90° using the OrthoPilot 3.0 software. Thus, we lacked full information on mid and deep flexion gaps (at 45° and >120°, respectively), which is a current limitation in gap adjustment. For TKA, increasing the posterior tibial slope has been found to lead to deeper flexion [31], whereas the mid flexion gap could be extended by less distal femoral resection,

more femoral flexion, and more tibial resection and slope [32]. For UKA, overall ligament balance adjustments are performed to maintain stability. If the knee is still unstable, an increase in the thickness of the polyethylene liner is required. The alignment, however, must be evaluated after all other adjustments are made and after ensuring that there is no valgus alignment during the fixed-bearing UKA. Our experience of navigated UKA demonstrated that navigation provided interactive simulation that could assess knee kinematics and alignment during surgery and implantation.

References

1. Matharu G, Robb C, Baloch K, Pynsent P. The Oxford medial unicompartmental knee replacement: survival and the affect of age and gender. Knee. 2012;19(6):913–7.
2. Hamilton WG, Ammeen DJ, Hopper RH Jr. Mid-term survivorship of minimally invasive unicompartmental arthroplasty with a fixed-bearing implant: revision rate and mechanisms of failure. J Arthroplast. 2014;29(5):989–92.
3. Lidgren L, Sundberg M, W-Dahl A, Robertsson O. Annual Report 2016: The Swedish Knee Arthroplasty Registry. http://www.myknee.se/pdf/SVK_2016_Eng_1.0.pdf. Accessed 06 June 2017.
4. New Zealand Orthopaedic Association: New Zealand Joint Registry. http://nzoa.org.nz/system/files/NZJR%2017%20year%20Report.pdf. Accessed 06 June 2017.
5. Berend KR, Lombardi AV Jr, Mallory TH, Adams JB, Groseth KL. Early failure of minimally invasive unicompartmental knee arthroplasty is associated with obesity. Clin Orthop Relat Res. 2005;440:60–6.
6. Argenson JN, Scuderi GR, Komistek RD, Scott WN, Kelly MA, Aubaniac JM. In vivo kinematic evaluation and design considerations related to high flexion in total knee arthroplasty. J Biomech. 2005;38(2):277–84.
7. Hauptmann SM, et al. Einfluss Der Retropatellararthrose Auf Das Funktionelle Ergebnis Nach Unikondylären Schlittenprothesen. Orthopade. 2005;34(11):1088–93.
8. Beard DJ, Pandit H, Gill HS, Hollinghurst D, Dodd CA, Murray DW. The influence of the presence and severity of pre-existing patellofemoral degenerative changes on the outcome of the Oxford medial unicompartmental knee replacement. J Bone Joint Surg Br. 2007;89(12):1597–601.
9. Murray DW, Goodfellow JW, O'Connor JJ. The Oxford medial unicompartmental arthroplasty: a ten-year survival study. J Bone Joint Surg Br. 1998;80(6):983–9.
10. Lustig S, Barba N, Magnussen RA, Servien E, Demey G, Neyret P. The effect of gender on outcome of unicompartmental knee arthroplasty. Knee. 2012;19(3):176–9.
11. W-Dahl A, Robertsson O, Lidgren L, Miller L, Davidson D, Graves S. Unicompartmental knee arthroplasty in patients aged less than 65. Acta Orthop. 2010;81(1):90–4.
12. Baker P, Jameson S, Critchley R, Reed M, Gregg P, Deehan D. Center and surgeon volume influence the revision rate following unicondylar knee replacement: an analysis of 23,400 medial cemented unicondylar knee replacements. J Bone Joint Surg Am. 2013;95(8):702–9.
13. Robertsson O, Knutson K, Lewold S, Lidgren L. The routine of surgical management reduces failure after unicompartmental knee arthroplasty. J Bone Joint Surg Br. 2001;83(1):45–9.
14. Hernigou P, Deschamps G. Alignment influences wear in the knee after medial unicompartmental arthroplasty. Clin Orthop Relat Res. 2004;423:161–5.
15. Sawatari T, Tsumura H, Iesaka K, Furushiro Y, Torisu T. Three-dimensional finite element analysis of unicompartmental knee arthroplasty—the influence of tibial component inclination. J Orthop Res. 2005;23(3):549–54.

16. Vasso M, Del Regno C, D'Amelio A, Viggiano D, Corona K, Schiavone Panni A. Minor varus alignment provides better results than neutral alignment in medial UKA. Knee. 2015;22(2):117–21.
17. Kim KT, Lee S, Kim TW, Lee JS, Boo KH. The influence of postoperative tibiofemoral alignment on the clinical results of unicompartmental knee arthroplasty. Knee Surg Relat Res. 2012;24(2):85–90.
18. Cassidy K, Tucker S, Rajak Y, Kia M, Imhauser C, Westrich G, et al. Kinematics of passive flexion following balanced and overstuffed fixed bearing unicondylar knee arthroplasty. Knee. 2015;22(6):542–6.
19. Hernigou P, Deschamps G. Posterior slope of the tibial implant and the outcome of unicompartmental knee arthroplasty. J Bone Joint Surg. 2004;86(3):506–11.
20. Weber P, Schröder C, Schwiesau J, Utzschneider S, Steinbrück A, Pietschmann M, et al. Increase in the tibial slope reduces wear after medial unicompartmental fixed-bearing arthroplasty of the knee. Biomed Res Int. 2017. https://doi.org/10.1155/2015/736826.
21. Jenny J, Boeri C. Unicompartmental knee prosthesis implantation with a non-image-based navigation system: rationale, technique, case-control comparative study with a conventional instrumented implantation. Knee Surg Sports Traumatol Arthrosc. 2002;11(1):40–5.
22. Valenzuela G, Jacobson N, Geist D, Valenzuela R, Teitge R. Implant and limb alignment outcomes for conventional and navigated unicompartmental knee arthroplasty. J Arthroplast. 2013;28(3):463–8.
23. Song E, N M, Lee S, Na B, Seon J. Comparison of outcome and survival after unicompartmental knee arthroplasty between navigation and conventional techniques with an average 9-year follow-up. J Arthroplast. 2016;31(2):395–400.
24. Australian Orthopedic Association: National Joint Replacement Registry. https://aoanjrr.sahmri.com/annual-reports-2016. Accessed 06 June 2017.
25. Jenny J, Ciobanu E, Boeri C. The rationale for navigated minimally invasive unicompartmental knee replacement. Clin Orthop Relat Res. 2007;463:58–62.
26. Casino D, Martelli S, Zaffagnini S, Lopomo N, Iacono F, Bignozzi S, et al. Knee stability before and after total and unicondylar knee replacement: in vivo kinematic evaluation utilizing navigation. J Orthop Res. 2009;27(2):202–7.
27. Schindler O, Scott W, Scuderi G. The practice of unicompartmental knee arthroplasty in the United Kingdom. J Orthop Surg. 2010;18(3):312–9.
28. Mont M. Excellent restoration of alignment using computer-assisted total knee arthroplasty for tibial deformities. JBJS Orthop Highlights Knee Surg. 2013;3(4):e5.
29. Garvin K, Barrera A, Mahoney C, Hartman C, Haider H. Total knee arthroplasty with a computer-navigated saw: a pilot study. Clin Orthop Relat Res. 2012;471(1):155–61.
30. Ong A, Jung K, Orozco F, Delasotta L, Lee D. Total knee arthroplasty using a hybrid navigation technique. J Orthop Surg Res. 2011;6(1):26.
31. Zelle J, Heesterbeek P, De Waal Malefijt M, Verdonschot N. Numerical analysis of variations in posterior cruciate ligament properties and balancing techniques on total knee arthroplasty loading. Med Eng Phys. 2010;32(7):700–7.
32. Baier C, Fitz W, Craiovan B, Keshmiri A, Winkler S, Springorum R, et al. Improved kinematics of total knee replacement following partially navigated modified gap-balancing technique. Int Orthop. 2013;38(2):243–9.

Chapter 6
Robotic UKA

Chumroonkiet Leelasestaporn

Abstract Unicompartmental knee arthroplasty (UKA) is a reliable, although technically challenging, treatment option for osteoarthritis. Successful clinical outcomes depend on accurate implant placement, lower limb alignment, and soft tissue balance intraoperatively. Robot-assisted systems aim to improve the surgical accuracy, precision, and reproducibility of clinical outcomes. Semi-active UKA systems with a minimally invasive approach have been developed and are becoming more interesting. These robotic systems can be either image-based or imageless. Recently, two robotic systems have been approved for UKA by the US Food and Drug Administration: the MAKO Robotic Arm, which is an image-based system, and the Navio Precision Free-Hand Sculptor (PFS), which is an image-free system. Several studies have shown that robotic UKA offers greater accuracy of the mechanical axis, implant positioning, and soft tissue balance than conventional UKA. They concluded that robot-assisted UKA achieved more reproducible, accurate, and precise bone cuts, suggesting that the system could improve surgical survivorship. Although robot-assisted UKA has a high capital cost, some studies have shown that it is cost-effective under the following conditions: (1) centers must perform at least 94 cases annually in (2) patients younger than age 67 years, and (3) the 2-year revision rate does not exceed 1.2%. Thus, these early results and cost-effectiveness analyses seem promising. The limitation of robotic surgery may be the longer learning curve regarding the operative time, although some studies reported that the robot-assisted UKA system significantly decreased the learning curve over that required for UKA with traditional instrumentation.

Keywords Partial knee arthroplasty · Robot · Robotic · UKA · Unicompartmental knee arthroplasty

C. Leelasestaporn
Department of Orthopaedic, Bhumibol Adulyadej Hospital, The Royal Thai Air Force, Bangkok, Thailand
e-mail: chumroonkiet_l@yahoo.com

N. Sugano (ed.), *Computer Assisted Orthopaedic Surgery for Hip and Knee*,
https://doi.org/10.1007/978-981-10-5245-3_6

6.1 Introduction

Unicompartmental knee arthroplasty (UKA) has achieved varying degrees of acceptance within the orthopedic community over the past three decades. During the 1980s, the popularity of UKA was limited because of the difficulty of achieving a well-balanced joint postoperatively [1] and the high incidence of early revision [2]. Many advantages of UKA, compared with total knee arthroplasty (TKA), have been reported, including lower morbidity [3, 4], lower risk of infection [5], less blood loss [6], faster recovery [7], and better postoperative range of knee motion [3, 7]. These are the reasons for the increasing popularity of UKA as a surgical option to isolate medial compartment osteoarthritis of the knee [8]. Some studies have reported the 10-year survivorship of UKA as inferior than that of TKA (85–90% vs. 95%, respectively) [8]. Others showed that UKA performed at high-volume centers had a higher survivorship than those at low-volume centers [9]. Several studies have shown that controlling postoperative leg alignment [10], balancing the soft tissue [11], maintaining the joint line [12, 13], proper component sizing [14], and adequate component fixation [15] could improve the clinical outcomes of UKA. Many advanced technologies have been applied to improve clinical outcomes, reduce complications, improve survivorship, and increase patient satisfaction, including computer navigation, patient-specific cutting guides, semi-customized patient-specific implants, and robot-assisted systems.

6.2 History of Robot-Assisted UKA

In 1992, the system designed by Paul and Bargar made history by being the first robot used clinically in orthopedic surgery [16]. Justin Cobb first introduced robotic assistance in 2000 and first reportd a prospective comparison of a tactile-guided robot-assisted UKA and conventional UKA performed with manual instrumentation [17]. There are currently several computer- and robot-assisted surgical systems that can be classified into three categories: passive, semi-active, and active [18]. *Passive systems* guide surgical instruments by navigation that is completely under the control of surgeons. *Active systems* automatically perform a preprogrammed task under the careful observation of surgeons. *Semi-active systems* require surgeon involvement, but the robotic platform provides feedback to augment the surgeon's control. The surgical procedure is performed by the surgeon under physically constrained movement of the tools to follow the preoperative bone-cut plan. These robotic systems can be either image-based or imageless. In image-based systems, the patient's knee anatomy registration and the preoperative imaging plus planning based on computed tomography (CT) or magnetic resonance imaging (MRI) are accomplished by mapping points on the bone with a digitizer during the operation to instruct the robot where the cutting tool is relative to the patient's knee anatomy. Image-free systems rely on intraoperative registration of the patient's knee anatomy, so the robotic system can create a virtual three-dimensional model.

Table 6.1 System summary of MAKO and Navio PFS

Name	Application	Control	Resection type	Platform	Preop image
MAKO	UKA	Semiautonomous haptic	Burr	Closed	CT images
Navio PFS	UKA	Semiautonomous	Burr	Open	None

To date, two robotic systems have been approved by the US Food and Drug Administration (FDA) for UKA (Table 6.1). The MAKO Robotic Arm Interactive Orthopedic System (Rio; MAKO Surgical Corporation, Fort Lauderdale, FL, USA) is a haptic-guided robotic system introduced in 2005. It was FDA-approved in 2008 and acquired by Stryker in 2013. The Navio Precision Free-Hand Sculptor (PFS) system (Blue Belt Technologies, Plymouth, MN, USA) was FDA-approved in 2012 and acquired by Smith & Nephew in 2014.

6.3 Robotic Systems

6.3.1 Stryker/MAKO Haptic-Guided Robot System (MAKOplasty)

The MAKO system (Fig. 6.1) is a semi-active tactile robotic system with a closed platform and an image-based system that requires preoperative computed tomography (CT) images. These images allow the surgeon to perform preoperative planning for optimal femoral and tibial component sizing and positioning. Intraoperatively, the movement of the robotic arm with a burr is controlled by the surgeon, while the system gives the surgeon real-time tactile feedback during the procedure, allowing the surgeon to adjust component positioning and alignment through a range of motion after intraoperative soft tissue tension registration. The system provides information about leg alignment, component position, and balancing of the soft tissue. The haptic system constrains the movement of the robot arm burr within the bone-cutting area because the surgeon's plan and the robotic arm do not allow bone resection outside the preplanned area.

The accuracy of the MAKO system has been evaluated in several studies (Table 6.2). Pearle and colleagues [19] evaluated the accuracy of the mechanical axis using the MAKO system in patients undergoing medial robot-assisted UKA. They reported that the intraoperative registration required 7.5 min, the duration of the robot-assisted burring was 34.8 min, and the postoperative leg alignment was within 1.6° of the alignment planned intraoperatively. Dunbar and colleagues [20] assessed the accuracy of component positioning of the MAKO system in patients undergoing medial UKA surgery by comparing preoperative and postoperative CT images. They reported that the femoral component was within 0.8 mm and 0.9° in all directions and the tibial component was within 0.9 mm and 1.7° in all directions. Plate and colleagues [11] assessed the accuracy of soft tissue balancing achieved with the MAKO system in patients undergoing medial UKA surgery by comparing the balance plan of the soft tissue tension before and after implantation. The MAKO system

Fig. 6.1 The Stryker/MAKO haptic-guided robot system (MAKOplasty)

Table 6.2 Summary of clinical outcome of the MAKO system [21]

Author	Year	Platform	Outcome summary
Lonner	2009	MAKO	Robotic arm-assisted UKA demonstrated increased accuracy in recreating the posterior tibial slope and coronal tibial alignment
Coon	2009	MAKO	Robotic UKA demonstrated short learning curve and excellent radiographic outcomes (2.5 times improvement in tibial alignment, lower SD)
Jinnah et al.	2009	MAKO	Learning curve of robot-assisted UKA procedures averages 13 cases. The learning cases did not present an increased risk to the patient
Lonner et al.	2010	MAKO	Tibial component alignment was found to be more accurate and less variable for MAKO robotic arm-assisted surgeries compared to those with manual instrumentation
Pearle et al.	2010	MAKO	The planned and intraoperative tibiofemoral angle was within 1°. The postoperative long film axis radiographs were within 1.6°
Citak et al.	2013	MAKO	UKA was more precise using a semi-active robotic system with femoral and tibial component position compared to the manual technique
Jones et al.	2013	MAKO	Robotic arm-assisted UKA resulted in significantly lower postoperative pain and greater functionality as measured by American Knee Scores compared with manual UKA
Coon et al.	2014	MAKO	MAKO UKA had a cumulative revision rate of 1.2% and high patient satisfaction at an average of 29.6 months follow-up
Coon et al.	2015	MAKO	At 2-year follow-up, 92% of patients indicated that they were either very satisfied or satisfied with their robotic arm-assisted UKA procedure
Stuart et al.	2016	MAKO	Robot-assisted surgical procedures with the use of the MAKO RIO lead to improved accuracy of implant positioning compared with conventional unicompartmental knee arthroplasty surgical techniques

quantified soft tissue balance as the millimeters of knee tightness or looseness at 0°, 30°, 60°, 90°, and 110° of flexion. The authors reported that the ligament balancing was accurate within 1 mm at all flexion angles.

6.3.2 Navio Precision Free-Hand Sculptor System

The Navio Precision Free-Hand Sculptor (PFS) (Fig. 6.2) is a handheld, image-free, semi-active, open-platform robotic system. The smart handheld instrument provides freehand sculpting for UKA. The interactive, surgeon-controlled, handheld cutting

Fig. 6.2 The Navio Precision Free-Hand Sculptor (PFS) system

Table 6.3 Summary of clinical outcome of the Navio PFS [21]

Author	Year	Platform	Outcome summary
Gregori et al.	2014	Navio PFS	Postsurgical mechanical axis alignment within 10 of the plan in 91%. Improved Oxford Knee Scores from preoperative to 6 weeks postoperative
Wallace et al.	2014	Navio PFS	Rapid learning curve of an average of 8 (5–11) procedures with the average time over the first 4 cases (tracker placement to trial acceptance) of 64.9 (27–102) min
Simons et al.	2014	Navio PFS	Narrowing learning curve of the Navio system from an initial case duration of 85–48 min after 5 surgeries
Lonner et al.	2015	Navio PFS	Medial UKA achieved accurate implantation of the surgical plan with small errors in implant placement

tool has an end-cutting burr that can extend and retract in the sleeve to remove only the bone, as planned. The Navio PFS robotic system requires intraoperative registration of the patient's knee anatomy by morphing the bony surface with a digitizer to create a three-dimensional virtual model of the knee and soft tissue tension registration data to allow the surgeon to plan optimal implant sizing, implant positioning, and soft tissue balancing. The system continuously tracks the position of the patient's lower limb and the handheld burr by navigation, so it is not necessary for the knee to be held completely rigid during the procedure. It also allows the surgeon to choose a preferred knee position and movement during the procedure. A semi-active system, the Navio PFS robot, monitors the surgeon's movement of the burring tool with safeguards in place to optimize both accuracy and safety via retraction of the burr tip when the edge of the planning bone removal volume is approached.

The accuracy of the Navio PFS system was investigated in several studies (Table 6.3) [21]. A clinical study by Picard et al. [22] reported on 65 patients undergoing medial UKA using Navio. The planned mechanical axis alignment was compared with the postsurgical alignment using full-length, double-stance, weight-bearing radiographs. The postoperative mechanical axis alignment in the coronal plane was within 1° of the intraoperative plan in 91% of the cases. Smith and colleagues [23] also assessed the accuracy of component positioning using the handheld robotic system and reported a maximum rotational error of 3.2°, an angular error of 1.46° in all orientations, and a maximum translation error of 1.18 mm in both the tibial and femoral implants. Lonner and colleagues [24] assessed the accuracy of component positioning of the medial UKA Navio PFS system in a cadaveric

study. The implant position was within the expected target value with low rotational, angular, and translation errors. Similar results were found by Smith and colleagues [23].

6.4 Robot-Assisted vs. Conventional UKA

Several studies compared the accuracy of the robot-assisted and conventional UKA procedures. Cobb and colleagues [25] performed a randomized clinical trial for patients treated undergoing UKA with the Acrobot system, compared with conventional UKA, and assessed differences in the mechanical axis. They reported that the mechanical axis was within 2° in 100% in the group of robot-assisted UKAs but only 40% in the conventional group ($P < 0.001$). Lonner and colleagues [26] compared the tibial component positioning between robot-assisted UKA with the MAKO system and conventional UKA. They found that the variance in tibial slope, tibial component alignment in the coronal plane, and varus/valgus alignment were all greater with conventional UKA than with robot-assisted UKA. Coon and colleagues [27] reported the preliminary results of a multicenter study of 854 patients and found survivorship of 98.9% and a satisfaction rate of 92% at a minimum 2-year follow-up. They suggested that robot-assisted UKA could improve survivorship short term compared with the results of other large conventional UKA cohorts [28]. MacCallum and colleagues compared the tibial baseplate position in a prospective clinical study of patients treated with conventional UKA and others treated with robot-assisted UKA with the MAKO system. They found that robot-assisted UKA was more precise regarding the coronal and sagittal planes and more accurate regarding coronal alignment than conventional UKA [29]. Danielle and colleagues retrospectively compared the polyethylene insert sizes between robotic ($N = 8421$) and conventional ($N = 27{,}989$) UKA, where 8- and 9-mm polyethylene inserts were used in 93.6% and 84.5%, respectively [30]. They concluded that robot-assisted UKA achieved more accurate and precise conservative bone resection than conventional UKA.

6.5 Cost-Effectiveness of Robot-Assisted UKA

One of the major concerns about robot-assisted UKA is its high initial capital cost. Only a few studies have performed cost-effectiveness analyses on UKA. Swank and colleagues [31] reviewed the hospital expenditures and profits associated with robot-assisted knee arthroplasty, citing up-front costs of approximately $800,000. They estimated a mean contribution profit of $5790 for robot-assisted UKA per case, assuming an inpatient/outpatient ratio of 1:3. Based on this study, they proposed that the capital cost of robot-assisted UKA could be recovered within as short a time as 2 years when 50, 70, and 90 cases were performed using robot-assisted

UKA during the first 3 consecutive years. Moschetti and colleagues [32] published the first 2-year follow-up study of robot-assisted UKA based on the aforementioned data from the MAKO system. They assumed an initial capital expenditure with an annual servicing cost of 10% (discounted annually) for 4 years, resulting in the total cost of the robotic system. Sensitivity analysis showed that robot-assisted UKA is cost-effective under the following conditions: (1) centers perform at least 94 cases annually in (2) patients who were <67 years of age, and (3) the 2-year revision rate did not exceed 1.2%. Based on these studies, the early results and cost-effectiveness analyses of robot-assisted UKA seem promising.

6.6 Discussion

Robotics may provide a tool to assist the surgeon plan an operation and increase the accuracy of intraoperative implant placement. Robotic tools have the potential to make bone preparation easier, quicker, and more accurate. Semi-active systems have been more interesting, and their development is increasing, especially those for UKA with a minimally invasive approach. The limitation of robotic surgery may be that it has a longer operative time during the learning curve, although some studies have shown that the robotic system significantly decreases the learning curve compared with that for UKAs using traditional instrumentation [33].

The learning curve of the MAKO robot-assisted UKA procedure averaged 13 cases, and the patients treated during the learning processes did not experience any increased risk [34]. The Navio system demontrated a fairly raapid learning curve of an average of 8 procedures (range 5–11) with the average time over the first 4 cases (tracker placement to trial acceptance) of 64.9 minutes (range 27–102) and another study narrowed the learning curve of the Navio system from an initial case duration of 85 minutes to 48 minutes after 5 surgies [35]. The strength of the MAKO system is that it is image-based, allowing surgeons to plan the implant size accurately prior to the surgery, thereby avoiding intraoperative planning, although the patient must bear the additional cost of, and time for, the preoperative CT scan.

The MAKO system is a haptic device, with the surgeon having to manually move the robotic arm that is attached to a high-speed burr. The haptic control system, however, allows the high-speed burr to remove only the bone, which had been determined during the preoperative planning.

The strength of the Navio PFS system is that it is image-free, thereby avoiding radiation exposure and the cost of a preoperative CT scan. Another advantage of the Navio PFS system is its open platform and compatibility with multiple implant designs, which allows surgeons the flexibility to choose among preferable implants (although its acquisition by Smith & Nephew may result in changing it to a closed platform). This system places control of the robot in a handpiece (rather than a robotic arm), which is lighter, smaller, handheld, and more portable than the robotic arm in the MAKO system. Because Navio PFS is an image-free system, the accuracy of intraoperative registration using a morphing technique depends on the expe-

rience of the surgeon. Incorrect registration could lead to an incorrect plan and could have potentially calamitous results.

6.7 Conclusion

Robotic UKA has been proven to improve the accuracy and precision of component positioning and soft tissue balance to create the optimal kinematics of UKA. The new robot-assisted UKA is potentially superior to conventional UKA. In the future, robotic surgery may become a valuable adjunct to the surgeon for optimizing patient-specific arthroplasty. The trend toward using robotic UKA is increasing the number of procedures. As new technology continues to be incorporated into practice, however, more studies of robotic UKA are needed to assess its additional value of providing functional outcomes, long-term surgical survivorship, and cost-effectiveness analysis.

References

1. Jamali AA, Scott RD, Rubash HE, Freiberg AA. Unicompartmental knee arthroplasty: past, present, and future. Am J Orthop (Belle Mead NJ). 2009;38(1):17–23.
2. Insall J, Aglietti P. A five to seven-year follow-up of unicondylar arthroplasty. J Bone Joint Surg Am. 1980;62(8):1329–37.
3. Newman JH, Ackroyd CE, Shah NA. Unicompartmental or total knee replacement? Five-year results of a prospective, randomised trial of 102 osteoarthritic knees with unicompartmental arthritis. J Bone Joint Surg Br. 1998;80(5):862–5.
4. Watanabe T, Abbasi AZ, Conditt MA, Cristopher J, Kreuzer S, Otto JK, Banks SA. In vivo kinematics of a robot-assisted uni-and multi-compartment knee arthroplasty. J Orthop Sci. 2014;19(4):552–7.
5. Robertson O, Borgquist L, Knutson K, Lewold S, Lidgren L. Use of unicompartmental instead of tricompartmental prostheses were compared with 10,624 primary medial or lateral unicompartmental prostheses. Acta Orthop Scand. 1999;70(2):170–5.
6. Schwab P-E, Lavand'homme P, Yombi JC, Thienpont E. Lower blood loss after unicompartmental than total knee arthroplasty. Knee Surg Sports Traumatol Arthrosc. 2015;23(12):3494–500.
7. McAllister CM. The role of unicompartmental knee arthroplasty versus total knee arthroplasty in providing maximal performance and satisfaction. J Knee Surg. 2008;21(4):286–92.
8. Borus T, Thornhill T. Unicompartmental knee arthroplasty. J Am Acad Orthop Surg. 2008;16(1):9–18.
9. Badly M, Espehaug B, Indrekvam K, Havelin LI, Furnes O. Higher revision risk for unicompartmental knee arthroplasty in low-volume hospitals. Acta Orthop. 2014;85(4):342–7.
10. Vass M, Del Regno C, D'Amelio A, Viaggiano D, Corona K, Schiavone Panni A. Minor varus alignment provides better results than neutral alignment in medial UKA. Knee. 2015;22(2):117–21.
11. Plate JF, Mofidi A, Mannava S, Smith BP, Lang JE, Poehling GG, Conditt MA, Jinnah RH. Achieving accurate ligament balancing using robotic-assisted unicompartmental knee arthroplasty. Adv Orthop. 2013;2013:837167.
12. Niinimaki TT, Murray DW, Partanen J, Pajala A, Leppilahti JI. Unicompartment knee arthroplasties implanted for osteoarthritis with partial loss of joint space have higher re-operation rates. Knee. 2011;18(6):432–5.
13. Zuiderbaan HA, Khamaisy S, Thein R, Nawabi DH, Pearle AD. Congruence and joint space width alternations of medial compartment following lateral unicompartmental knee arthroplasty. Bone Joint J. 2015;97-B(1):50–55.31.

14. Chau R, Gulati A, Pandit H, Beard DJ, Price AJ, Dodd CA, Gill HS, Murray DW. Tibial component overhang following unicompartmental knee replacement-does it matter? Knee. 2009;16(5):310–3.
15. Kendrick BJ, Kaptein BL, Valstar ER, Gill HS, Jackson WF, Dodd CA, Price AJ, Murray DW. Cemented versus cementless Oxford unicompartmental knee arthroplasty using radiostereometric analysis: a randomised controlled trial. Bone Joint J. 2015;97-B(2):185–91.
16. Jacofsky DJ, Allen M. Robotics in arthroplasty: a comprehensive review. J Arthroplast. 2016;31(10):2353–63.
17. Bargar WL. Robots in orthopaedic surgery: past, present, and future. Clin Orthop Relat Res. 2007;463:31–6.
18. DiGioia AM III. What is computer assisted orthopaedic surgery? Clin Orthop Relat Res. 1998;(354):2–4.
19. Pearle AD, O'Loughlin PF, Kendoff DO. Robot-assisted unicompartment knee arthroplasty. J Arthroplast. 2010;25(2):230–7.
20. Dunbar NJ, Roche MW, Park BH, Branch SH, Conditt MA, Banks SA. Accuracy of dynamic tactile-guided unicompartment knee arthroplasty. J Arthroplast. 2012;27(5):803–8.
21. Jacofsky DJ, Allen M. Robotic in arthroplasty: a comprehensive review. J Arthroplast. 2016;31:2353–63.
22. Picard F, Gregori A, Bellemans J, et al. Handheld robot-assisted unicondylar knee arthroplasty: a clinical review. Bone Joint J. 2014;96-B(Suppl 16):25.
23. Smith JR, Riches PE, Rowe PJ. Accuracy of a freehand sculpting tool for unicondylar knee replacement. Int J Med Robot. 2014;10(2):162–9.
24. Lonner JH, Smith JR, Picard F, Hamlin B, Rowe PJ, Riches PE. High degree of accuracy of a novel image-free handheld robot for unicondylar knee arthroplasty in a cadaveric study. Clin Orthop Relat Res. 2015;473(1):206–12.
25. Cobb J, Henckel J, Gomes P, Harris S, Jakopec M, Rodriguez F, Barrett A, Davies B. Hands-on robotic unicompartmental knee replacement: a prospective, randomised controlled study of the acrobot system. J Bone Joint Surg Br. 2006;88(2):188–97.
26. Lonner JH, John TK, Conditt MA. Robotic arm-assisted UKA improves tibial component alignment: a pilot study. Clin Orthop Relat Res. 2010;468(1):141–6.
27. Coon T, Roche M, Pearle AD, Dounchis J, Borus T, Buechel F Jr. Two year survivorship of robotically guided unicompartmental knee arthroplasty. Paper presented at: International Society for technology in arthroplasty 26th Annual Congress 16–19, 2013. Palm Beach, FL.
28. Pandit H, Jenkins C, Gill HS, Barker K, Dodd CA, Murray DW. Minimally invasive Oxford phase 3 unicompartmental knee replacement: results of 1000 cases. J Bone Joint Surg Br. 2011;93(2):198–204.
29. MacCallum KP, Danoff JR, Geller JA. Tibial baseplate positioning in robotic-assisted and conventional unicompartmental knee arthroplasty. Eur J Orthop Surg Traumatol. 2016;26(1):93–8.
30. Ponzio DY, Lonner JH. Robotic technology produces more conservative tibial resection than conventional techniques in UKA. Am J Orthop (Belle Mead NJ). 2016;45(7):E465–8.
31. Swank ML, Alkire M, Conditt M, Lonner JH. Technology and cost-effectiveness in knee arthroplasty: computer navigation and robotics. Am J Orthop (Belle Mead NJ). 2009;38(2 Suppl):32–6.
32. Moschetti WE, Konopka JF, Rubash HE, Genuario JW. Can robot-assisted unicompartmental knee arthroplasty be cost-effective? A Markov decision analysis. J Arthroplast. 2016;31(4):759–65.
33. Hamilton WG, Ammeen D, Engh CA Jr, Engh GA. Learning curve with minimally invasive unicompartmental knee arthroplasty. J Arthroplast. 2010;25(5):735–40.
34. Jinnah R, Horowitz S, Lippincott C, et al. The learning curve of robotically assisted UKA. 56th Annual Meeting of the Orthopaedic Research Society; p. 407.
35. Cobb J, Henckel J, Gomes P, et al. Hands-on robotic unicompartmental knee replacement: a prospective, randomised controlled study of the acrobot system. J Bone Joint Surg Br. 2006;88(2):188–97.

Part II
Computer-Assisted THA, Hip Osteotomy, and Tumor Surgery

Chapter 7
Pelvic and Femoral Coordinates and Implant Alignment Representations in THA

Masaki Takao, Takashi Sakai, Hidetoshi Hamada, and Nobuhiko Sugano

Abstract For three-dimensional study of total hip arthroplasty, including preoperative planning and biomechanical studies, it is important to indicate the systems used to define the cup and stem alignment and the pelvic and femoral coordinate systems that are used. Cup alignment may be represented radiographically, operatively, or anatomically. Stem alignment is based on the representation of stem anteversion. The pelvis may be defined using the anatomical coordinate system, the functional coordinate system, or the coordinate system recommended by the International Society of Biomechanics (ISB). The anatomical coordinate system uses the anterior pelvic plane as the reference plane, which consists of the bilateral anterosuperior iliac spines and the midpoint of the bilateral pubic tubercles. The functional coordinate system incorporates the pelvic sagittal inclination, or pelvic tilt, in the supine position. The ISB pelvic coordinate system uses the plane consisting of the bilateral anterosuperior iliac spines and the midpoint of the bilateral posterosuperior iliac spines. The two major femoral coordinate systems are the femoral retrocondylar coordinate system and the ISB femoral coordinate system. The femoral retrocondylar coordinate system uses the retrocondylar plane as a reference plane, which consists of the posterior edge of the great trochanter and the bilateral posterior condyles. The ISB femoral coordinate system uses the plane consisting of the femoral head center and the bilateral femoral epicondyles as a reference plane. We must recognize that these differences in the representation of cup and stem alignment and the reference bone coordinate system significantly influence the clinical outcome of total hip arthroplasty whether using three-dimensional planning, navigation, or robotics. Such misunderstanding could result in an incorrect clinical interpretation of biomechanical analysis results.

M. Takao, M.D., Ph.D. (✉) • N. Sugano, M.D., Ph.D.
Department of Orthopaedic Medical Engineering, Osaka University Graduate School of Medicine, 2-2 Yamadaoka, Suita, 565-0871 Osaka, Japan
e-mail: masaki-tko@umin.ac.jp

T. Sakai, M.D., Ph.D. • H. Hamada, M.D., Ph.D.
Department of Orthopaedic Surgery, Osaka University Graduate School of Medicine, 2-2 Yamadaoka, Suita, 565-0871 Osaka, Japan

N. Sugano (ed.), *Computer Assisted Orthopaedic Surgery for Hip and Knee*,
https://doi.org/10.1007/978-981-10-5245-3_7

Keywords Cup alignment · Stem alignment · Pelvic coordinate system · Femoral coordinate system · Anterior pelvic plane · Pelvic tilt · Femoral retrocondylar plane International Society of Biomechanics

7.1 Introduction

Plain radiography is the standard imaging modality for diagnosing and treating patients in the daily practice of orthopedics. We measure several anatomical parameters, such as Sharp's angle, the center-edge angle, and the femoral neck-shaft angle, to quantify bone shape on radiographs for diagnosis and posttreatment evaluation. We also use plain radiography for preoperative templating during total hip arthroplasty (THA). We know the limitations of radiographic measurements or templating because the magnification of radiographs is variable and bone shapes appear differently depending on the rotational position of the bone against the radiographic plane. To overcome these limitations of plain radiography for preoperative planning of THA, a three-dimensional (3D) planning based on computed tomography (CT) images has been shown to provide more accurate information for predicting implant size and adjusting to achieve the proper postoperative leg length and offset [1, 2]. Oversized implants may result in intraoperative fractures, and undersized implants may lead to early migration and fixation failure. Therefore, accurate prediction of implants is important for the success of THA and may reduce the implant inventory and cost. Moreover, CT images allow 3D simulation of prosthetic and bone impingement-free hip range of motion (ROM) [3–8].

Recent advancements in computer technology have enabled us to perform 3D planning and simulation more easily, and the number of articles published on this subject is increasing. However, the methods used to represent the alignment of cup and stem, the ROM, and a reference bone coordinate system are not standardized, making research results confusing because of the different methods used to represent the measurements in each study. As different reference bone coordinate systems result in different implant alignments and ROM, it is important to recognize the existing bone coordinate systems and which system is appropriate for each analysis. It is also important to recognize the methods used to represent implant alignment.

7.2 Methods for Representing Implant Alignment

7.2.1 Cup Alignment

The alignment of the cup is described by combining the inclination and anteversion angles. Murray [9] used three methods to represent cup alignment: radiographic, anatomical, and operative (Fig. 7.1). These cup alignment representation

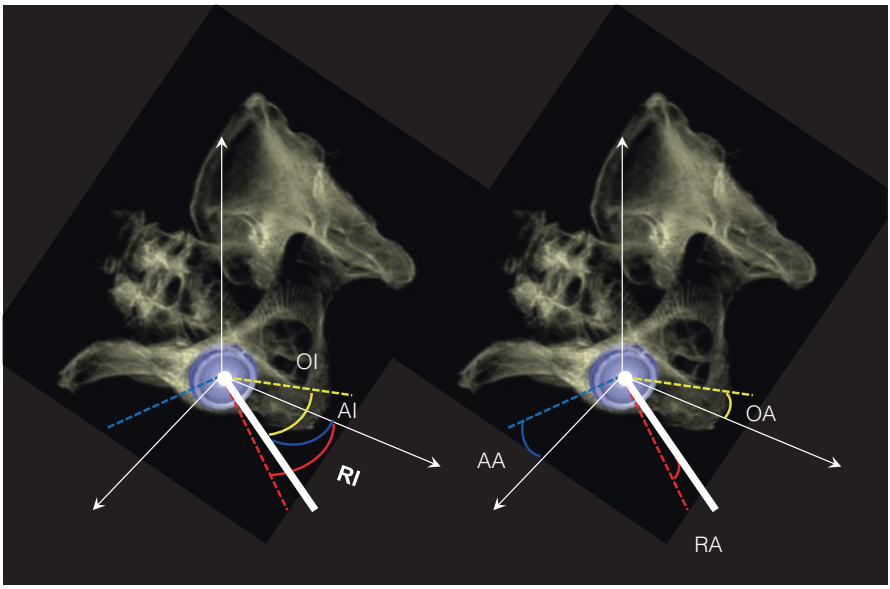

Fig. 7.1 Three definitions of cup inclination and anteversion. The white line represents the cup's polar axis. The broken red line represents the projected cup's polar axis on the coronal plane. The broken yellow line represents the projected cup's polar axis on the sagittal plane. The broken blue line represents the projected cup's polar axis on the transverse plane. *RA* radiographic anteversion, *AA* anatomical anteversion, *OA* operative anteversion, *RI* radiographic inclination, *OI* operative inclination (Reprinted with permissions from [10])

methods are defined by the projected plane of the cup's polar axis, which passes through the cup's center and is perpendicular to the cup's opening plane (Fig. 7.1).

The radiographic definition corresponds to the cup's inclination angle and anteversion angle measured on an anteroposterior radiograph of the hip joint. The cup opening circle is projected as an elliptical shape on the anteroposterior radiograph, the long and short axes of which are used to measure the radiographic inclination (RI) and anteversion of the cup. The RI is measured as the angle between a horizontal line and the cup's long axis [11, 12]. The radiographic anteversion (RA) angle is calculated from the ratio of the short axis and the long axis using a trigonometric function [11, 12].

The anatomical inclination (AI) angle is the angle between the cup's polar axis and the vertical axis. The anatomical anteversion (AA) angle is the angle between the horizontal axis and the cup's polar axis projected in the transverse plane.

The operative definition corresponds to the inclination and the anteversion angle of the cup from the surgeon's viewpoint. The operative inclination (OI) angle is the angle between the cup's polar axis and the sagittal plane. The operative anteversion

(OA) angle is the angle between the vertical axis and the cup polar axis projected in the sagittal plane.

Conversion formulas for radiographic, anatomical, and operative cup alignment angles are as follows [9]:

Conversion formula from RI and RA to OI and OA:

$$\mathrm{Sin(OI)} = \mathrm{Sin(RI)} \times \mathrm{Cos(RA)}\ \mathrm{Tan(OA)} = \mathrm{Tan(RA)} \div \mathrm{Cos(RI)}$$

Conversion formula from AI and AA to OI and OA:

$$\mathrm{Sin(OI)} = \mathrm{Sin(AI)} \times \mathrm{Cos(AA)}\ \mathrm{Tan(OA)} = \mathrm{Sin(AA)} \times \mathrm{Tan(AI)}$$

Conversion formula from OI and OA to AI and AA:

$$\mathrm{Cos(AI)} = \mathrm{Cos(OI)} \times \mathrm{Cos(OA)}\ \mathrm{Tan(AA)} = \mathrm{Sin(OA)} \div \mathrm{Tan(OI)}$$

Conversion formula from RI and RA to AI and AA:

$$\mathrm{Cos(AI)} = \mathrm{Cos(RI)} \times \mathrm{Cos(RA)}\ \mathrm{Tan(AA)} = \mathrm{Tan(RA)} \div \mathrm{Sin(RI)}$$

Conversion formula from OI and OA to RI and RA:

$$\mathrm{Tan(RI)} = \mathrm{Tan(OI)} \div \mathrm{Cos(OA)}\ \mathrm{Sin(RA)} = \mathrm{Sin(OA)} \times \mathrm{Cos(OI)}$$

Conversion formula from AI and AA to RI and RA:

$$\mathrm{Tan(RI)} = \mathrm{Tan(AI)} \times \mathrm{Cos(AA)}\ \mathrm{Sin(RA)} = \mathrm{Sin(AA)} \times \mathrm{Sin(AI)}$$

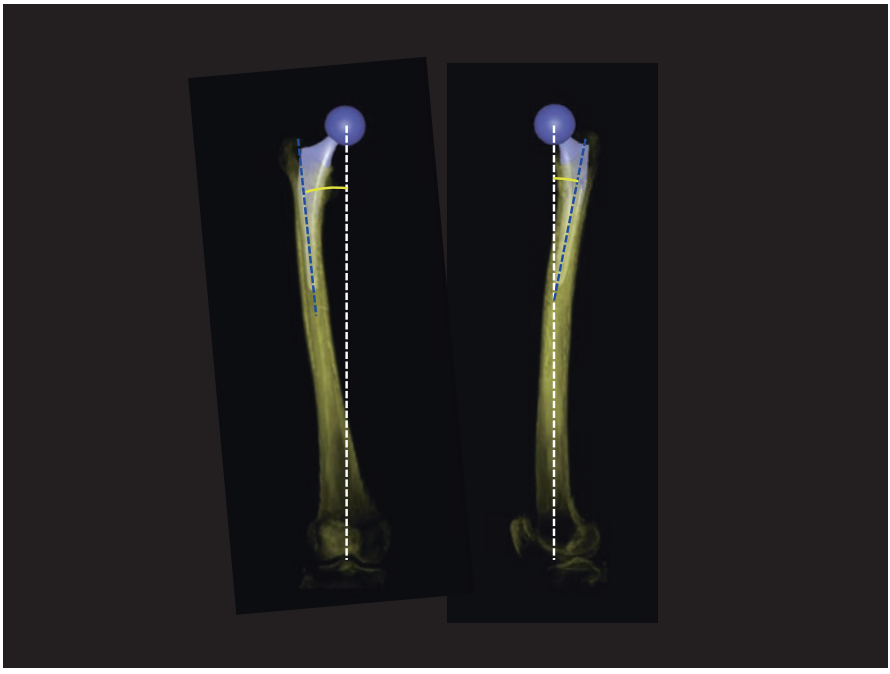

Fig. 7.2 A stem implanted in the femoral canal tilts posteriorly and in valgus position against the mechanical axis, passing through the femoral head center to the knee's center (white broken line) because of femoral lateral and anterior bowing. The broken blue line represents the stem body's axis (Reprinted with permissions from [10])

7.2.2 *Stem Alignment*

The alignment of the stem is described by three angles: the anteversion angle, posterior tilting angle, and varus (or valgus) angle. The stem implanted in the femoral canal is tilted posteriorly, and in valgus position against the mechanical axis passing through the femoral head center to the knee center because of femoral lateral and anterior bowing (Fig. 7.2) [13, 14]. There is no standardized term used to indicate the sagittal alignment of the stem (sagittal stem tilt angle, stem flexion angle, and stem extension angle have been used in the literature [13–16]).

There are two methods of representing stem alignment according to the stem anteversion (Fig. 7.3). In one method, the sagittal and coronal alignments are described as alignments of the stem body axis projected in the sagittal and coronal planes against the vertical and horizontal axes of the reference femoral coordinate system. Stem anteversion is described as the angle between the horizontal axis and the stem neck axis projected in the transverse plane. With the other method, stem alignment is described in the Euler angle representation in the following two orders:

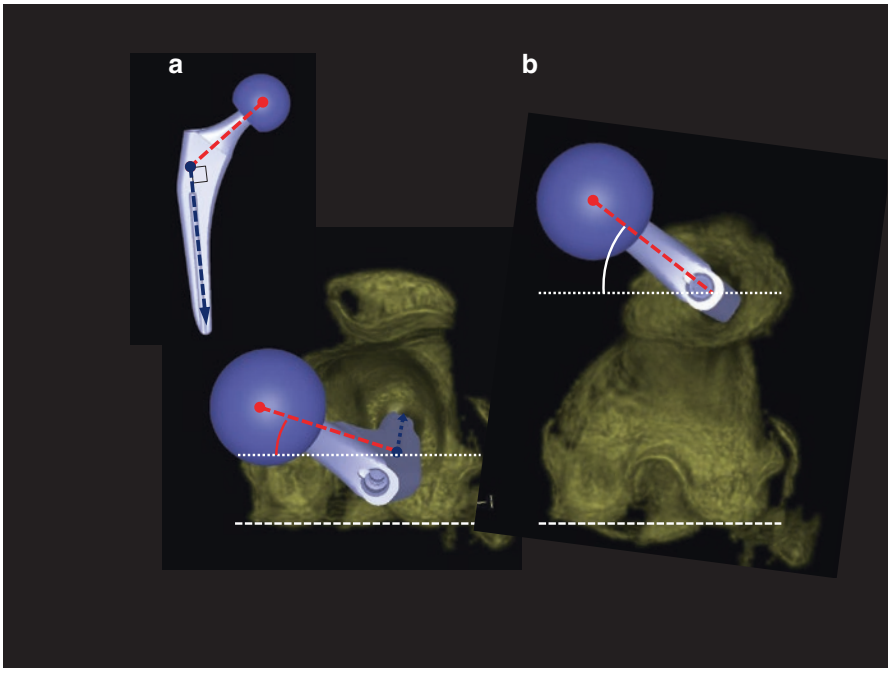

Fig. 7.3 Differences in stem anteversion angles measured according to two definitions. The red broken line represents the stem neck's axis. The broken blue line represents the stem body's axis. The stem anteversion measured as a rotational angle of the stem neck's axis around the stem body's axis (**b**) is larger than the stem's anteversion angle measured in the femoral retrocondylar coordinate system (**a**) (Reprinted with permissions from [10])

(1) posterior tilt, varus position, and anteversion or (2) varus position, posterior tilt, and anteversion. With this method, stem anteversion is described as a rotational angle around the stem body axis.

7.3 Bone Coordinate Systems

7.3.1 Pelvic Coordinate Systems

The three major pelvic coordinate systems are the anatomical coordinate system, the functional coordinate system, and the International Society of Biomechanics (ISB) coordinate system [17]. The anatomical coordinate system uses the anterior pelvic plane (APP), consisting of the bilateral anterosuperior iliac spine (ASIS), and the midpoint of the bilateral pubic tuberosities as the coronal plane (Fig. 7.4) [18, 19]. This coordinate system is useful for analyzing pelvic morphology to standardize the position of the pelvis [5, 6], but it is not optimal for representing cup alignment or ROM of the hip, as the sagittal inclination of the APP varies among patients in the supine position [20–23]. The average angle of the pelvic sagittal inclination in the supine position is reportedly 4°–10° (range −37° to +30°) [20–23].

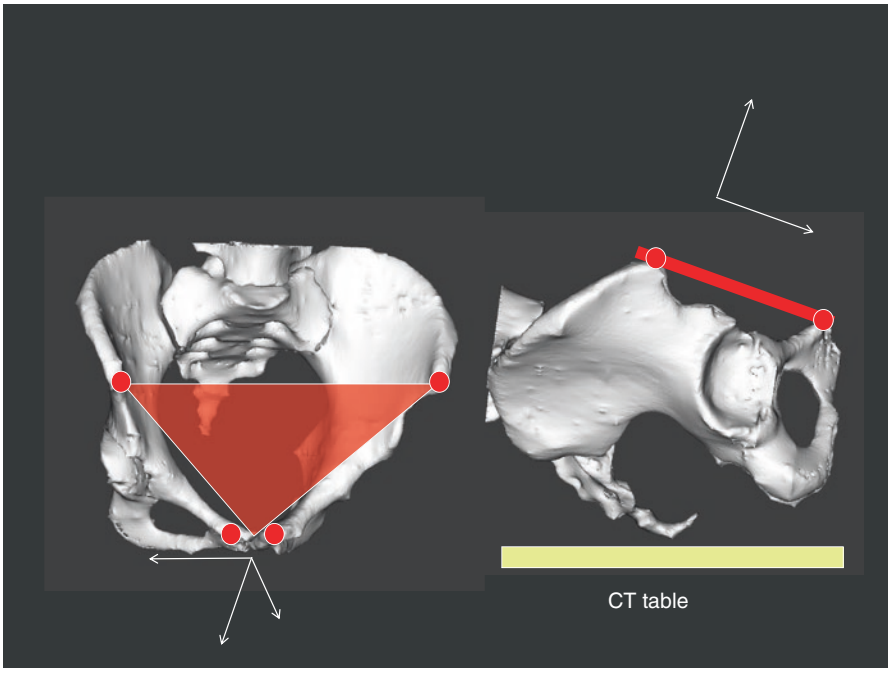

Fig. 7.4 Anatomical pelvic coordinate system (Reprinted with permissions from [10])

The functional coordinate system incorporates the pelvic sagittal inclination in the supine position. We recommend the functional coordinate system for 3D planning and navigation for the following four reasons. (1) Pelvic sagittal inclination varies among patients, even in the supine position. (2) In 90% of patients before THA, the difference in the pelvic sagittal inclination angle in the supine versus the standing position is within 10° [20]. (3) The ROM of the hip during daily living activities is not affected by changes in the pelvic tilt while standing [24]. The pelvis in supine position can be assumed to be the neutral, zero position. (4) Pelvic tilt in the supine position has shown no significant changes during a 10-year period after THA [25].

The functional pelvic coordinate system has three subtypes, each with different definitions of the horizontal axis and the anteroposterior axis. Subtype 1 is a simple system that incorporates the sagittal inclination of the APP in the supine position (Fig. 7.5) [3, 5, 6]. The horizontal axis is the line passing through the bilateral ASIS. Subtype 2 uses the line passing through the bilateral inferior edges of the acetabular fossae as the horizontal axis, which corresponds with the line passing through the bilateral tips of the teardrop shadows on an anteroposterior radiograph of the hip (Fig. 7.6) [26]. In subtype 3, the anteroposterior axis passes through the center of the first sacral vertebral body and the pubic symphysis, and the horizontal plane is in contact with the bilateral ischial tuberosities (Fig. 7.7) [27–29].

The ISB pelvic coordinate system, proposed in 2002, uses the plane consisting of the bilateral ASIS and the midpoint of the bilateral posterosuperior iliac

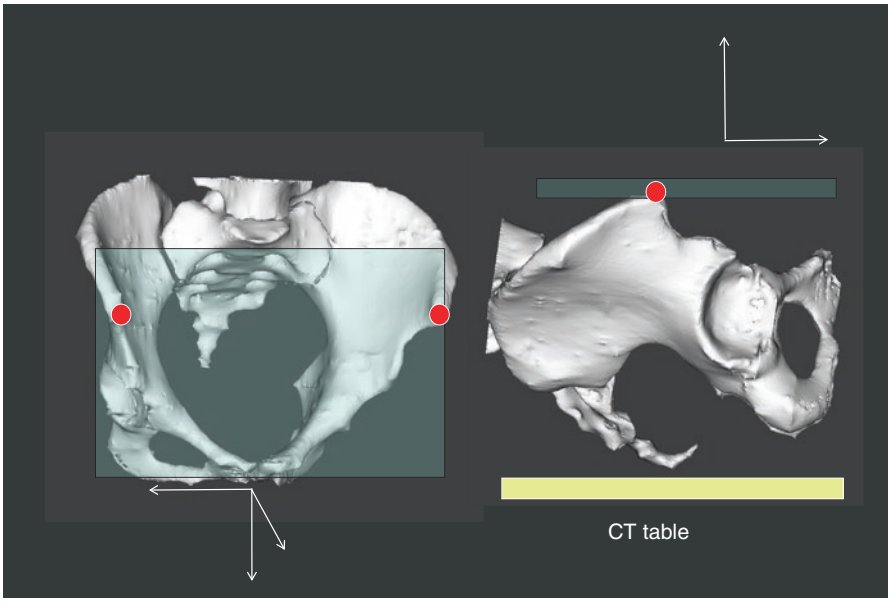

Fig. 7.5 Subtype 1 of the functional pelvic coordinate system (Reprinted with permissions from [10])

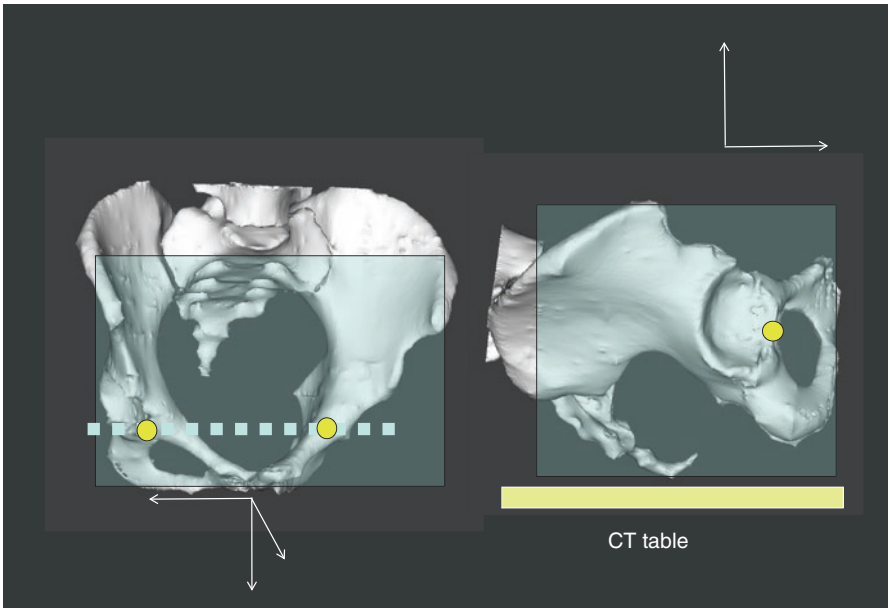

Fig. 7.6 Subtype 2 of the functional pelvic coordinate system (Reprinted with permissions from [10])

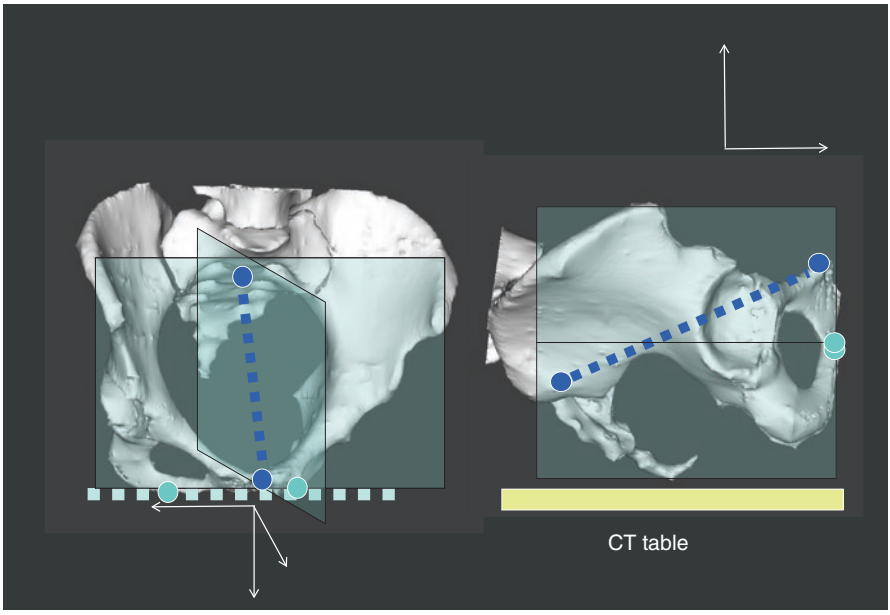

Fig. 7.7 Subtype 3 of the functional pelvic coordinate system (Reprinted with permissions from [10])

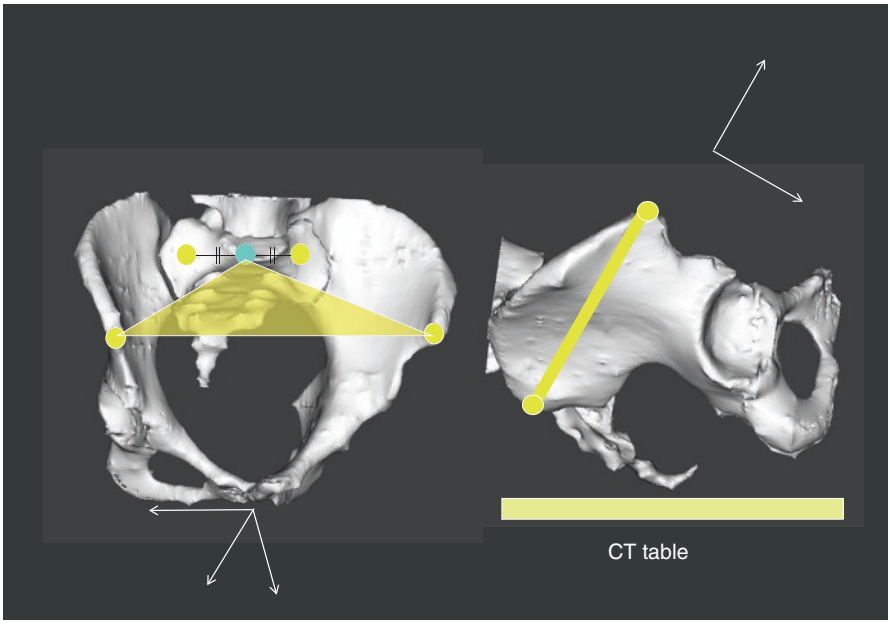

Fig. 7.8 Pelvic coordinate system recommended by the International Society of Biomechanics (Reprinted with permissions from [10])

spine (Fig. 7.8) [30]. This system uses landmarks that can be detected easily on the skin, which is useful during motion analysis using optical markers and cameras. However, this pelvic coordinate system does not reflect variations in pelvic sagittal inclination, so it is not optimal for representing cup alignment and ROM of the hip.

7.3.2 Femoral Coordinate Systems

There are two main femoral coordinate systems. One is the femoral retrocondylar coordinate system, which uses the retrocondylar plane consisting of the posterior edge of the great trochanter and the bilateral posterior condyles [31, 32]. The retrocondylar plane corresponds to the tabletop plane on which the femoral bone is placed, so it is also called the tabletop plane.

The femoral retrocondylar coordinate system is divided into two subtypes according to the definition of the vertical axis. Subtype 1 uses the projected line on the retrocondylar plane of the line passing through the trochanteric fossa and the most distal point of the intercondylar notch (Fig. 7.9) [13, 27–29, 33]. This construction is suitable for a reference coordinate system of stem alignment because it can be reconstructed even after THA [13]. Subtype 2 uses the projected line on the retrocondylar plane of the line that passes through the femoral head center and

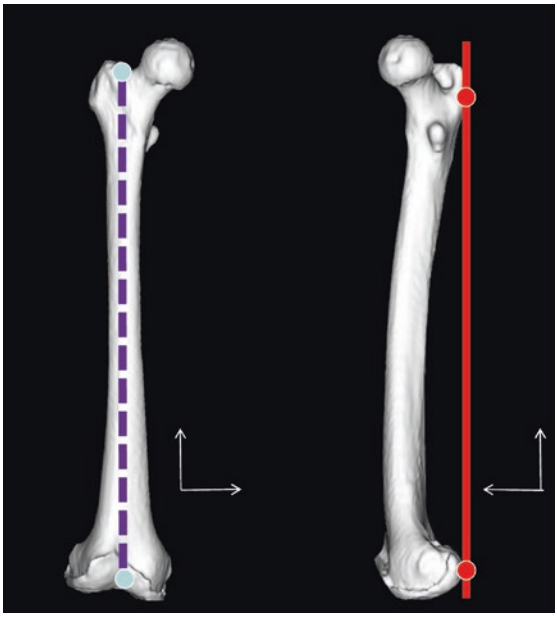

Fig. 7.9 Subtype 1 of the femoral posterior condylar coordinate system (Reprinted with permissions from [10])

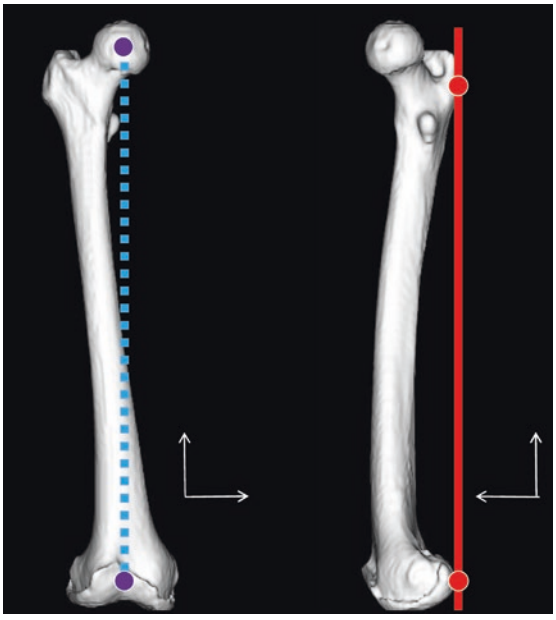

Fig. 7.10 Subtype 2 of the femoral posterior condylar coordinate system (Reprinted with permissions from [10])

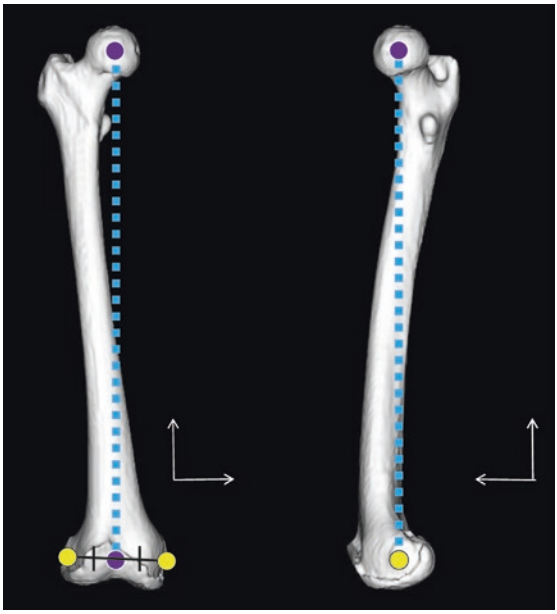

Fig. 7.11 Femoral coordinate system recommended by the International Society of Biomechanics (Reprinted with permissions from [10])

the most distal point of the intercondylar notch (Fig. 7.10) [3, 5, 6, 14]. This system is suitable for ROM analysis because the line passing through the femoral head center and the knee center is an appropriate reference line of hip joint movement [3, 5, 6].

The ISB femoral coordinate system uses the plane consisting of the femoral head center and the bilateral femoral epicondyles and the line passing through the femoral head center to the midpoint of the bilateral epicondyles as the vertical axis (Fig. 7.11) [30].

The definitions of the knee center are variable in the literature. They include the distal point of the intercondylar notch [34], the point of insertion of the posterior cruciate ligament [35], the midpoint of the bilateral femoral epicondyles [30], and the midpoint of the centers of the spheres approximated to the bilateral femoral condyles [36]. There is no consensus as to which definition is appropriate for 3D analysis of THA.

7.4 Conclusion

During 3D studies of THA, including those used for preoperative planning and biomechanical studies, it is important to indicate clearly which definitions of cup and stem alignment and which pelvic and femoral coordinate systems are used. The

three methods used to represent cup alignment are radiographic, operative, and anatomical alignments. The two methods of representing stem alignment are based on different representations of stem anteversion. There are three major ways to consider pelvic coordination, including the use of the anatomical coordinate system, the functional coordinate system, and the ISB coordinate system. The two major femoral coordinate systems are the femoral retrocondylar coordinate system and the ISB coordinate system.

We must recognize that these differences in the representation of cup and stem alignment and the reference bone coordinate systems significantly influence the clinical outcome of THA, whether using 3D planning, navigation, or robotics. Any misrepresentation could lead to incorrect clinical interpretation of biomechanical analysis results.

Acknowledgments The content of this chapter was written according to the guidelines of the 3D evaluation method of THA proposed in 2014 by the working group of the Japanese Society of Computer-Assisted Orthopedic Surgery (CAOS Japan). The authors thank the following members of the working group: Mitsuhiko Ikebuchi, Yutaka Inaba, Hiroyoshi Iwaki, Hironori Kaneko, Tokumi Kanemura, Masaaki Matsubara, Hidekazu Matsuda, Hidenobu Miki, Yukihide Minoda, Shigeru Mitani, Hiromasa Miura, Nobuo Nakamura, Takashi Nishii, Hirotsugu Ohashi, Takashi Sakai, Takashi Sato, Naofumi Shiota, Nobuhiko Sugano, Jun Takahashi, Masaki Takao, Ichiro Tatsumi, Kunihiko Tokunaga, and Shigeru Yanagimoto.

References

1. Sariali E, Mouttet A, Pasquier G, Durante E, Catone Y. Accuracy of reconstruction of the hip using computerised three-dimensional pre-operative planning and a cementless modular neck. J Bone Joint Surg Br. 2009;91(3):333–40. https://doi.org/10.1302/0301-620x.91b3.21390.
2. Sugano N, Ohzono K, Nishii T, Haraguchi K, Sakai T, Ochi T. Computed-tomography-based computer preoperative planning for total hip arthroplasty. Comput Aided Surg. 1998;3(6):320–4. https://doi.org/10.1002/(sici)1097-0150(1998)3:6<320::aid-igs6>3.0.co;2-o.
3. Hamada H, Takao M, Nakahara I, Sakai T, Nishii T, Sugano N. Hip range-of-motion (ROM) is less than normal after rotational acetabular osteotomy for developmental dysplasia of the hip: a simulated ROM analysis. J Orthop Res. 2016;34(2):217–23. https://doi.org/10.1002/jor.23024.
4. Miki H, Yamanashi W, Nishii T, Sato Y, Yoshikawa H, Sugano N. Anatomic hip range of motion after implantation during total hip arthroplasty as measured by a navigation system. J Arthroplast. 2007;22(7):946–52. https://doi.org/10.1016/j.arth.2007.02.004.
5. Nakahara I, Takao M, Sakai T, Miki H, Nishii T, Sugano N. Three-dimensional morphology and bony range of movement in hip joints in patients with hip dysplasia. Bone Joint J. 2014;96-b(5):580–9. https://doi.org/10.1302/0301-620x.96b5.32503.
6. Nakahara I, Takao M, Sakai T, Nishii T, Yoshikawa H, Sugano N. Gender differences in 3D morphology and bony impingement of human hips. J Orthop Res. 2011;29(3):333–9. https://doi.org/10.1002/jor.21265.
7. Miki H, Kyo T, Kuroda Y, Nakahara I, Sugano N. Risk of edge-loading and prosthesis impingement due to posterior pelvic tilting after total hip arthroplasty. Clin Biomech (Bristol, Avon). 2014;29(6):607–13. https://doi.org/10.1016/j.clinbiomech.2014.05.002.

8. Miki H, Kyo T, Sugano N. Anatomical hip range of motion after implantation during total hip arthroplasty with a large change in pelvic inclination. J Arthroplast. 2012;27(9):1641–1650. e1641. https://doi.org/10.1016/j.arth.2012.03.002.
9. Murray DW. The definition and measurement of acetabular orientation. J Bone Joint Surg Br. 1993;75(2):228–32.
10. Takao M, Sugano N. Current issues of three-dimensional evaluation of total hip arthroplasty. Rinsho Seikei Geka. 2015;50(8):765–71.
11. Widmer KH. A simplified method to determine acetabular cup anteversion from plain radiographs. J Arthroplast. 2004;19(3):387–90.
12. McLaren RH. Prosthetic hip angulation. Radiology. 1973;107(3):705–6. https://doi.org/10.1148/107.3.705.
13. Abe H, Sakai T, Takao M, Nishii T, Nakamura N, Sugano N. Difference in stem alignment between the direct anterior approach and the posterolateral approach in total hip arthroplasty. J Arthroplast. 2015;30(10):1761–6. https://doi.org/10.1016/j.arth.2015.04.026.
14. Takao M, Nishii T, Sakai T, Nakahara I, Shiomi T, Tsuda K, Yabuda K, Iwana D, Kitada M, Nakamura N, Yoshikawa H, Sugano N The effect of femoral anterolateral bowing on stem alignment in THA. In: O'Keefe RJ (ed) 56th Annual Meeting of the Orthopaedic Research Society, New Orleans, LA. 2010. p 2219.
15. Renkawitz T, Haimerl M, Dohmen L, Gneiting S, Lechler P, Woerner M, Springorum HR, Weber M, Sussmann P, Sendtner E, Grifka J. The association between Femoral Tilt and impingement-free range-of-motion in total hip arthroplasty. BMC Musculoskelet Disord. 2012;13:65. https://doi.org/10.1186/1471-2474-13-65.
16. Muller M, Crucius D, Perka C, Tohtz S. The association between the sagittal femoral stem alignment and the resulting femoral head centre in total hip arthroplasty. Int Orthop. 2011;35(7):981–7. https://doi.org/10.1007/s00264-010-1047-z.
17. Takao M, Nishii T, Sakai T, Nakahara I, Shiomi T, Tsuda K, Nakamura N, Yoshikawa H, Sugano N. Anterior pelvic plane can mislead leg length adjustments as well as cup alignments. In: 2010 Annual Meeting of American Academy of Orthopaedic Surgeons, New Orleans, LA. 2010. p 400.
18. McKibbin B. Anatomical factors in the stability of the hip joint in the newborn. J Bone Joint Surg Br. 1970;52(1):148–59.
19. Lewinnek GE, Lewis JL, Tarr R, Compere CL, Zimmerman JR. Dislocations after total hip-replacement arthroplasties. J Bone Joint Surg Am. 1978;60(2):217–20.
20. Nishihara S, Sugano N, Nishii T, Ohzono K, Yoshikawa H. Measurements of pelvic flexion angle using three-dimensional computed tomography. Clin Orthop Relat Res. 2003;411:140–51. https://doi.org/10.1097/01.blo.0000069891.31220.fd.
21. Babisch JW, Layher F, Amiot LP. The rationale for tilt-adjusted acetabular cup navigation. J Bone Joint Surg Am. 2008;90(2):357–65. https://doi.org/10.2106/jbjs.f.00628.
22. Tamura S, Takao M, Sakai T, Nishii T, Sugano N. Spinal factors influencing change in pelvic sagittal inclination from supine position to standing position in patients before total hip arthroplasty. J Arthroplast. 2014;29(12):2294–7. https://doi.org/10.1016/j.arth.2013.11.014.
23. Murphy WS, Klingenstein G, Murphy SB, Zheng G. Pelvic tilt is minimally changed by total hip arthroplasty. Clin Orthop Relat Res. 2013;471(2):417–21. https://doi.org/10.1007/s11999-012-2581-3.
24. Tamura S, Miki H, Tsuda K, Takao M, Hattori A, Suzuki N, Yonenobu K, Sugano N. Hip range of motion during daily activities in patients with posterior pelvic tilt from supine to standing position. J Orthop Res. 2015;33(4):542–7. https://doi.org/10.1002/jor.22799.
25. Tamura S, Nishihara S, Takao M, Sakai T, Miki H, Sugano N. Does pelvic sagittal inclination in the supine and standing positions change over 10 years of follow-up after total hip arthroplasty? J Arthroplast. 2016. https://doi.org/10.1016/j.arth.2016.08.035.
26. Sugano N, Nishii T, Miki H, Yoshikawa H, Sato Y, Tamura S. Mid-term results of cementless total hip replacement using a ceramic-on-ceramic bearing with and without computer navigation. J Bone Joint Surg Br. 2007;89(4):455–60. https://doi.org/10.1302/0301-620x.89b4.18458.

27. Iwana D, Nakamura N, Miki H, Kitada M, Hananouchi T, Sugano N. Accuracy of angle and position of the cup using computed tomography-based navigation systems in total hip arthroplasty. Comput Aided Surg. 2013;18(5–6):187–94. https://doi.org/10.3109/10929088.2013.818713.
28. Kitada M, Nakamura N, Iwana D, Kakimoto A, Nishii T, Sugano N. Evaluation of the accuracy of computed tomography-based navigation for femoral stem orientation and leg length discrepancy. J Arthroplast. 2011;26(5):674–9. https://doi.org/10.1016/j.arth.2010.08.001.
29. Sugano N, Takao M, Sakai T, Nishii T, Miki H, Nakamura N. Comparison of mini-incision total hip arthroplasty through an anterior approach and a posterior approach using navigation. Orthop Clin North Am. 2009;40(3):365–70. https://doi.org/10.1016/j.ocl.2009.04.003.
30. Wu G, Siegler S, Allard P, Kirtley C, Leardini A, Rosenbaum D, Whittle M, D'Lima DD, Cristofolini L, Witte H, Schmid O, Stokes I. ISB recommendation on definitions of joint coordinate system of various joints for the reporting of human joint motion—Part I: ankle, hip, and spine. International Society of Biomechanics. J Biomech. 2002;35(4):543–8.
31. Kingsley PC, Olmsted KL. A study to determine the angle of anteversion of the neck of the femur. J Bone Joint Surg Am. 1948;30A(3):745–51.
32. Uemura K, Takao M, Sakai T, Nishii T, Sugano N. The validity of using the posterior condylar line as a rotational reference for the femur. J Arthroplast. 2016;31(1):302–6. https://doi.org/10.1016/j.arth.2015.08.038.
33. Sugano N, Noble PC, Kamaric E. A comparison of alternative methods of measuring femoral anteversion. J Comput Assist Tomogr. 1998;22(4):610–4.
34. Grood ES, Suntay WJ. A joint coordinate system for the clinical description of three-dimensional motions: application to the knee. J Biomech Eng. 1983;105(2):136–44.
35. Yoshioka Y, Siu D, Cooke TD. The anatomy and functional axes of the femur. J Bone Joint Surg Am. 1987;69(6):873–80.
36. Sato T, Koga Y, Sobue T, Omori G, Tanabe Y, Sakamoto M. Quantitative 3-dimensional analysis of preoperative and postoperative joint lines in total knee arthroplasty: a new concept for evaluation of component alignment. J Arthroplast. 2007;22(4):560–8. https://doi.org/10.1016/j.arth.2006.06.020.

Chapter 8
Computed Tomography-Based Navigation for Total Hip Arthroplasty

Nobuhiko Sugano

Abstract CT-based navigation systems have been reported to be more accurate than conventional methods and even than imageless navigation in total hip arthroplasty. Although there is additional cost for preoperative CT images and it requires preoperative planning time, it may reduce the implant inventory cost by precisely predicting implant size and OR time by reducing the decision-making time regarding the final implant size and modular parts selection. It is particularly useful for complex cases such as DDH and post-traumatic deformities. It can be used through any surgical approaches or patient positions on the OR table. It can be used with either cementless or cemented implants. It can be also used for revision surgery. Because CT-based navigation accurately determines the best positioning and alignment of instruments and implants, it smooths the path for less-invasive THA with limited anatomic exposure.

Keywords Navigation · Total hip arthroplasty · Computer-assisted tomography · CT-based · 3D template

8.1 Introduction

Total hip arthroplasty (THA) is one of the most successful surgical operations used to reconstruct hip joints disabled because of osteoarthritis, arthritis, osteonecrosis, or trauma. Improvements in the materials, designs, and instruments of hip implants have reduced complications and improved the implant's durability. However, surgeons—or more accurately their surgical skills—are still the most significant factor affecting the outcomes.

Since the early 1990s, computer-assisted surgery (CAS) utilizing robot- or image-guided technologies has been introduced in various orthopedic fields [1] to help surgeons overcome limitations. There are several CAS systems for THA,

N. Sugano
Department of Orthopaedic Medical Engineering, Osaka University Graduate School of Medicine, Suita, Osaka, Japan
e-mail: n-sugano@umin.net

N. Sugano (ed.), *Computer Assisted Orthopaedic Surgery for Hip and Knee*,
https://doi.org/10.1007/978-981-10-5245-3_8

including computer-assisted preoperative planners, robotic devices, navigation devices, and patient-specific surgical instruments.

Navigation is a passive system in that it does not interact with the patient but provides information and guidance to the surgeon using conventional instruments to perform the surgery. Navigation uses optical sensors or magnetic sensors as three-dimensional (3D) position sensors to track the target bones and surgical tools or implants [2].

Optical systems use charged coupled device (CCD) cameras to obtain positional information. Infrared light-emitting diodes (active markers) or infrared light-reflecting markers (passive markers) are used for dynamic reference frames (DRFs) and are attached to the target bones and surgical tools to be tracked. Measurements by optical sensors are highly accurate and fast, but they require an uninterrupted line of sight between the CCD camera and the DRF. In contrast, there is no line-of-sight issue with magnetic sensors, although there are concerns about their accuracy, which may be reduced by interference from the motor of the operating room (OR) table or metallic tools.

Two types of navigation are used for THA: computed tomography (CT)-based navigation and imageless navigation. CT-based navigation was first introduced to accomplish accurate cup placement during THA by DiGioia's group [3]. Preoperative CT images are used for planning. For measuring cup alignment, pelvic coordinates are located on 3D reconstructed CT images based on anatomic landmarks, such as the anterosuperior iliac spine and the pubic tubercles. A plane through these landmarks, the anterior pelvic plane, is often used for pelvic coordinates when determining cup alignment (inclination and anteversion). HipNav (developed at Carnegie Mellon University) has been used to guide acetabular component placement [3, 4]. However, to assess the use of combined anteversion for optimal impingement-free hip range of motion and to evaluate limb length and offset, surgeons require information on both the acetabular and femoral sides. Therefore, in 1998, Sugano et al. developed a combined acetabular and femoral CT-based navigation system and later reported mid- to long-term outcomes showing the benefit of CT-based navigation for THA [5–7].

During the early 2000s, several commercially available CT navigations systems were launched. CT-based systems have been reported to be more accurate than conventional methods and even than imageless navigation [8–10]. Although there is additional cost for preoperative CT images and it requires preoperative planning time, it may reduce the implant inventory cost by precisely predicting implant size and OR time by reducing the decision-making time regarding the final implant size and modular parts selection [11]. The aim of this chapter, then, is to describe the elements of CT-based navigation for THA to help readers understand the pros and cons of this guidance system.

8.2 Preoperative Preparation and Planning

Preoperatively, a CT scanner is used to obtain transverse images from the bilateral pelvic brims to the distal end of the femurs. To maintain an accuracy of 1 mm and 1°, the minimum slice thickness and pitch should be ≤3 mm [5]. CT images are

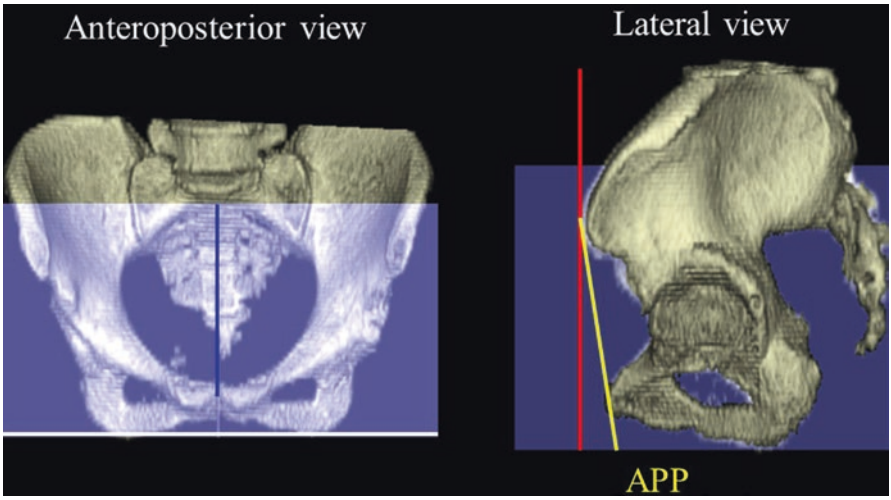

Fig. 8.1 Functional pelvic coordinates in supine position on computed tomography (CT) images. The coordinates are adjusted as follows: The anteroposterior axis is through the symphysis pubis and the sacral spine (left panel, blue line). The horizontal line is adjusted through the bottom of the bilateral ischia (left panel, white line). Therefore, the anterior pelvic plane (APP) on the lateral view shows a sagittal tilt (right panel, yellow line)

stored in Digital Imaging and Communication in Medicine format and transferred to a preoperative planning computer. Each coordinate of the pelvis and femurs is necessary to measure the position and alignment of the cup and stem. Two types of coordinates—anatomic and functional—were described in detail in the previous chapter in this book. My preference is to use anatomic femoral coordinates and functional pelvic coordinates. The functional pelvic coordinates refer to the position of the supine pelvis. Its axial rotation is adjusted by referring to the line through the symphysis pubis and the sacral spine. The horizontal axis refers to the line through the bottoms of the bilateral ischia (Fig. 8.1). The anatomic femoral coordinates are defined by several anatomic landmarks: tabletop plane, defined by the most posterior points of the trochanter and bilateral posterior condyles of the femur, and vertical axis, defined by the line through the trochanteric fossa and the most distal point of the femoral intercondylar notch (knee center), which is projected on the tabletop plane (Fig. 8.2).

After the pelvic and femoral coordinates are defined, the optimal design and size of the implant are selected and placed virtually in the acetabulum and proximal femur. Three orthogonal multiplanar reconstruction (MPR) CT images are useful for quickly verifying the implant size and position. By showing the MPR views through the acetabular center (Fig. 8.3a), a best-fit cup is selected and placed in the preferred alignment, which could be changed according to femoral stem anteversion. In anatomically simple cases, such as hips with primary osteoarthritis and osteonecrosis, the cup center is almost the same as the original acetabular center (Fig. 8.3b). In anatomically complex cases, however, such as a patient with devel-

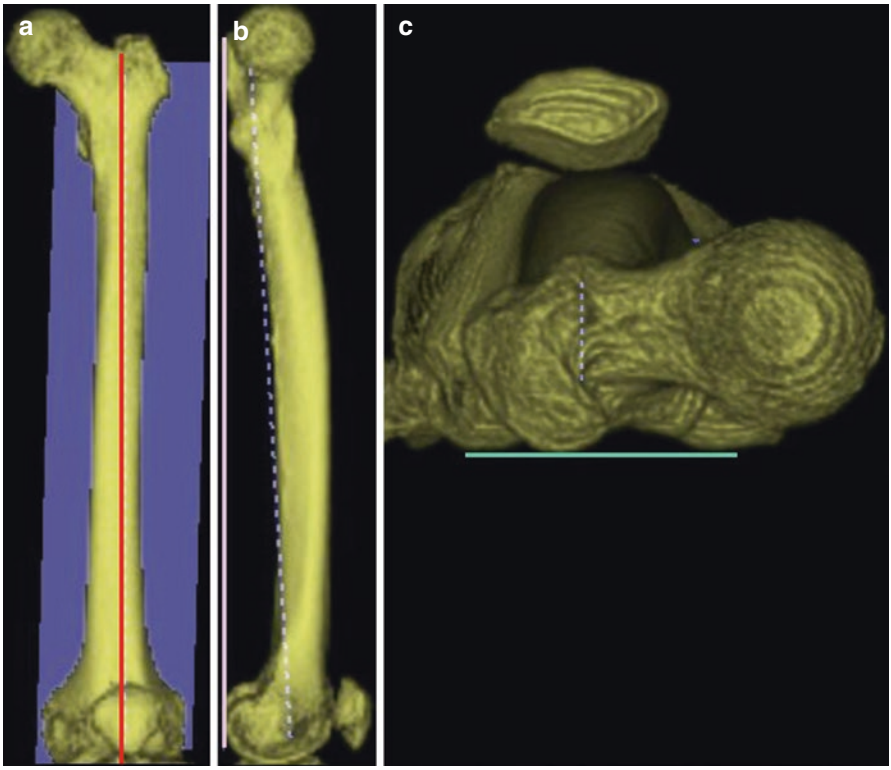

Fig. 8.2 Femoral coordinates are defined by several anatomic landmarks: top plane, which contacts the most posterior points of the trochanter; coronal plane, defined by the bilateral posterior condyles; and vertical axis, defined by the coronal plane of the femur and the line through the trochanteric fossa and the most distal point of the femoral intercondylar notch (knee center), which is projected onto the top plane. (**a**) frontal view, (**b**) lateral view, (**c**) axial view

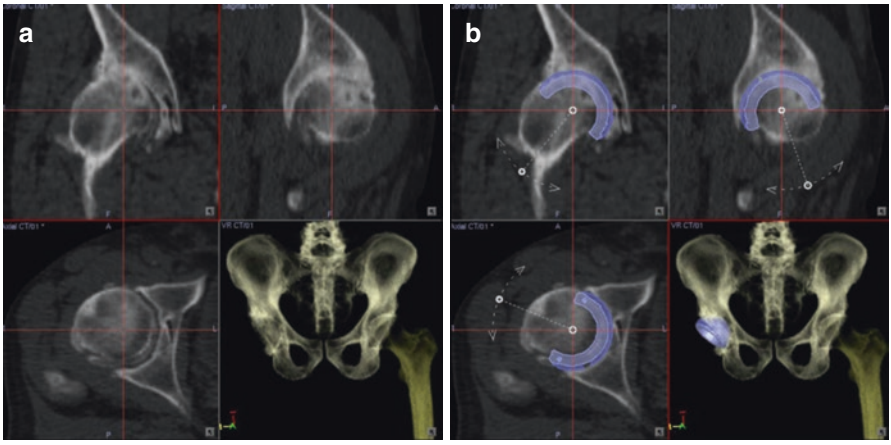

Fig. 8.3 (**a**) Multiplanar reconstruction CT views through the acetabular center. (**b**) The cup center is almost the same as the original acetabular center in knees with primary osteoarthritis

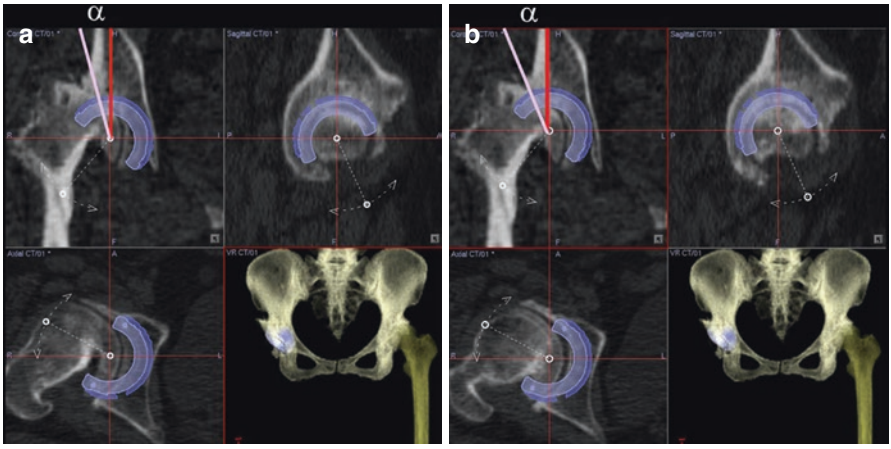

Fig. 8.4 In developmental dysplasia of the hip, the cup is moved medially (**a**) and then superiorly (**b**) to obtain sufficient bony coverage. The cup center-edge (CE) angle (α) is a good indicator for verifying lateral bone coverage. If the cup CE angle is ≥5°, no structural bone graft is needed, and a press-fit technique is sufficient to achieve stable fixation

opmental dysplasia of the hip, the cup is moved medially (Fig. 8.4a) and then superiorly (Fig. 8.4b) to obtain sufficient bone coverage. On the coronal view through the cup center, a certain level of lateral bone coverage is necessary for cementless press-fit fixation without dome screws. The center-edge angle of the cup (Fig. 8.4) is a good indicator by which to verify lateral bone coverage [12]. This angle is not affected by cup inclination. If it is ≥5°, no structural bone graft is needed, and a press-fit technique is sufficient to achieve stable fixation [13].

Femoral component planning requires a coronal view of the proximal femur through the center of the head, and the proximal medullary canal axis should be identified. An optimal stem design and size are then chosen that would have sufficient fit and would fill the medullary canal based on the fixation concept of each stem design. When a fit-and-fill straight stem such as Super Secur-Fit Plus (Stryker) is selected, the size of the implant is determined mainly by the distal canal size. The medial portion of the stem is seated in the medial femoral neck cortex (Fig. 8.5). On the coronal MPR view, the distal stem axis should be aligned with the proximal medullary canal axis, and the medial curved portion of the stem should be seated until endocortical contact is obtained. On the sagittal MPR view, the stem alignment should be neutral to increase the area of stem contact with the cortical bone. Because the distal canal size is not always proportional to the metaphyseal cavity, a different distal stem diameter can be selected with this design (Fig. 8.6). Several transverse MPR views—e.g., at the neck osteotomy, lesser trochanter, subtrochanter, and stem tip levels—should be evaluated to verify the fit of the stem. The proximal end of the greater trochanter is often used as a landmark to confirm the optimal center of the head. Although it has often been conceptually thought to be at the same level as the normal femoral head center, on average it is 8 mm above the normal femoral head center when measured along the proximal medullary canal axis [14, 15].

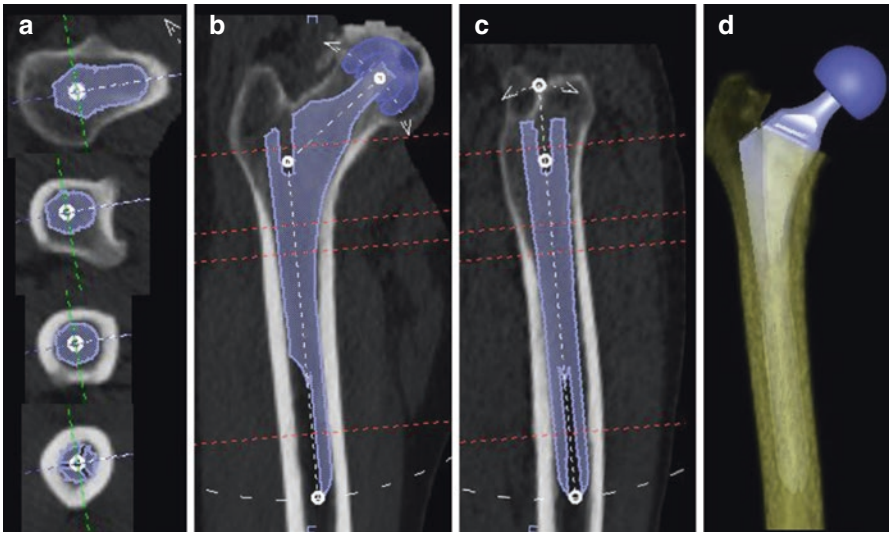

Fig. 8.5 The size of the Super Secur-Fit Plus (Stryker) is determined mainly by the size of the distal canal (in this case: 10 mm, with a 16 mm diameter distal stem). The coronal and sagittal stems are aligned with the proximal medullary axis. The medial part of the stem is seated in the medial femoral neck cortex. (**a**) Transverse sections obtained at neck osteotomies at the lesser trochanter, subtrochanter, and stem tip levels. (**b**) Coronal plane of the proximal femur. (**c**) Sagittal plane through the proximal medullary axis. (**d**) 3D anteroposterior (AP) view

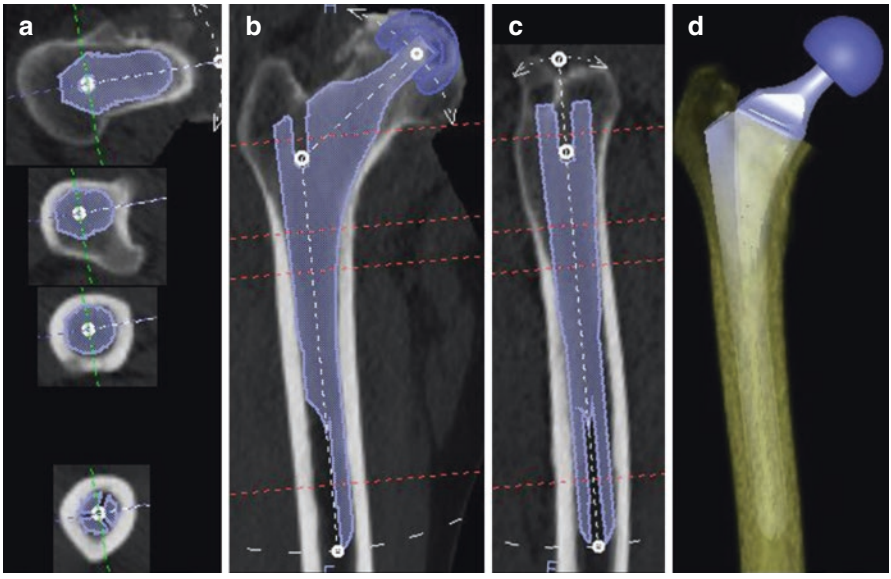

Fig. 8.6 There is room for a larger proximal body of the stem in the metaphysis with Super Secur-Fit Plus (size 10–16) in the case of Fig. 8.5. A two-sizes-larger proximal body of the Super Secur-Fit Plus (size 12–16) provides a better fit to the metaphysis in this case, although the head height and offset may be too great. (**a**) Transverse sections obtained during neck osteotomies at the lesser trochanter, subtrochanter, and stem tip levels. (**b**) Coronal plane of the proximal femur. (**c**) Sagittal plane through the proximal medullary axis. (**d**) 3D AP view

When a tapered wedge design is selected, such as Accolade II (Stryker), three areas—i.e., medial femoral neck and medial and lateral flares of the canal below the level of the lesser trochanter—are critical to achieve a proper fit (Fig. 8.7).

When an anatomic proximal-fit short stem such as CentPillar (Stryker) is selected, the stem size is chosen in the same fashion as for the tapered wedge design, but the sagittal alignment is adjusted according to its curved design (Fig. 8.8). The stem anteversion is usually matched to the original femoral neck anteversion. Head offset is determined by verifying the limb length and offset. Cup alignment is adjusted based on the range of motion (Fig. 8.9) according to a combined anteversion theory [16].

Finally, the registration procedure must be confirmed. The area of bone surface used for surface registration should be determined and the initial landmarks defined. The bone surface areas used for registration are different from those used with a posterior approach (Fig. 8.10) or an anterior or anterolateral approach (Fig. 8.11). The accuracy of registration depends on the accuracy of the bone surface models. Therefore, a tip for achieving accurate surface registration is to avoid using the articular surface area in patients with end-stage osteoarthritis because segmentation of the pelvic and femur models in the CT images is not reliable in these patients. Another tip is to assess only a few surface points in the presence of unique geometry, including those quite distant from the joint.

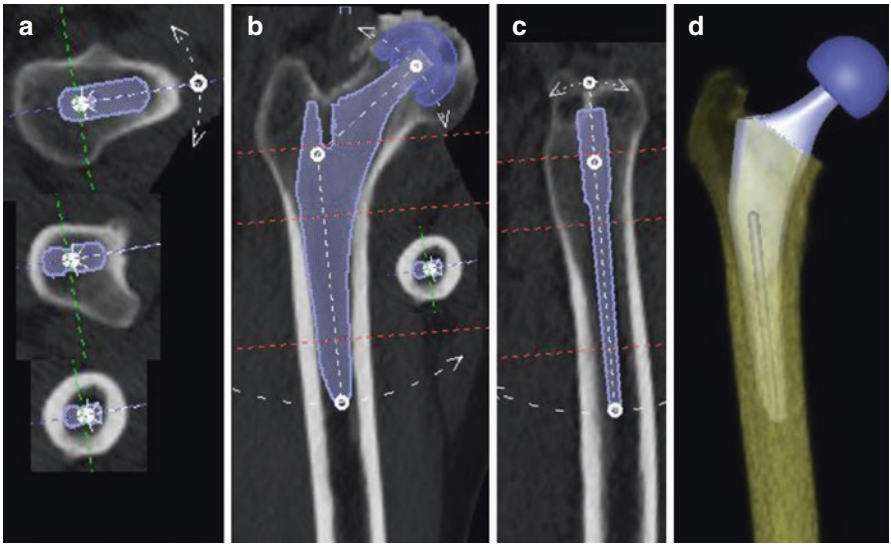

Fig. 8.7 The size of Accolade II (Stryker) is determined mainly by the fit of the stem to the proximal mediolateral flare of the canal at the lesser trochanter level (size 6 with a 127° neck–shaft angle in this case). Coronal/sagittal stem is aligned with the proximal medullary axis, but the sagittal alignment could be variable because of the thin AP dimension. (**a**) Transverse sections at the neck osteotomies at the lesser trochanter and stem tip levels. (**b**) Coronal plane of the proximal femur. (**c**) Sagittal plane through the proximal medullary axis. (**d**) 3D AP view

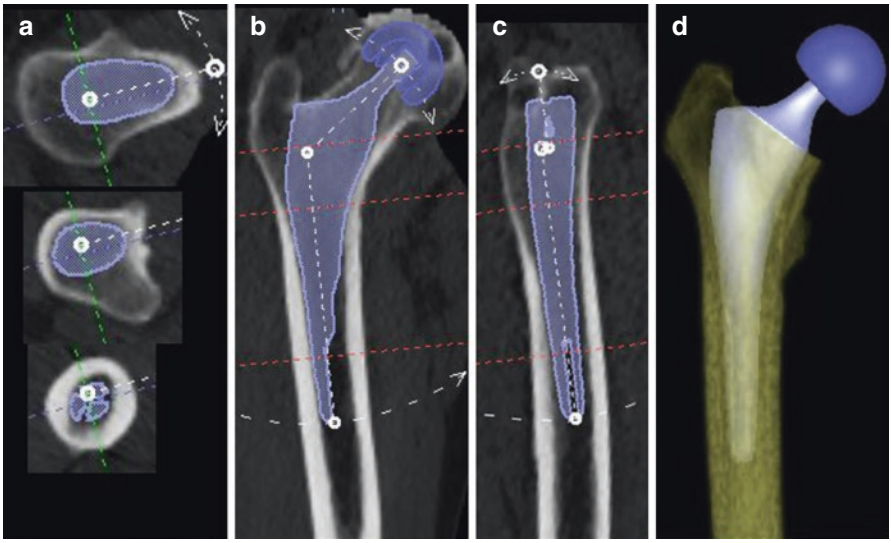

Fig. 8.8 The size of CentPillar (Stryker) is determined mainly by the fit and fill of the stem in the metaphysis of the femur from the neck osteotomy level to the proximal flare of the canal around the lesser trochanter (size 8 with a 127° neck–shaft angle in this case). The coronal and sagittal stem is aligned with the proximal medullary axis. Because CentPillar has an anatomic anterior bow, the most proximal body is shifted somewhat anteriorly from the proximal medullary axis. (**a**) Transverse sections at the neck osteotomy, lesser trochanter, and stem tip levels. (**b**) Coronal plane of the proximal femur. (**c**) Sagittal plane through the proximal medullary axis. (**d**) 3D AP view

8.3 Preoperative Preparation in the Operating Room and Intraoperative Activities

There are three important things to do in the OR before surgery. The data should be checked to determine if correct patient data have been installed. The navigation CCD camera should be placed at a distance from the surgical area where there is no interference with others. The navigation tools should be validated.

8.3.1 Registration and Confirmation of Accuracy

Immediately prior to skin incision, insert bone screw pins percutaneously into the pelvis and femur to fix each tracker (DRF) (Fig. 8.12). The pelvic brim is a good place to fix the pelvic tracker, and the femoral diaphysis has been used for the femoral tracker. Placing the trackers on the ilium and greater trochanter within the operative wound is also an option. CT-based navigation can be used through any approach or in any postural position, such as lateral and supine positions [17, 18]. After

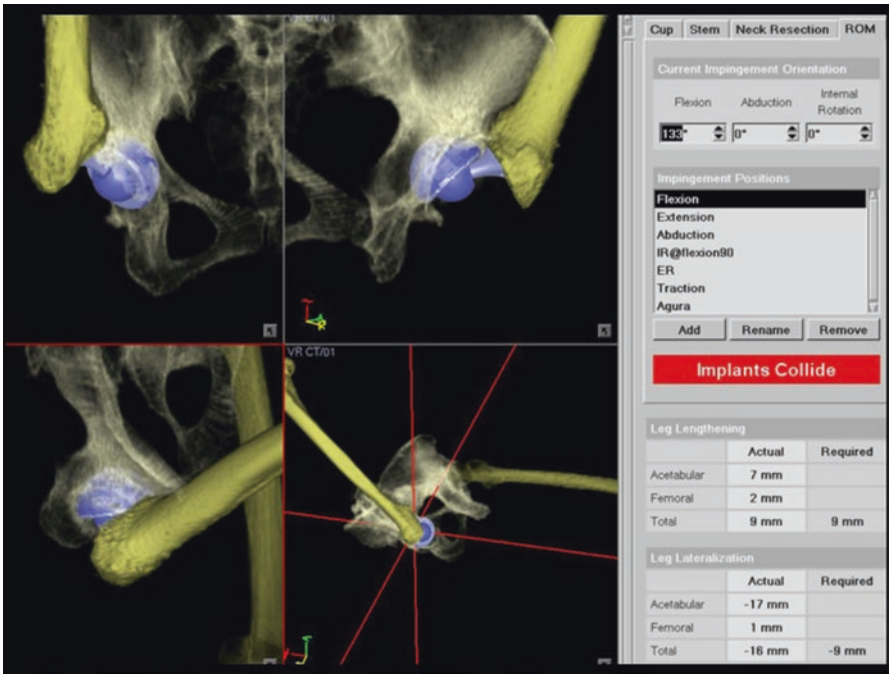

Fig. 8.9 Range-of-motion (ROM) simulation until implant–implant impingement. Cup orientation, liner design, head diameter, stem design, and alignment are the major factors influencing the ROM. The collision of stem and cup liner here is at 133° of flexion. Body positions can be simulated by changing the hip angle parameters of flexion/extension, abduction/adduction, and external rotation/internal rotation

registration, the root mean square of registration residue is a reliable parameter for determining the accuracy of registration. It should be <1 mm. It is always important, however, to confirm the accuracy by touching several bone surfaces with a pointer tool. If the pointer tip is just on the bone surface, the registration is acceptable (Fig. 8.13).

8.3.2 Bone Preparation, Implant Placement, and Intraoperative Measurements

After verifying registration accuracy, acetabular reaming is started with 1- or 2-mm portions, smaller than the planned size. If there is a thick osteophyte (double floor) in the acetabulum, the direction of the reamer should be turned toward the medial wall. At 3 mm before reaching the planned position, however, the direction of the reamer should be aligned with the axis of the planned cup angle to avoid stacking the cup in an incorrect position due to a distorted reaming pass [19]. If

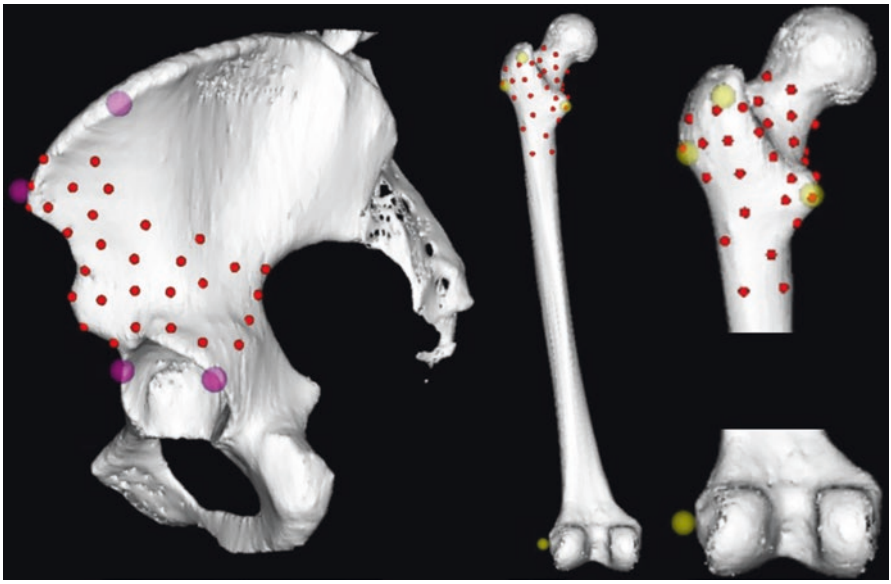

Fig. 8.10 Surface registration via a posterior approach. The four large purple dots on the pelvis and four yellow large dots on the femur are used for initial paired point matching. The 30 small red dots on the pelvis and femur are used for surface-based registration

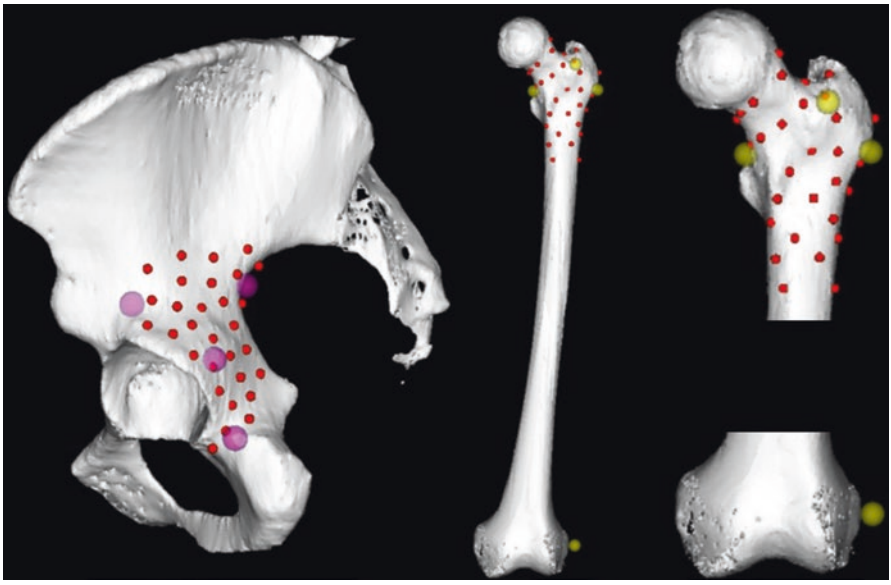

Fig. 8.11 Surface registration via an anterior or anterolateral approach. The four large purple dots on the pelvis and four large yellow dots on the femur are used for initial paired point matching. The 30 small red dots on the pelvis and femur are used for surface-based registration

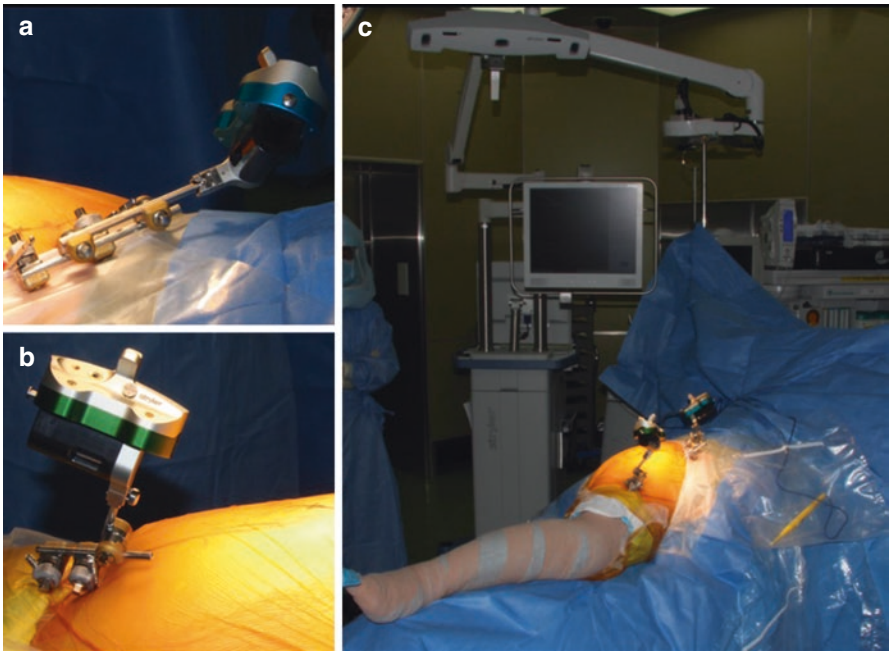

Fig. 8.12 Tracker fixation using percutaneous bone screw pins and an external fixation system. The pelvic tracker (**a**) is fixed to the pelvic brim and the femoral tracker (**b**) to the distal femur. The angles of trackers are adjusted so the CCD camera can detect the LED markers on the trackers in various hip positions (**c**)

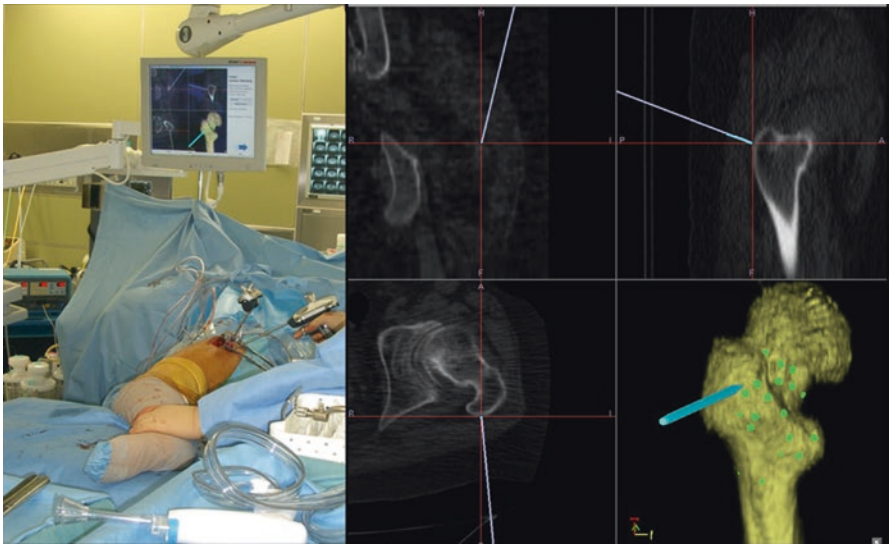

Fig. 8.13 Accuracy of registration can be determined by verifying the pointer tip location on multiplanar reconstruction CT scans by touching several bony landmarks to make sure that the tip of the pointer is just on the bone surface

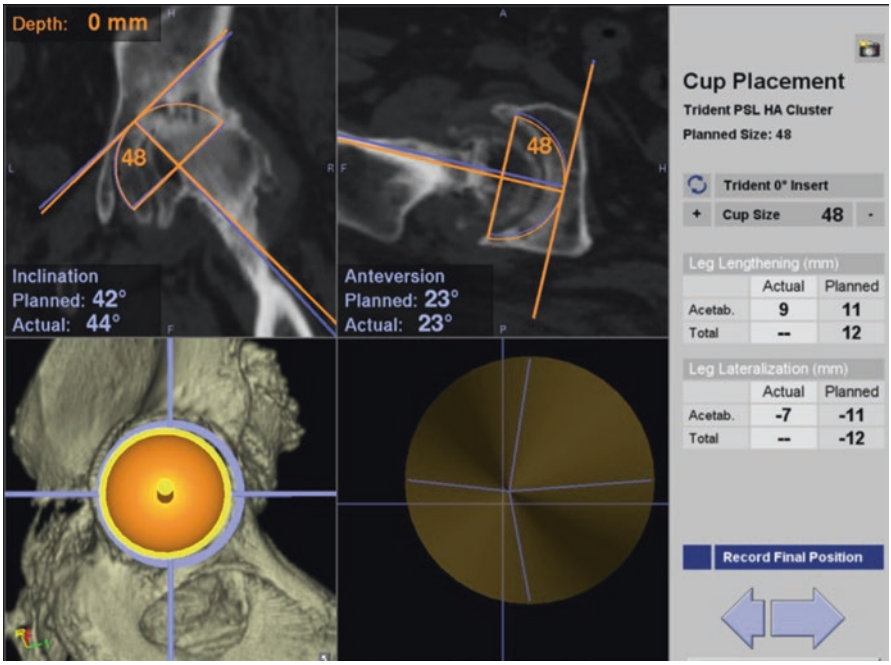

Fig. 8.14 Final position and size of the cup is recorded on the navigation computer

the final size of the reamed material is obtained prior to reaching the planned position, navigation can record the final reamer position. A trial cup is then provisionally placed on the acetabulum, and its stability is checked by gently moving the inserter. If inserter and pelvis move together, press-fit fixation is sufficient. At this point, an acetabular osteophyte protruding from the trial cup is removed with an osteotome or rongeurs to prevent bone impingement. The cup is then placed permanently under navigation, and the final position and orientation are recorded (Fig. 8.14).

For the femoral side, rasping can be monitored by navigation. It is useful to measure the rasp's position and alignment. When the surgeon believes that the maximum amount of rasping has been done, it is stopped. If the maximum rasp size is smaller than had been planned, the alignment (including varus/valgus, flexion/extension, and anteversion) may have been inappropriate. In such cases, navigation can provide useful information for making corrections or fine-tuning the procedure. When the final size rasp is inserted properly, the position of the rasp is recorded, and navigation can provide the information on stem alignment and offset as well as any limb-length change. If it is acceptable, the final stem is secured in the femur by tapping. The final stem position is recorded, and a proper offset of the modular head on the trunnion is ensured.

After repositioning the femur, the maximum range of motion is recorded (Fig. 8.15). The stability is evaluated in several postures, and soft tissue tension

Fig. 8.15 While checking the stability of the hip, the maximum range of motion can be recorded on the navigation computer

can be estimated by measuring femoral head separation from the cup when traction is applied [20].

8.4 Postoperative Evaluation of Navigation Accuracy

Cup alignment is often evaluated on plain radiographs with the use of a target zone such as the Lewinnek safe zone. However, anteversion of the cup is often shown to be smaller than the real one because of the nature of the plain radiography cone beam [21]. The coordinates of the pelvis for measuring cup alignment are determined by the pelvic position on the radiographic film or detector, which may not be reproducible. Moreover, the target zone concept is not patient specific, and only the precision of the cup alignment can be evaluated.

When CT-based navigation is used, target cup alignment is known. Therefore, we can evaluate the clinical accuracy and the absolute accuracy of navigation using postoperative CT images. The absolute accuracy of navigation is evaluated by comparing the recorded implant position/alignment and the postoperative implant position/alignment. The clinical accuracy of navigation is evaluated by comparing the preoperative plan and the postoperative implant position/alignment. Thus, the former represents the system accuracy of navigation, and the latter is influenced by the major technical factor, the surgeon. Several reports on the accuracy of CT-based navigation showed high accuracy, such as 1° of absolute accuracy and 4° of clinical accuracy regarding cup alignment [8, 9]. Recently, CT-based robotic cup placement systems have been developed, and some initial reports indicate that the accuracy of cup placement is as good with those systems as with CT-based navigation [22]. It will be interesting to see the differences in clinical outcomes between CT-based navigation and those using CT-based robotic systems.

8.5 Summary

CT-based preoperative planning is more predictable for determining the most advantageous implant size than when planning it using plain radiography. Computer simulation can provide useful information on postoperative impingement, free range of motion, and changes in offset and limb length. Therefore, after optimization of CT-based preoperative planning by fine-tuning the design/size of implants and their position/alignment, it remains for surgeons to execute the plan precisely in the OR in a less-invasive fashion. Because CT-based navigation accurately determines the best positioning and alignment of instruments and implants, it smooths the path for less-invasive THA with limited anatomic exposure.

Navigation systems, however, are not foolproof, and there is always a learning curve. Therefore, it is important to understand the basic concept of CT-based navigation and its knacks and pitfalls before applying it in the clinical setting.

References

1. Sugano N. Computer-assisted orthopaedic surgery and robotic surgery in total hip arthroplasty. Clin Orthop Surg. 2013;5:1–9.
2. Sugano N. Computer assisted orthopaedic surgery. J Orthop Sci. 2003;8:442–8.
3. Jaramaz B, DiGioia AM III, Blackwell M, Nikou C. Computer assisted measurement of cup placement in total hip replacement. Clin Orthop Relat Res. 1998;(354):70–81.
4. DiGioia AM, Jaramaz B, Blackwell M, Simon DA, Morgan F, Moody JE, Nikou C, Colgan BD, Aston CA, Labarca RS, Kischell E, Kanade T. The Otto Aufranc Award. Image guided navigation system to measure intraoperatively acetabular implant alignment. Clin Orthop Relat Res. 1998;355:8–22.
5. Sugano N, Sasama T, Sato Y, Nakajima Y, Nishii T, Yonenobu K, Tamura S, Ochi T. Accuracy evaluation of surface-based registration methods in a computer navigation system for hip surgery performed through a posterolateral approach. Comput Aided Surg. 2001;6(4):195–203.
6. Sugano N, Nishii T, Miki H, Yoshikawa H, Sato Y, Tamura S. Mid-term results of cementless total hip arthroplasty using a ceramic-on-ceramic bearing with and without computer navigation. J Bone Joint Surg Br. 2007;89B:455–60.
7. Sugano N, Takao M, Sakai T, Nishii T, Miki H. Does CT-based navigation improve the long-term survival in ceramic-on-ceramic THA? Clin Orthop Relat Res. 2012;470(11):3054–9.
8. Kitada M, Nakamura N, Iwana D, Kakimoto A, Nishii T, Sugano N. Evaluation of the accuracy of computed tomography-based navigation for femoral stem orientation and leg length discrepancy. J Arthroplast. 2011;26(5):674–9.
9. Iwana D, Nakamura N, Miki H, Kitada M, Hananouchi T, Sugano N. Accuracy of angle and position of the cup using computed tomography-based navigation systems in total hip arthroplasty. Comput Aided Surg. 2013;18(5–6):187–94.
10. Nakamura N, Maeda Y, Hamawaki M, Sakai T, Sugano N. Effect of soft-tissue impingement on range of motion during posterior approach Total Hip Arthroplasty: an in vivo measurement study. Comput Assist Surg (Abingdon). 2016;21(1):132–6.
11. Noble PC, Sugano N, Johnston JD, Thompson MT, Conditt MA, Engh CA Sr, Mathis KB. Computer simulation: how can it help the surgeon optimize implant position? Clin Orthop Relat Res. 2003;417:242–52.

12. Sugano N, Nishii T, Nakata K, Masuhara K, Takaoka K. Polyethylene sockets and alumina ceramic heads in cemented total hip arthroplasty. A ten-year study. J Bone Joint Surg Br. 1995;77(4):548–56.
13. Takao M, Nakamura N, Ohzono K, Sakai T, Nishii T, Sugano N. The results of a press-fit-only technique for acetabular fixation in hip dysplasia. J Arthroplast. 2011;26(4):562–8.
14. Sugano N, Noble PC, Kamaric E. Predicting the position of the femoral head center. J Arthroplast. 1999;14(1):102–7.
15. Sugano N, Noble PC, Kamaric E, Salama JK, Ochi T, Tullos HS. The morphology of the femur in developmental dysplasia of the hip. J Bone Joint Surg Br. 1998;80(4):711–9.
16. Sugano N, Tsuda K, Miki H, Takao M, Suzuki N, Nakamura N. Dynamic measurements of hip movement in deep bending activities after total hip arthroplasty using a 4-dimensional motion analysis system. J Arthroplast. 2012;27(8):1562–8.
17. Sugano N, Takao M, Sakai T, Nishii T, Miki H, Nakamura N. Comparison of mini-incision total hip arthroplasty through an anterior approach and a posterior approach using navigation. Orthop Clin North Am. 2009;40(3):365–70.
18. Maeda Y, Sugano N, Nakamura N, Hamawaki M. The accuracy of a mechanical cup alignment guide in total hip arthroplasty (THA) through direct anterior and posterior approaches measured with CT-based navigation. J Arthroplast. 2015;30(9):1561–4.
19. Nishii T, Sakai T, Takao M, Sugano N. Fluctuation of cup orientation during press-fit insertion: a possible cause of malpositioning. J Arthroplast. 2015;30(10):1847–51.
20. Takao M, Nishii T, Sakai T, Sugano N. Postoperative limb-offset discrepancy notably affects soft-tissue tension in total hip arthroplasty. J Bone Joint Surg Am. 2016;98(18):1548–54.
21. Kalteis T, Handel M, Herold T, Perlick L, Paetzel C, Grifka J. Position of the acetabular cup—accuracy of radiographic calculation compared to CT-based measurement. Eur J Radiol. 2006;58(2):294–300.
22. Kamara E, Robinson J, Bas MA, Rodriguez JA, Hepinstall MS. Adoption of robotic vs fluoroscopic guidance in total hip arthroplasty: is acetabular positioning improved in the learning curve? J Arthroplast. 2017;32(1):125–30.

Chapter 9
Imageless Computer-Assisted Navigation for Total Hip Arthroplasty

Kamal Deep

Abstract The introduction of computer-assisted surgery is an important landmark in the history of orthopedics. Its clinical use for total hip arthroplasty is recent. It can be image-based or imageless depending on the registration technique used: whether imageless or based on preoperative/intraoperative radiological images. It has changed the way surgeons perceive procedures. In this chapter, we describe an imageless method of computer navigation. It guides the surgeon through the various surgical steps that the surgeon could only speculate about previously. With this system, the surgeon sees the operation on a monitor in real time. It helps not only with acetabular orientation; it shows the cup's center shift at the time of reaming and cup insertion. Similarly, it can show femoral stem orientation and the changes it will make in leg length and its offset, thereby helping with final selection of the prosthesis. Its accuracy and precision have been reported by many to be >95% regarding cup orientation, offset, and leg-length reproducibility. There is, however, a learning curve. The initial cases take more time to complete, but with experience, the operating time is lengthened by only 5–10 min. The instrumentation and technique could (and no doubt will) be improved. Even now, however, it has allowed more accurate and reproducible surgery. The preoperative plan can be executed with unprecedented accuracy compared with that achieved using conventional techniques.

Keywords Navigation · Total hip replacement (THR) · Accuracy · Leg length · Offset · Computer-assisted surgery (CAS)

9.1 Introduction

Computer-assisted navigation has been one of the most important developments in orthopedics in recent times. Joint replacement arthroplasty was developed and became popular during the 1960–1990 era. More recently, during the twenty-first century, the most striking change seems to be a better understanding of the

K. Deep, FRCS, MCh Orth, FRCS Orth
Golden Jubilee National Hospital, Glasgow, UK

N. Sugano (ed.), *Computer Assisted Orthopaedic Surgery for Hip and Knee*,
https://doi.org/10.1007/978-981-10-5245-3_9

kinematics and dynamics of these joints. Computer-assisted surgery (CAS) has played a vital role in this arena and has taken us a step further in putting the theoretical preoperative plan into practical perioperative action by giving feedback to the surgeon in real time.

The standard process of imageless computer navigation involves four phases: setup, registration, planning, and execution. The setup involves attaching rigid bodies/reference frames (trackers) to the bones. Registration of the individual anatomical part to computer images may use sequences of kinematics and/or anatomical landmarks that are matched to the patient's anatomy. The planning phase allows us to perform the surgery while watching it on the screen as per the plan. Throughout the surgery, instruments equipped with infrared or electromagnetic (or other types of) trackers and the tracked bones are monitored in real time.

Despite its early development, during the 1990s, the clinical use of CAS for total hip replacement (THR) is recent and is gaining in popularity, although less so than total knee arthroplasty. The main reason for this difference is that improperly placed hip implants do not cause as many immediately visible problems as do incorrectly placed knee implants. With time, however, surgeons are realizing the potential advantages of CAS for THR because of their good results. The problems experienced following conventional THR surgery are related to implant malpositioning and include dislocation, impingement, leg-length discrepancy, and early failure [1–3]. Impingement has been highlighted recently to be a considerable problem especially when using ceramics [3, 4] and metal-on-metal bearings, which are highly sensitive to malpositioned implants [5]. Indeed, a malpositioned acetabulum during hip resurfacing arthroplasty can lead to the disastrous consequences of a patient's adverse reaction to metal debris, such as aseptic lymphocyte-dominant vasculitis-associated lesions and pseudotumors, which has led to a visible decline in the frequency of hip resurfacing use as well as metal-on-metal hip replacements [6]. There is no consensus on a standard position for acetabular cup placement, although some safe zones, such as that described by Lewinnek et al. [7], have been noted. The functional plane may be different for each individual, and contractures of various degrees may occur in an arthritic hip, leading to different degrees of pelvic tilt. This situation holds true for conventional as well as navigated surgery.

Most of the currently available computer navigation systems use the anterior pelvic plane as the reference plane for registering pelvic anatomy. This plane is determined by registering the two anterosuperior iliac spines (ASISs) and pubic symphysis during the registration phase. Although this plane gives consistent fixed bony points, it may not represent a true reference for individual functional positions because of the variation in pelvic tilt and spinal deformities. Thus, alternatives have been explored but have not proved to be better than the anterior pelvic plane. The alternatives have included the posterosuperior iliac spines, transverse acetabular ligament, and impingement cones of circumduction. The inherent acetabular axis has also been used as a reference to denote the anatomy

of the acetabulum [8]. The most commonly perceived difficulty with the anterior pelvic plane using imageless navigation is registration, especially if the surgeon uses lateral positioning for the surgery. We have found that, with consistent use, it is not as difficult as has been perceived. Although performing THR for primary osteoarthritis is relatively better understood and provides successful results using conventional techniques, the complexity increases if the patient's arthritis is secondary to an underlying cause. With complex primary THR, the acetabular anatomy of the hip is distorted, leading to loss of the usually available landmarks. In this situation, it is highly desirable that the surgeon obtains maximum guidance from any source available, such as the anterior pelvic plane. CAS can play a vital role in revising these hips. Not only can it guide the surgeon on the orientation of the components but also on positioning the center of the hip, which is constantly visible on the monitor during the operation, from which the surgeon can make important decisions and adjustments regarding placement of components. This is especially desirable for dysplastic hips and those destroyed by trauma, infection, inflammation, malignancy, or previous surgery or when using a minimally invasive approach.

Although the accuracy of the computer navigation systems in a laboratory environment is measured to the last degree or millimeter, issues are still encountered with this technology in the operating theater that can affect the accuracy and precision of component placement and orientation. Despite these issues, this technology offers irrefutable advantages, including component orientation and placement, offset, and leg length, as well as reproduction of the planned surgery, training, and research, among others.

9.2 Drawbacks of CAS in THR

9.2.1 Registration

Whether image-free or image-based technology is used, the registration of patient anatomy is still an issue affecting the finer points of accuracy during navigated surgery. Registration may not be as much of a problem when using image-based navigation, but it requires more complex software for the matching process and 3D images, both of which are more costly.

With imageless techniques, the registration accuracy may be questionable and is surgeon-dependent [9]. Also, when the surgeon operates with the patient in the lateral position, acquiring an anterior pelvic plane using the ASIS and pubic symphysis can be difficult, especially in morbidly obese patients. Therefore, other reference points have been suggested, although they have not proved superior to the anterior pelvic plane. A registration that is up to 2 cm inaccurate has limited impact on the accuracy of cup orientation—provided the contralateral registration of the ASIS and pubic symphysis in depth (anteroposterior direction) is accurate.

The effects of inaccurate registration are shown in Table 9.1 (craniocaudal direction) and Table 9.2 (transverse plane anteroposterior direction). Incorrect registration in the mediolateral direction of the ASIS does not affect the inclination or version of the cup. An error of up to 2 cm of the ASIS registration in most cases affects the orientation by only 1–4°. The most important point affecting overall accuracy is that of registration in the transverse plane (depth) for the contralateral ASIS as it could significantly affect anteversion. Although accurate pelvic plane registration is highly desirable, inaccurate pelvic registration does not affect leg length, offset, or femoral component guidance, which is a substantial advantage of computer-assisted navigation.

Table 9.1 Changes in inclination and anteversion of the acetabular cup in an average pelvis[a]

	Actual cup position			Actual cup position	
Right ASIS: Cranial(+) Caudal(−) Shift in mm	Inclination (°)	Anteversion (°)	Left ASIS: Cranial(+) Caudal(−) Shift in mm	Inclination (°)	Anteversion (°)
30	7	−2	30	−7	2
20	4	−1	20	−4	1
10	2	−1	10	−2	1
0	0	0	0	0	0
−10	−2	1	−10	2	−1
−20	−4	1	−20	4	−1
−30	−7	2	−30	7	−2

ASIS anterosuperior iliac spines

[a]The distance between the ASISs was 240 mm, with the right side being the treatment side and the effects of incorrect registration in the craniocaudal direction [31]

Table 9.2 Changes in inclination and anteversion of the acetabular cup of an average pelvis[a]

	Actual cup position			Actual cup position	
Right ASIS: Anterior(+) Posterior(−) Shift in mm	Inclination (°)	Anteversion (°)	Left ASIS: Anterior(+) Posterior(−) Shift in mm	Inclination (°)	Anteversion (°)
30	−3	−2	30	−2	−17
20	−2	−1	20	−2	−11
10	−1	−1	10	−1	−5
0	0	0	0	0	0
−10	1	1	−10	1	5
−20	2	1	−20	2	10
−30	4	1	−30	4	15

[a]The distance between ASISs was 240 mm, with the right side being the treatment side and the effects of wrong registration in the transverse plane [31]

9.2.2 Tracker-Related Problems

There is a potential for tracker attachment site morbidity because a hole must be made in the bone to attach the trackers. This potentially could lead to fracture (although it is a theoretical risk because we found none associated with THR navigation in the literature). If the tracker-attaching pins are not positioned carefully, there is a theoretical risk of neurovascular damage (again, none has been reported). More trivially, if a passive tracker is being used, contamination with fluid or blood could affect visibility, with the computer struggling to recognize the tracker. Trackers have the potential to move and be inadvertently touched by the surgeon or assistants because the pelvis may be osteoporotic in older patients. This situation would occur more frequently when using single pins with no rotary locking mechanism. In an experiment carried out at the University of Brisbane [10], the authors found that larger-diameter pins had a better hold, although 4- and 5-mm ratchet pins showed little difference (150–200 N). Double cortical pins had a better hold than single cortical pins. Triple-pin fixation of a tripod and bone-to-pin fixation did not fail before failure of the metal of the tripod itself. Pullout strength was much stronger (10–15 times) than translational strength. With a sudden bump or sustained force during the surgery, an assistant could produce a force of up to 150 N, which is much less than the force required to pull out the tracker pin and just less than translating a 4- or 5-mm diameter pin but more than the required forces to rotate the tracker [10]. Thus, the choice of the tracker-attaching device is important, and a compromise is sometimes necessary between reliability and invasiveness.

9.2.3 Duration of the Procedure

The procedure may take longer than a conventional technique. At the beginning of the learning curve, it can be as much as 30 min longer, which decreases to about 5–10 min after performing up to 50 cases, having mastered the learning curve. The operating environment, experience, and familiarity of the operating staff also have a bearing on the speed of the operation. The author's operating time for a typical primary navigated THR is 40–60 min.

9.3 Advantages of CAS for THR

One of the main benefits of CAS is to provide the surgeon with data on patient-specific anatomy, based on which the surgeon can formulate a plan for bone preparation, thereby producing the optimal result. In addition, placement and

orientation of both femoral and acetabular implants can be carefully planned and subsequently navigated during the execution phase.

9.3.1 Component Orientation

The acetabular cup during CAS can be displayed on the monitor in real time within 6 degrees of freedom in whatever orientation the surgeon is placing the cup. The monitor shows the inclination, anteversion, and flexion, as well as any anteroposterior, mediolateral, or superoinferior shifts that the surgeon produces, allowing them to be corrected during the surgery. Lewinnek et al. described a "safe zone" of 40 ± 10° for cup inclination and 15 ± 10° for anteversion to reduce the dislocation rate [7]. Barrack advocated positioning cups in 10–30° of anteversion [11], whereas McCollum and Gray recommended 20–40° of anteversion [12]. Regardless of the safe zone the surgeon chooses, freehand techniques and mechanical jigs have been shown to be unreliable [13–17]. Using conventional methods at a teaching hospital (Massachusetts General Hospital, Boston), Callanan et al. found that of 1952 hips, only 62% fell within their desired inclination of 30–45° [18]. In our experience with 259 navigated hips, 96% were within the desired inclination range of 30–50° [19] and 89% of our cups were within the inclination range of 30–45°. Other authors also have achieved better accuracy with navigated cups [1].

Similarly, for the femoral stem, the monitor can display flexion/extension, varus/valgus, anteversion/retroversion, offset, and leg-length change. Most of the systems available should be able to show these parameters, although some may differ. The surgeon is advised to look at these in detail before choosing a system.

9.4 Offset and Leg Length

Soft tissue balancing during total hip arthroplasty is extremely important, and offset and leg length form an integral part of it. It is well established that reproducing the native femoral offset is essential to achieving good abductor function and improving joint stability and implant longevity [20]. Restoration of the hip offset can lead to increased stability and improved range of motion, which in turn reduces wear and component loosening [21, 22]. Leg-length discrepancy (LLD) can lead to back pain, patient dissatisfaction, and medicolegal litigation [23]. LLD is a major problem associated with conventional hip replacement. In a study conducted in the United Kingdom, Konyves and Bannister found that, among 90 THRs, there was a mean lengthening of 9 mm, which was perceived by 43% patients at 3 months and 33% patients at 1 year [24]. The functional Oxford score was 27% worse at 3 months and

18% worse at 1 year compared with those who did not have any perception of the LLD, indicating that the functional outcome is worse with LLD [24].

We conducted a study of 228 THRs to identify how accurately we could reproduce the native hip offset and leg length with the help of navigation. We used the contralateral normal hip as the control to measure these parameters. Navigation enabled us to restore native hip offset to within 6 mm of other normal hips in 95.39% of cases. It also enabled us to restore leg length to within 6 mm of the other (normal) leg in 96.05% of cases. In all, 96% of the hips had the center of the joint within 5 mm of that of the contralateral hip in the craniocaudal direction.

Superior migration of the center of rotation of the hip by >5 mm results in distortion of the hip offset, leading to high offset stems. A higher center of rotation of the hip needs a higher offset to prevent impingement [25]. Other studies have also found better results using navigation than the conventional surgery in relation to offset and leg-length results [26]. Using computer navigation, Dastane et al.—based on the criteria of offset and limb-length restoration within 6 mm from the normal hip and contralateral lower limb—achieved those goals in 95% of patients for offset and 99% for limb length [26], similar to our findings [27]. Confalonieri et al., in a comparative study between computer navigation and freehand techniques, found that computer navigation produced significantly better results for offset (mean 2.8 ± 0.5 mm) and LLD (mean 4.1 ± 1.7 mm) restoration [28]. Computer-based navigation has also been shown to correct LLD better than conventional techniques [3, 28, 29].

9.4.1 Other Points

The pelvis and acetabulum are moving targets during the procedure without knowledge or control of the surgeon working blindly, leading to risk of incorrect placement and orientation of the cup. With navigation, any movement of the pelvis is detected by the computer, thereby reducing the chances of it being left uncorrected. In contrast, conventional surgery, using only the naked eye, cannot detect these problems. It is thus hoped that controlling the implant's position and orientation more cautiously could reduce the number of early failures and potentially lead to better function and increased survival of the implants. Because the CAS techniques are in their infancy, it is too early to state whether this goal will hold true, but it does appeal to common sense based on the early findings in the literature.

The proposed technique has been shown to be helpful for training young surgeons and gives consistent results in trainees' hands that compare well with those of experienced surgeons [30–32]. This method is also helpful if minimally invasive approaches are being used wherein the field of view is limited [33].

9.5 Operative Technique

The most commonly used imageless registration method is described, highlighting only the steps that are important from a navigation point of view. Before embarking on this technique, one must know how to perform conventional hip replacement arthroplasty because this new technique involves various stages as in conventional surgery. The method described here is the one we use, but there can be variations with different surgeons and the various commercial systems available. Because at present there is limited dedicated software available for complex or revision hips, in most situations primary total hip software is used and seems to serve the purpose. There is, however, software available for dysplastic hips.

9.5.1 Preoperative Planning

Preoperative planning is essential, especially for complex primary THR. It must be determined before the start of the surgery, based on radiological and clinical criteria, (1) in what direction and to what extent a change in the center of the hip is desired and (2) what changes in offset and leg length are needed. It is also important to note the anatomy of the acetabulum, if needed, by supplementing the data with preoperative computed tomography (CT) scans to determine the position, thickness, and any deficiency of the walls of the acetabular cavity. The femoral version, shape, and medullary canal dimensions should also be considered.

9.5.2 System Setup

Patient and anatomical part preparation is done as for conventional surgery. The patient may be positioned supine or lateral. It is important that the surgeon can access the knee, iliac crest, and pelvis for proper registration of the anatomy and for attaching the trackers to the bone. In obese individuals, if the patient is in the lateral position for a posterior approach, it may be easier to leave the patient first in a "sloppy" lateral position until registration of the pelvis is completed and then tighten the posterior supports. Echocardiographic patches with central knobs may also be used to guide the contralateral ASIS and pubic symphysis under the drapes for registration of the pelvic plane.

Patient data and the operated side are then fed into the system. The trackers and instruments are registered and calibrated if needed by the system and then attached to the pelvis and femur with various means depending on the system being used (Fig. 9.1).

The site of attachment on the pelvis can be the iliac crest or supra-acetabular area. The femoral tracker may be attached to the trochanteric region or the distal

Fig. 9.1 Tracker attachment devices for the pelvis (supra-acetabular area) and femur (*C* clamp for the trochanteric region), attached through the same incision

Fig. 9.2 Camera is adjusted in the right direction and distance from the operative site so it focuses on the sensors and data is shown on the screen

shaft away from the main operative incision. The means of attachment vary from one to three pins to a square nail. Whatever means is used, the fixation should be secure, stable, and not interfere with the main operation. The camera (Fig. 9.2) is adjusted so it can focus on both trackers. It should also be a proper distance (usually 1.6–2.5 m) from the surgical field and give accurate readings. Normally, the computer screen indicates if the camera cannot see the trackers properly.

9.5.3 Registration of Pelvis and Acetabulum

The registration of the pelvis and acetabulum can be image-based or imageless. For the image-based method, preoperative CT or fluoroscopy may be used. We use the imageless method for registration. The pelvis is registered in the frontal plane, which is composed

of the two ASISs and pubic tubercles or pubic symphysis. These points are intact in most primary or complex primary hips and hence act as good references for orientation. Some systems also register a functional plane composed of the mid-axillary point and greater trochanter with the leg in neutral position. This arrangement is sometimes difficult to reproduce as neither point is a single discrete bony point and thus is open to error.

The hip joint is then exposed as in conventional surgery, neck osteotomy is performed, and the femoral head is extracted. Acetabular registration is performed by denoting the true medial wall (floor), acetabular surface, and/or circumference of the margin. These points give an approximate diameter of the acetabulum and native anatomy. A cup trial or reamer of the same diameter as the acetabulum can be inserted in the acetabulum, with the center of the trial/reamer registered by the computer as the center of the hip. The orientation of the inherent acetabulum can also be recorded. This center acts as a reference for further calculations. It is important to note that in complex hips, the acetabular anatomy may not be clear, and preoperative planning then comes into play. The local acetabular anatomy may not be much help for orienting the acetabular cup in complex hips, in which case the pelvic plane is a good guide.

9.5.4 Femoral Registration

There are various methods for registration used by different systems. The anterior mid-patellar point and anterior midpoint of the ankle with the knee bent to 90° is used by one system. With another system, the trochanteric fossa is registered first, followed by the popliteal fossa, which can be registered as a single point or as two femoral epicondyles. The knee is then bent to 90° to avoid any effects of leg rotation, and the midpoint of the Achilles tendon is registered. These registrations form a virtual femoral plane by combining all of the points to act as a reference for the femoral components. One must consider the inherent anatomy of the femur and be vigilant that these are the planes generated by the computer to give the orientation between the various registered points. It ignores the intervening shaft anatomy, which may be bent, especially if there are any previous fractures or malformations. The surgeon must then take that situation into consideration.

9.5.5 Acetabular Cup

After good exposure is achieved, acetabular reamers are used to prepare the cup bed. The reamer handle is attached to a tracker (Fig. 9.3), which communicates with the computer to give the orientation and position of the reamer in all 6 degrees of freedom, including inclination, version, flexion, and the superoinferior, anteroposterior, and mediolateral positions.

Reaming is executed in accordance with the preoperative plan (Fig. 9.4).

Fig. 9.3 Passive tracker with reflective balls is attached to the reamer handle for acetabular reaming relative to the reference plane identified by the pelvic tracker

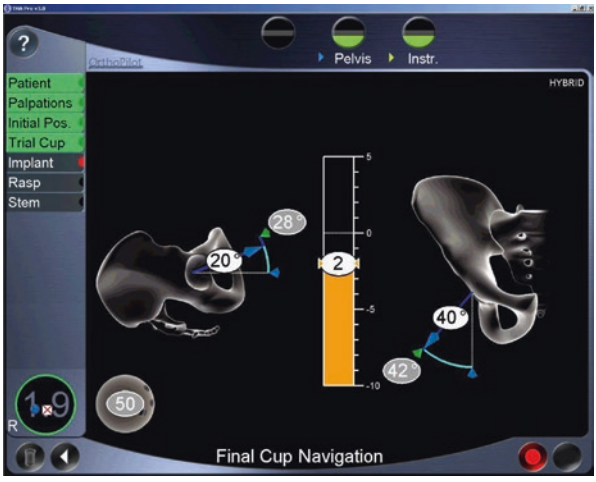

Fig. 9.4 Acetabular reaming screen shows the reamer size and the anteroposterior, mediolateral, and craniocaudal positions. It also shows the inclination, anteversion, and distance to the true floor in the central column

Similar information is provided when the cup is inserted as a tracker attached to the cup insertion handle. For uncemented cups, it is important to be careful when preparing the reamers so they are in correct orientation. For cemented cups, one can change the position of the cup within the cement mantle to some extent before it sets.

9.5.6 Femoral Stem

The femur is prepared in a conventional fashion, taking care that it is in the correct orientation, which is shown by the computer as the tracker is attached to the femoral broach handle. It shows the position of the broach, including version, offset, and lengthening (Fig. 9.5).

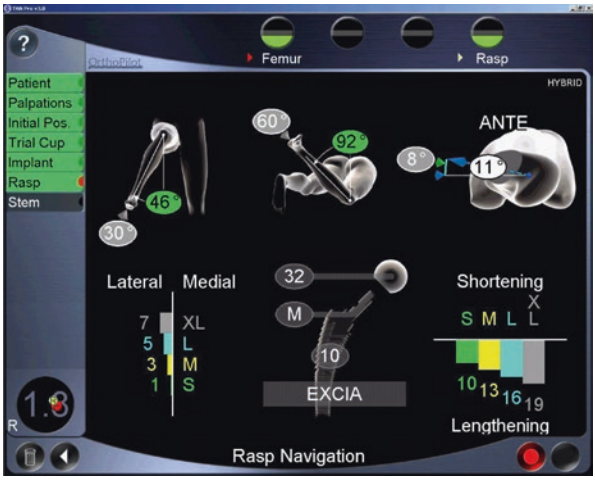

Fig. 9.5 Femoral rasping shows flexion, internal and external rotations that will be achieved by the shown anteversion of the rasp position. The lower part of the screen shows a virtual trial, including the offset; the sizes of the head, neck, and stem; and the change it could make to the leg length using different neck lengths (*S* small, *M* medium, *L* long, *XL* extra long)

Similar readings are given when inserting the stem component. It is important not to forget the preoperative planning, noting any specific anomalies in the femoral shape. Some software even gives the virtual range of motion that a specific position of the femoral component could produce and thus helps plan the version of the component. Again, for uncemented stems, it is important to be careful during preparation of the bed, whereas with cemented stems, the position can be altered to some extent in the cement mantle.

9.5.7 Final Steps

A virtual reduction can be seen on the monitor, and the effect of various lengths of the femoral neck can be seen even without the actual hip trial reduction (Fig. 9.5). Trial reduction is then done with selected components, and the new hip center appears. A change in leg length and offset is seen, which can be changed to any extent, even at this stage, by varying the neck length. The final range of movements and points of impingement are recorded in the computer, and the procedure is competed after the wound is closed, as with the conventional technique.

9.6 Conclusion

CAS has given us a technique that makes the surgery more accurate and reproducible. The preoperative plan can be executed with much more conviction and accuracy than

with conventional techniques. Further development of the technique, such as registration and instrumentation, are needed to make it more user-friendly and easier for adoption before it is accepted more widely than the conventional technique. Education and training will play a large part in spreading the use of this technology.

9.7 Future of CAS

It is my opinion that this technology will eventually become much simpler and more user-friendly. Software and instrumentation are currently being designed to cater to complex situations and revision procedures. Some of these designs will be used to perform preoperative and postoperative evaluations of kinematics and implants and to track their progress over time, thereby possibly recognizing a pending early failure. They will also be helpful for training surgeons and acting as evaluation tools for examination purposes. Their potential for research and understanding the biomechanics of humans is huge and will no doubt assist us to provide better outcomes for our patients.

Conflict of Interest The author's department has received research funding from several companies (nonexhaustive list): Zimmer; Stryker, BBraun, Mathys, Convatec, Blue Belt Technology. The author has received consulting fees from BBraun Aesculap.

References

1. Wixson RL. Computer-assisted total hip navigation. Instr Course Lect. 2008;57:707–20.
2. Ecker TM, Murphy SB. Application of surgical navigation to total hip arthroplasty. Proc Inst Mech Eng H. 2007;221(7):699–712.
3. Sugano N, Nishii T, Miki H, Yoshikawa H, Sato Y, Tamura S. Mid-term results of cementless total hip replacement using a ceramic-on-ceramic bearing with and without computer navigation. J Bone Joint Surg Br. 2007;89(4):455–60.
4. Murali R, Bonar SF, Kirsh G, Walter WK, Walter WL. Osteolysis in third-generation alumina ceramic-on-ceramic hip bearings with severe impingement and titanium metallosis. J Arthroplasty. 2008;23(8):1240.e13–9.
5. Onda K, Nagoya S, Kaya M, Yamashita T. Cup-neck impingement due to the malposition of the implant as a possible mechanism for metallosis in metal-on-metal total hip arthroplasty. Orthopaedics. 2008;31(4):396.
6. Langton DJ, Joyce TJ, Jameson SS, et al. Adverse reaction to metal debris following hp resurfacing – the influence of component type, orientation and volumetric wear. J Bone Joint Surg Br. 2011;93B(2):164–71.
7. Lewinnek GE, Lewis JL, Tarr R, Compere CL, Zimmerman JR. Dislocations after total hip-replacement arthroplasties. J Bone Joint Surg Am. 1978;60(2):217–20.
8. Hakki S, Bilotta V, Oliveira D, Dordelly L. Acetabular central axis; Is it the future of hp navigation? Orthopaedics. 2010;33(10 Suppl):43–7.
9. Pinoit Y, May O, Girard J, Laffargue P, Ala Eddine T, Migaud H. Low accuracy of anterior pelvic plane to guide the position of the cup with imageless computer assistance. Variation of position in 106 patients. Rev Chir Orthop Reparatrice Appar Mot. 2007;93(5):455–60.
10. Deep K, Ward N, Donnelly W, Tevelan G, Crawford R. Biomechanical force displacement analysis of strength of fixation of tracker holding devices to bone in computer aided joint replacements. J Bone Joint Surg Br. 2006;88B(Supp):439.

11. Barrack R. Dislocation after total hip arthroplasty: implant design and orientation. J Am Acad Orthop Surg. 2003;11:89.
12. McCollum DE, Gray WJ. Dislocations after total hip arthroplasty: causes and prevention. Clin Orthop. 1990;261:159.
13. Di Gioia AM, Jaramaz B, Blackwell M, et al. The Otto Aufranc Award. Image guided navigation system to measure intraoperatively acetabular implant alignment. Clin Orthop Relat Res. 1998;355:8–22.
14. Kalteis T, Handel M, Herold T, et al. Greater accuracy in positioning of the acetabular cup by using an image-free navigation system. Int Orthop. 2005;29(5):272–6.
15. Najarian BC, Kilgore JE, Markel DC. Evaluation of component positioning in primary total hip arthroplasty using an imageless navigation device compared with traditional methods. J Arthroplasty. 2009;24(1):15–21.
16. Saxler G, Marx A, Vandevelde D, et al. The accuracy of free-hand cup positioning: a CT based measurement of cup placement in 105 total hip arthroplasties. Int Orthop. 2004;28:198–201.
17. Hassan DM, Johnston GH, Dust WN, Watson G, Dolovich AT. Accuracy of intraoperative assessment of acetabular prosthesis placement. J Arthroplasty. 1998;13(1):80–4.
18. Callanan MC, Jarrett B, Bragdon CR, Zurakowski D, Rubash HE, Frieberg AA, Malchau H. Risk factors for cup malpositioning: quality improvement through a joint registry in a tertiary hospital. Clin Orthop Relat Res. 2011;469(2):319–29.
19. Deep K, Khan MS, Deakin A. Assessment of precision and accuracy of computer navigation in total hip Arthroplasty. Bone Joint J. 2013;95-B(Suppl 28):47.
20. Lecerf G, et al. Femoral offset: anatomical concept, definition, assessment, implications of preoperative templating and hip arthroplasty. Orthop Traumatol Surg Res. 2009;95:210–9.
21. Sakalkale DP, Sharkey PF, Eng K, et al. Effect of femoral component offset on polyethylene wear in total hip arthroplasty. Clin Orthop Relat Res. 2011;388:125.
22. Little NJ, Busch CA, Gallagher JA, Rorabeck CH, Bourne RB. Acetabular polyethylene wear and acetabular inclination and femoral offset. Clin Orthop Relat Res. 2009;467:2895–900.
23. Maloney WJ, Keeney JA. Leg length discrepancy after total hip arthroplasty. J Arthroplasty. 2004;19(Suppl 1):108.
24. Konyves A, Bannister GC. The importance of leg length discrepancy after total hip replacement. J Bone Joint Surg. 2005;87B(2):155–7.
25. Dolhain P, et al. The effectiveness of dual offset stems in restoring offset during total hip replacement. Acta Orthop Belg. 2002;68:490–9.
26. Dastane M, Dorr LD, Tarwala R, Wan Z. Hip offset in total hip arthroplasty: quantitative measurement with navigation. Clin Orthop Relat Res. 2011;469:429–36.
27. Ellapparadja P, Mahajan V, Deakin AH, Deep K. Reproduction of hip offset and leg length in navigated total hip arthroplasty: how accurate are we? J Arthroplasty. 2015;30(6):1002–7.
28. Confalonieri N, Manzotti A, Montironi F, Pullen C. Leg length discrepancy, dislocation rate, and offset in total hip replacement using a short modular stem: navigation vs conventional freehand. Orthopaedics. 2008;31(10 Suppl 1)
29. Ellapparadja P, Mahajan V, Atiya S, Sankar B, Deep K. Leg length discrepancy in computer navigated total hip arthroplasty - how accurate are we? Hip Int. 2016;26(5):438–43.
30. Gofton W, Dubrowski A, Tabloie F, Backstein D. The effect of computer navigation on trainee learning of surgical skills. J Bone Joint Surg Am. 2007;89(12):2819–27.
31. Deep K, Picard F. Computer assisted navigation in primary total hip arthroplasty. Orthopaedics Trauma. 2014;28(5):309–14.
32. Picard F, Deep K. Role of Computer assisted surgery in training and outcomes. Orthopaedics Trauma. 2014;28(5):322–6.
33. Judet H. Five years of experience in hip navigation using a mini-invasive anterior approach. Orthopaedics. 2007;30(10 Suppl):S141–3.

Chapter 10
Patient-Specific Surgical Guide for Total Hip Arthroplasty

Takashi Sakai

Abstract In combination with the advancements of three-dimensional printing, a patient-specific surgical guide (PSG) for total hip arthroplasty (THA) is a convenient surgical instrument and has been implicated in the ideal positioning of the components, including acetabular and femoral components. PSG is designed and manufactured based on either preoperative computed tomography (CT) data or magnetic resonance imaging data. PSGs for THA are mainly classified into three types: PSG for guidewire insertion, PSG for bone cutting, and PSG for bone reaming and implant fixation. PSG positioning accuracy depends on the PSG design and contact area on the bone surface. PSGs for the acetabular component, for the conventional femoral component, and for the resurfacing femoral component have been clinically used. Based on the removal of soft tissues and preparation needed to confirm PSG setting, PSGs for THA do not always mean minimal invasive surgery.

Keywords Patient-specific surgical guide · Total hip arthroplasty · Guidewire insertion · Bone cutting · Accuracy

10.1 Introduction

PSG for the orthopedic surgery has been introduced by Radermacher et al. as a computer-assisted surgical tool [1]. In the total hip arthroplasty (THA) procedure, ideal orientation and positioning of hip implants are necessary to prevent postoperative dislocation [2, 3], satisfactorily perform daily living activities [4], and enhance implant longevity [5]. In combination with the advancements of three-dimensional printing, a PSG for hip arthroplasty is a convenient surgical instrument and has been implicated in the ideal positioning of the components, including acetabular and femoral components, based on preoperative planning (Fig. 10.1) [6–15].

T. Sakai
Department of Orthopaedic Surgery, Osaka University Graduate School of Medicine, Osaka, Japan
e-mail: tsakai-osk@umin.ac.jp

N. Sugano (ed.), *Computer Assisted Orthopaedic Surgery for Hip and Knee*,
https://doi.org/10.1007/978-981-10-5245-3_10

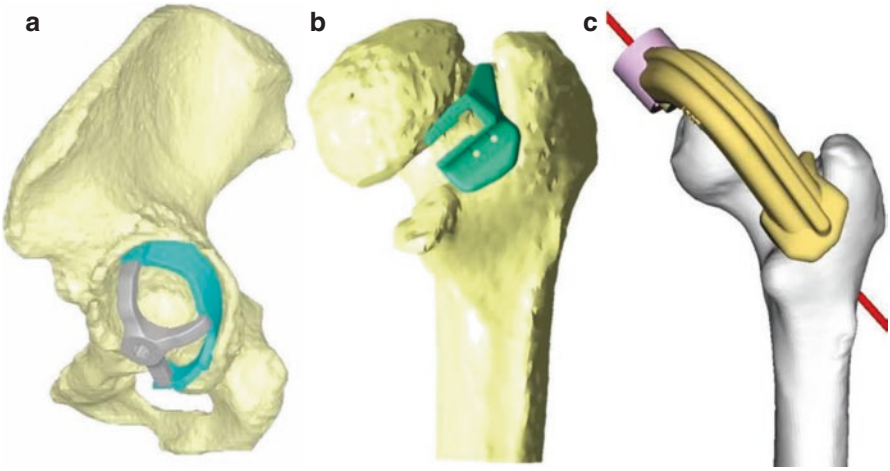

Fig. 10.1 PSGs for total hip arthroplasty. (**a**) PSG for acetabular component, (**b**) PSG for femoral neck cut, (**c**) PSG for resurfacing total hip arthroplasty

10.2 Design and Manufacturing of PSG

A PSG is designed to match the surface of the three-dimensional bone models based on either preoperative computed tomography (CT) data or magnetic resonance imaging data. PSGs are made by various materials, including resin. We used the helical CT data, reconstructed at 1-mm intervals and transferred to a workstation in STL format. PSGs for THA were designed based on preoperative planning using an image-processing software (e.g., Mimics, Materialise, Leuven, Belgium). PSGs are made from resins and produced by a machine (e.g., FORMIGA, EOS GmbH, Krailling, Germany) using a rapid prototyping method. The interoperator error of producing PSGs is 0.048 ± 0.25 mm [14].

10.3 Functional-Type Classification of PSGs for THA

PSGs for THA are mainly classified into three types: PSG for guidewire insertion [6–15], PSG for bone cutting [14], and PSG for bone reaming and implant fixation [14]. PSGs for guidewire insertion have been used to regulate the direction of the acetabular component and the resurfacing femoral component. These guides do not regulate the three-dimensional position of the component but regulate the two-dimensional position and direction. While the guidewire of the resurfacing femoral component is at the center of the component and regulates the two-dimensional position and the direction of the component [8, 9, 11, 13, 14], there are two types of guidewire of the acetabular components. The first type of guidewire is the same as the resurfacing femoral component [10, 12]. The second type of guidewire regulates

the direction of the acetabular component only [6, 7, 15]. In the second type, surgeons attempt to fix acetabular components parallel to the inserted guidewire around the acetabular rim.

PSGs for bone cutting have been used for femoral neck cutting in conventional THA. These guides regulate the neck-cut height and the direction [14, 18]. When the surgeons insert and fix the femoral component, some guides have additional parts to regulate the stem anteversion. PSGs for bone reaming and implant fixation have been particularly reported for acetabular reaming and acetabular component fixation [14]. Although these guides are set around the acetabular rim, these guides are influenced and moved by the tremor of the reamer and impaction of the socket holder.

10.4 PSG Positioning on the Bone Surface

To achieve the accurate positioning of THA implants using PSGs, accurate PSG positioning on the bone surface based on preoperative planning is necessary. The soft tissue covering the bony surface where PSGs will be set, including the joint capsule, acetabular limbus, and synovium, has to be removed completely. Otherwise, PSGs cannot be set on the bony surface accurately, and guidewire insertion and/or bone cutting cannot be performed precisely based on preoperative planning. Additionally, surgeons must confirm that PSGs are placed on the bony surface without any gaps. Based on the removal of soft tissues and preparation needed to confirm PSG setting, PSGs for THA do not always mean minimal invasive surgery.

10.5 PSG Positioning Accuracy

There are no clinical data concerning the accuracy of PSG positioning on the bone surface. In a cadaver study [14, 18], PSGs had four metal sphere markers (2 mm in diameter) for the evaluation of the accuracy of PSG positioning on the bone surface. The accuracy between preoperative planning and PSG positioning depends on the design and the contact area of PSGs.

In PSGs for the femoral neck cut through the posterior approach, there were no significant differences in PSG positioning between the wide-base-contact type and the narrow-base-contact type [14]. The absolute errors (wide vs. narrow) are 1.6 ± 0.7° vs. 1.6 ± 1.3° in the neck-cut angle on the coronal plane, 1.0 ± 0.4° vs. 0.7 ± 0.7° in the neck-cut angle on the sagittal plane, and 1.2 ± 0.8 mm vs. 0.8 ± 0.5 mm in the medial neck-cut height.

In PSGs for acetabular component implantation, all rim contact types showed more accuracy in PSG positioning than non-anterior rim contact types [14]. The absolute errors (all rim contact vs. non-anterior contact) are 1.0 ± 0.9° vs. 3.4 ± 2.4° in the inclination angle and 1.7 ± 1.1° vs. 3.6 ± 2.8° in the anteversion angle ($p = 0.03$).

10.6 PSGs for the Acetabular Component

There are three types of PSGs according to the functional classification: (1) guidewire outside the acetabulum (acetabular rim) to regulate the direction (inclination and anteversion) of the acetabular component [6, 7, 15], (2) guidewire inside the acetabulum to regulate the direction and the two-dimensional position of the acetabular component [10, 12], and (3) PSGs to regulate the direction and the three-dimensional position of the acetabular component [14]. The accuracy of computer-assisted modality between the preoperative planning and cup implantation is shown in Table 10.1.

10.6.1 Guidewire Insertion Around the Acetabular Rim

The PSG design is matched with the bony surface of the acetabular rim and/or the bony surface inside the acetabulum, avoiding contact with the remaining degenerative cartilages [6, 7, 15]. PSG has one hole for guidewire insertion around the acetabular rim. This guidewire regulates the direction, namely, inclination and anteversion of the acetabular component, based on preoperative planning. After reaming the acetabular bone and preparing the acetabular component, the cup holder is parallel to the guidewire, and the surgeons hit the cup holder to implant the acetabular component. The accuracy between the preoperative planning and cup implantation is determined by comparing the preoperative and postoperative CT

Table 10.1 Comparison of accuracy of computer-assisted total hip arthroplasty

Cup implantation in total hip arthroplasty				
	Subjects (hips)	Device	Inclination (°)	Anteversion (°)
Hananouchi et al. [6]	24	PSG[a] (parallel guidewire)	2.8 ± 2.1	3.7 ± 2.7
Hananouchi et al. [7]	38	PSG[a] (parallel guidewire)	3.2 ± 2.3	3.7 ± 2.7
Zhang et al. [10]	11	PSG[a] (reaming guidewire)	1.6 ± 0.4	1.9 ± 1.1
Buller et al. [12]	14 model bone	PSG[a] (cup holder guidewire)	1.4 ± 0.2	5.2 ± 5.5
Sakai et al. [14]	16 cadaveric	PSG[a] (cup holder, non-anterior rim) PSG[a] (cup holder, anterior rim contact)	6.7 ± 4.2 3.4 ± 2.1	8.4 ± 4.8 6.6 ± 4.7
Small et al. [15]	18	PSG[a] (parallel guidewire)	−1.96 ± 7.3	−0.22 ± 6.9
Steppacher et al. [17]	70	Mechanical navigation instrument	1.3 ± 3.4	1.0 ± 4.1
Kitada et al. [18]	30	CT-based navigation	1.5 ± 3.5	1.4 ± 5.6

Values are mean ± standard deviation
[a]Patient-specific surgical guide

data, and the absolute errors have been reported to be 3.2 ± 2.3° in the inclination of the acetabular component and 3.7 ± 2.7° in the anteversion of the acetabular component [7].

10.6.2 Guidewire Inside the Acetabulum

PSG is designed and manufactured as the abovementioned type. PSG has one hole for guidewire insertion or for the reaming handle/cup holder inside the acetabulum [10, 12]. This guidewire regulates the two-dimensional position and the direction (inclination and anteversion) of the acetabular component based on preoperative planning. Surgeons use the hollow reamer holder through the guidewire and prepare the acetabular component implantation. After reaming, surgeons use the hollow cup holder through the guidewire and implant the acetabular component. The accuracy between the preoperative planning and cup implantation is determined by comparing the preoperative and postoperative CT data, and the absolute errors have been reported to be 1.6 ± 0.4° in the inclination of the acetabular component and 1.9 ± 1.1° in the anteversion of the acetabular component [10].

10.6.3 Reaming Guide and Cup Holder in the Acetabulum (Fig. 10.2)

The PSG design is matched with the bony surface of the acetabular rim, avoiding contact with the remaining degenerative cartilages. PSG has one hole where the reamer handle and the cup holder pass [14]. It regulates both the two-dimensional position and the direction (inclination and anteversion) of the reamer handle and cup holder based on preoperative planning. Although this PSG can theoretically regulate the three-dimensional position (the depth of the acetabular component),

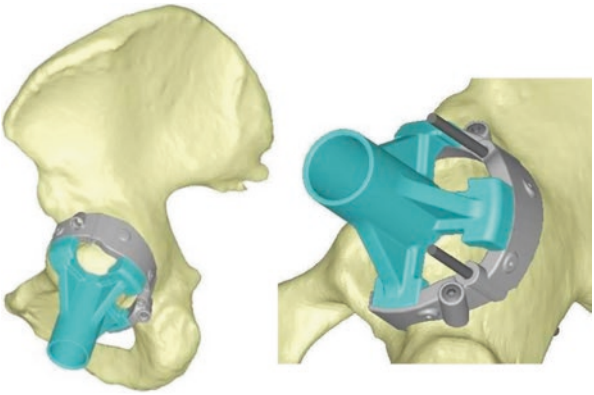

Fig. 10.2 PSG for acetabular component. This PSG regulates the direction and three-dimensional position of the reaming guide and the cup holder in the acetabulum

cup impaction affects the PSG setting. In a cadaver study, the absolute errors have been reported to be 3.4 ± 2.1° in the inclination of the acetabular component and 6.6 ± 4.7° in the anteversion of the acetabular component [14]. These PSGs have the risk of moving because of the tremor of the reamer and the cup impactor.

10.7 PSGs for the Conventional Femoral Component (Fig. 10.3)

There are two types of PSGs according to the functional classification: (1) a PSG that regulates the height and the direction of the neck-cut line [14, 16] and (2) a PSG that regulates the coronal/sagittal alignment and the anteversion of the femoral component.

10.7.1 PSG Regulates the Height and the Direction of the Neck-Cut Line

The PSG design is matched with the bony surface of the femoral neck [14]. The posterior aspect is chosen as the PSG positioning area in the posterior approach, while the anterior aspect is chosen in the anterior approach [16]. PSG regulates the height and direction of the neck-cut line. Through the metal slit, the blade contacts the bony surface and cuts the femoral neck. After the neck cut, the conventional stem is inserted and fixed based on the neck-cut line, including height and direction. In the cadaver study, the absolute errors between the preoperative planning and postoperative stem implantation, by comparing the preoperative and postoperative CT data, are

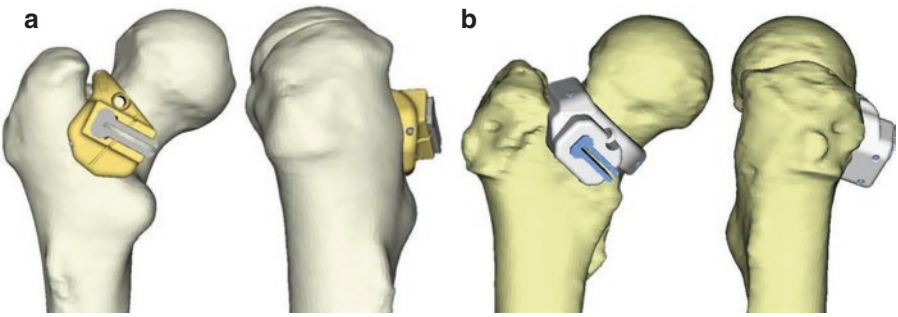

Fig. 10.3 PSG for the conventional femoral component. PSG regulates the height and the direction of the neck-cut line. (**a**) PSG for the posterolateral approach, (**b**) PSG for the anterior approach

1.4 ± 0.8° for the coronal alignment (varus/valgus), 3.0 ± 1.4° for the sagittal alignment (flexion/extension), and 0.7 ± 0.5 mm for the medial neck-cut height through the posterior approach [14].

10.7.2 PSG Regulates the Coronal/Sagittal Alignment and the Anteversion of the Femoral Component

PSG is designed and manufactured as the abovementioned type. This PSG regulates the height, the coronal/sagittal alignment, and the anteversion using the additional part attached to the neck-cut plane. After the neck cut, the conventional stem is inserted and fixed based on the neck-cut line, including height and direction as well as the anteversion direction.

10.8 PSG for the Resurfacing Femoral Component (Fig. 10.1c)

The PSG design is matched with the bony surface of the posterior aspect of the femoral neck and the saddle. This PSG regulates the position on the femoral head and the direction (stem-shaft angle and anteversion) of the guidewire insertion. PSG for the resurfacing femoral component is most practical [8, 9, 11, 13, 14], and optimal results have been reported (Table 10.2). The precision of the procedure using PSG has been reported to be as excellent as the CT-based navigation system [13].

Table 10.2 Comparison of accuracy of computer-assisted resurfacing total hip arthroplasty

Femoral guidewire insertion in resurfacing total hip arthroplasty					
	Subjects (hips)	Device	Stem-shaft angle (°)	Anteversion (°)	Insertion point (mm)
Kunz et al. [8]	45	PSG[a]	Mean 1.14	Mean 4.49	
Raaijmaakers et al. [9]	5	PSG[a]		Mean 2.02 (1.5–2.9)	Mean 1.84 (1.6–2.1)
Andenaert et al. [11]	6	PSG[a]		4.1 ± 1.8	2.7 ± 2.0
Sakai et al. [14]	16 cadaveric	PSG[a] (narrow base) PSG[a] (wide base)	2.6 ± 2.8 0.8 ± 0.6	2.4 ± 1.8 1.7 ± 2.0	3.7 ± 2.6 2.6 ± 1.5

Values are mean ± standard deviation
[a]Patient-specific surgical guide

10.9 PSG for the Corrective and Shortening Osteotomy Combined with THA

In some hip osteoarthritis patients who underwent preoperative femoral osteotomy, THA combined with the corrective and shortening osteotomy is needed. For such cases, PSG is useful like PSGs in the corrective osteotomy for the deformed upper extremities [19]. The PSG design is matched with the bony surface of the deformed femur. This PSG regulates the angle of the corrective osteotomy and the shortening distance.

References

1. Radermacher K, Portheine F, Anton M, Zimolong A, Kaspers G, Rau G, Staudte HW. Computer assisted orthopaedic surgery with image based individual templates. Clin Orthop Relat Res. 1998;354:28–38.
2. Widmer KH, Zurfluh B. Compliant positioning of total hip components for optimal range of motion. J Orthop Res. 2004;22:815–21.
3. Miki H, Yamanashi W, Nishii T, Sato Y, Yoshikawa H, Sugano N. Anatomic hip range of motion after implantation during total hip arthroplasty as measured by a navigation system. J Arthroplasty. 2007;22:946–52.
4. Jolles BM, Zangger P, Leyvraz PF. Factors predisposing to dislocation after primary total hip prosthesis. J Arthroplasty. 2002;17:282–8.
5. Kennedy JG, Rogers WB, Soffe KE, Sullivan RJ, Griffen DG, Sheehan LJ. Effect of acetabular component orientation on recurrent dislocation, pelvic osteolysis, polyethylene wear, and component migration. J Arthroplasty. 1998;13:530–4.
6. Hananouchi T, Saito M, Koyama T, Hagio K, Murase T, Sugano N, Yoshikawa H. Tailor-made surgical guide based on rapid prototyping technique for cup insertion in total hip Arthroplasty. Int J Med Robot. 2009;5:164–9.
7. Hananouchi T, Saito M, Koyama T, Sugano N, Yoshikawa H. Tailor-made surgical guide reduces incidence of outliers of cup placement. Clin Orthop Relat Res. 2010;468:1088–95.
8. Kunz M, Rudan JF, Xenoyannis GL, Ellis RE. Computer-assisted hip resurfacing using individualized drill templates. J Arthroplasty. 2010;25:600–6.
9. Raaijmaakers M, Gelaude F, De Smedt K, Clijmans T, Dille J, Mulier M. A custom-made guide-wire positioning device for hip surface replacement Arthroplasty: description and first results. BMC Musculoskelet Disord. 2010;11:161–7.
10. Zhang YZ, Chen B, Lu S, Yang Y, Zhao JM, Liu R, Li YB, Pei GX. Preliminary application of computer-assissted patient-specific acetabular navigational template for total hip arthroplasty in adult single development dysplasia of the hip. Int J Med Robot Comput Assist Surg. 2011;7:469–74.
11. Andenaert E, De Smedt K, Gelaude F, Clijmans T, Pattyn C, Geebelen B. A custom-made guide for femoral component positioning in hip resurfacing arthroplasty: development and validation study. Comput Aided Surg. 2011;16:304–9.
12. Buller L, Smith T, Bryan J, Klika A, Barsoum W, Iannti JP. The use of patient-specific instrumentation improves the accuracy of acetabular component placement. J Arthroplasty. 2013;28:631–6.
13. Kitada M, Sakai T, Murase T, Hanada T, Nakamura N, Sugano N. Validation of the femoral component placement during hip resurfacing: a comparison between the conventional jig, patient-specific template, and CT-based navigation. Int J Med Robot. 2013;9:223–9.

14. Sakai T, Hanada T, Murase T, Kitada M, Hamada H, Yoshikawa H, Sugano N. Validation of patient specific surgical guides in total hip arthroplasty. Int J Med Robot. 2014;10:113–20.
15. Small T, Krebs V, Molloy R, Bryan J, Klika AK, Barsoum WK. Comparison of acetabular shell position using patient specific instruments vs. standard surgical instruments: a randomized clinical trial. J Arthroplasty. 2014;29:1030–7.
16. Sakai T, Hamada H, Takao M, Murase T, Yoshikawa H, Sugano N. Validation of patient-specific surgical guides for femoral neck cutting in total hip arthroplasty through the anterolateral approach. Int J Med Robot. 2017;13(3)
17. Steppacher SD, Kowal JH, Murphy SB. Improving cup positioning using a mechanical navigation instrument. Clin Orthop Relat Res. 2011;469:423–8.
18. Kitada M, Nakamura N, Iwana D, Kakimoto A, Nishii T, Sugano N. Evaluation of the accuracy of computed tomography-based navigation for femoral stem orientation and leg length discrepancy. J Arthroplasty. 2011;26:674–9.
19. Murase T, Oka K, Moritomo H, Goto A, Yoshikawa H, Sugamoto K. Three-dimensional corrective osteotomy of malunited fractures of the upper extremity with use of a computer simulation system. J Bone Joint Surg Am. 2008;90:2375–89.

Chapter 11
Robotic Primary and Revision THA for the Femoral Side

Nobuo Nakamura

Abstract Robot-assisted THA for femoral side is one of the oldest appreciations of robotics in orthopedic surgery. The first active robotic system, ROBODOC, has been used in many countries. Originally, it utilized pin-based registration system and required locator pin implantation in the patient femur before THA. Subsequently, non-pin-based surface registration technique was developed, which eliminated the need for pin implantation and pin-related complications. Besides the function of femoral milling during primary THA, this system can also selectively remove bone cement from the femoral canal during revision THA. Although one study shows a higher revision rate of robotic femoral surgery than a conventional technique, many studies show accurate femoral preparation, same or slightly better postoperative function, better alignment of the stem, less fat embolism, less stress shielding, and a lower incidence of femoral fracture by using the robot than conventional techniques.

Keywords Robotic · Primary total hip arthroplasty · Revision total hip arthroplasty · Femoral

11.1 Introduction

Historically, there were two robotically assisted systems for femoral milling during total hip arthroplasty (THA): ROBODOC (Think Surgical, Fremont, CA, USA) and CASPAR (URS Ortho, Rastatt, Germany). ROBODOC was the first active robotic system designed to improve outcomes on the femoral side of cementless total hip arthroplasty (THA) by reducing technical errors [1]. During the 1980s, the clinical results using cementless THA were not stable because of bone ingrowth failure and persistent thigh pain. Manual preparation of the femoral cavity was thought to be one of the major causes of the problem [2]. Initial pilot studies were performed in dogs, and clinical use of this system was initiated in 1992 [2].

N. Nakamura
Kyowakai Hospital, Suita, Osaka, Japan
e-mail: nnakamu@abox2.so-net.ne.jp

N. Sugano (ed.), *Computer Assisted Orthopaedic Surgery for Hip and Knee*,
https://doi.org/10.1007/978-981-10-5245-3_11

The US Food and Drug Administration (FDA) authorized a multicenter study that started in 1994. Although the robotic system used in that study required insertion of three locator pins, and the average operative time was more than 240 min, the study demonstrated better fit and positioning of the femoral component in the robot-assisted group [1]. Later, there were further system improvements that included reduction in the number of locator pins used (from three to two) and improved milling speed and cutting paths to reduce surgical invasiveness and robot milling time [1].

The European Union approved the system in 1994 [3], although the early trials in Germany led to multiple lawsuits and negative media coverage because of the high complications rate [4]. In Japan, we initiated a multicenter clinical trial in 2000 to acquire approval by our Ministry of Health, Labour, and Welfare. Subsequently, a "pinless" registration system was developed that utilized the bone surface for registration. In 2008, it received FDA approval for its use in THA. The ROBODOC system has now been used for more than 28,000 joint arthroplasties, including those in the knee.

CASPAR was the other image-based active robotic system. Although preliminary in vitro studies showed better bone-implant contact than manual implantation [5] and accuracy comparable to that of the ROBODOC system [6], the CASPAR system has been shown to have low accuracy regarding the postoperative stem anteversion angle compared with that in the original plan [7]. In addition, in a prospective trial, the CASPAR system had worse outcomes in terms of blood loss, dislocation, revision rate, and heterotopic ossification than the conventional group at the average 18 months of follow-up [8]. This system is no longer available for clinical use [4]. In this chapter, therefore, we address the ROBODOC system.

11.2 Techniques

11.2.1 Primary THA Using a Pin-Based System

ROBODOC is a fiducially based registration system. It consists of three units: a robotic arm with a high-speed end-milling device, a control cabinet, and a preoperative planning workstation (ORTHODOC; Think Surgical) (Fig. 11.1). Additional disposable equipment (e.g., sterilized drill bits and drapes) are needed for each robotic operation.

Using this pin-based system, each procedure consists of locator pin implantation, computed tomography (CT) scanning, preoperative planning using the workstation, robotic diagnostics and preparation, exposure and registration of pins, and robotic milling of the femur. For femoral registration, two locator pins are implanted: one in the greater trochanter and the other in the lateral condyle of the femur (Fig. 11.2). After pin implantation, which is performed with the patient under local anesthesia prior to THA, a CT scan is obtained according to the manufacturer's specified protocol.

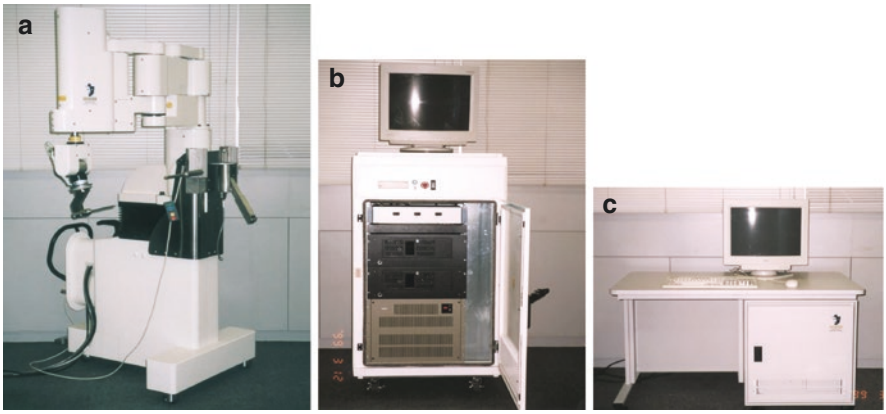

Fig. 11.1 ROBODOC surgical robot system. (**a**) ROBODOC surgical assistant, a five-axis SACARA-type surgical robot. (**b**) Control cabinet. (**c**) ORTHODOC, a three-dimensional (3D) preoperative planning workstation

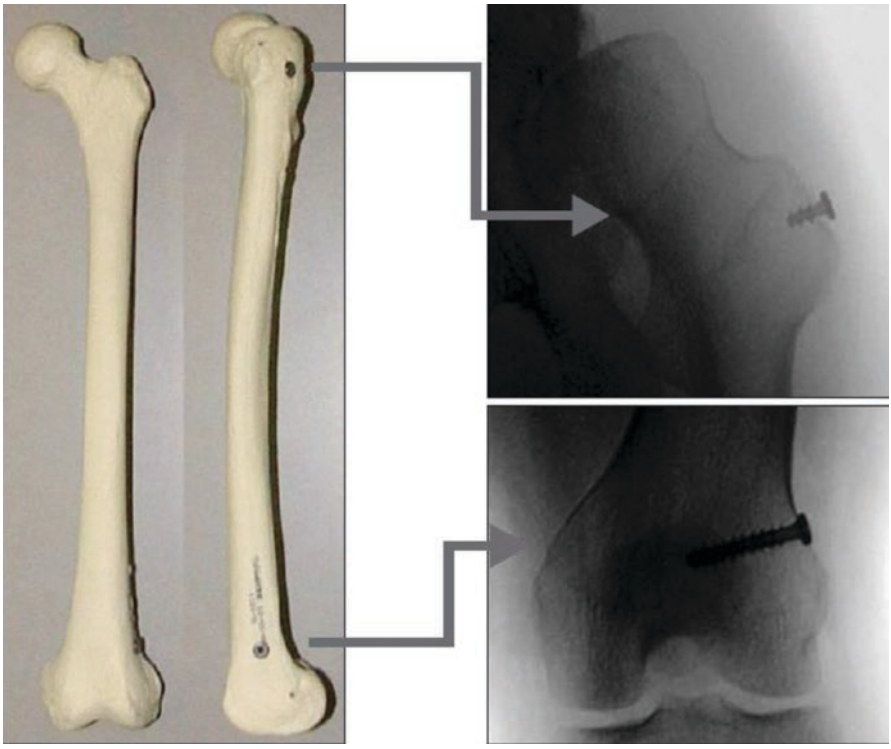

Fig. 11.2 Fiducial screws for registration. The screws are inserted in the greater trochanter and femoral condyles, and computed tomography (CT) images are obtained

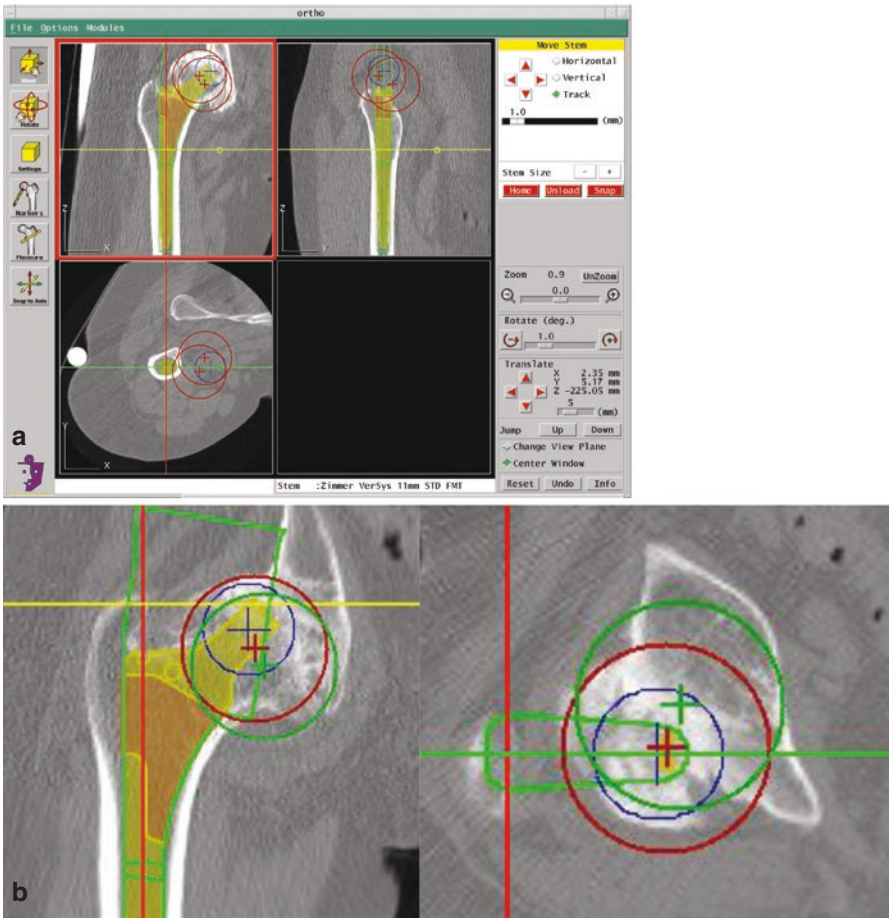

Fig. 11.3 Preoperative planning using the workstation. (**a**) Using the CT data, the surgeon constructs a 3D plan for prosthesis implantation. (**b**) Green lines around the stem indicates the cutting path, by which the surgeon can identify any risk to soft tissues and/or the possibility of bone injury

At the workstation, using the CT image data for the patient, the surgeon can create a three-dimensional (3D) preoperative plan to select the size of the prosthesis and its position in the femur (Fig. 11.3a). As the workstation shows the cutting paths three-dimensionally, the surgeon can identify any risk of abductor tendon injury and/or damage to the greater trochanter (Fig. 11.3b). When the implant is optimally positioned (virtually, at the workstation), the preoperative planning data are recorded on a compact disk (CD). Prior to the surgical procedure, the surgeon loads the patient data on the CD into the robot-assisted system and performs self-start-up diagnostics of the robot.

During the operation, the surgeon exposes the pins and secures the patient's lower extremity to the robot with a femoral positioning clamp (Fig. 11.4). The surgeon then

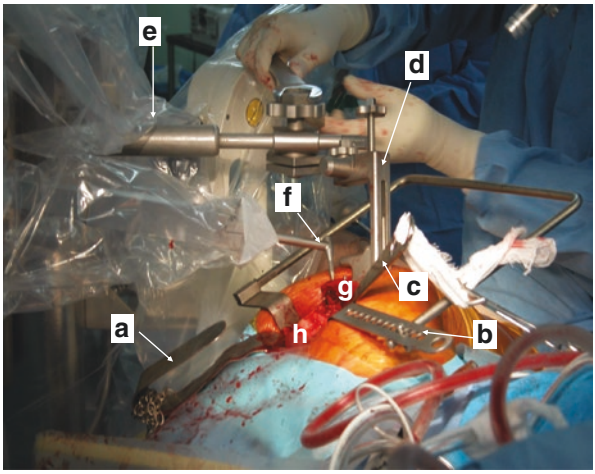

Fig. 11.4 Surgical exposure of the left hip via a posterior approach. Femoral head and neck are elevated by an abdominal spatula (**a**). Gluteus maximus is retracted with a Charnley retractor (**b**). Gluteus medius and minimus muscles are retracted with a Hohmann retractor (**c**). A femoral positioning clamp (**d**) is then applied to the proximal femur (just below the lesser trochanter) to connect it with the robot (**e**). Finally, a bone motion monitor (**f**) is placed on the bone surface. (**g**) Greater trochanter; (**h**) femoral head

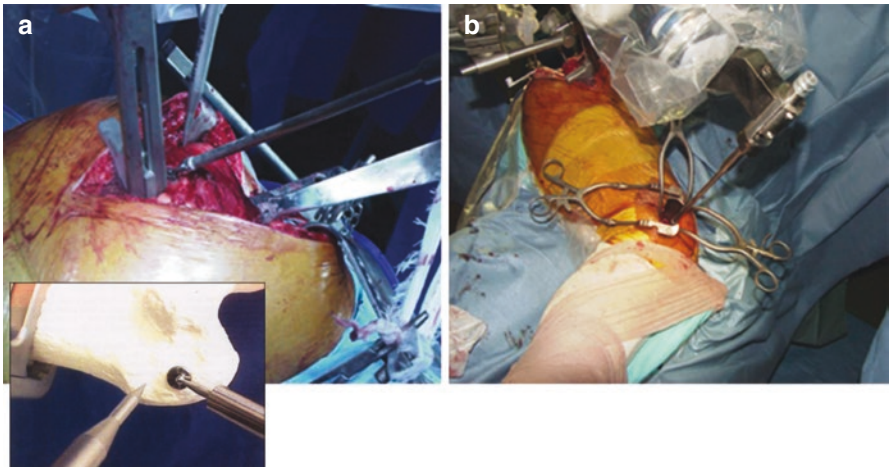

Fig. 11.5 Exposure and registration of the two locator pins: one in the greater trochanter (left panel) and the other in the lateral condyle of the femur (right panel). Inset: Robotic probe is touching the pins for registration

moves the robot arm by guiding its probe into contact with the pins (Fig. 11.5). The robot-assisted system computer records the pin locations and automatically performs registration and verification of its accuracy.

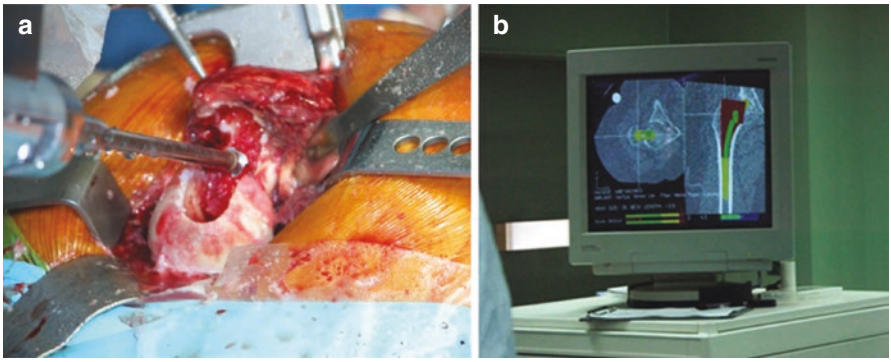

Fig. 11.6 (**a**) Robotic milling of the proximal femur. The gluteus medius and minimus muscles were retracted anteriorly without any damage. (**b**) Monitor on the control cabinet shows the milling process by the robot in real time

The surgeon then installs a drill bit and guides the robotic arm in front of the bone to begin milling the femur (Fig. 11.6a). While the robot mills the femoral canal, the monitor shows the milling process (Fig. 11.6b). The surgeon can stop the machine at any time by pressing a "pause" button. We prefer a posterior approach so the gluteus medius and minimus muscles are easily retracted anteriorly to avoid damage (Fig. 11.6a). After the milling is complete, the surgeon inserts the implant in the usual fashion. It is easy to determine the osteotomy level of the femoral neck because the medial cortex of this level has already been milled by the robot.

11.2.2 Primary THA Using a Pinless System

To eliminate the need for locator pin implantation and its potential pin-related complications (e.g., postoperative pain at the site of pin implantation [9]), a proprietary non-pin-based surface registration technique was developed by the manufacturer in 2000. First, a CT scan of the femur is performed according to the manufacturer's specified protocol. The CT data are then imported into the workstation, and surface models of the proximal and distal femur are created for surface registration (Fig. 11.7). A preoperative plan is created in the same manner as with the pin-based registration system (Fig. 11.3). Once the surface bone model is successfully created and the optimal surgical plan completed, the surgeon transfers the data to a CD.

Prior to the surgical procedure, the surgeon loads the CD's information into the robotic system and performs routine setup and diagnostic checks. During surgery, the surgeon secures the patient's leg in the femoral fixator of the robot and then locates the bone surface points on the femur using a digitizer (Think Surgical) (Fig. 11.8a). In the present study, 14 points from the proximal femur and three points from the distal femur were digitized (Fig. 11.8b). The robotic computer recorded the spatial information of surface points and matched them to the coordinate surface model that was created preoperatively on the workstation. This procedure is called *surface*

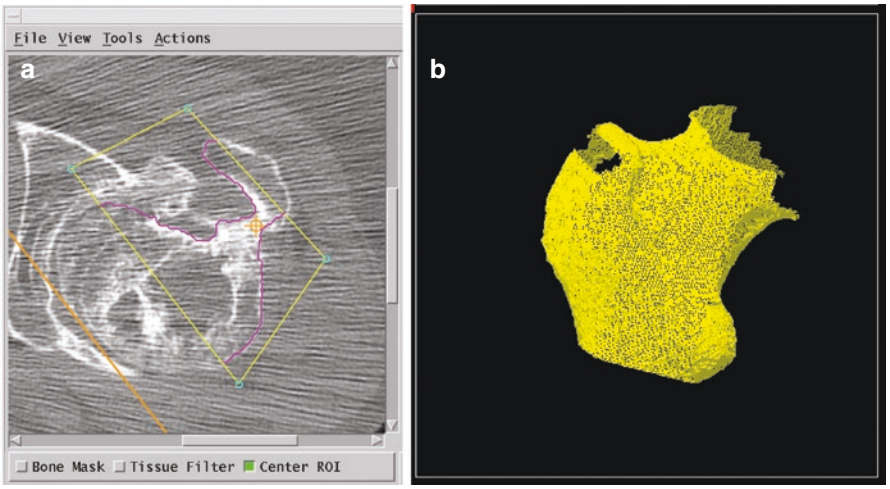

Fig. 11.7 Preoperative creation of the surface models of the femur on the workstation for pinless registration. (**a**) The bone surface is defined (pink line) on each CT slice. (**b**) Acquired bone surface model of the proximal femur. *ROI* region of interest

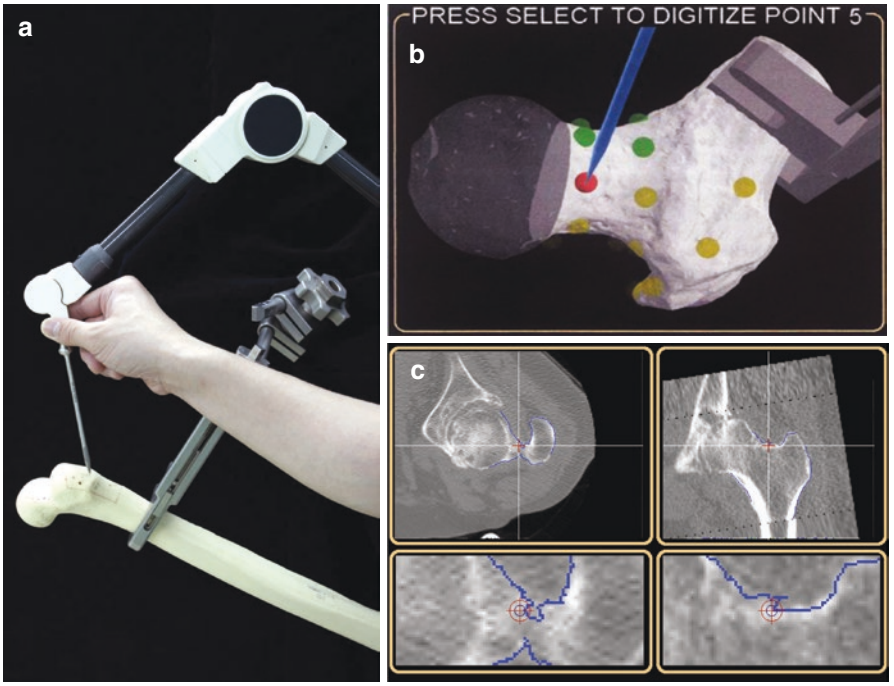

Fig. 11.8 Pinless registration technique. (**a**) During the operation, the surgeon oriented the robot by selecting points on the femoral surface using a "digitizer." (**b**) Registration of the proximal femur. Fourteen points were chosen, as shown on the monitor. The surgeon verified the registration accuracy by touching the bone surfaces with the digitizer. (**c**) If the locations coincided with the bone surface points on the monitor, the surgeon accepted the registration

registration. When the registration has been completed, the surgeon verifies its accuracy by touching bone surfaces with the digitizer. If the difference between the digitization-based surface contour and the CT-derived surface contour is within 1 mm, the registration is considered acceptable (Fig. 11.8c). A drill bit is then installed, and the milling of the femur begins.

11.2.3 Cement Removal During Revision THA Using a Pin-Based System

The pin-based registration system can also selectively remove bone cement from the femoral canal during revision THA. Prior to the surgery, two locater pins are implanted into the affected femur under local anesthesia. CT scans are obtained, and their data are imported into a preoperative planning workstation. The long axis of the femur is aligned. At least eight cross sections are defined, and the surgeon demarcates a perimeter around the bone cement on axial views of the femur. From these data, the workstation program automatically creates a 3D cutting path for cement removal (Fig. 11.9). At this point, the surgeon can check and modify the

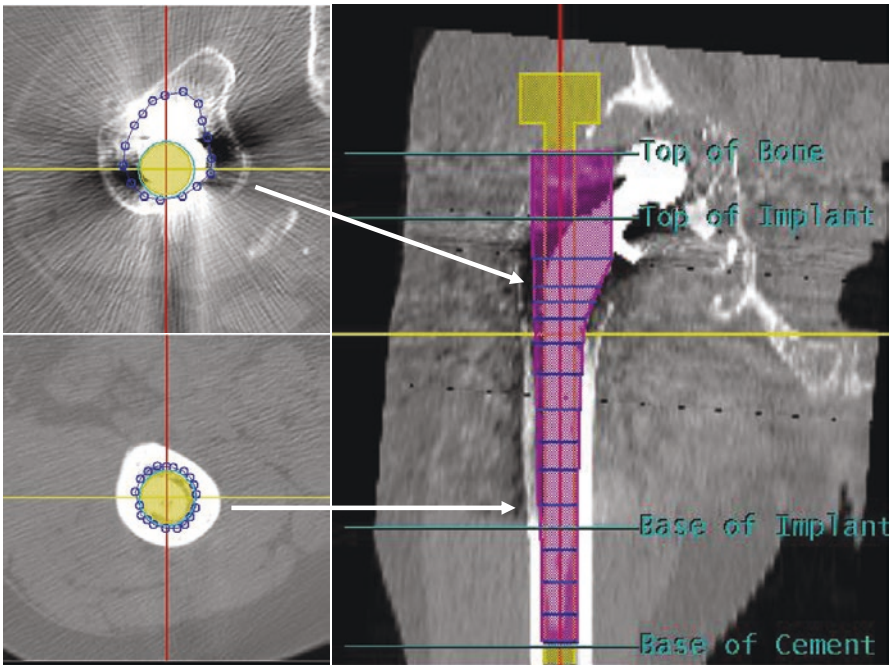

Fig. 11.9 At the planning workstation, multiplanar reconstruction view of the proximal femur is used to plan robotic cement removal. A minimum of eight cross sections are defined on a coronal view. A perimeter around the bone cement is demarcated on each section (blue lines). The cutting path (purple) is then created automatically

cutting path. These preoperative planning data are recorded on a CD. During the operation, the femur is exposed and the femoral component removed using a conventional procedure. After the patient's leg is fixed to the robot and surgical table, registration is performed using the two locater pins. After soft tissues are firmly retracted, the robot mills the femoral canal to remove the bone cement. Finally, the surgeon manually reams the femoral canal and inserts the stem.

11.3 Clinical Outcomes

11.3.1 Primary THA Using the Pin-Based System

The clinical accuracy (75 hips) of the pin-based system using postoperative CT images was <5% for the canal fill, <1 mm for the gap, and <1° for the mediolateral and anteroposterior alignment [10]. In our prospective, randomized study (78 hips underwent robotic milling, 78 underwent hand rasping) using a posterolateral approach, the robotic milling group showed significantly superior Merle d'Aubigne hip scores at 2 years. Compared with the robotic milling group, the hand rasping group had more intraoperative femoral fractures (0 vs. 5), more stem undersizing, higher vertical seating, and more femoral anteversion causing inferior fit of the implant [11]. At the 5-year follow-up (71 hips with robotic milling, 75 with hand rasping), there was significantly less variance in limb-length inequality and less stress shielding of the proximal femur in the robotic milling group, although differences in the clinical scores were not significant [12]. This tendency was also true at the 10-year follow-up [13]. At 2 years postoperatively, a dual energy X-ray absorptiometry study suggested that robotic milling was effective in facilitating proximal load transfer around the femoral component and minimizing bone loss after cementless THA [14].

The robotic femoral milling system reportedly reduces the development of intraoperative pulmonary embolisms. Using transesophageal echocardiography (46 hips with robotic milling, 25 with hand rasping), Hagio et al. found that the incidence of severe embolic events was lower in the robotic-milling group than in the hand-rasping group [15]. In contrast, Honl et al., who conducted a prospective, randomized study with 2 years of follow-up (74 hips with robotic milling, 80 with hand rasping using an anterolateral approach), found that 18% of the attempted robotic implantation procedures required conversion to manual implantation because the robotic system failed. They also found more complications in the robotic milling group, including nerve palsy (7%), dislocation (18%), and abductor dysfunction requiring reoperation (15%) [16].

One reason for the difference could be the surgical approach. It is possible that the posterolateral approach allows better retraction of the abductor muscles and thus better access for robotic milling than the anterolateral approach. However, Bach et al. reported that, when the insertion of the hip abductor muscles was protected appropriately, gait analysis showed no functional impairment after robotic procedures, even

with an anterolateral approach [17]. Another reason could be the surgeons' learning curve with this system. The preoperative planning workstation shows the cutting paths three-dimensionally, and the well-trained surgeon can then make the appropriate decisions preoperatively and intraoperatively to avoid abductor tendon injury by choosing the appropriate implant and/or approach for each patient [12].

11.3.2 Primary THA Using a Pinless System

We have reported a comparison study of the pinless system (40 hips) versus the pin-based system (78 hips). The average duration of the surgery was 25 min longer with the pinless system because more time was required for registration, including verification. Differences in the average blood loss and complications (e.g., nerve palsy, femoral fissure, dislocation, thigh pain) were not significant. At an average of 38 months postoperatively, Japanese Orthopaedic Association hip scores were significantly better in the pinless group than in the pin-based group, probably because patients with the pinless system had no pin-related knee pain. The accuracy of postoperative stem alignment of the pinless system was comparable to that of the pin-based method [18].

The pinless system received FDA approval in 2008. The advantages of this system are that there is no need for prior pin implantation surgery and no concern about pin-related knee pain.

11.3.3 Revision THA

Yamamura et al. reported 19 cases that required robotic bone cement removal from the femoral canal. The mean robotic milling time was 34 min (range 17–51 min). None of the patients suffered perforation or fracture of the femur during surgery or follow-up. No patients displayed nerve palsy or infection. Dislocation was seen in one patient. Radiographically, the bone cement was completely removed in all cases. Stem subsidence was seen in two cases. At final follow-up (76–150 months), all stems were considered stable. Early weight bearing was possible because of circumferential preservation of the femoral cortex. In nine cases, full weight bearing was achieved within 1 week postoperatively, which was better than that achieved with extended trochanteric osteotomy. Robotic bone cement removal thus seems safe and effective [19].

11.4 Discussion

There are several advantages of a robotic milling system. It enables precise preoperative 3D planning and execution of the plan. It enables better fit and increased bony ingrowth between the implant and the host bone. It reduces the incidence of

complications, such as intraoperative pulmonary embolism, femoral fractures, and limb-length inequality. Its disadvantages are increased surgical invasiveness, longer operation time, an extended learning curve, and higher cost. In addition, surgeons cannot modify the surgical plan intraoperatively [4].

There have also been several reports of technical complications, such as having to halt a procedure because of bone motion during cutting, thereby requiring reregistration, femoral shaft fissures requiring wire cerclage, acetabular rim damage during milling, milling of a defect of the greater trochanter, and registration failures [20, 21]. To avoid these errors and complications, surgeons and staff must be fully educated regarding the use of the robotic milling system. Being familiar with the equipment and its use can minimize negative occurrences and optimize the safety and usefulness of the robot. Surgeons should keep in mind that, with this system, preoperative planning is part of the surgery, and an inappropriate plan results in failure. During surgery, the surgeon needs to understand the workspace and appropriate positioning of the patient and robot, carefully watch the moving path of the cutter, and listen to the sound of the milling to detect any abnormalities [22].

Future designs of the robotic system should include fail-safe mechanisms and tracking to prevent inadvertent injuries. For example, combining it with a navigation system would help avoid the need for reregistration as a result of bone motion. An improved user–machine interface could reduce the incidence of registration failure and subsequent incorrect execution of the surgery.

References

1. Bargar WL, Bauer A, Borner M. Primary and revision total hip replacement using the Robodoc system. Clin Orthop. 1998:82–91.
2. Paul HA, Bargar WL, Mittlestadt B, Musits B, Taylor RH, Kazanzides P, Zuhars J, Williamson B, Hanson W. Development of a surgical robot for cementless total hip arthroplasty. Clin Orthop. 1992:57–66.
3. Bargar WL. Robots in orthopaedic surgery: past, present, and future. Clin Orthop Relat Res. 2007;463:31–6.
4. Jacofsky DJ, Allen M. Robotics in arthroplasty: a comprehensive review. J Arthroplasty. 2016;31:2353. https://doi.org/10.1016/j.arth.2016.05.026.
5. Wu LD, Hahne HJ, Hassenpflug J. The dimensional accuracy of preparation of femoral cavity in cementless total hip arthroplasty. J Zhejiang Univ Sci. 2004;5:1270–8. https://doi.org/10.1631/jzus.2004.1270.
6. Schneider J, Kalender W. Geometric accuracy in robot-assisted total hip replacement surgery. Comput Aided Surg. 2003;8:135–45.
7. Mazoochian F, Pellengahr C, Huber A, Kircher J, Refior HJ, Jansson V. Low accuracy of stem implantation in THR using the CASPAR-system: anteversion measurements in 10 hips. Acta Orthop Scand. 2004;75:261–4. https://doi.org/10.1080/00016470410001178.
8. Siebel T, Kafer W. Clinical outcome following robotic assisted versus conventional total hip arthroplasty: a controlled and prospective study of seventy-one patients. Z Orthop Ihre Grenzgeb. 2005;143:391–8. https://doi.org/10.1055/s-2005-836776.
9. Nogler M, Maurer H, Wimmer C, Gegenhuber C, Bach C, Krismer M. Knee pain caused by a fiducial marker in the medial femoral condyle: a clinical and anatomic study of 20 cases. Acta Orthop Scand. 2001;72:477–80.

10. Nishihara S, Sugano N, Nishii T, Tanaka H, Nakamura N, Yoshikawa H, Ochi T. Clinical accuracy evaluation of femoral canal preparation using the ROBODOC system. J Orthop Sci. 2004;9:452–61.
11. Nishihara S, Sugano N, Nishii T, Miki H, Nakamura N, Yoshikawa H. Comparison between hand rasping and robotic milling for stem implantation in cementless total hip arthroplasty. J Arthroplasty. 2006;21:957–66.
12. Nakamura N, Sugano N, Nishii T, Kakimoto A, Miki H. A comparison between robotic-assisted and manual implantation of cementless total hip arthroplasty. Clin Orthop Relat Res. 2010;468:1072–81.
13. Nakamura N, Sugano N. Sakai T. Nakahara I. Comparison between robotic-assisted and manual implantation of primary cementless total hip arthroplasty; minimum ten years follow-up results. Proceedings of International CAOS meeting, 2014. 2014.
14. Hananouchi T, Sugano N, Nishii T, Nakamura N, Miki H, Kakimoto A, Yamamura M, Yoshikawa H. Effect of robotic milling on periprosthetic bone remodeling. J Orthop Res. 2007;25:1062–9.
15. Hagio K, Sugano N, Takashina M, Nishii T, Yoshikawa H, Ochi T. Effectiveness of the ROBODOC system in preventing intraoperative pulmonary embolism. Acta Orthop Scand. 2003;74:264–9.
16. Honl M, Dierk O, Gauck C, Carrero V, Lampe F, Dries S, Quante M, Schwieger K, Hille E, Morlock MM. Comparison of robotic-assisted and manual implantation of a primary total hip replacement. A prospective study. J Bone Joint Surg Am. 2003;85:1470–8.
17. Bach CM, Winter P, Nogler M, Gobel G, Wimmer C, Ogon M. No functional impairment after Robodoc total hip arthroplasty: gait analysis in 25 patients. Acta Orthop Scand. 2002;73:386–91.
18. Nakamura N, Sugano N, Nishii T, Miki H, Kakimoto A, Yamamura M. Robot-assisted primary cementless total hip arthroplasty using surface registration techniques: a short-term clinical report. Int J Comput Assist Radiol Surg. 2009;4:157–62.
19. Yamamura M, Nakamura N, Miki H, Nishii T, Sugano N. Cement removal from the femur using the ROBODOC system in revision total hip arthroplasty. Adv Orthop. 2013;2013:347–58. https://doi.org/10.1155/2013/347358.
20. Schulz AP, Seide K, Queitsch C, von Haugwitz A, Meiners J, Kienast B, Tarabolsi M, Kammal M, Jurgens C. Results of total hip replacement using the Robodoc surgical assistant system: clinical outcome and evaluation of complications for 97 procedures. Int J Med Robot. 2007;3:301–6.
21. Chun YS, Kim KI, Cho YJ, Kim YH, Yoo MC, Rhyu KH. Causes and patterns of aborting a robot-assisted arthroplasty. J Arthroplasty. 2011;26:621–5. https://doi.org/10.1016/j.arth.2010.05.017.
22. Sugano N. Computer-assisted orthopaedic surgery and robotic surgery in total hip arthroplasty. Clin Orthop Surg. 2013;5:1–9. https://doi.org/10.4055/cios.2013.5.1.1.

Chapter 12
Computer-Assisted Orthopedic Surgery for Hip Osteotomy

Masaki Takao, Takashi Sakai, Hidetoshi Hamada, and Nobuhiko Sugano

Abstract Developmental dysplasia of the hip (DDH) is a common cause of secondary osteoarthritis. Various types of periacetabular osteotomy that reorient the dysplastic acetabulum have been developed to prevent the early onset of secondary osteoarthritis. Bernese periacetabular osteotomy and rotational acetabular osteotomy are now commonly used as surgical treatments for symptomatic DDH. Periacetabular osteotomies are technically demanding procedures that require detailed anatomical knowledge of the pelvic anatomy and three-dimensional (3D) cognitive skills because surgeons must avoid intra-articular perforation of chisels, thin acetabular fragments, posterior column fracture, and vascular and nerve injury. Preoperative 3D simulation of the osteotomy would be useful to avoid these perioperative complications. Computer-assisted systems such as navigation and custom cutting guides would be powerful tools with which to accurately execute the 3D osteotomy plan. A few reports have described the clinical application of a navigation system or custom cutting guide for periacetabular osteotomy. However, no navigation system that can track movement of the acetabular fragment has been developed. Some researchers have been developing such navigation systems with a focus on tracking the acetabular fragment.

Keywords Bernese periacetabular osteotomy · Rotational acetabular osteotomy · Curved periacetabular osteotomy · Navigation · Patient-specific surgical guide

M. Takao, M.D., Ph.D. (✉) • N. Sugano, M.D., Ph.D.
Department of Orthopaedic Medical Engineering, Osaka University Graduate School of Medicine, 2-2 Yamadaoka, Suita, 565-0871 Osaka, Japan
e-mail: masaki-tko@umin.ac.jp

T. Sakai, M.D., Ph.D. • H. Hamada, M.D., Ph.D.
Department of Orthopaedic Surgery, Osaka University Graduate School of Medicine, 2-2 Yamadaoka, Suita, 565-0871 Osaka, Japan

N. Sugano (ed.), *Computer Assisted Orthopaedic Surgery for Hip and Knee*,
https://doi.org/10.1007/978-981-10-5245-3_12

12.1 Need for Computer Technology in Periacetabular Osteotomy

Developmental dysplasia of the hip (DDH) is a common cause of secondary osteoarthritis. Various types of periacetabular osteotomy that reorient the dysplastic acetabulum have been developed to prevent the early onset of secondary osteoarthritis [1–3], including Eppright's dial osteotomy [4], Wagner's spherical acetabular osteotomy [5], Ganz's Bernese periacetabular osteotomy [1], rotational acetabular osteotomy (RAO) [2], and curved periacetabular osteotomy (CPO) [6]. Bernese periacetabular osteotomy and RAO are now commonly used as surgical treatments for symptomatic DDH in Europe, North America, and Japan [7]. Clinical application of computer technology has also been reported mainly for Bernese periacetabular osteotomy, RAO, and CPO.

Bernese periacetabular osteotomy was first described in 1988 by Ganz et al. [1] and has been performed in Europe and North America. Its polygonal osteotomy design involves three cuts in the ilium, pubis, and ischial bones through a modified Smith-Petersen approach and maintains the integrity of the posterior column. RAO is a reorientational periacetabular osteotomy first described by Ninomiya and Tagawa in 1984 [2]. The surgical approaches and procedures of RAO have been modified, and it is currently widely used throughout Japan for patients with the early stages of osteoarthritis secondary to DDH. The design of the osteotomy is spherical, allowing the acetabular fragment to easily rotate and increasing the bone contact area between fragments for stability and bone healing (Fig. 12.1). RAO also maintains the integrity of the posterior column. CPO was modified from periacetabular osteotomy by Naito et al. [6]; the osteotomy design is spherical and performed through a modified Smith-Petersen approach.

The common aims of these techniques are to improve femoral head vertical coverage with articular cartilage and restore the femoral head from its subluxated position. Most of these osteotomies are technically demanding procedures. Insufficient lateral and anterior acetabular coverage as well as excessive anterior coverage after periacetabular osteotomy reportedly leads to early osteoarthritis [8]. Thus, many researchers have attempted to develop a three-dimensional (3D) system with which to evaluate the acetabular coverage of the femoral head [9–13], a 3D planning system [10, 14, 15], and a surgical guidance system for periacetabular osteotomy that includes navigation [16–22] and a custom cutting guide [23, 24]. Periacetabular osteotomy requires detailed anatomical knowledge of the pelvic anatomy and 3D cognitive skills because surgeons must avoid intra-articular perforation of chisels, thin acetabular fragments, posterior column fracture, and vascular and nerve injury [25–27].

Preoperative 3D simulation of the osteotomy would help to avoid these perioperative complications. Computer-assisted systems such as navigation and custom cutting guides would be powerful tools with which to accurately execute the 3D osteotomy plan. Many authors have reported the usefulness of navigation in total hip arthroplasty to reduce malpositioning of components and minimize leg-length

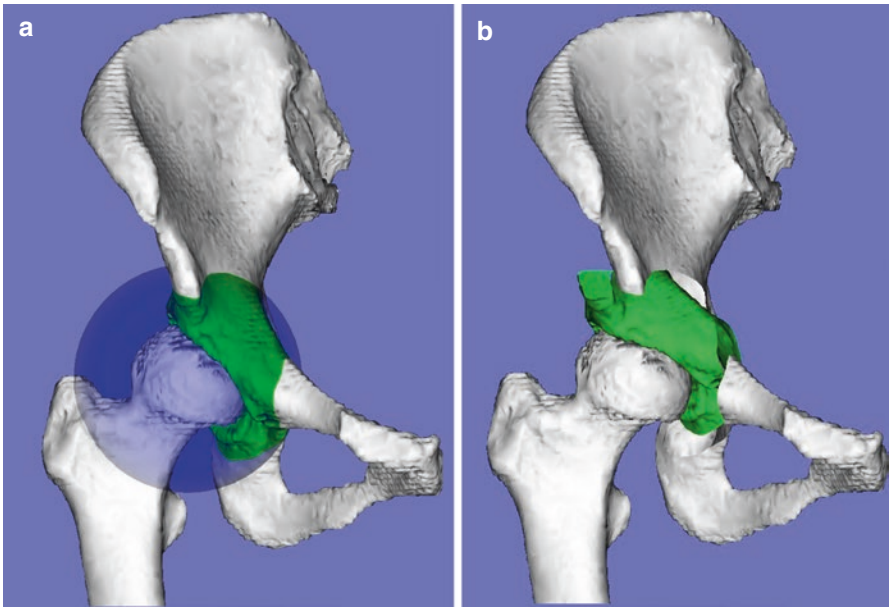

Fig. 12.1 (**a**) Design of rotational acetabular osteotomy and (**b**) position and alignment of a reoriented acetabulum were simulated three-dimensionally. Reprinted from [32]

discrepancy regardless of the incision length, approach, or surgeon's experience [28]. However, a few reports have described the clinical application of a navigation system or custom cutting guide for periacetabular osteotomy (Table 12.1) [16–19, 22–24, 29–32].

12.2 Periacetabular Osteotomy Using Navigation

Langlotz et al. [16] developed their original image-guided freehand navigation of surgical instruments and applied it to Bernese periacetabular osteotomy for 12 patients with 12 dysplastic hips. Their system did not incorporate the preoperative planning of osteotomies, reorientation, or refixation, but could visualize the osteotome in real time. The real-time visualization initiated a modification of the established surgical technique in the form of an alteration of the direction of the pubis osteotomy. The system indicated that the risk of endangering the hip joint during this osteotomy could be reduced by a less markedly inclined cut. The authors also reported the outcomes of 14 cases of computer-navigated osteotomy [17]. They found that although the operative time was 20–30 min longer and the operative blood loss volume was higher than those for nonimage-guided interventions, no intraoperative or postoperative complications were observed, and an accurate and safe pelvic osteotomy could be performed.

Table 12.1 Literature on clinical application of navigation to periacetabular osteotomy

Author	Study design	No. of patients (hips)	Follow-up period	Osteotomy name	Osteotomy design	Approach	Navigation system	Planning software	Display of plan
Langlotz F (1997) [16]	Case series	12 (12)	Average 10.5 months	Bernese periacetabular osteotomy	Polygonal	Modified Smith-Petersen	Original	+	None
Langlotz F (1998) [17]	Case series	14 (14)	Average 10.5 months	Bernese periacetabular osteotomy	Polygonal	Modified Smith-Petersen	Original	+	None
Nakahodo K (2000) [18]	Case series	2	N/A	Rotational acetabular osteotomy	Spherical	Transtrochanteric	Original	+	Osteotomy line and reoriented acetabulum
Mayman DJ (2002) [19]	Case series	7 (8)	N/A	Kingston periacetabular osteotomy	Polygonal	Transtrochanteric	Original	+	Osteotomy line (iliac and ischical osteotomies)
Hsieh PH (2006) [30]	Comparative study	18 (18) navigation, 18 (18) non-navigation	Minimum 24 months	Modified periacetabular osteotomy	Spherical	Transtrochanteric	VectorVision Hip Navigation (Brainlab)	-	None
Akiyama H (2010) [29]	Case series	3 (3)	28 months (12–37 months)	Curved periacetabular osteotomy	Spherical	Modified Smith-Petersen	Stealth Station TRIA Plus (Medtronic)	-	None

Sugano N (2016) [22]	Case series	29 (36)	8 years (5 to 15 years)	Rotational acetabular osteotomy	Spherical	Transtrochanteric	Original	+	Osteotomy line and reoriented acetabulum
Inaba Y (2016) [31]	Comparative study	22 (23) navigation, 20 (23) non-navigation	N/A	Rotational acetabular osteotomy	Spherical	Transtrochanteric	OrthoMap 3D (Stryker)	+	Osteotomy line and reoriented acetabulum
Takao M (2016) [32]	Case series	24 (25)	3.2 years (2 to 5.1 years)	Rotational acetabular osteotomy	Spherical	Transtrochanteric	OrthoMap 3D (Stryker)	+	Osteotomy line and reoriented acetabulum

Mayman et al. [19] developed an original CT-based navigation system and applied it to periacetabular osteotomy through a transtrochanteric approach for seven patients with eight dysplastic hips. The iliac and ischial osteotomies were marked in three dimensions using an optically tracked drill following the preoperative plan. The superior pubic rami osteotomy was performed under fluoroscopic guidance. They reported that computer enhancement of periacetabular osteotomy allows the surgeon to take the preoperative plan to the operating room and carry out that plan with accuracy, reliability, and safety. This exposure allows the experienced hip surgeon to perform the procedure safely under direct vision, even if the computer enhancement fails.

Nakahodo and Sugano et al. [18] developed an original CT-based navigation system that could guide both the surgical instruments and movement of the fragment as well as reconstruct the intraoperative change in the acetabular fragment model. Three screws were placed around the acetabular rim just before the osteotomy, and the movement of the acetabular fragment was determined by measuring the movement of the position of each screw head. They applied the navigation system not only to two cases of RAO but also to two cases of Chari medialization osteotomy. Sugano et al. [22] reported the 8-year follow-up outcomes of RAO using this CT-based navigation system. The position of the acetabular fragment was estimated by touching the edge points of the rim and osteotomy line with a navigation probe. No perioperative complications such as infection, nonunion, avascular necrosis, or neurovascular injuries occurred, but variations in the postoperative center-edge (CE) angle and acetabular roof angle were not smaller than the preoperative angles despite the fact that the preoperative plan targeted a CE angle of 35°. This indicates that the landmark matching technique to evaluate the position of the reorientated acetabulum is not as accurate as real-time tracking of the navigated osteotome. An additional tool with which to track the acetabular fragment, such as a fiducial marker or a tracker, might improve the accuracy of reorientation. Radiographic progression of osteoarthritis was found in one hip, but no hips were converted to total hip arthroplasty.

Hsieh et al. [30] performed a randomized comparative study of 36 patients undergoing periacetabular osteotomy through a transtrochanteric approach using either the commercially available CT-based navigation system (VectorVision Hip Navigation System; Brainlab Inc., Westchester, IL) or the conventional technique. They reported a reduced number of intraoperative radiographic images and a reduced operation time using the navigation system than using the conventional technique. No significant differences in the operative blood loss volume, transfusion requirement, radiographic correction of deformity, or clinical functional improvement were found after a 2-year follow-up. The authors concluded that the navigation system offers little additional benefit when the surgery is performed by an experienced surgeon. However, their navigation system did not show the preoperative plan superimposed on the bone model data, and only the tip of the osteotome was shown as a line on the monitor. Therefore, the small number of cases and the use of navigation with a primitive user interface without preoperative planning may have failed to show a benefit.

Akiyama et al. [29] applied a commercially available CT-based navigation system (Stealth Station TRIA Plus; Medtronic Surgical Navigation Technologies, Louisville, CO, USA) to CPO through a modified Smith-Petersen approach and achieved an accurate osteotomy without intraoperative complications. The navigation system neither shows the intraosseous location and direction of the osteotome nor follows an osteotomy line during an osteotomy. It cannot track the rotation of the osteotomized acetabular fragment.

Inaba et al. [31] applied a commercially available CT-based navigation system (OrthoMap 3D Navigation System; Stryker Orthopaedics, Mahwah, NJ, USA) to RAO in 23 hips of 23 patients and compared the clinical and radiographic results with those of RAO performed in 23 hips of 20 patients without navigation before introduction of the navigation system. No significant difference in the operative time or blood loss was observed between the two groups. Additionally, no significant differences in the radiological assessments were observed between the navigation and non-navigation groups. The authors performed precise 3D preoperative planning, and the navigation system could track the tip position of the osteotome and vitalize the osteotomy line and target position of the acetabular fragment; however, it could not track the movement of the acetabular fragment.

Takao et al. [32] also applied the abovementioned CT-based navigation system (OrthoMap 3D Navigation System; Stryker Orthopaedics) to RAO in 25 hips of 24 patients. They compared the outcomes of RAO performed by experienced surgeons (16 hips) and less-experienced surgeons (9 hips) using this navigation system. The navigation system could track the tip position of the osteotome and vitalize the osteotomy line and target position of the acetabular fragment (Fig. 12.2), but it could not track the movement of the acetabular fragment. There were no significant differences in the clinical or radiographic results after a minimum 2-year follow-up between the high-experience and low-experience groups. The use of navigation combined with a preoperative CT-based plan enabled less-experienced surgeons to perform RAO through a mini-incision as safely and reliably as that performed by experienced surgeons. The authors also evaluated the accuracy of the osteotomy position and acetabular movement using image registration between the preoperative and postoperative CT data.

Preoperative planning and accurate bone cutting are major benefits of CT-based navigation. However, no commercially available navigation system can track movement of the acetabular fragment. Sugano et al. [22] attempted to estimate the position of the acetabular fragment by touching the edge points of the rim and osteotomy line with a navigation probe. However, there were two outliers (6%) that showed >10° of difference from the targeted CE angle of 35°. Takao et al. [32] confirmed anterior and lateral femoral head coverage with the moved acetabular fragment by visualization of the planned position of the acetabular fragments on the navigation monitor. The position of the reoriented acetabulum was assessed by touching the anterior and lateral edges of the reoriented acetabulum with the navigation pointer with reference to the 3D plan on the navigation monitor (Fig. 12.3). However, there were five overcorrections (20%) that showed a CE angle of >40°. A navigation system that can track the acetabular fragment is necessary to improve the accuracy of both rotation of the

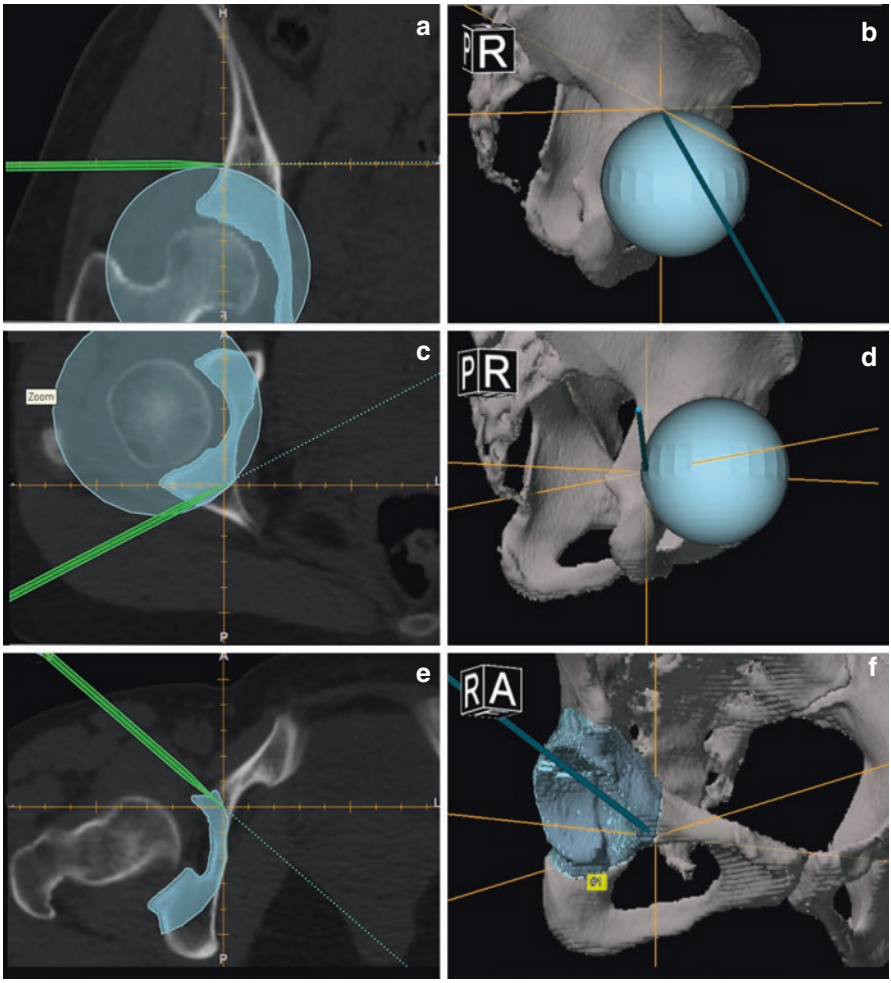

Fig. 12.2 Display of the navigation system shows the position and direction of the curved chisels during (**a**, **b**) iliac osteotomy, (**c**, **d**) ischial osteotomy, and (**e**, **f**) pubic osteotomy on (**a**) coronal, (**c**) axial, and (**e**) sagittal images centered on the tip of the chisel. (**b**, **d**, **f**) Three-dimensional views. (**a**, **c**, **e**) Green lines and (**b**, **d**, **f**) blue lines represent the tangential direction of the tip of the curved chisel. Reprinted from [32]

acetabular fragment and medialization of the femoral head [20, 21]. Some researchers have developed a navigation system that focuses on tracking of the acetabular fragment. Pflugi et al. [20] developed a cost-effective surgical navigation system to measure the orientation of the acetabular fragment during Bernese periacetabular osteotomy using commercially available inertial measurement units. They used plastic bones in the operating room to compare a previously developed optical navigation system with their inertial-based navigation system. The mean absolute difference was <4°. Murphy et al. [21] developed a biomechanical guidance system that incorporated

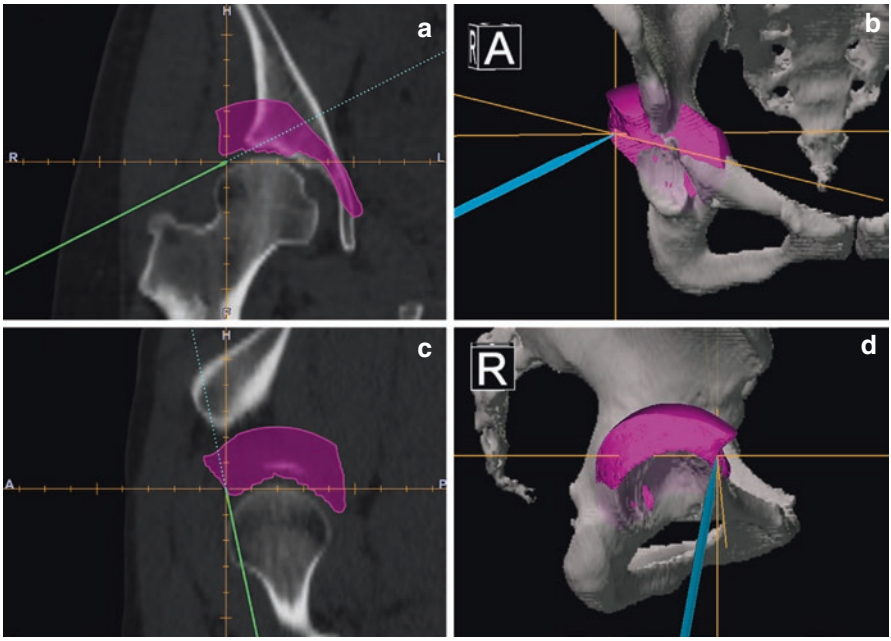

Fig. 12.3 Acquired lateral femoral head coverage by the acetabulum was checked on a (**a**) coronal image and a (**b**) three-dimensional image by touching the lateral edge of the reoriented acetabulum with the navigation pointer. The acquired anterior femoral head coverage was checked on a (**c**) sagittal image and a (**d**) three-dimensional image by touching the anterior edge of the reoriented acetabulum with the navigation pointer. (**a**, **c**) Green lines and (**b**, **d**) blue lines represent the navigation pointer. Reprinted from [32]

intraoperative acetabular fragment tracking and acetabular characterization through radiographic angles and joint biomechanics and used the system for 11 patients who underwent 12 Bernese periacetabular osteotomies. The system collected information on acetabula positioning by digitizing the four divots created on the acetabular fragment by a bone burr. The measured acetabular positioning showed strong agreement with the postoperative CT measurements (−0.3° to 9.2°; mean, 3.7°).

12.3 Periacetabular Osteotomy Using a Custom Cutting Guide

Navigation has several advantages such as real-time tracking of surgical tools, intraoperative validation of registration using landmarks, and intraoperative confirmation of the reoriented acetabular position. However, it has also some drawbacks such as expensive equipment and a learning curve for preparation and registration. Some researchers have attempted to develop a custom guide for hip osteotomy using 3D printing technology to overcome these drawbacks.

Radermacher et al. [23] developed individual templates to create a cutting guide of triple osteotomy, which involves three individual osteotomies in the ilium, pubis, and ischium. They applied individual templates for iliac osteotomy and compared 13 interventions using individual templates with 11 interventions performed in the conventional manner. The mean effective time of intraoperative X-ray monitoring was reduced by >75%, and the mean time of intervention was reduced by 25% compared with the conventional procedures. They concluded that the exact positioning of the osteotomies resulted in optimal mobility of the acetabulum.

Otsuki et al. [24] designed a custom cutting guide made of titanium for CPO and applied it to the C-shaped osteotomy of seven patients. They evaluated the accuracy of the osteotomy position by measuring the actual cutting radius and the planned cutting radius at three different points of the C-shaped osteotomy. The difference was <5 mm in all measurements.

12.4 Target 3D Acetabular Coverage in Periacetabular Osteotomy

Technological advancements in navigation systems and custom surgical guide systems might improve clinical outcomes by reducing the risk of postoperative instability due to undercorrection or impingement due to over-rotation. However, the optimal range of acetabular coverage of the femoral head remains unclear. The postoperative lateral acetabular coverage of the femoral head is a very important factor because it is reportedly a determinant of long-term outcomes of periacetabular osteotomy [8, 33]. Hartig-Andreasen et al. [34] reported that the postoperative lateral CE angle of periacetabular osteotomy should be 30–40° at the 4- to 12-year follow-up evaluations. They found the risk of conversion to total hip arthroplasty to be doubled if acetabular reorientation was not confined to this range. Albers et al. [8] found a lateral CE angle of <22° to be a risk factor for failure. Tannast et al. [35] reported that a normal lateral CE angle is within the range of 23–32°, which is quite a narrow target for periacetabular osteotomy.

The appropriate anterior acetabular coverage after periacetabular osteotomy is also a controversial topic. Overcorrection of anterior acetabular coverage may reportedly cause reduced range of motion [36] and postoperative femoral acetabular impingement [8]. Nakahara et al. [37, 38] analyzed acetabular and femoral morphologies on 3D CT images and found that the anterior and lateral acetabular coverage of both normal and dysplastic hips showed wide variations. In normal hips, the mean lateral 3D CE angle was 35.6° (range, 21.4–59.2°), and the mean anterior 3D CE angle was 58.6° (34.6–73.9°). Hamada et al. [36] simulated the range of motion of 52 DDH-affected hips after RAO with several patterns of femoral head coverage and compared them with those of 73 normal hips using

computer models reconstructed from CT images. After RAO with a lateral 3D CE angle of 30° and an anterior 3D CE angle of 55° producing coverage similar to that of normal hips, the maximal flexion and maximal internal rotation at 110° flexion with 20° adduction were significantly smaller than those of the normal group. Yasunaga et al. [39] reported that the radiographic crossover sign did not influence the radiographic progression of osteoarthritis after RAO during a mean 13-year follow-up. Imai et al. [40] reported that patients with a postoperative vertical-center-anterior angle of >46° had impairment of activities of daily living associated with limitations in hip flexion after RAO. The vertical-center-anterior angle was measured on the false-profile radiographic view obtained with the patients in the standing position; thus, it was necessary to estimate changes in pelvic sagittal inclination from the supine to standing position in CT-based planning. Postoperative range of motion was determined by acetabular and femoral morphologies, so individual biomechanical planning with range-of-motion simulation and estimation of peak contact pressure during activities of daily living would be necessary.

12.5 Computer-Assisted Orthopedic Surgery for Proximal Femoral Osteotomy

Intertrochanteric osteotomy had been performed mainly for the adult sequelae of DDH (varus, valgus, or derotational according to the final geometry of the proximal femur). Because of the success of periacetabular osteotomy, isolated intertrochanteric osteotomy is indicated only occasionally [41]. Transtrochanteric rotational osteotomy (TRO) [42] and curved varus osteotomy (CVO) [43] are performed to preserve the joint in patients with femoral head osteonecrosis. Because of the success of total hip arthroplasty, the technical demanding nature of the procedure, and the unstable clinical results, TRO and CVO are also indicated occasionally. Navigation systems have been used in the proximal femoral region in surgeries including stem orientation in total hip arthroplasty [44], femoral component placement in hip resurfacing [45–48], removal of bone cement in revision total hip arthroplasty [49], and open reduction and fixation of proximal femur fractures [50, 51]. To the best of our knowledge, no reports have described the clinical application of a navigation system in proximal femoral osteotomy. In TRO and CVO for femoral head osteonecrosis, the ratio of the transposed intact articular surface of the femoral head to the weight-bearing surface of the acetabulum on postoperative anteroposterior radiographs (postoperative intact ratio) is the most critical factor in preventing progression of femoral head collapse [42, 43, 52–56]. An appropriate indication and surgical procedure are needed to obtain good postoperative outcomes of TRO and CVO. Preoperative 3D simulation of TRO using 3D CT images and/or 3D magnetic resonance images is reportedly useful to determine the proper indications for these procedures [57].

References

1. Ganz R, Klaue K, Vinh TS, Mast JW. A new periacetabular osteotomy for the treatment of hip dysplasias. Technique and preliminary results. Clin Orthop Relat Res. 1988;232:26–36.
2. Ninomiya S, Tagawa H. Rotational acetabular osteotomy for the dysplastic hip. J Bone Joint Surg Am. 1984;66(3):430–6.
3. Murphy SB, Ganz R, Muller ME. The prognosis in untreated dysplasia of the hip. A study of radiographic factors that predict the outcome. J Bone Joint Surg Am. 1995;77(7):985–9.
4. Eppright RH. Dial osteotomy of the acetabulum in the treatment of dysplasia of the hip. J Bone Joint Surg Am. 1975;57(8):1172.
5. Wagner H. Experiences with spherical acetabular osteotomy for the correction of the dysplastic acetabulum. In: Weil UH, editor. Acetabular dysplasia: skeletal dysplasias in childhood. Berlin: Springer; 1978. p. 131–45. https://doi.org/10.1007/978-3-642-66737-4_7.
6. Naito M, Shiramizu K, Akiyoshi Y, Ezoe M, Nakamura Y. Curved periacetabular osteotomy for treatment of dysplastic hip. Clin Orthop Relat Res. 2005;433:129–35.
7. Yasunaga Y, Yamasaki T, Ochi M. Patient selection criteria for periacetabular osteotomy or rotational acetabular osteotomy. Clin Orthop Relat Res. 2012;470(12):3342–54. https://doi.org/10.1007/s11999-012-2516-z.
8. Albers CE, Steppacher SD, Ganz R, Tannast M, Siebenrock KA. Impingement adversely affects 10-year survivorship after periacetabular osteotomy for DDH. Clin Orthop Relat Res. 2013;471(5):1602–14. https://doi.org/10.1007/s11999-013-2799-8.
9. Klaue K, Wallin A, Ganz R. CT evaluation of coverage and congruency of the hip prior to osteotomy. Clin Orthop Relat Res. 1988;232:15–25.
10. Millis MB, Murphy SB. Use of computed tomographic reconstruction in planning osteotomies of the hip. Clin Orthop Relat Res. 1992;274:154–9.
11. Dutoit M, Zambelli PY. Simplified 3D-evaluation of periacetabular osteotomy. Acta Orthop Belg. 1999;65(3):288–94.
12. Mechlenburg I, Nyengaard JR, Romer L, Soballe K. Changes in load-bearing area after Ganz periacetabular osteotomy evaluated by multislice CT scanning and stereology. Acta Orthop Scand. 2004;75(2):147–53. https://doi.org/10.1080/00016470412331294395.
13. Armiger RS, Armand M, Lepisto J, Minhas D, Tallroth K, Mears SC, Waites MD, Taylor RH. Evaluation of a computerized measurement technique for joint alignment before and during periacetabular osteotomy. Comput Aided Surg. 2007;12(4):215–24. https://doi.org/10.3109/10929080701541855.
14. Hipp JA, Sugano N, Millis MB, Murphy SB. Planning acetabular redirection osteotomies based on joint contact pressures. Clin Orthop Relat Res. 1999;364:134–43.
15. Liu L, Ecker TM, Schumann S, Siebenrock KA, Zheng G. Evaluation of constant thickness cartilage models vs. patient specific cartilage models for an optimized computer-assisted planning of periacetabular osteotomy. PLoS One. 2016;11(1):e0146452. https://doi.org/10.1371/journal.pone.0146452.
16. Langlotz F, Stucki M, Bachler R, Scheer C, Ganz R, Berlemann U, Nolte LP. The first twelve cases of computer assisted periacetabular osteotomy. Comput Aided Surg. 1997;2(6):317–26. https://doi.org/10.1002/(sici)1097-0150(1997)2:6<317::aid-igs1>3.0.co;2-2.
17. Langlotz F, Bachler R, Berlemann U, Nolte LP, Ganz R. Computer assistance for pelvic osteotomies. Clin Orthop Relat Res. 1998;354:92–102.
18. Nakahodo K, Sasama T, Sato Y, Sugano N, Ohzono K, Nishii T, Nishihara S, Yonenobu K, Ochi T, Tamura S. Intraoperative update of 3D bone model during computer navigation of pelvic osteotomies using real-time 3D position data. In: Lemke H, Vannier M, Inamura K, Farman A, Doi K, editors. Computer assisted radiology and surgery. 14th International Symposium and Exhibition (CARS 2000), San Francisco, CA, 2000. Amsterdam: Elsevier; 2000. p. 252–6.
19. Mayman DJ, Rudan J, Yach J, Ellis R. The Kingston periacetabular osteotomy utilizing computer enhancement: a new technique. Comput Aided Surg. 2002;7(3):179–86. https://doi.org/10.1002/igs.10041.

20. Pflugi S, Liu L, Ecker TM, Schumann S, Larissa Cullmann J, Siebenrock K, Zheng G. A cost-effective surgical navigation solution for periacetabular osteotomy (PAO) surgery. Int J Comput Assist Radiol Surg. 2016;11:271. https://doi.org/10.1007/s11548-015-1267-1.
21. Murphy RJ, Armiger RS, Lepisto J, Mears SC, Taylor RH, Armand M. Development of a biomechanical guidance system for periacetabular osteotomy. Int J Comput Assist Radiol Surg. 2015;10(4):497–508. https://doi.org/10.1007/s11548-014-1116-7.
22. Sugano N, Takao M, Sakai T, Nishii T, Miki H. Safety and accuracy of CT-based navigation for rotational acetabular osteotomy. Formosan J Musculoskelet Disord. 2016;7(1):44–50. https://doi.org/10.6492/fjmd.20151007.
23. Radermacher K, Portheine F, Anton M, Zimolong A, Kaspers G, Rau G, Staudte HW. Computer assisted orthopaedic surgery with image based individual templates. Clin Orthop Relat Res. 1998;354:28–38.
24. Otsuki B, Takemoto M, Kawanabe K, Awa Y, Akiyama H, Fujibayashi S, Nakamura T, Matsuda S. Developing a novel custom cutting guide for curved peri-acetabular osteotomy. Int Orthop. 2013;37(6):1033–8. https://doi.org/10.1007/s00264-013-1873-x.
25. Azuma H, Taneda H. Rotational acetabular osteotomy in congenital dysplasia of the hip. Int Orthop. 1989;13(1):21–8.
26. Kambe T, Naito M, Asayama I, Koga K, Fujisawa M, Yamaguchi T, Yatsunami M. Vascular anatomy for rotational acetabular osteotomy: cadaveric study. J Orthop Sci. 2003;8(3):323–8. https://doi.org/10.1007/s10776-002-0630-7.
27. Matsui M, Masuhara K, Nakata K, Nishii T, Sugano N, Ochi T. Early deterioration after modified rotational acetabular osteotomy for the dysplastic hip. J Bone Joint Surg. 1997;79(2):220–4.
28. Xu K, Li YM, Zhang HF, Wang CG, Xu YQ, Li ZJ. Computer navigation in total hip arthroplasty: a meta-analysis of randomized controlled trials. Int J Surg (London, England). 2014;12(5):528–33. https://doi.org/10.1016/j.ijsu.2014.02.014.
29. Akiyama H, Goto K, So K, Nakamura T. Computed tomography-based navigation for curved periacetabular osteotomy. J Orthop Sci. 2010;15(6):829–33. https://doi.org/10.1007/s00776-010-1520-y.
30. Hsieh PH, Chang YH, Shih CH. Image-guided periacetabular osteotomy: computer-assisted navigation compared with the conventional technique: a randomized study of 36 patients followed for 2 years. Acta Orthop. 2006;77(4):591–7. https://doi.org/10.1080/17453670610012656.
31. Inaba Y, Kobayashi N, Ike H, Kubota S, Saito T. Computer-assisted rotational acetabular osteotomy for patients with acetabular dysplasia. Clin Orthop Surg. 2016;8(1):99–105. https://doi.org/10.4055/cios.2016.8.1.99.
32. Takao M, Nishii T, Sakai T, Sugano N. Comparison of rotational acetabular osteotomy performed with navigation by surgeons with different levels of experience of osteotomies. Int J Comput Assist Radiol Surg. 2017;12:841. https://doi.org/10.1007/s11548-016-1494-0.
33. Hasegawa Y, Iwase T, Kitamura S, Kawasaki M, Yamaguchi J. Eccentric rotational acetabular osteotomy for acetabular dysplasia and osteoarthritis: follow-up at a mean duration of twenty years. J Bone Joint Surg Am. 2014;96(23):1975–82. https://doi.org/10.2106/jbjs.m.01563.
34. Hartig-Andreasen C, Troelsen A, Thillemann TM, Soballe K. What factors predict failure 4 to 12 years after periacetabular osteotomy? Clin Orthop Relat Res. 2012;470(11):2978–87. https://doi.org/10.1007/s11999-012-2386-4.
35. Tannast M, Hanke MS, Zheng G, Steppacher SD, Siebenrock KA. What are the radiographic reference values for acetabular under- and overcoverage? Clin Orthop Relat Res. 2015;473(4):1234–46. https://doi.org/10.1007/s11999-014-4038-3.
36. Hamada H, Takao M, Nakahara I, Sakai T, Nishii T, Sugano N. Hip range-of-motion (ROM) is less than normal after rotational acetabular osteotomy for developmental dysplasia of the hip: a simulated ROM analysis. J Orthop Res. 2016;34:217. https://doi.org/10.1002/jor.23024.
37. Nakahara I, Takao M, Sakai T, Miki H, Nishii T, Sugano N. Three-dimensional morphology and bony range of movement in hip joints in patients with hip dysplasia. Bone Joint J. 2014;96-b(5):580–9. https://doi.org/10.1302/0301-620x.96b5.32503.

38. Nakahara I, Takao M, Sakai T, Nishii T, Yoshikawa H, Sugano N. Gender differences in 3D morphology and bony impingement of human hips. J Orthop Res. 2011;29(3):333–9. https://doi.org/10.1002/jor.21265.
39. Yasunaga Y, Yamasaki T, Matsuo T, Ishikawa M, Adachi N, Ochi M. Crossover sign after rotational acetabular osteotomy for dysplasia of the hip. J Orthop Sci. 2010;15(4):463–9. https://doi.org/10.1007/s00776-010-1489-6.
40. Imai H, Kamada T, Takeba J, Shiraishi Y, Mashima N, Miura H. Anterior coverage after eccentric rotational acetabular osteotomy for the treatment of developmental dysplasia of the hip. J Orthop Sci. 2014;19(5):762–9. https://doi.org/10.1007/s00776-014-0592-5.
41. Turgeon TR, Phillips W, Kantor SR, Santore RF. The role of acetabular and femoral osteotomies in reconstructive surgery of the hip: 2005 and beyond. Clin Orthop Relat Res. 2005;441:188–99.
42. Sugioka Y. Transtrochanteric anterior rotational osteotomy of the femoral head in the treatment of osteonecrosis affecting the hip: a new osteotomy operation. Clin Orthop Relat Res. 1978;130:191–201.
43. Sakano S, Hasegawa Y, Torii Y, Kawasaki M, Ishiguro N. Curved intertrochanteric varus osteotomy for osteonecrosis of the femoral head. J Bone Joint Surg Br. 2004;86(3):359–65.
44. Kitada M, Nakamura N, Iwana D, Kakimoto A, Nishii T, Sugano N. Evaluation of the accuracy of computed tomography-based navigation for femoral stem orientation and leg length discrepancy. J Arthroplasty. 2011;26(5):674–9. https://doi.org/10.1016/j.arth.2010.08.001.
45. Kitada M, Sakai T, Murase T, Hanada T, Nakamura N, Sugano N. Validation of the femoral component placement during hip resurfacing: a comparison between the conventional jig, patient-specific template, and CT-based navigation. Int J Med Robot Comput Assist Surg. 2013;9(2):223–9. https://doi.org/10.1002/rcs.1490.
46. Bailey C, Gul R, Falworth M, Zadow S, Oakeshott R. Component alignment in hip resurfacing using computer navigation. Clin Orthop Relat Res. 2009;467(4):917–22. https://doi.org/10.1007/s11999-008-0584-x.
47. Olsen M, Schemitsch EH. Avoiding short-term femoral neck fracture with imageless computer navigation for hip resurfacing. Clin Orthop Relat Res. 2011;469(6):1621–6. https://doi.org/10.1007/s11999-010-1607-y.
48. Schnurr C, Michael JW, Eysel P, Konig DP. Imageless navigation of hip resurfacing arthroplasty increases the implant accuracy. Int Orthop. 2009;33(2):365–72. https://doi.org/10.1007/s00264-007-0494-7.
49. Akiyama H, Kawanabe K, Goto K, Ohnishi E, Nakamura T. Computer-assisted fluoroscopic navigation system for removal of distal femoral bone cement in revision total hip arthroplasty. J Arthroplasty. 2007;22(3):445–8. https://doi.org/10.1016/j.arth.2006.11.010.
50. Hamelinck HK, Haagmans M, Snoeren MM, Biert J, van Vugt AB, Frolke JP. Safety of computer-assisted surgery for cannulated hip screws. Clin Orthop Relat Res. 2007;455:241–5. https://doi.org/10.1097/01.blo.0000238815.40777.d2.
51. Liebergall M, Ben-David D, Weil Y, Peyser A, Mosheiff R. Computerized navigation for the internal fixation of femoral neck fractures. J Bone Joint Surg Am. 2006;88(8):1748–54. https://doi.org/10.2106/jbjs.e.00137.
52. Zhao G, Yamamoto T, Ikemura S, Motomura G, Mawatari T, Nakashima Y, Iwamoto Y. Radiological outcome analysis of transtrochanteric curved varus osteotomy for osteonecrosis of the femoral head at a mean follow-up of 12.4 years. J Bone Joint Surg Br. 2010;92(6):781–6. https://doi.org/10.1302/0301-620x.92b6.23621.
53. Atsumi T, Kajiwara T, Hiranuma Y, Tamaoki S, Asakura Y. Posterior rotational osteotomy for nontraumatic osteonecrosis with extensive collapsed lesions in young patients. J Bone Joint Surg Am. 2006;88(Suppl 3):42–7. https://doi.org/10.2106/jbjs.f.00767.
54. Zhao G, Yamamoto T, Ikemura S, Motomura G, Iwasaki K, Yamaguchi R, Nakashima Y, Mawatari T, Iwamoto Y. Clinico-radiological factors affecting the joint space narrowing after transtrochanteric anterior rotational osteotomy for osteonecrosis of the femoral head. J Orthop Sci. 2012;17(4):390–6. https://doi.org/10.1007/s00776-012-0238-4.

55. Hamanishi M, Yasunaga Y, Yamasaki T, Mori R, Shoji T, Ochi M. The clinical and radiographic results of intertrochanteric curved varus osteotomy for idiopathic osteonecrosis of the femoral head. Arch Orthop Trauma Surg. 2014;134(3):305–10. https://doi.org/10.1007/s00402-013-1919-y.
56. Sugano N, Takaoka K, Ohzono K, Matsui M, Saito M, Saito S. Rotational osteotomy for nontraumatic avascular necrosis of the femoral head. J Bone Joint Surg Br. 1992;74(5):734–9.
57. Koyama T, Sugano N, Nishii T, Miki H, Takao M, Sato Y, Yoshikawa H, Tamura S. MRI-based surgical simulation of transtrochanteric rotational osteotomy for femoral head osteonecrosis. J Orthop Res. 2009;27(4):447–51. https://doi.org/10.1002/jor.20568.

Chapter 13
CAOS in Bone Tumor Surgery

Kwok Chuen Wong

Abstract Wide local resection with an adequate margin is a crucial step in the management of patients with bone sarcoma. Inaccurate resection with an inadequate margin is associated with a high risk of local recurrence and poor patient survival. Orthopedic oncologist surgeons are often faced with the dilemma of how much normal tissue to preserve to retain good function without compromising an adequate margin. With the advent of medical imaging and computer technology, tumor surgeons are increasingly using computer-assisted surgery for bone tumor resection. Computer-assisted orthopedic surgery helps surgeons replicate their preoperative plans, and this improved accuracy may have clinical benefits. This chapter provides an overview of the techniques that have emerged in bone tumor surgery over the past decade, including (1) three-dimensional (3D) surgical planning, intraoperative navigation-assisted resection, and patient-specific instrumentation (PSI)-assisted bone tumor resection, (2) clinical indications and early results of these techniques, and (3) possible future developments. The workflow includes 3D surgical planning with fusion of preoperative computed tomography/magnetic resonance imaging results and the integration of digital data for computer-aided design tumor implants or allografts. Computer navigation and PSI are the tools needed to implement 3D surgical planning. The current indications for computer-assisted tumor surgery (CATS) in patients with bone tumors include the following: (1) pelvic and sacral tumors that are at anatomically complex locations with nearby vital structures; (2) technically demanding resections, such as joint-preserving operations or multiplanar tumor resections; and (3) resections that must accommodate a custom tumor implant or match an allograft for reconstruction. The early clinical results suggest that the technique is feasible and safe, and it improves surgical accuracy. Nevertheless, surgeons must be aware of the potential errors when using the technique. An all-in-one planning platform for all users and the integration of 3D printing technology into the CATS workflow are potential areas for future development. Larger studies with longer follow-up periods are essential to determine the real clinical efficacy of the technique.

K.C. Wong
Orthopaedic Oncology, Department of Orthopaedics and Traumatology, Prince of Wales Hospital, The Chinese University of Hong Kong, Hong Kong, SAR, China
e-mail: skcwong@ort.cuhk.edu.hk

N. Sugano (ed.), *Computer Assisted Orthopaedic Surgery for Hip and Knee*,
https://doi.org/10.1007/978-981-10-5245-3_13

Keywords Computer navigation · Patient-specific instruments · 3D surgical planning · Computer-assisted tumor surgery (CATS) · Image fusion · Computer-aided design (CAD) prosthesis

13.1 Introduction

The orthopedic tumor surgeon performs bone sarcoma resections that include some normal tissue beyond the boundary of the tumor. The amount of the margin is based on an analysis of the preoperative medical images. Wide local resection with an adequate margin is a crucial step in the management of patients with bone sarcoma. Inaccurate resection with an inadequate margin is associated with a high risk of local recurrence and poor patient survival [1]. When resecting the tumor, however, surgeons may be forced to remove more tissue than necessary to avoid any mistaken assumptions about an adequate margin. In such cases, more normal tissue than necessary may be sacrificed, resulting in less favorable reconstruction and limb function.

Thus, in orthopedic oncology, surgeons are often faced with a dilemma of deciding how much normal tissue to preserve to retain good function without compromising the resection margin. Surgical planning for resecting a bone tumor and reconstructing the defect requires detailed analysis of preoperative images. The surgeon must mentally integrate the two-dimensional (2D) images and then formulate a three-dimensional (3D) surgical plan for tumor resection with clear margins in the desired plane. Such preoperative mental planning and its intraoperative implementation are particularly difficult when the tumor is in a complex anatomical area, such as the pelvis or sacrum, or when the resection is technically demanding, such as a joint-saving or multiplanar resection. Therefore, the main responsibility of the tumor surgeon is to replicate the planned resections accurately and precisely. Given that bone sarcomas are not common and these tumors vary in extent and location, tumor surgeons may not have adequate operative experience to mitigate surgical inaccuracy.

Resection accuracy in bone sarcoma surgery was not properly addressed until 2008, when, in an experimental study, four experienced tumor surgeons operated on simulated plastic pelvic models. The probability of an experienced surgeon obtaining a 10-mm surgical margin with ±5 mm tolerance was only 52% (95% confidence interval 37–67). Also, the degree of host–graft contact for reconstruction was poor [2]. Advanced computer-assisted orthopedic surgery (CAOS), which was already well established for joint arthroplasty and spinal surgery, has been investigated for use with bone sarcomas over the past decade. The use of computed tomography (CT)-based navigation for pelvic and sacral tumor resection was first reported in 2004 [3, 4]. Those authors used navigation tools to guide the orientation of osteotomies during surgery and suggested that computer-assisted surgery might help increase the accuracy of anatomically and surgically complex tumor resection. The report aroused much interest in the field of orthopedic oncology because the technique might provide a potential solution to the long-standing issue of surgical inaccuracy during bone sarcoma surgery.

This chapter provides an overview of the techniques that have emerged in CAOS for bone tumor surgery during the past decade. It covers the subjects of three-dimensional (3D) surgical planning, intraoperative navigation-assisted bone tumor resection, and patient-specific instrumentation (PSI)-assisted bone tumor resection as well as the clinical indications and early results of the techniques and possible future developments.

13.2 Computer-Assisted Tumor Surgery

For computer-assisted tumor surgery (CATS), computer-assisted preoperative planning is as important as intraoperative implementation of the surgical plan. Oncology surgeons can replicate a planned resection and achieve the surgical goal of achieving an adequate surgical margin only if they prepare a detailed, accurate surgical plan. Computer navigation has been utilized in both surgical planning and its intraoperative implementation. Patient-specific instrumentation (PSI) has been recently investigated as an alternative to computer navigation for replicating surgical plans. The clinical workflow of CATS is summarized in Fig. 13.1.

13.2.1 3D Surgical Planning

In contrast to the surgical planning used in other orthopedic disciplines, bone tumor surgery often involves a detailed analysis of multimodal medical images for planning the bone resection. The planning regimen integrates all available information, such as regarding the implants or allografts used for skeletal reconstruction. 3D

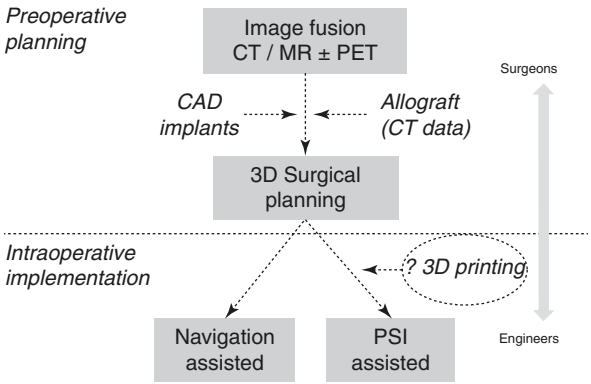

Fig. 13.1 Clinical workflow of computer-assisted tumor surgery (CATS) from preoperative three-dimensional (3D) surgical planning through intraoperative implementation of the plan. The workflow requires close collaboration between tumor surgeons and engineers. The 3D printing technology may facilitate the use of patient-specific instrumentation (PSI) and computer-aided design (CAD) implants

surgical planning has been described for navigation systems that facilitate the process of this complex exercise [5–8]. CT and magnetic resonance imaging (MRI) provide the preoperative images that are essential for planning a bone tumor resection [9]. CT provides good bony details, and MRI shows the extent of the tumor and its relations with surrounding vital structures. In addition to fusion of these 2D CT/MR images, 3D images can be reconstructed and individual structures (e.g., vessels, the tumor) isolated. A 3D bone tumor model can then be created. Thus, using all of the 2D and 3D processed images for the surgical planning, tumor surgeons can then obtain an excellent mental picture of the resection, including surgical access, tumor exposure, and the sites and orientations of the required osteotomies before actual implementation of their surgical plan in the operating theater (Fig. 13.2).

Planning the reconstruction of the skeletal defect after tumor resection is thus facilitated as surgeons can now define the exact location of the planned resection in

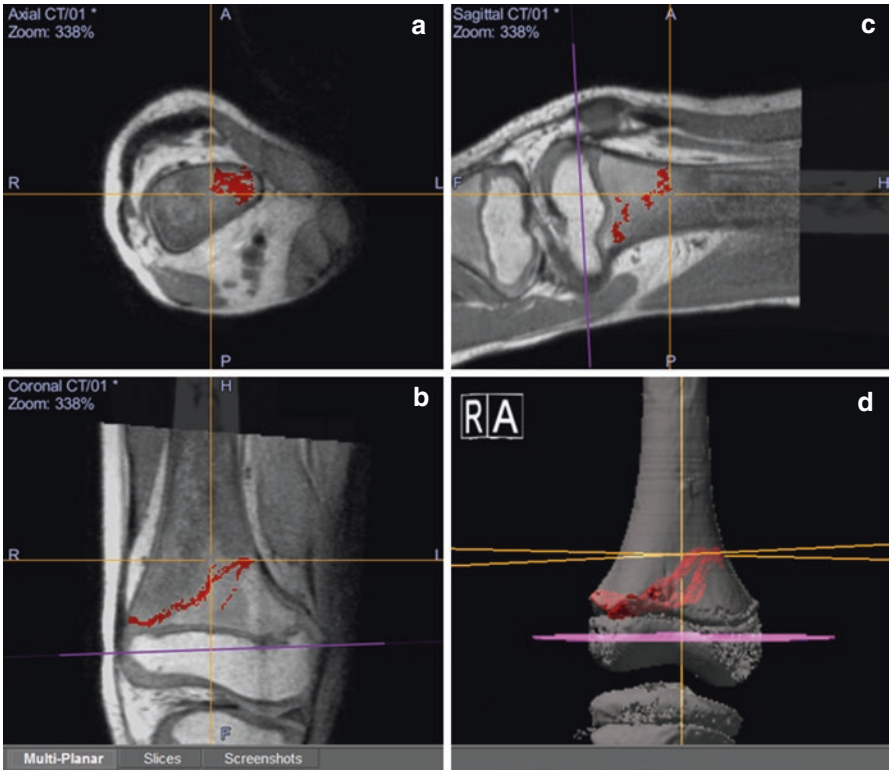

Fig. 13.2 Patient was a 9-year-old boy with osteosarcoma of the right distal femur. Computed tomography/magnetic resonance imaging (CT/MR) fusion images are shown on the navigation display. Joint-preserving resection and reconstruction with a custom tumor implant were performed under navigational guidance. MR images are overlaid and realigned on the base CT images, so the femur has the same spatial coordinates on both images. The distal intramedullary tumor margin (*red*) is outlined on MR images. Axial (**a**), reformatted coronal (**b**), and sagittal (**c**) views and a 3D bone tumor model (**d**) were used for 3D surgical planning to define the osteotomy plane (*purple*) at the distal femur epiphysis

the navigational software. Implant engineers can then design a custom implant to match the defect defined by the surgeons [6, 10, 11]. The same resection planning can also be carried out on the CT data for the allograft, which has dimensions similar to those of the host bone. Shaping the allograft can now be conformed more closely to the host bone, resulting in better allograft–host bone contact, thereby minimizing the chance of nonunion [12–14].

Although contemporary engineering by computer-aided design (CAD) software allows advanced surgical planning (e.g., virtual resection simulation, custom CAD design, biomechanical analysis of the bone reconstruction), the information cannot be readily or directly used for navigational planning because of system incompatibility. Hence, a technique for integrating CAD data into the navigational system was devised [10]. CAD planning and CAD custom prostheses can now be translated and visualized in the navigational system (Fig. 13.3), which greatly enhances the capability of navigational planning for bone tumor surgery.

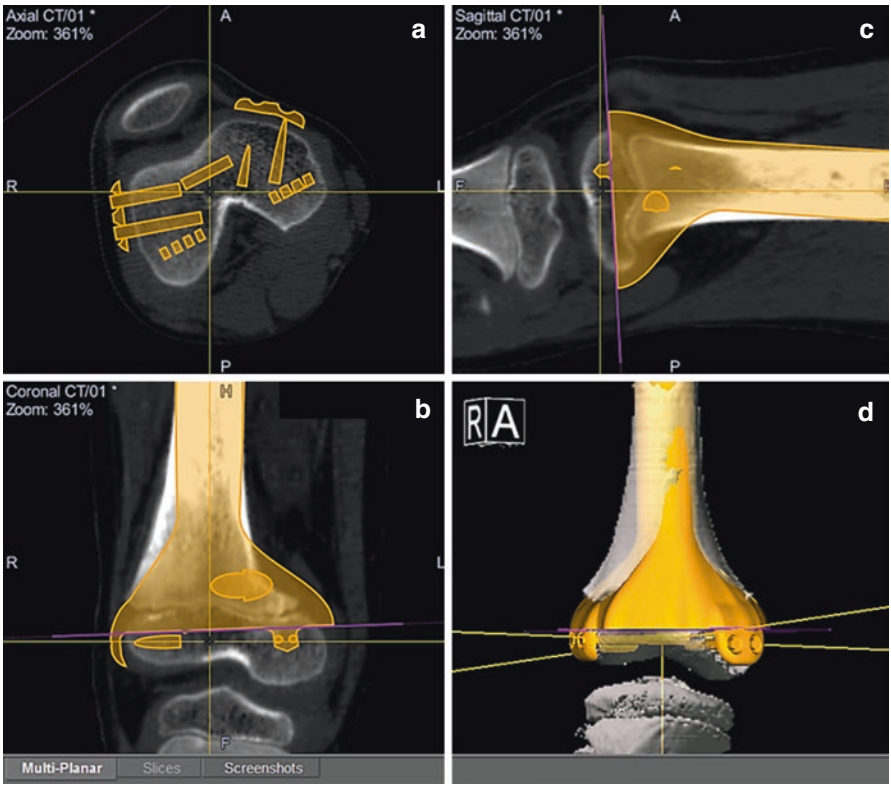

Fig. 13.3 Patient was a 9-year-old boy with osteosarcoma of the right distal femur. Preoperative axial (**a**), coronal (**b**), and sagittal (**c**) views and a 3D model for navigation planning are shown on the navigational monitor. The CAD implant (*yellow*) could be integrated into the navigation planning and visualized on CT images. This integration facilitates precise definition of the intended resection planes (*purple*) at the distal femur epiphysis

13.2.2 Implementation Tools for CATS

13.2.2.1 Image-Based Navigation

CT-based navigation has been adopted as the image-based navigational system for implementing 3D planning for bone tumor surgery [15–17]. Thin slices of CT images with an excellent resolution are acquired. 2D CT images, with various reformatted views and 3D models, can be generated more easily than MR images and offer the best visualization and representation of the patient's anatomy and pathology. Image-to-patient registration is a process by which the anatomy of the operative site is matched to preoperatively acquired imaging data. This is the most crucial intraoperative step in CATS. A CT-based navigational system allows accurate image-to-patient registration, which is the main determinant of overall accuracy of the CATS technique. At the time of surgery, only if patients' operative anatomy can be matched to their preoperative images and the operated bones can be physically tracked by the navigational system can the surgeon trust and rely on the virtual images to execute their 3D surgical plans. Although the amount of registration error—representing the degree of mismatch between the patient's anatomy and the virtual preoperative images—acceptable during CATS has not been defined, the mean error is reported to be <2 mm [15, 16, 18–21].

After conventional surgical exposure around bone tumors, a patient's tracker is placed in the operated bone. Manual registration using paired points and surface matching is then performed. In addition to the registration error generated from the navigational machine, the registration accuracy is further verified by checking some anatomical landmarks or tracing the exposed bone surface with a navigational pointer (Fig. 13.4). Because the current navigational system does not support a navigated saw, the sites of intended osteotomies are identified by the navigation. The osteotomies are then performed manually, with the orientation of the saw blade guided by the navigational pointer (Fig. 13.5).

13.2.2.2 Patient-Specific Instrument

The PSI is customized on the basis of the 3D surface model of the bony anatomy, which is generated by image segmentation of a patient's imaging data [22]. In addition to the cutting platform for guided osteotomies, PSI has a footprint that accurately fits the bone surface. The chosen bone contact surface should have enough contoured surface for stable, consistent positioning of the PSI (Fig. 13.6). Because the PSI in bone tumor surgery involves few instruments and a simple operative setup compared with navigational surgery, it offers a simpler alternative for replicating surgical plans. The use of PSI has recently been described in bone tumor surgery. In a cadaveric study simulating pelvic tumor resections, the PSI technique enabled surgeons to reproduce the virtual surgical plan with similar accuracy but less bone resection time when compared with navigational assistance [23]. A case series

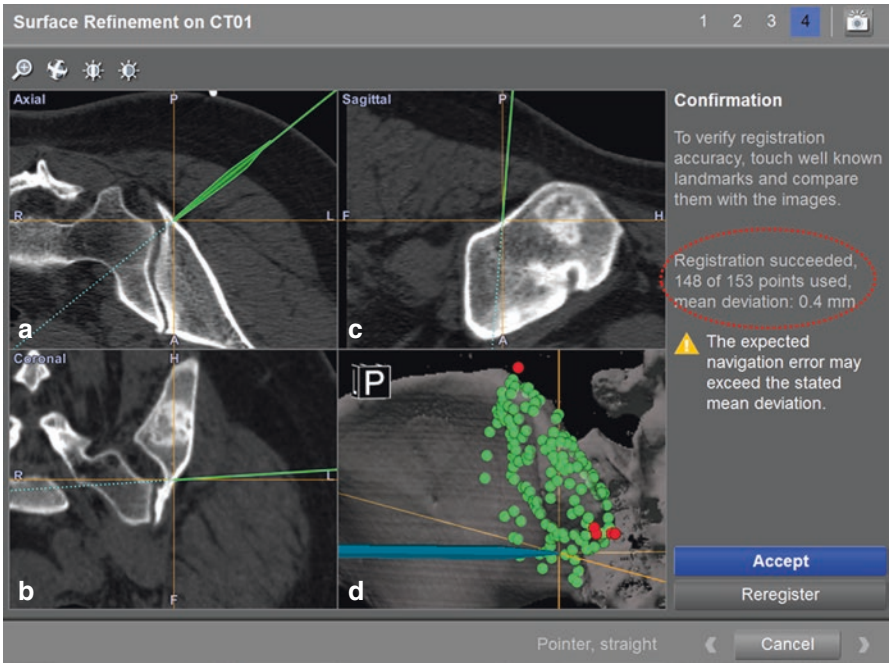

Fig. 13.4 Patient was a 27-year-old woman with a malignant bone tumor at the left posterior iliac crest. Preoperative axial (**a**), coronal (**b**), and sagittal (**c**) views and a 3D model of CT images are shown on the navigation monitor. Following paired points and surface matching, the registration error was 0.4 mm. The registration accuracy was further verified by touching the bone surface with a navigation pointer. The virtual tip of the navigation pointer was exactly on the bone surface. The navigation system was considered accurate only if there was exact matching between the image on the navigational monitor and the patient's skeletal anatomy

Fig. 13.5 Because the navigational system does not support a navigated saw, the osteotomy was performed manually using an osteotome (*red arrow*) with an orientation under navigational guidance in a patient with an iliac bone tumor

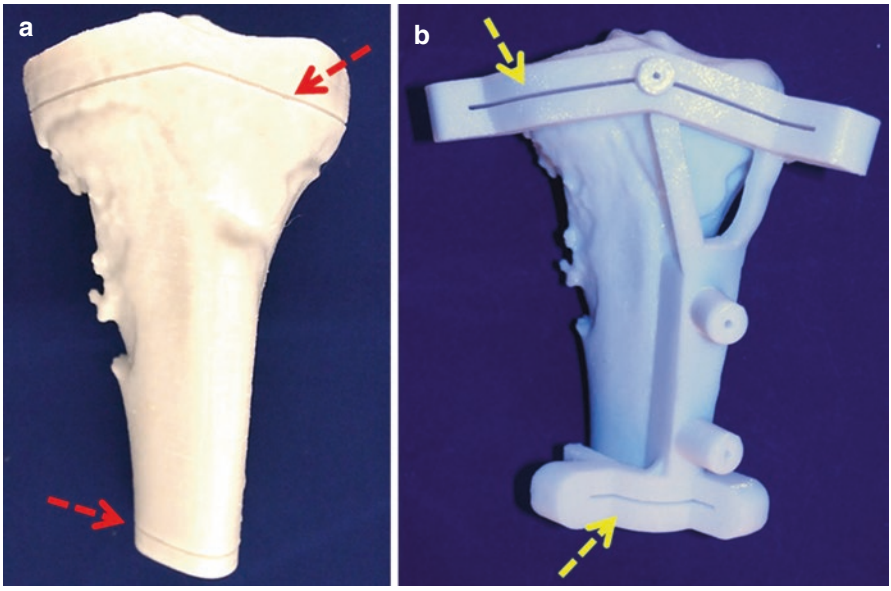

Fig. 13.6 Patient was a 10-year-old girl with a left proximal tibia osteosarcoma. She was to undergo joint-preserving resection and reconstruction with a custom tumor implant. A 3D-printed bone tumor model (**a**) and patient-specific instrumentation (PSI) (**b**) were used. The intended resection planes (red p) were marked on the model for easy reference during the operation. The orientations of the cutting slits (*yellow arrows*) in the PSI were designed and fabricated to confine the oscillating saw blade along the intended resections

suggested that this technique might help improve bone resection accuracy for oncological clearance [24]. The technique also might facilitate the matching of a customized tumor implant to the bone defect after tumor resection [25, 26].

13.2.3 Indications and Clinical Results

Given the complexity of 3D surgical planning and the additional time and facilities required for intraoperative implementation, the CATS technique is not used routinely for bone tumor surgery but may be applied if difficulty is anticipated in (1) achieving accurate tumor resection with a clear margin, (2) obtaining a correct resection plane to accommodate a custom tumor implant, or (3) shaping an allograft to reconstruct a bone defect after resection [5, 27]. The computer-assisted approach, which was developed to improve surgical accuracy, may offer a greater chance of achieving clear resection margins and better oncological results. Because the technique is still in its early development, there are no randomized controlled trials to determine its clinical efficacy compared with that achieved using the traditional surgical approach to bone tumor surgery. It is yet to be determined if the improved surgical accuracy can provide better oncological and functional results.

The early results are promising. A few short-term clinical studies at various centers reported that the CATS technique helps carry out the surgical plan with good accuracy and allows safe tumor resection. It may also help preserve unaffected sacral nerve roots during sacral tumor resection [15–17, 28]. A recent large clinical series of 31 patients with pelvic or sacral malignant bone tumors undergoing resection with CATS tended to support the theoretical advantage of improved surgical accuracy. Its use reduced intralesional resections from 29.0% to 8.7% [17]. Because CATS enables surgeons to perform complex osteotomies, more technically demanding operations, such as joint-preserving surgery [11, 20, 29] and multiplanar tumor resection [7, 16, 17], are possible. More conservative resections can be performed, thereby preserving more unaffected bone with better postoperative function (Fig. 13.7).

A 3D navigational system has also been applied to the treatment of benign bone tumors. A recent study used 3D surgical navigation to guide radio-frequency ablation in 32 patients with osteoid osteomas [30]. Accurate localization of the tiny nidus of an osteoid osteoma in the bone cortex is difficult, and the real-time image-guided technique was reported to be feasible and safe, guiding and enabling surgeons to place the radio-frequency ablation needle in the tiny nidus at the correct and difficult-to-access anatomical locations. The success rate was 96.8%.

13.2.4 Limitations

With navigation-assisted tumor surgery, surgeons rely on preoperative virtual images for surgical planning and intraoperative implementation of the intended tumor resection. Following skin incision and surgical manipulation, however, soft tissue deforms and the preoperative virtual images no longer represent the actual intraoperative locations of the soft tissue. Therefore, the technique enables surgeons to replicate accurately only bone resection, thus avoiding intralesional tumor resection. It cannot navigate soft-tissue resection, however, which still requires a traditional surgical technique.

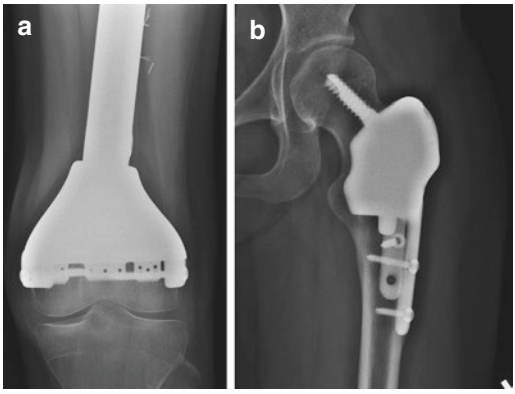

Fig. 13.7 Anteroposterior radiographs show satisfactory positioning of custom implants following uniplanar joint-preserving tumor resection at the distal femur at 1 year after surgery (**a**) and after multiplanar tumor resection of the proximal femur at 5.5 years after surgery (**b**)

Tumor surgeons must understand the CATS workflow and should be aware of the potential errors that could occur during 3D surgical planning and intraoperative implementation of the technique. These errors and ways to minimize them are discussed in detail elsewhere [11, 31]. Incorrect interpretation of the navigational information may result in inaccurate bone resections, with possible adverse clinical outcomes.

The PSI technique makes the same errors as the navigational technique during the surgical planning. It also does not provide intraoperative imaging feedback to check the correct placement of the PSI on the bone surface as determined when designing the PSI with engineering software [25]. Accurate intraoperative PSI placement, then, relies mainly on the subjective feeling of the fit by the surgeon. No objective methods are yet available to verify quantitatively the correct placement of PSI during the surgery.

Because the new method requires additional surgical time and more time to set up the operating room, there is a learning curve, which was evaluated for the navigation-assisted technique in 78 patients with bone tumors [21]. Intraoperative technical problems resulted in the navigation portion of the operation not being completed in four (5%) of the 78 patients. These four cases occurred among the first 20 cases in which the technology was used. Surgical time decreased as surgeons performed more of the navigated procedures. The authors concluded that larger studies are needed to justify the value of the technology for routine use in bone tumor surgery [21].

13.3 Potential Future Development of CATS

The clinical workflow of CATS in bone tumor surgery involves various stakeholders, including orthopedic tumor surgeons, radiologists, engineers, and implant companies. Although the current workflow provides the link for communication, it requires different software. To improve the learning curve and increase the popularity of the technique among orthopedic tumor surgeons, an all-in-one integrated computer platform is essential to allow easy 3D surgical planning and seamless, effective communication with other care providers. Thus, the digital orthopedic data should be integrated to facilitate personalized treatment in bone tumor patients [22].

During the last decade, the use of 3D printing has been increasing and has become more prevalent in medical applications. The additive manufacturing technology has superior flexibility in fabricating free-form objects from a digital model that is distinct from the traditional subtractive manufacturing method. In addition, custom implants can be 3D-printed to match the patient's unique bone defect after tumor resection. The personalized implant is a metal monobloc with a porous lattice that not only reduces implant stiffness but allows better osseointegration at the bone–implant junction [26]. Because tumor surgeons are more capable of performing difficult osteotomies with guidance tools (e.g., computer navigation, PSI), complex 3D-printed tumor implants may become more common in bone tumor surgery as more advances are made in the technology.

It remains to be seen if the improved surgical accuracy offered by CATS can translate into better clinical outcomes. Future large, multicenter studies with longer follow-up assessments are needed to determine the real clinical efficacy of CATS.

13.4 Conclusion

With the advances in medical imaging and computer technology, orthopedic tumor surgeons have increasingly been using computer-assisted surgery for bone tumor resection. CATS helps surgeons replicate preoperative surgical plans and improve surgical accuracy, which may offer clinical benefits. The workflow includes 3D surgical planning, the fusion of preoperative CT/MR images, and integration of digital data of CAD tumor implants or allografts. Computer navigation and PSI are the tools needed to implement 3D surgical planning. The current indications for the use of CATS to resect bone tumors are (1) the presence of pelvic and sacral tumors located at anatomically complex sites with nearby vital structures, (2) technically demanding resections, such as joint-preserving operations or multiplanar tumor resections, or (3) resections after which the defect must accommodate a custom tumor implant or match an allograft for reconstruction. The early clinical results suggest that the technique is feasible and safe and it improves surgical accuracy, although surgeons must be aware of the potential errors when using the techniques. Potential areas for future development of CATS include an all-in-one planning platform for all users and the integration of 3D printing technology into the CATS workflow. Larger studies with longer follow-up are essential to determine the real clinical efficacy of the new technique.

Declaration of Conflict of Interest The author, Kwok Chuen Wong, declares that there are no conflicts of interest. The Stryker, Materialise, and Stanmore Implants companies did not fund or sponsor this research in any way.

References

1. Picci P, Sangiorgi L, Rougraff BT, Neff JR, Casadei R, et al. Relationship of chemotherapy-induced necrosis and surgical margins to local recurrence in osteosarcoma. J Clin Oncol. 1994;12:2699–705.
2. Cartiaux O, Docquier PL, Paul L, Francq BG, Cornu OH, Delloye C, et al. Surgical inaccuracy of tumor resection and reconstruction within the pelvis: an experimental study. Acta Orthop. 2008;79(5):695–702.
3. Krettek C, Geerling J, Bastian L, Citak M, Rücker F, Kendoff D, Hüfner T. Computer aided tumor resection in the pelvis. Injury. 2004;35(Suppl 1):S-A79–83.
4. Hüfner T, Kfuri M Jr, Galanski M, Bastian L, Loss M, Pohlemann T, Krettek C. New indications for computer-assisted surgery: tumor resection in the pelvis. Clin Orthop Relat Res. 2004;426:219–25.

5. Wong KC, Kumta SM, Chiu KH, et al. Precision tumour resection and reconstruction using image-guided computer navigation. J Bone Joint Surg Br. 2007;89:943–7.
6. Wong KC, Kumta SM, Chiu KH, Cheung KW, Leung KS, Unwin P, Wong MC. Computer assisted pelvic tumor resection and reconstruction with a custom-made prosthesis using an innovative adaptation and its validation. Comput Aided Surg. 2007;12(4):225–32.
7. Aponte-Tinao LA, Ritacco LE, Ayerza MA, Muscolo DL, Farfalli GL. Multiplanar osteotomies guided by navigation in chondrosarcoma of the knee. Orthopedics. 2013;36(3):e325–30.
8. Ritacco LE, Milano FE, Farfalli GL, Ayerza MA, Muscolo DL, Aponte-Tinao LA. Accuracy of 3-D planning and navigation in bone tumor resection. Orthopedics. 2013;36(7):e942–50.
9. Wong KC, Kumta SM, Antonio GE, Tse LF. Image fusion for computer-assisted bone tumor surgery. Clin Orthop Relat Res. 2008;466:2533–41.
10. Wong KC, Kumta SM, Leung KS, Ng KW, Ng EW, Lee KS. Integration of CAD/CAM planning into computer assisted orthopaedic surgery. Comput Aided Surg. 2010;15:65–74.
11. Wong KC, Kumta SM. Joint-preserving tumor resection and reconstruction using image-guided computer navigation. Clin Orthop Relat Res. 2013;471(3):762–73.
12. Docquier PL, Paul L, Cartiaux O, Delloye C, Banse X. Computer-assisted resection and reconstruction of pelvic tumor sarcoma. Sarcoma. 2010;2010:125162. https://doi.org/10.1155/2010/125152.
13. Gerbers JG, Ooijen PM, Jutte PC. Computer-assisted surgery for allograft shaping in hemicortical resection: a technical note involving 4 cases. Acta Orthop. 2013;84(2):224–6.
14. Aponte-Tinao L, Ritacco LE, Ayerza MA, Muscolo DL, Albergo JI, Farfalli GL. Does intraoperative navigation assistance improve bone tumor resection and allograft reconstruction results? Clin Orthop Relat Res. 2015;473(3):796–804. https://doi.org/10.1007/s11999-014-3604-z.
15. Cho HS, Oh JH, Han I, Kim HS. The outcomes of navigation assisted bone tumour surgery: minimum three-year follow-up. J Bone Joint Surg Br. 2012;94(10):1414–20.
16. Wong KC, Kumta SM. Computer-assisted tumor surgery in malignant bone tumors. Clin Orthop Relat Res. 2013;471(3):750–61.
17. Jeys L, Matharu GS, Nandra RS, Grimer RJ. Can computer navigation-assisted surgery reduce the risk of an intralesional margin and reduce the rate of local recurrence in patients with a tumour of the pelvis or sacrum? Bone Joint J. 2013;95-B(10):1417–24.
18. So TY, Lam YL, Mak KL. Computer-assisted navigation in bone tumor surgery: seamless workflow model and evolution of technique. Clin Orthop Relat Res. 2010;468(11):2985–91. https://doi.org/10.1007/s11999-010-1465-7.
19. Ieguchi M, Hoshi M, Takada J, Hidaka N, Nakamura H. Navigation-assisted surgery for bone and soft tissue tumors with bony extension. Clin Orthop Relat Res. 2012;470:275–83.
20. Li J, Wang Z, Guo Z, Chen GJ, Yang M, Pei GX. Irregular osteotomy in limb salvage for juxta-articular osteosarcoma under computer-assisted navigation. J Surg Oncol. 2012;106(4):411–6.
21. Farfalli GL, Albergo JI, Ritacco LE, Ayerza MA, Milano FE, Aponte-Tinao LA. What is the expected learning curve in computer-assisted navigation for bone tumor resection? Clin Orthop Relat Res. 2017;475:668.
22. Wong KC. 3D-printed patient-specific applications in orthopaedics. Orthopaedic Res Rev. 2016;8:57–66. dx.doi.org. https://doi.org/10.2147/ORR.S99614.
23. Wong KC, Sze KY, Wong IO, Wong CM, Kumta SM. Patient-specific instrument can achieve same accuracy with less resection time than navigation assistance in periacetabular pelvic tumor surgery: a cadaveric study. Int J Comput Assist Radiol Surg. 2016;11(2):307–16. https://doi.org/10.1007/s11548-015-1250-x.
24. Gouin F, Paul L, Odri GA, Cartiaux O. Computer-assisted planning and patient-specific instruments for bone tumor resection within the pelvis: a series of 11 patients. Sarcoma. 2014;9:842709.
25. Wong KC, Kumta SM, Sze KY, Wong CM. Use of a patient-specific CAD/CAM surgical jig in extremity bone tumor resection and custom prosthetic reconstruction. Comput Aided Surg. 2012;17(6):284–93.

26. Wong KC, Kumta SM, Geel NV, Demol J. One-step reconstruction with a 3D-printed, biomechanically evaluated custom implant after complex pelvic tumor resection. Comput Aided Surg. 2015;20(1):14–23.
27. Wong KC, Kumta SM. Use of computer navigation in orthopedic oncology. Curr Surg Rep. 2014;2:47. Review
28. Yang YK, Chan CM, Zhang Q, Xu HR, Niu XH. Computer navigation-aided resection of sacral chordomas. Chin Med J (Engl). 2016;129(2):162–8. https://doi.org/10.4103/0366-6999.173465.
29. Cho HS, Oh JH, Han I, Kim HS. Joint-preserving limb salvage surgery under navigation guidance. J Surg Oncol. 2009;100(3):227–32.
30. Outani H, Hamada K, Takenaka S, Imura Y, Oshima K, Sotobori T, Naka N, Araki N, Yoshikawa H, Myoui A. Radiofrequency ablation of osteoid osteoma using a three-dimensional navigation system. J Orthop Sci. 2016;21(5):678–82. https://doi.org/10.1016/j.jos.2016.05.005.
31. Saidi K. Potential use of computer navigation in the treatment of primary benign and malignant tumors in children. Curr Rev Musculoskelet Med. 2012;5(2):83–90. https://doi.org/10.1007/s12178-012-9124-0.

Part III
Statistical Shape Modelling for Computer-Assisted Hip and Knee Surgery

Chapter 14
Application of Statistical Shape Modeling for CAOS: A Tutorial

Yoshinobu Sato

Abstract Statistical shape models (SSMs) are useful for representing intersubject variabilities of anatomical shapes and anatomical shape deformations specific to diseases (e.g., osteoarthritis) as well as preoperative planning of anatomical reconstructive surgery (e.g., fracture reduction and arthroplasty). This chapter presents the mathematical foundations of such applications for SSMs, especially aiming at intuitive understanding of the role of SSMs in Bayes estimation, which is a basic framework of various estimations and prediction problems, including anatomical reconstruction and diagnostic/therapeutic applications.

Keywords Musculoskeletal anatomy modeling · Bayesian estimation · Hip replacement

14.1 Introduction

A statistical shape model (SSM), also known as an active shape model [1, 2], is useful for addressing various medical problems related to intersubject variabilities of anatomical structures. Statistical shape modeling and related methodologies are commonly used to represent these variabilities. An SSM is constructed from a set of training data from several subjects, typically for a specific category of an anatomical structure (e.g., the female pelvis). Regarding its application to computer-assisted orthopedic surgery (CAOS), some good surveys are available [3, 4]. The main difference between this chapter and the existing surveys is that our chapter provides intuitive explanations of its mathematical foundations, especially on the role of SSMs in Bayesian estimations.

From a theoretical viewpoint, an ideal model for representing the shape variabilities must satisfy three criteria—i.e., specificity, generalization, and compactness [5]—which allow the model to generate any shape within a targeted category (generalization)

Y. Sato
Nara Institute of Science and Technology, Ikoma, Nara, Japan
e-mail: yoshi@is.naist.jp

N. Sugano (ed.), *Computer Assisted Orthopaedic Surgery for Hip and Knee*,
https://doi.org/10.1007/978-981-10-5245-3_14

using only a few number of parameters (compactness) while excluding any shape outside the category (specificity). An acceptable SSM approximately satisfies these three criteria in a well-balanced manner. Because of this special feature, unknown shapes of a known category can be reconstructed and predicted from partial, incomplete, degenerated, and/or noisy data via SSM fitting to the data. SSMs are considered to provide statistic-based, category-specific interpolation (and even extrapolation) methods, unlike conventional smoothness-based methods (e.g., splines) or analytical function-based methods (e.g., linear regression). With CAOS, reconstruction of musculoskeletal anatomy—including bones [6–11], muscles [12], and cartilage [13], among other tissues—from images and spatial data has been addressed. The mathematical aspects of SSMs are described in an intuitively understandable manner in this chapter, and anatomical shape reconstruction using SSMs is described, with special emphasis on the role of SSMs in the Bayesian estimation framework.

Surgeons improve their capability through gaining experience with a wide variety of clinical cases. From the clinical viewpoint, an SSM is used to represent inter-patient variabilities in clinical cases when modeling the improvement process of surgeons' capability. High levels of generalization and specificity are directly related to the capability of diagnostic and therapeutic decisionmaking based on patient data. Similar to human surgeons, an SSM would gain higher generalization and specificity by increasing the number of training data. CAOS applications of SSMs include diagnosing osteoarthritis [14, 15] and treatment planning for arthroplasties [16], fracture reduction [17], and bone tumors [18, 19]. We address this issue using an SSM that represents the clinical skill of acetabular cup alignment as an example, which is also formulated as a Bayesian estimation [16].

14.2 Intuitive Understanding of Mathematical Aspects of SSM

An SSM is constructed from a dataset of a targeted anatomical shape category of many subjects. Figure 14.1a shows the simplest SSM, which is constructed from two shapes of the category "hemi-pelvis" from various subjects. Here, we consider three-dimensional (3D) shapes. To construct the SSM, their average is first computed. For this purpose, dense point-to-point correspondences on surfaces are needed between the two shapes, which is a key process when constructing SSMs and has been addressed by many researchers [20–22]. Once the point-to-point correspondences between two shapes have been established, their average shape is generated by taking the midpoint of every corresponding point (vertex) pair. Here, we denote the calculation of the average shape S_{ave} of two shapes S_1 and S_2 simply as

$$S_{\text{ave}} = \frac{S_1 + S_2}{2}$$

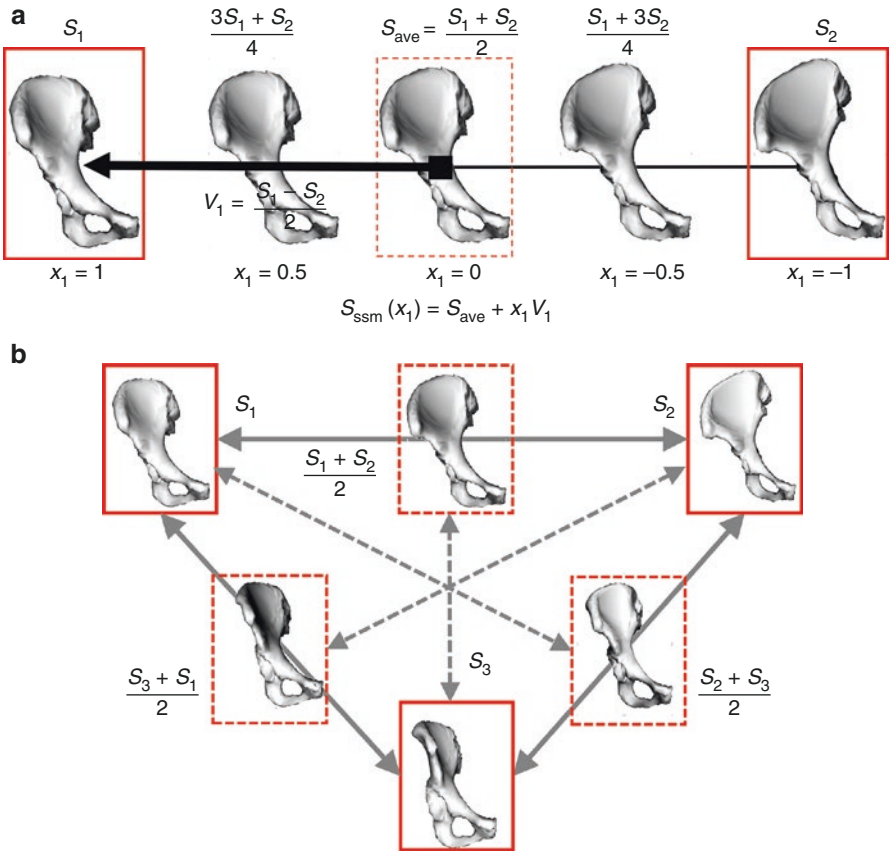

Fig. 14.1 Intuitive illustrations of simple cases of statistical shape models (SSMs). (**a**) Simplest SSM constructed from two shapes of different subjects. In this case, shapes generated from an SSM are equivalent to interpolated shapes by simple morphing between the two shapes based on dense point-to-point correspondences on their surfaces. (**b**) Morphing among three shapes. Morphing is possible not only between two of the three shapes (solid lines) but also an interpolated shape of two of them and the other shape (dotted lines)

Using the established correspondences, continuously interpolated shapes between S_1 and S_2 can be generated (Fig. 14.1a). That is, "morphing" between the two shapes is possible, which is regarded as the simplest SSM, expressed as

$$S_{\text{ssm}}\left(x_1\right) = S_{\text{ave}} + x_1 V_1$$

where x_1 is a coefficient of variation mode V_1 given by

$$V_1 = \frac{S_1 - S_2}{2}$$

As shown in Fig. 14.1b, given three shapes, morphing is possible not only between two of the three shapes but also between a shape interpolated from the two shapes and the other shape (Fig. 14.1b). Therefore, three shapes can be combined to generate multiple interpolated shapes as their weighted average (dotted lines in Fig. 14.1b), which defines an SSM with two variation modes.

Generally, an SSM constructed from n training shape data has $n - 1$ variation modes, V_1, V_2, …, V_{n-1}, which is expressed as

$$S_{\text{ssm}}(X') = S_{\text{ave}} + x_1V_1 + x_2V_2 \cdots + x_{n-1}V_{n-1} = S_{\text{ave}} + \sum_{i=1}^{n-1} x_iV_i$$

where $X' = (x_1, x_2, \cdots, x_{n-1})$. By setting certain parameter values for X', $S_{\text{ssm}}(X')$ generates any shape, represented only as a weighted average of training shape data, which ensures high *specificity*. In addition, given training data that cover a sufficiently wide variability of a target category, high *generalization* is expected.

Figure 14.2 outlines the construction, utilization, and mathematical interpretation of SSMs. As shown in the top left frames, principal component analysis (PCA) is typically used to obtain the variation modes that are vectors orthogonal to each other and listed in the order of the standard deviation (SD). The SD is the amount of variation in each mode and is regarded as the importance of each mode. Using the PCA, we can use the first m ($m < n - 1$) mode. Thus, we have

$$S_{\text{ssm}}(X) = S_{\text{ave}} + x_1V_1 + x_2V_2 \cdots + x_mV_m = S_{\text{ave}} + \sum_{i=1}^{m} x_iV_i$$

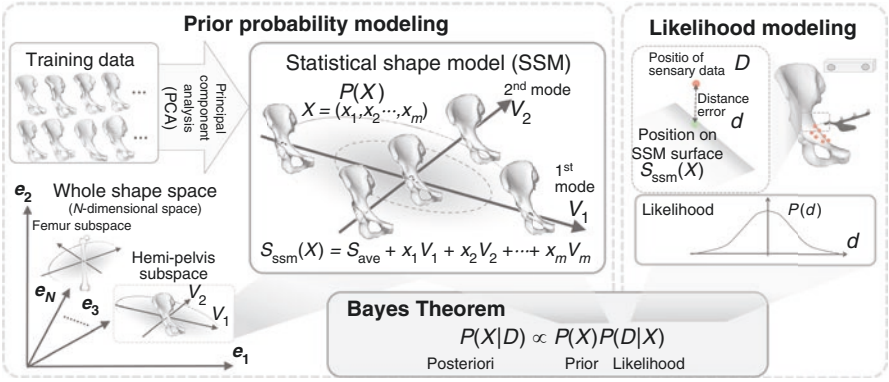

Fig. 14.2 Construction (top, left) and mathematical interpretation (bottom, left) of an SSM and its integration into a Bayesian estimation for anatomical reconstruction from incomplete and noisy data (right). Left: Prior probability modeling. SSM is considered to provide a prior probability distribution, $P(X)$, in the Bayes theorem, with $P(X)$ defined as a dimensionality-reduced subspace in the whole shape space. Right: Likelihood modeling. Using the analysis of sensory data generation, a likelihood in Bayes theorem is modeled (e.g., as additive Gaussian noise)

where $X = (x_1, x_2, \cdots, x_m)$. Hereafter, X is referred to as "SSM parameters." $S_{\text{ssm}}(X)$ generates a specific shape of the trained category as an approximation to a weighted average of training shape data. Most importantly, the probability distribution of a shape category, $P(X)$, is provided as an m-dimensional Gaussian distribution defined by the average shape S_{ave} and variation modes V_i associated with the SD values, σ_i ($i = 1, 2, \cdots, m$).

Figure 14.3 shows examples of SSMs. An SSM can represent not only variabilities of a single shape but also those of a combined shape of multiple object shapes [23]. In an SSM of combined shapes, variabilities in spatial relations between two bones are represented in addition to those of bone shapes. In the example of a combined shape shown in Fig. 14.3, variabilities represented by an SSM include inter-subject variabilities of the hip joint configuration in the supine position during computed tomography (CT) imaging.

A 3D shape is typically represented by a polygon mesh that consists of vertices (3D points) and faces. Let N be the number of vertices. Then, a 3D shape is regarded as a vector in a $3N$-dimensional space that includes any shapes represented by N vertices (because three coordinate values of N vertices are concatenated to produce a $3N$-dimensional vector), which here we call "whole shape space." Its concept is shown in the left-lower frame of Fig. 14.2. Therefore, an SSM provides a probability distribution of a specific category of shapes as a Gaussian distribution in a dimensionally reduced subspace within the whole shape space.

In one case [24], $N = 1500$ vertices were used to represent the shape of a hemi-pelvis. The actual values of n and m were $n = 200$ and $m = 60$, respectively. The dimension of the hemi-pelvis subspace, $m = 60$, was largely reduced from the original dimension of the whole shape space, $3N = 4500$. Typically, the first few modes are essential to represent unknown shapes in the category, and later modes become

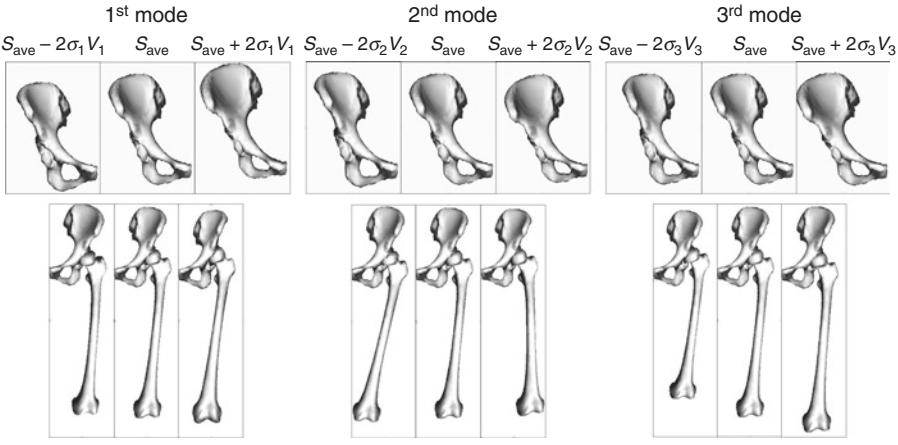

Fig. 14.3 Examples of statistical shape models (SSMs). First three modes are shown. Top: SSM of the hemi-pelvis shape. Bottom: SSM of the combined shape of the hemi-pelvis and femur, where variabilities in spatial relations between the two bones are represented as well as the shape variabilities in each bone

less important or even exert a negative influence. Therefore, a (much) smaller m than $n-1$ occurs often enough, so the *compactness* requirement is satisfied. An appropriate m is usually determined by the cumulative contribution ratio or accuracy assessment through cross-validation within training dataset. In the case described [24], $m = 60$ modes were selected so that the cumulative contribution ratio was 99.9%.

14.3 Anatomical Reconstruction Using SSMs as Bayesian Estimation

One of the earliest CAOS applications of SSMs was reconstruction of femoral and tibial shapes from intraoperatively digitized 3D position data on bone surfaces [6, 7]. CT [8] and magnetic resonance imaging [12, 13] data, as well as (tracked and calibrated) plain radiography [9, 10] and ultrasonography [11] image data, are also used for SSM-based reconstruction. We refer to all these data types as "sensory data D." We use X to refer to "shape X" because SSM parameters X generate a targeted anatomical shape. The problem is viewed as the estimation of shape X from sensory data D. We apply the concept of Bayes theorem, written as

$$P(X|D) \propto P(X)P(D|X)$$

to the problem. Figure 14.2 provides an overview of Bayesian estimation. Its details, including explanations of $P(X|D)$, $P(X)$, and $P(D|X)$, are described below.

$P(X|D)$, referred to as "the posteriori probability," refers to a probability distribution of shape X after observed sensory data D is taken into account. We want to find the shape X that maximizes $P(X|D)$—i.e., the most probable shape X of the target anatomy estimated from observed sensory data D. This estimation framework is called the "maximum a posteriori" estimation. Although direct formulation of $P(X|D)$ is not easy, Bayes theorem ensures that maximization of $P(X|D)$ is equivalent to that of $P(X) \times P(D|X)$.

The left panel of Fig. 14.2 corresponds to modeling of "the prior probability" distribution of shape X, $P(X)$, which represents the more probable or more unlikely shape of the target anatomy without (prior to) observing the sensory data. $P(X)$ is regarded as knowledge about the targeted anatomical shape, modeled by a Gaussian function using an SSM.

The right panel of Fig. 14.2 shows modeling of "the likelihood," $P(D|X)$—representing a probability distribution of sensory data D—that is expected to be observed from shape X. $P(D|X)$ is regarded as knowledge on generation processes of sensory data from anatomical shapes. When D is a set of 3D measured positions of the surface of shape X, $P(D|X)$ is typically formulated as the Gaussian distribution of distance errors, d, added to the surface positions on $S_{\mathrm{ssm}}(X)$. In actual situations, outliers must be considered, so a simple Gaussian distribution is insufficient. In such cases, $P(D|X)$ is often modified from the Gaussian distribution, so it is robust against outliers [25].

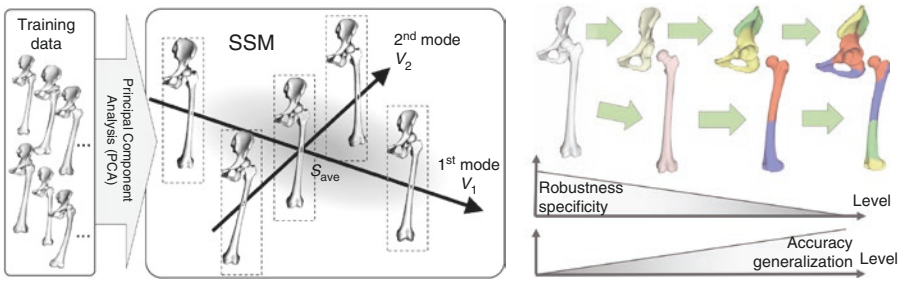

Fig. 14.4 Hierarchical statistical shape modeling of the combined shapes of the hemi-pelvis and femur. (**a**) SSM of combined hemi-pelvis and femur shapes at the coarsest level. (**b**) Hierarchical decomposition of SSMs into sub-shapes at the finer levels. Robustness and specificity ability are better at coarser levels, whereas accuracy and generalization ability are better at finer levels

According to Bayes theorem, $P(X)$, knowledge of targeted anatomical shape X, and $P(D|X)$, knowledge on generation processes of data D from shape X, are combined to find the most probable shape X of the targeted anatomy estimated from observed sensory data D. Next, the key issues for successful applications are to develop effective methods for (1) modeling of $P(X)$ and $P(D|X)$ and (2) finding the optimal X to maximize $P(X) \times P(D|X)$. These two issues are related. More accurate modeling of $P(X)$ and $P(D|X)$ is desirable, but it may result in less chance of finding the optimal X. A possible approach to finding a good compromise between accurate modeling and stable optimization is hierarchical modeling of $P(X)$.

Figure 14.4 shows an example of hierarchical modeling, wherein the SSM of a combined shape of the pelvis and femur is constructed at the coarsest level (Fig. 14.4a). SSMs of the pelvis and femur are then modeled individually. Furthermore, each model (pelvis and femur) is decomposed into sub-shapes hierarchically at the finer levels (Fig. 14.4b) [8, 24]. An initial estimate of X is obtained at the coarsest level, where optimization is stable (i.e., will not make a big mistake) because of the high *specificity*, but reconstruction accuracy may be insufficient because of the low *generalization*. At the finer levels, accuracy can be improved using decomposed models of higher *generalization*, and stability is maintained because of a good initial estimate obtained at the coarser level.

14.4 Applications to Diagnostic and Treatment Planning Assistance Using SSMs

Typical SSM applications to diagnostic assistance depend on finding the relations between disease-specific deformation patterns and the coefficients of the variation modes of an SSM [26]. For instance, the diagnosis of osteoarthritis has been addressed by several studies [14, 15], which have been well summarized [3]. With respect to therapeutic planning, SSMs are useful for surgical planning that involves

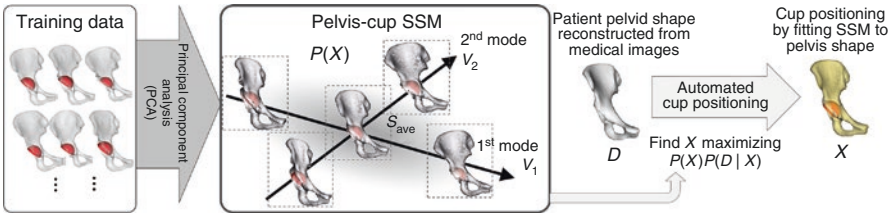

Fig. 14.5 Automated preoperative planning of acetabular cup alignment as a Bayesian estimation. Preferred spatial relation between the patient's pelvis and cup, X, is encoded in the SSM, which provides a prior probability distribution $P(X)$. Given the patient pelvis shape D, the problem is formulated as finding X, maximizing $P(X) \times P(D|X)$

predicting desirable postoperative (implanted) anatomy from preoperatively deformed/injured/defective anatomy such as with arthroplasty [16], fracture reduction [17], and reconstruction of bone from which a tumor has been resected [18, 19].

Here, specifically, we describe a Bayesian formulation of automated preoperative planning for acetabular cup placement during total hip arthroplasty (THA) (Fig. 14.5). The problem of acetabular cup planning could be described as finding the best cup size from the data regarding the host's bone shape. To formulate $P(X)$, an SSM of the combined shape of the pelvis and cup in a preoperative plan (pelvis-cup SSM) is constructed, which is regarded as knowledge on the alignment of the acetabular cup with respect to the pelvis. Training data (for preoperative planning of the cup) on the pelvis, X, for various patients were previously prepared by an experienced surgeon. The shape of the patient's pelvis, segmented from CT data, is regarded as observed data D, and $P(D|X)$ is modeled by the Gaussian distribution of distance from each surface point of the pelvic part (without the cup) in shape X to observed data D. That is, given the patient's pelvic shape, the cup shape is statistically predicted (or extrapolated) by fitting the pelvic-cup SSM to the patient's pelvic shape [16]. Similar principles are used for other therapeutic applications.

14.5 Summary

Intuitive understanding of the mathematical aspects of an SSM was reviewed, with the role of an SSM discussed especially within the framework of Bayesian estimation. The problems associated with anatomical shape reconstruction from sensory data and therapeutic planning from patient anatomy were addressed as representative CAOS applications of SSMs. An SSM represents knowledge of anatomical shape categories and anatomy-related therapeutic planning, such as the position and alignment of the acetabular cup, which provides a "prior probability" distribution within the Bayesian framework. Although only shape modeling was addressed here, statistical intensity modeling can be combined with SSM, which has been

successfully applied to the reconstruction of 3D distributions of bone mineral density [27]. The methodologies for SSMs are now sufficiently well established. Going forward, systematic collection and classification of training data will be key to initiating clinical application.

References

1. Cootes TF, Taylor CJ, Cooper DH, Graham J. Active shape models-their training and application. Comput Vision Image Understand. 1995;61(1):38–59.
2. Heimann T, Meinzer H-P. Statistical shape models for 3D medical image segmentation: a review. Med Image Anal. 2009;13(4):543–63.
3. Sarkalkan N, Weinans H, Zadpoor AA. Statistical shape and appearance models of bones. Bone. 2014;60:129–40.
4. Lamecker H, Zachow S. Statistical shape modeling of musculoskeletal structures and its applications. In: Computational radiology for orthopaedic interventions. New York, NY: Springer International Publishing; 2016. p. 1–23.
5. Styner MA, Rajamani KT, Nolte L-P, Zsemlye G, Székely G, Taylor CJ, Davies RH. Evaluation of 3D correspondence methods for model building. In: Biennial International Conference on Information Processing in Medical Imaging. Berlin: Springer; 2003. p. 63–75.
6. Fleute M, Lavallée S. Building a complete surface model from sparse data using statistical shape models: application to computer assisted knee surgery. In: Medical Image Computing and Computer-Assisted Intervention—MICCAI'98. London: Springer; 1998. p. 879–87.
7. Fleute M, Lavallée S, Julliard R. Incorporating a statistically based shape model into a system for computer-assisted anterior cruciate ligament surgery. Med Image Anal. 1999;3(3):209–22.
8. Yokota F, Okada T, Takao M, Sugano N, Tada Y, Sato Y. Automated segmentation of the femur and pelvis from 3D CT data of diseased hip using hierarchical statistical shape model of joint structure. Med Image Comput Comput Assist Interv. 2009;12:811–8.
9. Zheng G, Gollmer S, Schumann S, Dong X, Feilkas T, Ballester MAG. A 2D/3D correspondence building method for reconstruction of a patient-specific 3D bone surface model using point distribution models and calibrated X-ray images. Med Image Anal. 2009;13(6):883–99.
10. Baka N, Kaptein BL, de Bruijne M, van Walsum T, Giphart JE, Niessen WJ, Lelieveldt BPF. 2D–3D shape reconstruction of the distal femur from stereo X-ray imaging using statistical shape models. Med Image Anal. 2011;15(6):840–50.
11. Barratt DC, Chan CSK, Edwards PJ, Penney GP, Slomczykowski M, Carter TJ, Hawkes DJ. Instantiation and registration of statistical shape models of the femur and pelvis using 3D ultrasound imaging. Med Image Anal. 2008;12(3):358–74.
12. Baudin P-Y, Azzabou N, Carlier PG, Paragios N. Prior knowledge, random walks and human skeletal muscle segmentation. In: International Conference on Medical Image Computing and Computer-Assisted Intervention. Berlin: Springer; 2012. p. 569–76.
13. Fripp J, Crozier S, Warfield SK, Ourselin S. Automatic segmentation and quantitative analysis of the articular cartilages from magnetic resonance images of the knee. IEEE Trans Med Imaging. 2010;29(1):55–64.
14. Gregory JS, Waarsing JH, Day J, Pols HA, Reijman M, Weinans H, Aspden RM. Early identification of radiographic osteoarthritis of the hip using an active shape model to quantify changes in bone morphometric features: can hip shape tell us anything about the progression of osteoarthritis? Arthritis Rheum. 2007;56(11):3634–43.
15. Bredbenner TL, Eliason TD, Potter RS, Mason RL, Havill LM, Nicolella DP. Statistical shape modeling describes variation in tibia and femur surface geometry between Control and Incidence groups from the osteoarthritis initiative database. J Biomech. 2010;43(9):1780–6.

16. Kagiyama Y, Otomaru I, Takao M, Sugano N, Nakamoto M, Yokota F, Tomiyama N, Tada Y, Sato Y. CT-based automated planning of acetabular cup for total hip arthroplasty (THA) based on hybrid use of two statistical atlases. Int J Comput Assist Radiol Surg. 2016;11(12):2253–71.
17. Gong RH, Stewart J, Abolmaesumi P. Multiple-object 2-D–3-D registration for noninvasive pose identification of fracture fragments. IEEE Trans Biomed Eng. 2011;58(6):1592–601.
18. Sleiman HB, Ritacco LE, Aponte-Tinao L, Muscolo DL, Nolte L-P, Reyes M. Allograft selection for transepiphyseal tumor resection around the knee using three-dimensional surface registration. Ann Biomed Eng. 2011;39(6):1720–7.
19. Krol Z, Skadlubowicz P, Hefti F, Krieg AH. Virtual reconstruction of pelvic tumor defects based on a gender-specific statistical shape model. Comput Aided Surg. 2013;18(5-6):142–53.
20. Rueckert D, Sonoda LI, Hayes C, Hill DLG, Leach MO, Hawkes DJ. Nonrigid registration using free-form deformations: application to breast MR images. IEEE Trans Med Imaging. 1999;18(8):712–21.
21. Faisal Beg M, Miller MI, Trouvé A, Younes L. Computing large deformation metric mappings via geodesic flows of diffeomorphisms. Int J Comput Vision. 2005;61(2):139–57.
22. Vercauteren T, Pennec X, Perchant A, Ayache N. Diffeomorphic demons: efficient non-parametric image registration. Neuroimage. 2009;45(1):S61–72.
23. Frangi AF, Rueckert D, Schnabel JA, Niessen WJ. Automatic construction of multiple-object three-dimensional statistical shape models: application to cardiac modeling. IEEE Trans Med Imaging. 2002;21(9):1151–66.
24. Yokota F, Okada T, Takao M, Sugano N, Tada Y, Tomiyama N, Sato Y. Automated CT segmentation of diseased hip using hierarchical and conditional statistical shape models. In: International Conference on Medical Image Computing and Computer-Assisted Intervention. Berlin: Springer; 2013. p. 190–7.
25. Huber PJ. Robust statistics. Berlin: Springer; 2011.
26. Golland P, Grimson WEL, Shenton ME, Kikinis R. Detection and analysis of statistical differences in anatomical shape. Med Image Anal. 2005;9(1):69–86.
27. Whitmarsh T, Humbert L, De Craene M, Barquero LMDR, Frangi AF. Reconstructing the 3D shape and bone mineral density distribution of the proximal femur from dual-energy X-ray absorptiometry. IEEE Trans Med Imaging. 2011;30(12):2101–14.

Chapter 15
Statistical Shape Models and Atlases: Application to 2D-3D Reconstruction in THA

Guoyan Zheng

Abstract This chapter introduces both a statistically shaped model (SSM)-based surface model reconstruction method and an atlas-based intensity volume reconstruction method under the context of 2D-3D reconstruction-based planning for total hip arthroplasty (THA). It shows that, despite successful application of the SSM-based method for planning cup components to be used during THA, it has limitations regarding planning stem components because of missing information about intramedullary canal geometry. This deficit motivated us to develop an atlas-based intensity volume reconstruction method to derive the patient-specific intensity volume of the proximal femur, which facilitates precise planning of stem components.

Keywords Statistical shape model · Atlas · 2D-3D reconstruction · THA

15.1 Introduction

Meticulous preoperative planning and templating are becoming an integral part of total hip arthroplasty (THA). Preoperative planning and templating allow surgeons to search for an optimal fit of the hip implant components and for the best technique to reconstruct leg length and the position of the center of rotation, each of which depends on the implant size and positioning. Successful preoperative planning can prevent the use of undersized or oversized hip implants, whereas inadequate preoperative planning and inaccurate templating may lead to various complications, including femoral fracture, limb length inequality, insufficient offset, instability, and failure to achieve ingrowth.

In the past, both digital and analog radiography-based preoperative planning systems have been introduced, but the reported accuracy for these systems varies. Della Valle et al. [1] showed that the template size corresponded to the actual component

G. Zheng
Institute for Surgical Technology and Biomechanics, University of Bern, Bern, Switzerland
e-mail: Guoyan.zheng@ieee.org

N. Sugano (ed.), *Computer Assisted Orthopaedic Surgery for Hip and Knee*,
https://doi.org/10.1007/978-981-10-5245-3_15

used in approximately 78% and 83% of cases with cemented femoral prostheses and combined cemented and cementless acetabular components, respectively. Eggli et al. [2] reported similar results, wherein more than 90% of the cases in the series used cement fixation. For cementless prostheses, Carter et al. [3] reported that the exact size of the femoral components was predicted in approximately 50% of 74 cases, and Unnanuntana et al. [4] noted that the size of the prosthesis was exactly predicted for only 42% of acetabular components and 68.8% of femoral components. The error in determining accurate radiographic magnification and the projection characteristics of two-dimensional (2D) radiography contributed significantly to the prediction errors of these systems. In addition, insufficient definition of the intramedullary anatomy on plain radiography reduces the accuracy of proper implant selection. There is currently a trend to perform preoperative planning of THA using three-dimensional (3D) computed tomography (CT) data.

Compared with plain radiography, CT-based 3D planning of THA offers several advantages [5–8]: avoiding errors resulting from magnification and incorrect patient positioning and providing true 3D depiction of the underlying anatomy and accurate information on bone quality. Preoperative planning for THA using 3D CT data has usually been performed in an interactive manner [5], although an automated solution was recently introduced [8]. More specifically, with such a system, the sizes of the implants and their 3D positions and orientations with respect to the host bones can be automatically computed based on 3D surface models segmented from the CT data. A randomized comparison between 3D CT-based planning and 2D plain radiography-based templating for THA [6] showed that the prediction rate for the stem and the cup sizes for the 3D CT-based planning is twice as accurate as that for 2D plain radiography-based templating. The concern about 3D CT-based planning of THA, however, is the increased radiation dosage to the patient and the associated CT acquisition cost [6, 7]. One way to address this concern is to reconstruct 3D patient-specific surface models or intensity volumes from 2D plain radiographic images.

Constructing 3D models or volumes from a limited number of calibrated 2D radiographic images, however, is challenging. A priori information is often required to handle this otherwise ill-posed problem. Previously, atlas-based methods [9, 10] and statistically shaped model (SSM)-based methods [11–13] have been proposed. More specifically, an atlas-based method starts with establishing spatial correspondence between an atlas—which could be a generic object or a template obtained via averaging—and the given images, followed by sequential scaled rigid and nonrigid registration steps until the simulated projections of the atlas are similar to the given radiographic images. In contrast, instead of using one generic object as the prior information, the methods in the second category use SSMs obtained from a statistically shaped analysis. Thus, because an SSM captures the mean shape and geometric variability of a collection of sample models of a given population using a limited number of parameters, it can be used for robust 2D-3D reconstruction.

We introduce both an SSM-based surface model reconstruction method and an atlas-based intensity volume reconstruction method under the context of 2D-3D reconstruction-based planning of THA. We show that, despite successful application

of the former method in planning cup components for THA, such a method has limitations in regard to planning stem components because of missing information about intramedullary canal geometry. This situation motivated us to develop an atlas-based intensity volume reconstruction method to derive a patient-specific intensity volume of the proximal femur, which facilitates precise planning of stem components.

15.2 SSM-Based Surface Model 2D-3D Reconstruction Method

Existing feature-based 2D-3D reconstruction algorithms [9–11] have difficulty reconstructing concave structures because they depend on areas of correspondence between the contours detected from the plain radiographic images and the silhouettes extracted from the SSMs. For THA, however, surgeons are interested not only in accurate reconstruction of the overall shape of the anatomical structures but also of the specific acetabular joint, which consists of two surfaces: the acetabular surface and the proximal femoral surface. The accuracy of reconstructing the acetabular joint depends on the accuracy of the preoperative planning. Although the 2D-3D reconstruction scheme that we previously developed could be used to reconstruct a patient-specific model of the proximal femur surface [11], its direct application to reconstruction of the acetabular surface may lead to less-than-accurate results.

To explain why we need to develop a new 2D-3D reconstruction scheme, we must analyze the established 2D-3D correspondence and thus generation of the silhouette. Figure 15.1 shows a calculated silhouette of the pelvis. Based on this image, it seems clear that whatever does not generate a silhouette cannot contribute to the final solution because it cannot be used to establish correspondence. To obtain more points of correspondence, more contours must be drawn on the radiograph and, accordingly, identified on the SSM. This is realized with so-called features [13] and patches [14].

The "features" that build points of correspondence—and therefore contribute to the reconstruction—were selected for the SSM with an SSM construction application that was developed in-house. The acetabular rim was split into anterior and posterior parts. The boundary where the anterior part starts and ends was defined. Figure 15.2 (left) shows the selected feature points for the anterior and posterior parts of the acetabular rim, respectively, as well as a list of features and patches used for our method. The rim points were chosen as features because they are almost all located at the same position for all view angles because of a relatively sharp edge.

The left and right hemi-pelvis and the acetabular fossa were introduced as "patches," defined as subregions of a surface. A patch is handled differently from a feature in the developed application. As the patch describes a subregion of the surface model, a silhouette can be calculated, depending on the viewing direction.

Fig. 15.1 Limitations of the existing two-/three-dimensional (2D-3D) reconstruction scheme. This anteroposterior (AP) view shows the 3D pelvic surface model and the calculated silhouettes. Certain parts (i.e., anterior acetabulum rims) do not contribute to silhouette generation. Thus, they cannot participate in the 2D-3D reconstruction process

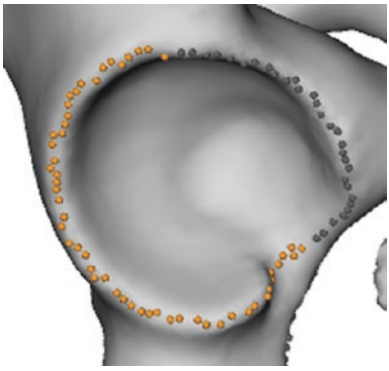

A list of features and patches used in our method

Anatomical name	Feature	Patch
Left hemi-pelvis		X
Right hemi-pelvis		X
Left anterior rim	X	
Left posterior rim	X	
Right anterior rim	X	
Right posterior rim	X	
Left acetabular fossa		X
Right acetabular fossa		

Fig. 15.2 Left: anterior (gray points) and posterior (yellow points) acetabular rims defined on the statistically shaped model as "features." Right: a list of features and points

All additional features and patches are shown in Fig. 15.2 (right). There is no differentiation on the radiographic images between contours building correspondence with a patch, a feature, or the model. The contours for the acetabular anterior and posterior rims, however, are not drawn on all of the radiographic images. Although the rims are on an edge, the contour cannot be well identified on these images as it is not necessarily the outermost contour. Therefore, the decision was made to draw only the inner (more medial) rim contours, except on the anteroposterior (AP) image, where all contours are assigned because the outermost contour can be clearly assigned to the rim. Examples of the AP and outlet images with their assigned contours are shown in Fig. 15.3.

As the feature points do not generally coincide with the silhouette points, they are projected individually onto the image plane. To ensure that no incorrect correspondence points are found, the 2D contours are assigned specifically to a feature or

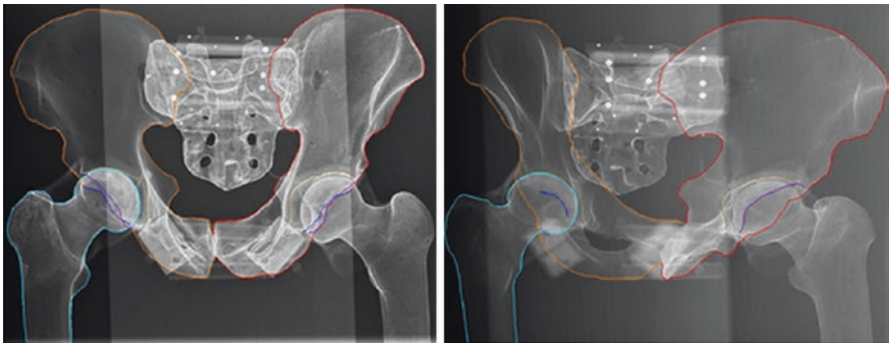

Fig. 15.3 Contours assigned on AP (left) and oblique (right) plain radiographic images for hierarchical 2D-3D reconstruction. Red, left hemi-pelvis contour; orange, right hemi-pelvis contour; light brown, left/right acetabular fossa; blue, left/right anterior acetabular rim; dark purple, left/right posterior acetabular rims; cyan, femoral contours

a patch. Instead of trying to find a matching point pair in the whole contour data set, we consider only the contour assigned with the feature by its name. As now all the related features and patches contribute to the 2D-3D reconstruction process, it is expected that more accurate reconstruction of the hip joint models will be obtained [13, 14]. Figure 15.4 shows an example of the reconstruction.

To evaluate the accuracy of the reconstructions, we conducted validation experiments based on calibrated plain radiographs. Three bones—i.e., two cadaveric hips (models 1 and 2, respectively, each with a cadaveric femur) and one plastic hip containing two femurs with metallic coating (models 3 and 4)—were used in the experiment. Three calibrated plain radiographic images (AP, oblique, outlet) were acquired for each of the four hip joints and were used as the input models for the reconstruction algorithms. For model 1, we reconstructed the right hip joint and for model 2 the left hip joint. For the plastic "bone," we reconstructed both left and right hip joints.

The present hierarchical 2D-3D reconstruction algorithm was compared with the 2D-3D reconstruction algorithm introduced elsewhere [11]. Surface models segmented from CT images of each bone were regarded as the ground truth. To evaluate the accuracy of the reconstruction, the surface models reconstructed from the plain radiographic images were transformed to the coordinate system of the associated ground truth models with surface-based rigid registration before a surface-to-surface error could be computed. When the 2D-3D reconstruction algorithm introduced earlier [11] was used, the mean surface reconstruction errors were 1.1 and 2.1 mm for the femur and the pelvis, respectively. Using the present 2D-3D reconstruction algorithm led to lower corresponding mean surface distance errors of 0.8 mm and 1.9 mm, respectively.

The method presented here can be used to derive patient-specific surface models of both the pelvis and proximal femur and has been successfully used to plan cup components for THA [15]. No intensity information or information about cortical bone, however, is available. The method is therefore not ready for planning a

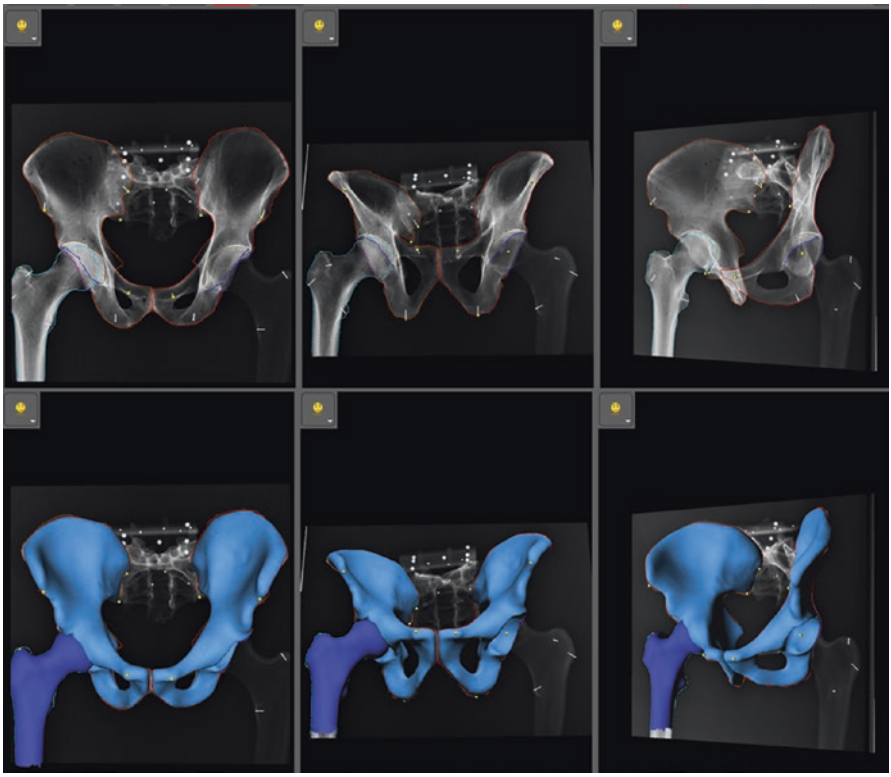

Fig. 15.4 Contour definition (top) and the models (bottom) obtained with our hierarchical 2D-3D reconstruction algorithm

cementless stem component because of the missing information about proximal femur morphology and intramedullary anatomy. This lacking information motived us to develop an atlas-based intensity volume reconstruction method.

15.3 Atlas-Bases Intensity Volume Reconstruction

Figure 15.5 shows the schema for our atlas-based 2D-3D intensity volume reconstruction algorithm, which depends on a control point-based 2D-3D registration process that we previously described [16]. More specifically, starting from a volumetric atlas and a pair of given plain radiographic images, the nonrigid registration is done with a hierarchical two-stage strategy: scaled rigid 2D-3D registration followed by regularized deformable b-spline 2D-3D registration. During the first stage, we estimated the scaled rigid transformation between the reference space of the given radiographic images and the space of the volumetric atlas. Then, during the second stage, we estimated a deformation field from the radiographic image

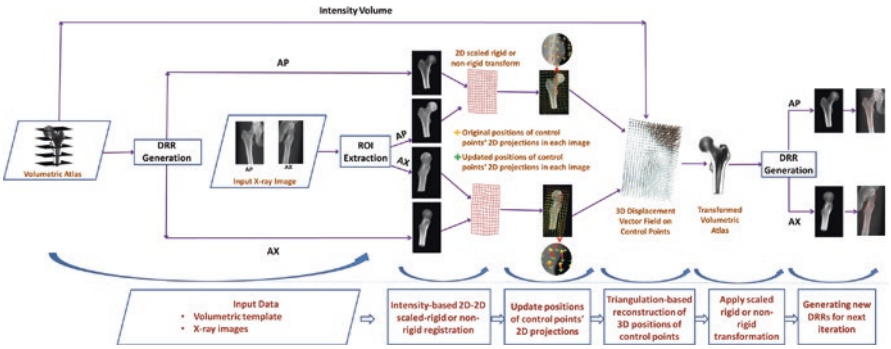

Fig. 15.5 Schema of our atlas-based intensity volume reconstruction method

reference space to the volumetric atlas space. Obtaining this deformation field allows us to warp the volumetric atlas to the radiographic reference space to derive a patient-specific intensity volume. For details, please refer to our earlier study [16].

The present method was evaluated using anonymized data of 44 patients, taking measurements from the CT scan of each patient as the ground truth. The mean absolute surface distance, mean Dice coefficient, mean cortical bone region absolute surface distance, and mean cortical bone region Dice coefficient between the reconstructed volumes and the ground truth CT volumes were 0.9 ± 0.2 mm, $94.4\% \pm 1.1\%$, 0.7 ± 0.2 mm, and $85.1\% \pm 2.9\%$, respectively.

15.4 Conclusion

We introduced two 2D-3D reconstruction methods. The first is an SSM-based 2D-3D surface model reconstruction method that can be used to plan cup components for THA but not stem components because of missing information about intramedullary canal anatomy. This lacking information motivated us to develop an atlas-based 2D-3D intensity volume reconstruction method, which facilitates the planning of stem components for THA. We believe that the combination of the SSM-based 2D-3D reconstruction and the atlas-based intensity volume 2D-3D reconstruction provides a solution for precise planning of both cup and stem components for THA.

References

1. Gonzalez Della Valle A, et al. The Precision and usefulness of preoperative planning for cemented and hybrid primary total hip arthroplasty. J Arthroplasty. 2005;20:51–8.
2. Eggli S, Pisan M, Mueller M. The value of preoperative planning for total hip arthroplasty. J Bone Joint Surg Br. 1998;80:382–90.

3. Carter LW, Stovall DO, Young TR. Determination of accuracy of preoperative templating of noncemented femoral prostheses. J Arthroplasty. 1995;10:507–13.
4. Unnanuntana A, Wagner D, Goodman SB. The accuracy of pre-operative templating in cementless total hip arthroplasty. J Arthroplasty. 2009;24:180–6.
5. Viceconti M, Lattanzi R, et al. CT-based surgical planning software improves the accuracy of total hip replacement preoperative planning. Med Eng Phys. 2003;25:371–7.
6. Sariali E, Mauprivez R, et al. Accuracy of the preoperative planning for cementless total hip arthroplasty. A randomized comparison between three-dimensional computerized planning and conventional templating. Orthop Traumatol Surg Res. 2012;98:151–8.
7. Huppertz A, Radmer S, et al. Computed tomography for preoperative planning in minimal-invasive total hip arthroplasty: radiation exposure and cost analysis. Eur J Radiol. 2011;78:406–13.
8. Otomaru I, Nakamoto M, et al. Automated preoperative planning of femoral stem in total hip arthroplasty from 3D CT data: atlas-based approach and comparative study. Med Image Anal. 2012;16:415–26.
9. Mitton D, Deschenes S, et al. 3D reconstruction of the pelvis from bi-planar radiography. Comput Methods Biomech Biomed Engin. 2006;9:15.
10. Kadoury S, Cheriet F, et al. Three-dimensional reconstruction of the scoliotic spine and pelvis from uncalibrated biplanar X-ray images. J Spinal Disord Tech. 2007;20:160–7.
11. Zheng G, Gollmer S, Schumann S, et al. A 2D/3D correspondence building method for reconstruction of a patient-specific 3D bone surface model using point distribution models and calibrated X-ray images. Med Image Anal. 2009;13:883–99.
12. Zheng G. Personalized X-ray reconstruction of the proximal femur via intensity- based non-rigid 2D-3D registration. Med Image Comput Comput Assist Interv. 2011;14(2):598–606.
13. Schumann S, Liu L, Tannast M, Bergmann M, Nolte L-P, Zheng G. An integrated system for 3D hip joint reconstruction from 2D X-rays: a preliminary validation study. Ann Biomed Eng. 2013;41:2077–87.
14. Balestra S. Statistical shape model-based articulated 2D-3D reconstruction. Master thesis, Institute for Surgical Technology and Biomechanics, University of Bern, 2013.
15. Schumann S, Sato Y, Nakanishi Y, Yokota F, Takao M, Sugano S, Zheng G. Cup implant planning based on 2-D/3-D radiographic pelvis reconstruction - first clinical results. IEEE Trans Biomed Eng. 2015;62:2665–73.
16. Yu W, Chu C, Tannast M, Zheng G. Fully automatic reconstruction of personalized 3D volumes of the proximal femur from 2D X-ray images. Int J Comput Assist Radiol Surg. 2016;11:1673–85.

Chapter 16
Construction and Application of Large-Scale Image Database in Orthopedic Surgery

Yoshito Otake, Masaki Takao, Futoshi Yokota, Norio Fukuda, Keisuke Uemura, Nobuhiko Sugano, and Yoshinobu Sato

Abstract Databases of medical images are valuable resources not only for clinical studies such as the analysis of disease progression or a large-scale population analysis of morphological characteristics but also for those engaged in image analysis. Databases can serve as a compendium against which newly developed algorithms can be tested and a common platform for performance comparisons with existing state-of-the-art algorithms. Several database projects that have focused on certain target modalities and diseases have been successful, including the Cancer Imaging Archive, the Alzheimer's Disease Neuroimaging Initiative, and the Osteoarthritis Initiative. Here, we introduce our efforts to construct a database of medical images and treatment records of Japanese patients who underwent hip surgery. This database currently contains computed tomography images, radiographs, and the log files of a surgical navigation system, including preoperative plans, intraoperative procedures, and postoperative outcomes (alignment). Herein, we also introduce our attempts in three applications: statistical analysis of the alignment in functional (standing) position, muscle function, and statistical analysis of surgeons' expertise from the surgical log. Open access is an important aspect for the research community, but privacy is a concern, especially for large-scale databases where per-patient consent is difficult to obtain as well as with images of patients with specific diseases wherein complete de-identification is extremely difficult. We believe our effort serves as a step toward augmentation of social acceptability of the strength of medical image databases for accelerating advanced medical treatment.

Keywords Image database · Image segmentation · 2D-3D registration · Muscle fiber analysis · Automated surgical planning

Y. Otake (✉) • F. Yokota • N. Fukuda • Y. Sato
Nara Institute of Science and Technology, Ikoma, Nara, Japan
e-mail: otake@is.naist.jp

M. Takao • K. Uemura • N. Sugano
Osaka University Graduate School of Medicine, Suita, Osaka, Japan

N. Sugano (ed.), *Computer Assisted Orthopaedic Surgery for Hip and Knee*,
https://doi.org/10.1007/978-981-10-5245-3_16

16.1 Introduction

A number of medical image databases, such as the Cancer Imaging Archive [1], the Alzheimer's Disease Neuroimaging Initiative [2], and the Osteoarthritis Initiative [3], provide valuable opportunities for clinical and engineering researchers engaged in population analysis of various diseases, analysis of pathology, and/or development and validation of algorithms of new analysis or diagnostic tools and techniques. In this chapter, we introduce our attempt to construct an image database of a cohort of Japanese patients with hip diseases.

16.2 Overview of the Database

The database consists of computed tomography (CT) images, plain radiographs, and the log files of a surgical navigation system, including the preoperative surgical plan and intraoperative procedures (registration results and transformation data representing the actual placement of an implant with respect to the bones). To date, 1147 total hip arthroplasties, performed between 2005 and 2015, were collected. The database contains images of four time phases (Fig. 16.1) in 70 patients that are useful for analyzing disease progression and recovery of muscles after treatment.

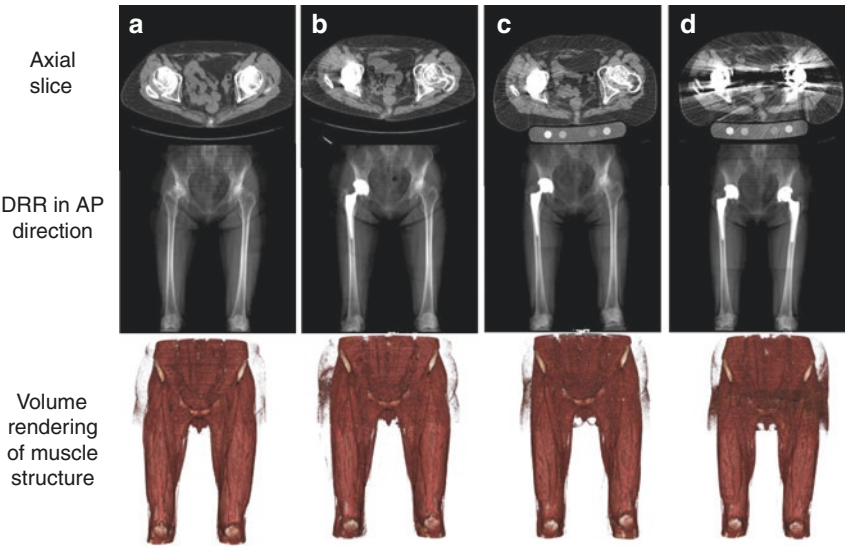

Fig. 16.1 Example of a series of computed tomography (CT) images in the data set of one patient. (**a**) Prior to right hip surgery. (**b**) After the surgery. (**c**) Prior to contralateral hip surgery. (**d**) After the second surgery. These images allow various follow-up analyses, such as disease progression, muscle atrophy, and/or recovery. *DRR* digitally reconstructed radiograph, *AP* anteroposterior

16.3 Segmentation of Anatomical Structures

The anatomical structures of bones (Fig. 16.2a) and muscles (Fig. 16.2c) were reconstructed using automated segmentation algorithms that we developed [4, 5]. Identifying the boundary between the femoral head and acetabulum is not easy, especially in patients with an end-stage osteoarthritic or collapsed hip due to osteonecrosis or arthritic erosion. The approach employed in our study [4] uses statistical shape models (SSMs), called hierarchical SSMs and conditional SSMs. The specificity and generality of the model are compromised by dividing the target structure hierarchically. The segmentation of each muscle was achieved using the multi-atlas method, which was originally developed for brain parcellation in a hierarchical manner using a training data set consisting of 19 hips and thigh muscles of 20 patients [5].

16.4 Application Areas

16.4.1 Statistical Modeling of Standing Position

Skeletal alignment in a functional position was one of our target areas of application (Fig. 16.3). Radiographs of the hip obtained with the patient in standing position, for example, can be used to measure functional hip alignment. Conventionally, the pelvic sagittal inclination angle has been measured by generating multiple virtual radiographic images from CT images (called digitally reconstructed radiographs) at various inclination angles and compared the shape of the pelvic foramen with the

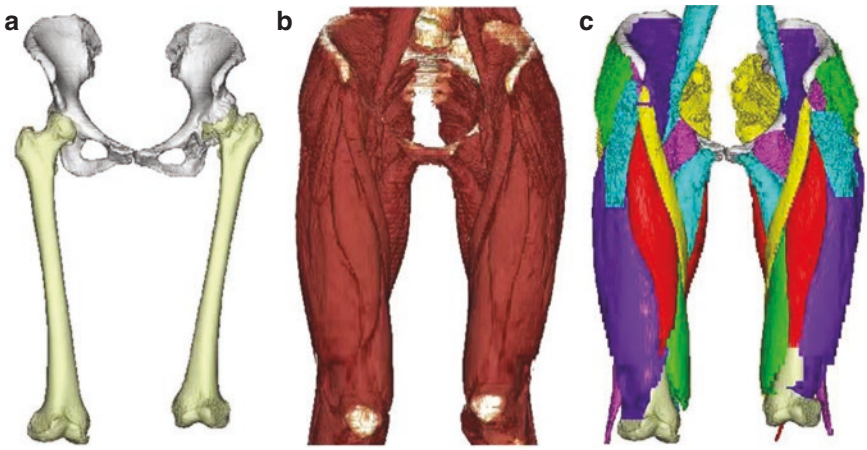

Fig. 16.2 Results of the segmentation of the bone (**a**), muscle region (**b**), and each unit of a muscle (**c**). Quantitative analyses of anatomical structures are possible using the segmented models

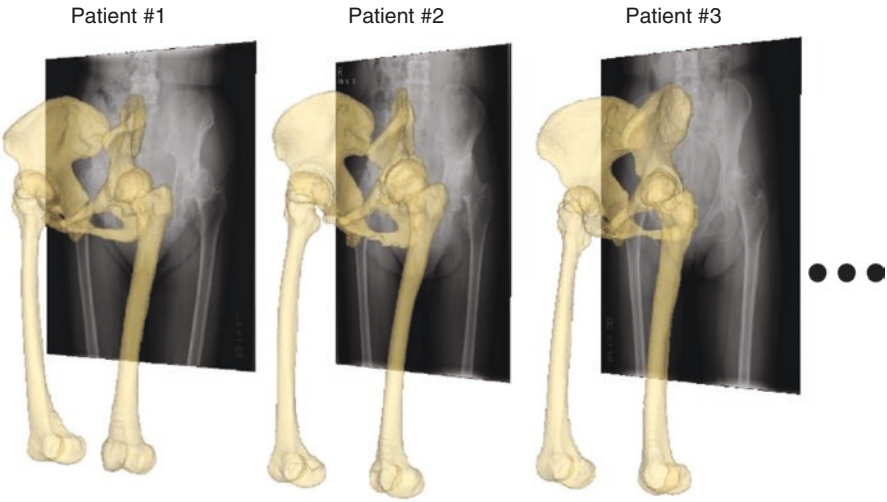

Fig. 16.3 Analysis of a hip joint angle in the standing position using two-/three-dimensional (2D-3D) registration of the CT image and the radiograph. Our fully automated analysis schema is especially advantageous for large-scale analyses of populations

obtained radiograph to find the true inclination angle [6]. Our approach—combining the automated segmentation of the skeletal structures [4] with the two-/three-dimensional (2D-3D) image registration method [7, 8]—allows a fully automatic analysis of the pelvic sagittal inclination angle in various postures. It is applicable to a large-scale population analysis [9]. The method compares the digitally reconstructed radiograph with the obtained radiograph more than a million times within a few minutes and provides an accurate three-dimensional position of the target bone with respect to the X-ray detector coordinate system. The same methodology has been applied to other anatomical structures such as the spine [10], patella [11], and ribs [12].

16.4.2 Statistical Modeling of Muscle Anatomy and Function

Analysis of muscle anatomy and function is one area on which we focus using the database. For example, variations in muscle fiber arrangement of a certain muscle in a population are analyzed with CT images (Fig. 16.4) [13]. For this analysis, we first create a model of the bones and individual muscles using the previously described automated segmentation method. We then identify the muscle attachment areas using a method that we previously proposed [14], wherein we created a probabilistic atlas of the attachment areas based on measurements in cadaver specimens to identify the most likely area for the muscle's attachment. Then, a geometric template representing the muscle's fiber arrangement is mapped to the muscle regions using information about the local orientation at each voxel derived by computing

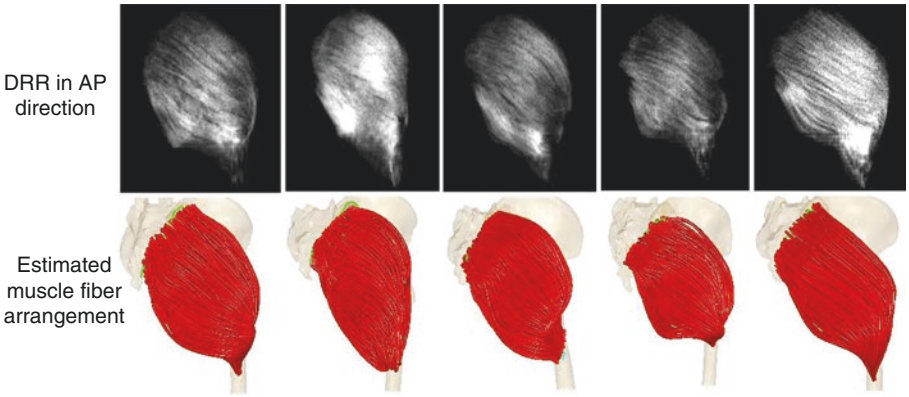

Fig. 16.4 Example of an analysis of the muscle fiber arrangement of the gluteus maximus muscle in five patients. The algorithm we proposed allows muscle fiber analysis using only a CT image, which would address the possibility of an accurate patient-specific musculoskeletal model that could be used, for example, for biomechanical simulations

the structure tensors of the CT images. The patient-specific fiber arrangement allows not only in vivo analysis of detailed muscle anatomy but also patient-specific biomechanical analysis, such as for planning treatment and rehabilitation for a patient requiring orthopedic surgery [e.g., [15]].

16.4.3 Statistical Modeling of Surgeons' Expertise in Surgical Planning

Our database contains the surgical planning data that was performed by expert surgeons in the past. In order to exploit the surgeon's expertise, we developed a system where we learn the relationship between the patient's anatomy and the surgical plan (i.e., selection of the size and placement of the implant) and automatically generate a plan for a new patient that matches the expert surgeons' preference [16, 17]. Figure 16.5a illustrate the workflow of the proposed system. Figure 16.5b shows the plans for example 6 patients generated by the system.

16.5 Conclusion

This chapter summarized our effort on constructing a large-scale medical image database in orthopedic surgery, which currently includes CT images, radiographs, and surgical logs that were recorded by a surgical navigation system. We described three example application scenarios using the database. We are aware of great importance of making the database openly accessible from all researchers. We hope

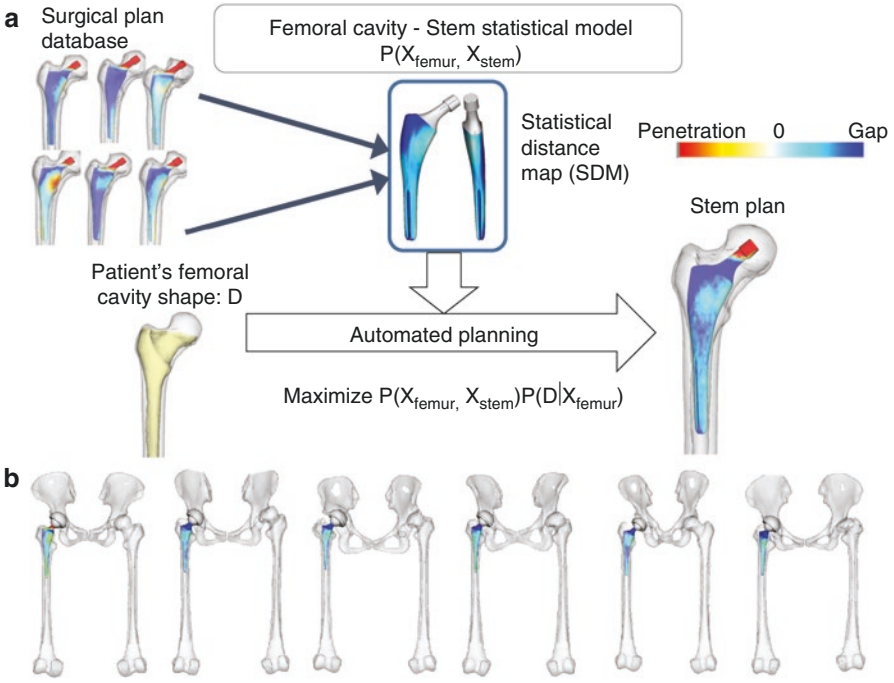

Fig. 16.5 (**a**) Workflow of an automated surgical planning system. (**b**) Example of the results of the surgical plan generated by the system. The system uses the database of expert surgeons' plans for past patients as a training data set to generate a plan for a new patient that matches the expert surgeons' preference

this database will provide one of the new venues for the discussion of the privacy concern in terms of legal, technical, and social aspects.

References

1. Clark K, et al. The Cancer Imaging Archive (TCIA): maintaining and operating a public information repository. J Digit Imaging. 2013;26(6):1045–57.
2. Alzheimer's Disease Neuroimaging Initiative (ADNI). Available from: adni.loni.usc.edu.
3. The Osteoarthritis Initiative (OAI). Available from: http://www.oai.ucsf.edu/.
4. Yokota F, et al. Automated CT segmentation of diseased hip using hierarchical and conditional statistical shape models. In: Medical Image Computing and Computer-Assisted Intervention – MICCAI 2013: 16th International Conference, Nagoya, Japan, September 22–26, 2013, Proceedings, Part II. Berlin: Springer; 2013.
5. Yokota F, et al. Automated muscle segmentation from 3D CT data of the hip using hierarchical multi-atlas method. In: Proceedings of the 12th Annual Meeting of the International Society for Computer Assisted Orthopaedic Surgery, Seoul. 2012.

6. Tamura S, et al. Does pelvic sagittal inclination in the supine and standing positions change over 10 years of follow-up after total hip arthroplasty? J Arthroplasty. 2017;32(3):877–82.
7. Otake Y, et al. Intraoperative image-based multiview 2D/3D registration for image-guided orthopaedic surgery: incorporation of fiducial-based C-arm tracking and GPU-acceleration. IEEE Trans Med Imaging. 2012;31(4):948–62.
8. Otake Y, et al. 3D–2D registration in mobile radiographs: algorithm development and preliminary clinical evaluation. Phys Med Biol. 2015;60(5):2075.
9. Uemura K, et al. Change in pelvic sagittal inclination from supine to standing position before hip arthroplasty. J Arthroplasty. 2017;32:2568.
10. Lo SF, et al. Automatic localization of target vertebrae in spine surgery: clinical evaluation of the levelcheck registration algorithm. Spine (Phila Pa 1976). 2015;40:E476.
11. Otake Y, et al. Robust patella motion tracking using intensity-based 2D-3D registration on dynamic bi-plane fluoroscopy: toward quantitative assessment in MPFL reconstruction surgery. 2016.
12. Hiasa Y., et al. Constrained piecewise rigid 2D3D registration for patient specific analysis of rib cage motion using X ray video. In: Computer Assisted Radiology and Surgery. 2016.
13. Otake Y, et al. Analysis of muscle fiber structure using clinical CT: preliminary analysis with cadaveric images. Proceedings of the 16th Annual Meeting of the International Society for Computer Assisted Orthopaedic Surgery, Osaka, 2016.
14. Fukuda N, et al. Estimation of attachment regions of hip muscles in CT image using muscle attachment probabilistic atlas constructed from measurements in eight cadavers. Int J Comput Assist Radiol Surg. 2017;12:733–42.
15. Rajagopal A, et al. Full-body musculoskeletal model for muscle-driven simulation of human gait. IEEE Trans Biomed Eng. 2016;63(10):2068–79.
16. Otomaru I, et al. Automated preoperative planning of femoral stem in total hip arthroplasty from 3D CT data: atlas-based approach and comparative study. Med Image Anal. 2012;16(2):415–26.
17. Kagiyama Y, et al. CT-based automated planning of acetabular cup for total hip arthroplasty (THA) based on hybrid use of two statistical atlases. Int J Comput Assist Radiol Surg. 2016;11(12):2253–71.

Chapter 17
Future Perspectives on Statistical Shape Models in Computer-Aided Orthopedic Surgery: Beyond Statistical Shape Models and on to Big Data

Leo Joskowicz

Abstract Statistical shape modeling (SSM) of bone surfaces is now the state of practice in industry and is gaining relevance in the clinical setting. In this chapter, we review the main technical, clinical, and scientific uses of SSMs and their associated techniques. We then survey the leading companies that use SMMs and related modeling techniques as part of their core technology to provide a variety of services and discuss three key issues they raise: What is the scope of SSM generation methodologies? How should the resulting SSMs be validated? How can the individual surface models and SSMs be made available to the community? We conclude with considerations of the main challenges that lie ahead for SSMs and the expected effect of "Big Data" on them.

Keywords Computer-aided orthopedic surgery · Statistical shape models · State-of-the-art review · Future assessment

17.1 Statistical Shape Models: Background and Uses

Statistical shape modeling (SSM) of bone surfaces is the current state of practice in industry and is gaining relevance in the clinical setting. The original concept of SSMs, starting from active contour models, was developed during the mid-1990s for the segmentation of structures in digital photographs and medical images [1, 2]. Since then, novel techniques have been developed for an increasing number of medical two-dimensional (2D) and three-dimensional (3D) shapes [3]. In orthopedics,

L. Joskowicz
CASMIP Lab – Computer Aided Surgery and Medical Image Processing Laboratory, School of Computer Science and Engineering, The Hebrew University of Jerusalem, Jerusalem, Israel
e-mail: josko@cs.huji.ac.il

N. Sugano (ed.), *Computer Assisted Orthopaedic Surgery for Hip and Knee*,
https://doi.org/10.1007/978-981-10-5245-3_17

Table 17.1 Main technical, clinical, and scientific uses of statistical shape models of bones in orthopedics

Technical	Clinical	Scientific
Surface reconstruction	Computer-aided diagnosis	Population studies
Intraoperative registration	Preoperative planning	Pathology studies
Automatic segmentation of structures in CT/MRI scans	Intraoperative spatial visualization and navigation	Identification of anatomical parameters
Advanced biomechanical analysis	Postoperative and longitudinal assessment of implants	Derivation of indications
Design and manufacturing of implants and instrumentation	Design of custom implants	Implant performance evaluation
	Design and 3D printing of custom templates	Quantitative evaluation methods
	Replacement of CT scans with X-ray imaging and SSMs	
	Training and education	

SSMs and the techniques to generate and use them were developed a decade ago for bone structures, with significant progress during the past few years [4–7]. In particular, specific SSMs were developed for hip and knee bone structures [8–11].

SSMs have a wide variety of technical, clinical, and scientific uses in orthopedics (Table 17.1). The main technical uses of SSMs include the following:

- *Surface reconstruction* of bone surfaces from two or more 2D plain radiographic images. This technique allows direct 3D reconstruction of the bone surface using triangular meshes based on the corresponding bone contours determined from preoperative plain radiographic images or intraoperative 2D fluoroscopic radiographic images. The missing surface information is extrapolated from the corresponding bone SSM. The result is a patient-specific 3D model suitable for a variety of tasks, including planning, navigation, manual and robotic surface machining, and designing custom templates and implants. In certain circumstances, the model can obviate the need of a computed tomography (CT) scan whose sole purpose is to obtain an image of the outer surface of a bone.
- *Intraoperative registration* of 2D fluoroscopic radiographic images to preoperative CT scans, 3D surface bone models obtained from them, and/or a preoperative plan (e.g., the desired positions of the cutting jigs, the implant location with respect to the bones). This technique is used to provide valuable spatial shape and location information for the operator during surgery, thereby potentially increasing the accuracy of the surgical manipulations and reducing the use of fluoroscopy (with its associated time requirement and ionizing radiation doses).
- *Automatic segmentation* of structures (e.g., bones, cartilage) on CT images and magnetic resonance imaging (MRI). SSMs provide a high-quality initialization shape for active and deformable contours' segmentation methods, such as fast

marching level sets [12]. This capability helps reduce segmentation errors and improves the accuracy and robustness of the resulting segmentation, which is used to create the 3D surface mesh and intensity bone models required for various technical, clinical, and research tasks.

- *Advanced biomechanical analysis*, including kinematic and dynamic simulations of knee and hip joints, bone-loading analysis, and fracture risk analysis. These simulations and analyses can be patient-specific, derived from information obtained from the patient's CT images, or they can be performed on population-based SSMs and statistical intensity models for use in advanced biomechanical simulations.
- *Design and manufacturing of implants and instrumentation*, including custom knee and hip implants, cutting jigs, and surgical instruments based on population-wide anatomical models. The SSMs encode the bone geometry and its variability, obviating the need to collect and process numerous individual CT scans.

The main clinical uses of SSMs include the following:

- *Computer-aided diagnosis* based on qualitative spatial visualization and quantitative comparison of a bone surface model obtained from CT images of patients with the corresponding bone SSM. The comparison yields quantitative measures on variations from normal anatomy, in support of clinical decision-making.
- *Preoperative planning* for implant selection and positioning, osteotomy planning, and cutting jigs' positioning based on patient-specific 3D surface models derived from plain radiographic or CT images [13]. The SSMs obviate the need for a CT scan during procedures where it is not routinely required.
- *Intraoperative spatial visualization and navigation* based on patient-specific 3D models derived from plain radiographic or CT images, following intraoperative registration. The models and their spatial locations are displayed together with tracked surgical instruments or are overlaid on fluoroscopic radiographic images or CT slices, thereby providing an updated, real-time view of the surgical site.
- *Postoperative and longitudinal assessment* of spatial implant positioning from plain radiographic images and from CT scans on which quantification is difficult because of the implant's metal artifacts. Emerging uses include longitudinal quantification of tissue/morphological changes (e.g., tibiofemoral osteoarthritis, rheumatoid arthritis, osteoporosis, osteophytes, fracture risk analysis).
- *Design and 3D printing of custom templates*, including cutting and targeting templates based on patient-specific 3D models derived from plain radiographic or CT images. The custom templates are then sterilized and used during surgery by mounting them on the patient's bone, similar to standard jigs. The advantage of these custom templates is that no adjustments are necessary during surgery.
- *Design of custom implants* based on patient-specific 3D models derived from plain radiographic or CT images, thereby obviating the need for a CT scan whose main purpose is to obtain an image of the outer surface of a bone.
- *Replacement of CT scans with plain radiographic imaging and SSMs* to reduce the cost and radiation exposure to the patient during both preoperative planning and postoperative follow-up.

- *Training and education*, including anatomical visualization of a wide and rich variety of cases for preoperative planning training and/or intraoperative execution simulation to learn how to address difficult/rare cases before attempting real-time surgery.

The main scientific and basic science uses include the following interests:

- *Population studies* that characterize the anatomical variability of population subgroups by age, race, and sex based on individual CT images
- *Pathology studies* that characterize pathologies such as bone deformities (e.g., cam deformities, genu valgum and varus deformities, cartilage wear)
- *Identification of anatomical parameters* that are clinically relevant to specific population subgroups and pathologies (e.g., acetabular orientation variability, symmetry) [14]
- *Derivation of indications* for implant types and their placement (e.g., determining the optimal pelvic coordinate system to serve as a reference for cup alignment) [15]
- *Implant performance evaluation* based on longitudinal plain radiographic images and population-wide models created by an SSM
- *Quantitative evaluation methods* for longitudinal studies and clinical trials

These lists indicate that the ability to generate 3D bone surface models automatically from CT and plain radiographic images and to create SMMs is both wide and far-reaching. It is starting to have a profound, across-the-board effect [16].

17.2 Current Trends and Issues

17.2.1 Trends

A growing number of leading companies use SMMs and related modeling techniques as part of their core technology to provide a variety of services, including implant design, testing, and evaluation. For example, Stryker has developed SOMA® (Stryker Orthopaedics Modeling and Analytics) from more than 15,000 patient-specific bone models computed from clinical CT scans [17]. Other examples include ZiBRA® (Zimmer's Bone Resection Atlas), a platform for bone research and analysis, and Mimics® (Materialize). Depuy Synthes reports that the Attune® Knee System was designed using SSM technology. Other companies, such as Imorphics (now owned by Stryker) sell enabling SSM technology. Research platforms have also been developed, such as Statismo, a tool for principal component analysis (PCA)-based statistical model creation [18], 1000shapes [19], and ShapeWorks® (ShapeWorks 2016), to name a few. There is a clear growth trend in the services and companies relying on SSMs and modeling technologies. SSMs and modeling technologies are enablers of new technologies and workflows, and they have been shown to increase the use of automation and provide quantitative measurements.

17.2.2 Issues

The proliferation of SSMs and modeling technologies raises three key issues: What is the scope of SSM generation methodologies? How should the resulting SSMs be validated? How can the individual surface models and SSMs be made available to the community?

17.2.2.1 Scope of SSM Generation Methodologies

Most, if not all, methods for generating musculoskeletal SSMs assume that the anatomical variability can be modeled with a set of linear equations, usually derived by PCA. This assumption has clear computational advantages, as the models can be efficiently generated, modified, and updated [11]. This modeling assumption, however, requires validation and may hold only for specific population subgroups categorized by age, race, sex, and personal characteristics (e.g., height, weight, type of pathology). Other modeling assumptions that require further investigation are the reliance on landmark points—manually or automatically selected—and probabilistic population distribution models, Gaussian or other. For example, Zhang and Golland [20] recently discussed the evolution of SSM representations and techniques from landmarks to diffeomorphisms. Another key aspect is reliance on the set of training samples used to construct the SSMs. Further studies are required to determine the minimum/optimal number of individual shape samples and their distribution necessary to create an SSM.

17.2.2.2 Validation of SSMs

Once an SSM has been created from a training set, how do we ensure that it faithfully represents the target population or, more generally, what type of population does it represent? Currently, SSMs are created with several tens of examples and can seldom be validated with a single test set. A second issue is how to quantify the downstream effect of the model's inaccuracy/lack of coverage on subsequent tasks, such as a custom template design and/or an advanced biomechanical analysis (e.g., load analysis).

17.2.2.3 Availability of Individual Surface Models and SSMs

Every month, hundreds of 3D models of musculoskeletal anatomy—healthy and pathological bone; bone regions of the hip, knee, and pelvis; and spine osseous anatomy—are engineered by industry. The models are created by automatic segmentation and are usually corrected and validated by an engineer and/or a surgeon

before they are used. These high-quality models are accumulating slowly but surely. Companies now have large collections of such models that are used in-house for the specific needs of the company. Unfortunately, universities and research laboratories do not have access to the databases of such large individual CT and surface models or to the SSMs created from them. Also, they do not have the ability to generate them. This valuable repository of high-quality models presents untapped opportunities for the development of advanced and refined SSMs and techniques.

17.3 The Future

Statistical shape and intensity models of musculoskeletal structures—including bones, cartilage, ligaments, muscles, and their associated pathologies—will undoubtedly play an increasingly important role in all aspects of orthopedics, particularly knee and hip surgery. There are main challenges that lie ahead for the short- to midterm future including:

1. The collection and validation of large sets of individual CT images and MRI scans as well as the automatic generation of high-quality segmentation for the creation of statistical shape and intensity models
2. The validation and certification of the resulting statistical models
3. The development of statistical models of bone fractures and bone pathology (e.g., bone tumors, osteoporosis)
4. The development of clinician-friendly statistical models technology that can be used by clinical practitioners without the need for technical intermediaries

The advent of Big Data and its associated technology is perhaps the most significant expected development in the long term. Big Data has made great strides in consumer goods, finance, and insurance industries and is poised to revolutionize radiology [21]. We can thus expect Big Data to make a major long-term difference in orthopedic radiology and orthopedic surgery. SSMs play a key role by being enablers for population-wide data mining, treatment personalization, and automation of a variety of clinical tasks. Indeed, data availability and size lead to paradigm changes, as is being appreciated in other fields. The current paradigm change is occurring because SSMs are being created from individual models or from a few tens of models to SSMs with hundreds or thousands of models. In the coming years, the hundreds of individual models will become thousands. This arena has the potential to yield specialized SSMs for subpopulations and specific groups of pathologies. As the trend continues over the next few years, the next disruptions could come as the order of magnitude increases. Think of what we could accomplish at each stage with all these data and models.

17.4 Conclusion

There is a great opportunity to create vendor-neutral, publicly available SSMs from the thousands of models being created in industry. The widespread availability of these models could greatly facilitate and speed up current and future technical, clinical, and scientific efforts. An international nonprofit scientific association such as the International Society for Computer Aided Orthopaedic Surgery (CAOS-International) is uniquely positioned to lead this trend.

References

1. Cootes TF, Hill A, Taylor CJ, Haslam J. The use of active shape models for locating structures in medical images. Image Vision Comput. 1994;12(6):355–66.
2. Cootes TF, Cooper D, Taylor CJ, Graham J. Active shape models - their training and application. Comput Vision Image Understand. 1995;61(1):38–59.
3. Heimann T, Meinzer HP. Statistical shape models for 3D medical image segmentation: a review. Med Image Anal. 2009;13:543–63.
4. Albrecht T, Lüthi M, Gerig T, Vetter T. Posterior shape models. Med Image Anal. 2013;17:959–73.
5. Blanc R, Seiler C, Székely G, Nolte LP, Reyes M. Statistical model based shape prediction from a combination of direct observations and various surrogates: application to orthopaedic research. Med Image Anal. 2012;16:1156–66.
6. Kozic N, Gonzalez Ballester MA, Buchler M, Reimers N, Nolte LP, Linguraru MG, Reyes M. Population-specific evaluation of implant bone fitting using PCA shape space and level sets. In: Proc. IEEE Int. Symp. on Biomedical Imaging. Washington, DC: IEEE; 2009. p. 883–6.
7. Sarkalkan N, Weinans H, Zadpoor AA. Statistical shape and appearance models of bones. Bone. 2014;60:129–40.
8. Baldwin MA, Langenderfer JE, Rullkoetter JA, Laz PL. Development of subject-specific and statistical shape models of the knee using an efficient segmentation and mesh-morphing approach. Comput Methods Programs Biomed. 2010;9(7):232–40.
9. Bryan R, Mohan PS, Hopkins A, Galloway F, Taylor M, Nair PB. Statistical modelling of the whole human femur incorporating geometric and material properties. Med Eng Phys. 2010;32:57–65.
10. Smoger L, Fitzpatrick CK, Clary CW, Cyr AJ, Maletsky LP, Rullkoetter PJ, Laz PJ. Statistical modeling to characterize relationships between knee anatomy and kinematics. J Orthop Res. 2015;33:1620.
11. Zheng G, Li S. Computational radiology for orthopaedic interventions. Lecture notes in computational vision and biomechanics. New York: Springer; 2016.
12. Sethian JR. Level set methods and fast marching methods evolving interfaces in computational geometry, fluid mechanics, computer vision, and materials science. Cambridge monograph on Applied and computational mathematics. Cambridge: Cambridge University Press; 1999.
13. Kovler I, Joskowicz L, Kronman A, Weill Y, Salavarrieta J. Haptic computer-assisted patient specific preoperative planning for orthopaedic fracture surgery. Int J Comput Aid Radiol Surg. 2015;10(10):1535–46.
14. Lubovsky O, Peleg E, Joskowicz L, Liebergall M, Khoury A. Acetabular orientation variability and symmetry based on CT scans of adults. Int J Comput Aid Radiol Surg. 2010;5(5):449–54.

15. Takao M, Nishii T, Sakai T, Sugano N. What is the optimal pelvic coordinate system as a reference of cup alignment? Bone Joint J. 2016;98(Supp. 4):47.
16. Joskowicz L, Hazan E. Computer aided orthopaedic surgery: incremental shift or paradigm change? Med Image Anal. 2016;33:84–90.
17. Banerjee S, Faizan A, Nevelos J, Kreuzer S, Burgkart R, Harwin SF, Mont MA. Innovations in hip arthroplasty three-dimensional modeling and analytical technology (SOMA). Surgical Technology International. Orthopaed Surg. 2013;24:280–94.
18. Lüthi M, Blanc R, Albrecht T, Gass T, Goksel O, Buchler P, Kistler M, Bousleiman H, Reyes M, Cattin PC, Vetter T. Statismo - a framework for PCA based statistical models. Insight Journal. 2012. http://hdl.handle.net/10380/3371. Accessed Dec 10, 2016.
19. Lamecker H, Zachow S. Statistical shape modeling of musculoskeletal structures and its applications. 2015. https://www.1000shapes.com/. Accessed Dec 10, 2016.
20. Zhang M, Golland P. Statistical shape analysis: from landmarks to diffeomorphisms. Med Image Anal. 2016;33:155–8.
21. Kansagra AP, Yu JP, Chatterjee AR, Lenchik L, Chow DS, Prater AB, Yeh J, Doshi AM, Hawkins CM, Heilbrun ME, Smith SE, Oselkin M, Gupta P, Ali S. Big Data and the future of radiology informatics. Acad Radiol. 2016;23(1):30–42.

Websites

1000shapes. https://www.1000shapes.com/. Accessed Dec 10, 2016.
CAOS International. International Society for Computer Aided Orthopaedic Surgery. http://www.caos-international.org/. Accessed Dec 10, 2016.
Depuy Synthes. https://www.depuysynthes.com/hcp/knee/products/qs/ATTUNE-Knee-System. Accessed Dec 10, 2016.
Imorphics. http://imorphics.com/. Accessed Dec 10, 2016.
Materialize. http://biomedical.materialise.com/anatomical-models Accessed Dec 10, 2016.
ShapeWorks. https://www.sci.utah.edu/software/shapeworks.html Accessed Dec 10, 2016.